RADIATION EXPOSURE LEVELS AND EXCESS LIFETIME CANCER RISK ASSOCIATED WITH SOIL, WATER AND SUB-SURFACE ROCKS IN KARGI AREA, MARSABIT - KENYA

WILLIS OUGO AGUKO

DOCTOR OF PHILOSOPHY

(Physics)

JOMO KENYATTA UNIVERSITY
OF
AGRICULTURE AND TECHNOLOGY

2024

Radiation Exposure Levels and Excess Lifetime Cancer Risk Associated with Soil, Water and Sub-Surface Rocks in Kargi Area, Marsabit - Kenya

Willis Ougo Aguko

A Thesis Submitted in Partial Fulfillment of the Requirements for the Degree of Doctor of Philosophy in Physics of the Jomo Kenyatta University of Agriculture and Technology

2024

DECLARATION

This thesis is my original work and has not been presented for a degree in any other university.

Signature……Date……...

Willis Ougo Aguko

This Thesis has been submitted for examination with our approval as University Supervisors.

Signature……Date……...

Prof. Robert Kinyua, PhD

JKUAT, Kenya

Signature……Date……...

Prof. John Githiri, PhD

JKUAT, Kenya

DEDICATION

I dedicate this thesis work to my wife Lillian, daughter Tough, sons Ron, Val and Trevor, my mother Esta Aguko, my late father Edwin Aguko, my sisters and brothers for the support they gave me during my study period.

ACKNOWLEDGEMENT

Special thanks to Prof. Robert Kinyua and Prof. John Githiri, my supervisors, for guiding and supporting me throughout the research work.

I am really indebted to Kenya Bureau of Standards (KEBS) for the use of dryer and hand-held survey meter, National Oil Corporation of Kenya for their advice and support in geomagnetic maps, JKUAT civil engineering labs for the use of the grinder and Institute of Nuclear Science, University of Nairobi for the use of Hyper-germanium detector.

I am grateful to Prof. Githiri for his constant advice and encouragement, Dr. Ominde and Dr. Kiroe, current and former chairman, Physics department, and to all staff of Physics department, JKUAT.

It gives me great pleasure to acknowledge Selma Sanya of KEBS organic lab for her assistance during the sample preparation and drying, Lydia Moraa Okemwa who walked the journey with me as a research assistant, Domnick Ondoro and Birgen Rono for their support during the period.

Without the continuous encouragement of my family, this would not have been completed. I thank them all.

Finally, for the good health and sound knowledge during this period, I thank God the Almighty.

TABLE OF CONTENTS

LIST OF TABLES

LIST OF FIGURES

LIST OF APPENDICES

ABBREVATIONS AND ACRONYMS

A	Absorbed gamma dose rate
ADC	Analog to Digital Converter
AGED	Annual Gonadal Equivalent Dose
CB	Chemical/Biological
D	Absorbed dose rate
De	Effective dose rate
DNA	Deoxyribo Nucleic Acid
EC	Electron capture
ELCR	Excess lifetime cancer risk
EM	Electromagnetic
EPA	Environmental Protection Agency
FFT	Fast Fourier Transform
FOM	Figure of Merit
FWHM	Full Width at Half Maximum
Ge (Li)	Germanium Lithium-doped
GPS	Global Positioning System
GRS	Gamma-Ray Spectrometer
HBRA	High Background Radiation Area
HD_TDR	Horizontal component of magnetic measurement
HPGe	Hyper Pure Germanium
$h.yr^{-1}$	Hours per year
IAEA	International Atomic Energy Agency

IAEA-TECDOC	International Atomic Energy Agency Technical Document
ICRP	International Commission on Radiological Protection
ICRU	Internal Commission on Radiation Units
IDC	Individual Dose Criterion
IGRF	International Geomagnetic Reference Field
KERMA	Kinetic Energy Released in Matter
MC	Monte Carlo
MCA	Multi-Channel Analyzer
mrem	Milli Roentgen Equivalent Man
NaI(TI)	Sodium Iodide Thallium Activated Detector
NBC	Nuclear/Biological/Chemical
NORM	Naturally Occurring Radioactive Materials
OECD	Organization for Economic Cooperation and Development
PET	Positron Emission Tomography
PM	Photomultiplier
Rad	Radiation Absorbed Dose
Rem	Roentgen Equivalent Man
ROI	Region of Interest
RAPS	Radially Average Power Spectrum
RTP	Reduction to the Pole
TECDOC	Technical Document
TDR	Tilt Derivative
TMI	Total magnetic intensity

UCSD	University of Califonia, San Diego
UNSCEAR	United Nations Scientific Committee on the Effects of Atomic Radiation
WHO	World Health Organisation
WR	World Resources
x	Sample Thickness (or effective thickness)

LIST OF SYMBOLS AND UNITS

$\mathbf{A_K}$	Activity Concentration of Potassium
$\mathbf{A_{Ra}}$	Activity Concentration of Radium
$\mathbf{A_{Th}}$	Activity Concentration of Thorium
B	Total Magnetic Field
Bq	Becquerel
$\mathbf{Bql^{-1}}$	Becquerel per Litre
$\mathbf{Bq/m^3}$	Becquerel per Cubic Metre
$\mathbf{Bqkg^{-1}}$	Becquerel per Kilogram
°C	Degrees Celsius
C	^{222}Rn Concentration
$\mathbf{C_k}$	Activity Concentration of Potassium
$\mathbf{C_{Ra}}$	Activity Concentration of Radium
$\mathbf{C_{Th}}$	Activity Concentration of Thorium
Ci	Curie
E	East; Energy, In Joules
Gy	Gray
$\mathbf{H_{ex}}$	External Hazard Index
$\mathbf{H_{in}}$	Internal Hazard Index
I	Intensity after Attenuation
$\mathbf{I_o}$	Intensity without Attenuation
J/kg	Joules per Kilogram

keV	Kilo Electron Volt
kg	Kilogram
L	Litre
LN_2	Liquid Nitrogen
M	Mass, in Kilogram
m	Metre
MeV	Mega Electron Volt
N	North; Sample Total Count Rate, Count Per Minute
N_B	Background Count Rate, Count per Minute
t	Time, in Seconds
$mSvy^{-1}$	Mili Sieverts per Year
$nGyh^{-1}$	Nano Gray per Hour
pCi	Picocurie
pCi/L	Picocurie per Litre
s	Second
Sv	Sieverts
Svy^{-1}	Sieverts per Year
SvGy	Sieverts Gray
α	Alpha radiation
β	Beta particle
γ	Gamma rays
λ	^{222}Rn Decay Factor, 1.26 X 10^{-4} per Minute

κ	Magnetic susceptibility
μ	Linear Attenuation Coefficient, cm^{-1}
μ_m	Mass Attenuation Coefficient, $\mu_m = \mu/\rho$, cm^{-2}/g
μs	Microsecond

ABSTRACT

Radiometric and Magnetic studies were carried out in Kargi area, located between latitudes 2.476944° and 2.520833° and longitudes 37.542778° and 37.601944°, with approximately 31.26 km^2 coverage area. Escalated number of cancer disease cases among humans and animal deaths in this region led to this research work. The aim of the study was to characterize radioactivity in soil and water, magnetic intensities, delineating subsurface structures, anomalous zones with depth to magnetic sources. Gamma ray spectrometer, Proton magnetometer, together with GPS were used for radiometric, magnetic and location points respectively. 14 water and 117 soil samples were collected from the area, examined to have their natural radioactivities due to ^{40}K, ^{232}Th and ^{226}Ra radionuclides measured. 51 magnetometer readings were taken on the eastern part of Kargi, covering an area of 13 km^2. Gamma spectrometry method making use of a high purity germanium (HPGe) detector and proton magnetometer were used to gauge the radiological hazard of radioactivities and measure magnetic field respectively. Surfer 10 and Geosoft^R Oasis Montaj software were used to map and process magnetic data respectively. Results from radioactivities for ^{40}K, ^{232}Th and ^{226}Ra, gave mean calculated activities as 353.19 ± 110.07, 7.98 ± 3.98 and 7.37 ± 2.60 $Bq \cdot kg^{-1}$ for soil and 56.93±20.16, 2.80±2.45, 4.31±2.52 and 11.19±5.74 Bql^{-1} for water respectively. Evaluation of magnetic images showed lows and highs with variation in amplitude between -791 nT to 420 nT, an indication of lineament structures. Euler Deconvolution was used to image structures and estimate depths to the magnetic basement. Radially averaged power spectrum showed depth estimates to magnetic sources ranging between 100 m to 480. Since internal, external, radium equivalent indices and annual effective dose values are lower than the worldwide acceptable limits, these soils and/or rocks are safe and are recommended for use in building with proper ventilation as any amount of radiation is still harmful.

CHAPTER ONE

INTRODUCTION

1.1 Background Information

Radiation is the process of transfer or emission of energy or wave or energetic particles from one space or medium to another. The major types of radiation include ionizing and non-ionizing radiation. These radiations are harmful to the organisms and their activity is likely to cause changes to the natural environment. The ionizing power tends to damage the molecules of matter, and thus similar effect occurs when living tissues are exposed to the radiation. The direct impairment of living tissues by ionization involves the breakage of the chemical bonds of bio-molecules considered essential in the human body; for instance, the DNA. As such, the chemical radicals in cells (from water molecules) tend to damage the living cells indirectly, which eventually causes chemical invasion to the biological molecules (UNCEAR, 1993). The damaged molecules are to some extent repaired or restored naturally through bio-processes. The repair or restoration efficacy depends on the degree of damage incurred by the cell. For a faulty cell repair, or incomplete bio-process, the living cell may undergo (Cember, 1996):

i. Cell death

ii. Impairment of cell's natural function resulting in somatic effects; that is, the physical effect or reaction endured by the irradiated individual; for instance, cancer

iii. Permanent alteration or metamorphosis of the cell, a condition transmittable throughout the generations, which resembles a genetic mutation.

The radionuclides or radioisotopes have always existed naturally in the environment. The external exposure of the radionuclides from the gamma-radiation is mainly contributed naturally by thorium and uranium, together with potassium 40 (^{40}K) when small quantities of these come in contact with the earth's surface or any other matter such as building materials (UNSCEAR 2008).

Long-lived radioactive elements like potassium, uranium and thorium and any of their products like radon and radium are examples of Naturally Occurring Radioactive Materials (NORM). The said elements have always been present in the crust of the earth and atmosphere. NORM issue relates to radon exposure in homes, particularly those built on granitic ground. Occupational health issues include the exposure of flight crew to higher levels of cosmic radiation, the exposure of tour guides to radon in caves, exposure of miners to radon underground, and exposure of workers in the oil and gas and mineral sands industries to elevated radiation levels in the materials they handle. The list of isotopes that contribute to natural radiation can be divided into those materials which come from the ground (terrestrial sources – vast majority) and those which are produced as a result of the interaction of atmospheric gases with cosmic rays (cosmogenic). Large discrepancies in dose rates both for terrestrial together with cosmic radiation are realised depending on where the measurements are made. The altitude above sea-level and the radionuclide activity concentration in the ground are major reasons for this discrepancy. By making use of building materials with relatively elevated activity concentration of ^{226}Ra and building techniques that stipulate the influx of radon coming from the ground, for instance, well insulated-housing, the radiation dose to the public dose is still further increased *(*Aguko *et al.,* 2013).

Throughout the history of life on earth, organisms have been continuously exposed to cosmic rays in the atmosphere, and from naturally occurring radionuclides which are ubiquitously distributed in all living and non-living components of the biosphere (Whicker and Schults, 1982). All living material contains a certain amount of potassium isotopes because no discrimination of potassium isotopes occurs in living systems. ^{238}U series contributes to an effective dose equivalent of 0.09 mSvy^{-1} from internal radiation, thus giving a total of 1.04 mSvy^{-1}. The members of ^{238}U series within the body do not irradiate it uniformly, and the dose to the organs affected is predominantly due to alpha particles irradiation. The above values are averages for the entire earth, and the variation from region to region may be rather large depending on the contribution of radionuclides from the ^{238}U and ^{232}Th series (UNSCEAR, 1988).

A broad span of activity concentrations in a broad variation of materials is reported. Examples of ores found to be in association with higher levels radionuclide concentrations are those of uranium, tin, tantalum, niobium, aluminium, copper, gold and phosphate. Mining and processing of these ores can lead to further increases in radionuclide concentrations in the residues, by-products or products (IAEA-TECDOC-1660, 2011).

Natural radioactivity concentrations depend mainly on geographical and/or geological conditions and tends to appear at different levels in soils of different geological regions (UNSCEAR, 2000). Soil radionuclide activity concentration is one of the main determinants of the natural background radiation. When rocks are disintegrated through natural process, radionuclides are carried to soil by rain and flows (Taskin *et al.,* 2009). In addition to the natural sources, soil radioactivity is also affected by human-made activities (Avwiri *et al.,* 2014).

Natural atmospheric radioactivity is determined by the concentration of radon and its daughter elements in air. Radon is formed in the decay chain of naturally occurring primordial radionuclides ^{232}Th, ^{238}U and ^{235}U present in the earth's crust. When radon is formed, it may diffuse from the rocks and soils to enter the atmosphere. The extent to which radon will diffuse into the atmosphere depends on the geological (type of rock or soil matrix, water content) and meteorological (atmospheric temperature, pressure) factors (Schery and Wasiolek, 1998; Nazaroff, 1992; Schubert and Schulz, 2002; Sannappa *et al.,* 1997, 1999; UNSCEAR, 1993). Radioactivity is due to alpha (α), beta (β) and gamma (γ) radiation from the unstable isotopes in the composition. For the most part, minerals that contain uranium (U), thorium (Th) and potassium (K) are radioactive.

Water is a major constituent of the human body and is essential for life. Human activities and some natural phenomenon pollute and affect water quality. Some of the waste disposals associated with the human activities affecting water quality often contain radioactive materials which contribute significantly to the background activity of the water bodies. Drinking waters usually contain several natural radionuclides: tritium, radon, radium, uranium isotopes, etc. Their concentrations vary widely since

they depend on the nature of the aquifer, namely, the prevailing lithology and whether there is air in it or not (Cristina and Forte 2012).

Drinking water sourced from deep wells and boreholes are usually expected to have higher concentration of radionuclides. This is because they pass through fractures in bedrock or within the soil which contain mineral deposits that might have radioactive constituents and thus leaking into the water ways (Njinga *et al*., 2015). Many salts of radium are soluble in water, and therefore surface, drinking and mineral waters may be enriched in radium and its descendant radon.

Radioactivity in drinking water is one of the major ways in which radionuclides gets into the human body, which might consequently lead to radiation-induced disorder (USEPA 2010). There is evidence from both human and animal studies that radiation exposure at lower to moderate doses, may increase the long-term incidence of cancer and that the rate of genetic malformations may increase by radiation exposure (Otton, 1994). It is therefore important to determine the amount of radioactivity in drinking water for every area where people reside, so as to guard against its deleterious effects (WHO, 2006). WHO guidelines for drinking water suggest performing an indirect evaluation of individual dose criterion (IDC) of 0.1 $mSvy^{-1}$ by measuring gross alpha and beta radioactivity and checking compliance of radionuclide activity concentration to derived guidance levels (WHO, 2011).

Estimation of the radiation dose distribution is vital in assessing the health risk to a population and serves as a reference for documenting changes in environmental radioactivity due to anthropogenic activities (Obed *et al*., 2005).

Humans are also exposed by food chain contamination which occurs as a result of deposition of radionuclides on plant leaves, uptake by roots from contaminated soil, water or sediment (Arogunjo *et al*., 2004), and from direct ingestion of contaminated water (Avwiri and Agbalagba, 2007).

Long-term exposure to radiation is assumed to have some risks of causing cancer. This means that all people have a risk of getting cancer. “Excess lifetime cancer risk” (ELCR) is additional risk that someone might have of getting cancer if that person is exposed to cancer-causing materials for a longer time (Aziz *et al.,* 2014). Cancer is a

class of diseases characterized by out-of-control cell growth. It is a disease of the cells in the body. There are over 100 different types of cancer, and each is classified by the type of cell that is initially affected. The World Health Organisation estimates that, worldwide, there were 14 million new cancer cases and 8.2 million cancer-related deaths in 2012 (their most recent data) (http://www.medicalnewstoday.com/info/cancer-oncology, Medical News Today – Newsletter, 2016). Many cancers seem to develop for no apparent reason. However, certain risk factors are known to increase the chance that one or more of the cells will become abnormal and lead to cancer. Risk factors include chemical carcinogens, age, radiation, infection, immune system and genetic 'makeup'.

Okpoli and Akingboye (2016) in their study of Magnetic, Radiometric and Geochemical Survey of Quarry Sites in Ondo State, South-western Nigeria used radiometric profiles to establish evidences from the geologic formations about the radiation level of the three quarries investigated in the study area. 3D Euler deconvolution and RAPS images used showed different range of depth estimates between 100 m to 800 m indicating the total depth estimate to the top of geologic sources that produced the observed anomalies. The varying magnetic intensity suggests varying magnetic materials associated with the rock types in the area.

Their study revealed that the quarrying activities in the study area have affected the geologic formation causing more fracturing in rocks and pronounced subsurface structures as a result of blasting and crushing that could serve as passage for leachates from pollutants as well as the level of radiation in the study area. Chemical concentration from explosives and machineries thereby increasing the level of chemical concentrations and elements in the soil, which in later years could lead to poisonous concentrates in soil, surface water and groundwater.

Githiri, *et al.,* 2011, while studying the depths to the top of magnetic bodies in magadi area of Kenya used Euler deconvolution method and found presence of deep sedimentary basins in some regions in the study area.

1.2 Geology of Kargi

Geology of study area is contained in sheet 20, a remote 12200 km^2 tract of the northern Kenya which was geologically mapped and geochemically surveyed at a reconnaissance scale in late 1984 by use of helicopter support. The sheet is bounded by latitudes 1° and 3° N and longitudes 37° and 38° E (Reconnaissance, 1987) as seen from figure 1.0.

From the reconnaissance report, Kargi is found to be covered by Basalt-capped mesas rocks. These rocks never rise more than 50 m above adjacent plain and consisting of a thin (about less than 20 m) basalt cap always overlying sedimentary rock. A monotonous sand-rich soil mantles the flat desert floor. However, there are subdued sand mounds which suggests that this area may formerly have been part of an extensive dune field.

Around Kargi reactivation of the sand is producing new dunes. These are relatively small longitudinal dunes parallel to the prevailing WNW directed winds (Reconnaissance, 1987).

Basalt from Algas, near Kargi on the western margin of the Marsabit lava, has been dated to 2.5 ± 0.3 Ma. Basalt rocks contain plagioclase feldspar which is rich in radioactive minerals. Plagioclase feldspar is a member of feldspar group originating from igneous rocks (Reconnaissance, 1987). Feldspar is from granite rocks, which are considered rich in minerals. Two main groups of feldspar are Potassium feldspar ("K-spar") and plagioclase ("plag"). Potassium (Potassic feldspar), Uranium (Uraninite, Urathorite, etc) and Thorium (Monazite, Zircon, etc) bearing minerals are traced to this rock type.

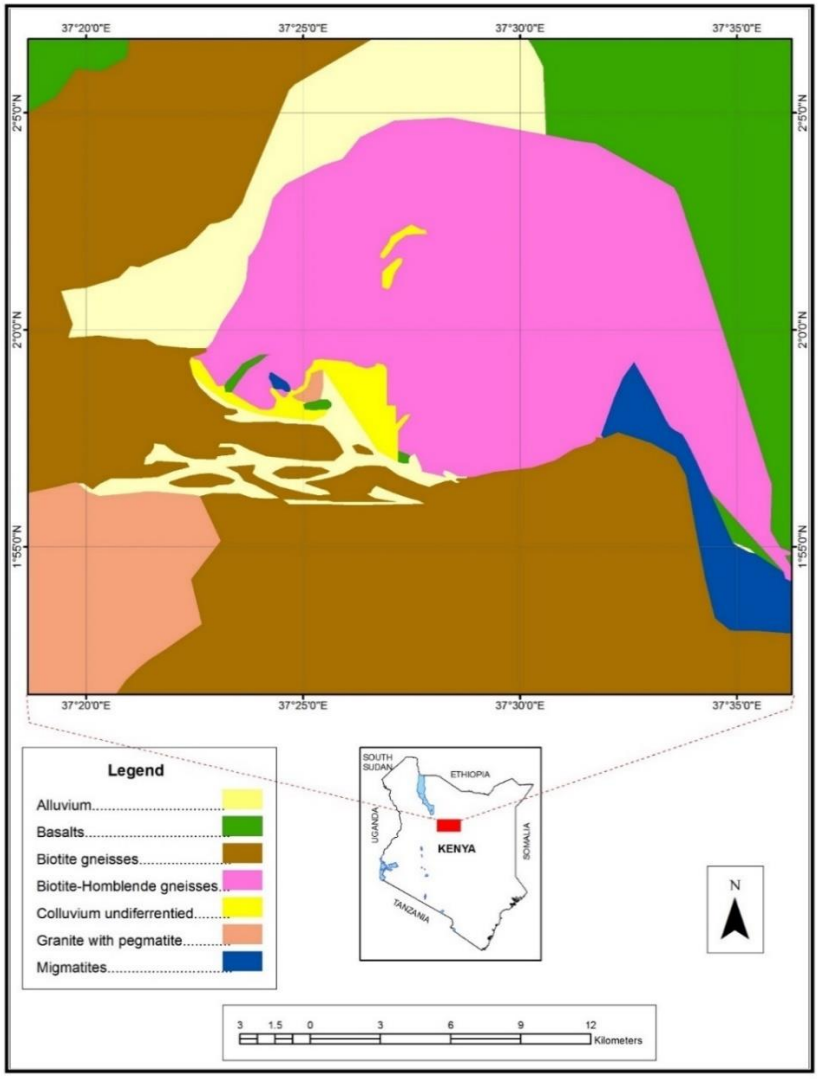

Figure 1.1: Geology Map of Kargi, Marsabit (Reconnaissance, 1987)

1.3 Problem Statement

Long-lived radioactive elements such as potassium, uranium and thorium and any of their decay products like radium and radon are examples of Naturally Occurring Radioactive Materials (NORM). NORM is considered as radioactive materials occurring naturally and from which human activities increase the exposure of people to ionizing radiation. IAEA-TECDOC-1660 reports a wide range of concentrations for activity and in a wider variety of materials. Uranium, tantalum, tin, rare earths, niobium, aluminium, copper, gold and phosphate are some ores that have been found to be linked with elevated radionuclide concentration. In his report titled “Manyattas

of death" in a story of the online Standard Newspapers of 2013, Gisesa Nyambega explains how cancer sweeps Kargi area (https://www.standardmedia.co.ke/article/2000095804/up-to-500-deadand-counting-as-mystery-cancer-devastates-marsabit). Kargi residents suspect that some toxic substances were long time buried in their land thereby causing the killer disease to the community. It is reported that exposure to naturally occurring radiation is responsible for the majority of an average person's yearly radiation dose. Therefore, there is need to carry out studies that will investigate the dose levels of such suspected high background radiation areas (HBRA) which may have health impacts on the people living and working around these areas.

1.4 Justification

We consider radiation as one of the possible cancer disease causes. However small radiation dosage can be, it is still harmful to health. Reports of abrupt animal deaths together with a number of cancer disease cases have greatly interfered with the healthy status of Kargi area. In order to make Kargi area safe for human living, it is good practice that the cause of the disease be checked and dealt with. Searching for cancer causes in this area is therefore important in order to give help to the health community on control measures of the disease and better health practices. People living as well as working around Kargi area may be exposed to high levels of background radiation without their knowledge. The impact of high concentrations of ^{40}K, ^{226}Ra and ^{232}Th may have health implications on the people living and working around this area, which could be high risk of cancer. This research was carried out in order to try and find out if radiation levels in Kargi can be a probable cause of the disease. Magnetic measurements were involved to help understand whether radiation in the area is from natural causes or from foreign bodies in the soil.

1.5 Objectives

1.5.1 Main Objective

The general objective is to investigate the human exposure level to natural sources of radiation in Kargi area within Marsabit County, Kenya.

1.5.2 Specific Objectives

i. To determine the levels of naturally occurring radionuclide ^{226}Ra, ^{232}Th and ^{40}K in soil/water samples from Kargi area.
ii. To determine the surface distribution of ionizing radiation dose in Kargi area.
iii. To carry out ground magnetic survey and interpret anomalies possibly mapping granite rocks that are rich in radionuclides.

CHAPTER TWO

LITERATURE REVIEW

2.1 Previous Studies on Terrestrial Radionuclides

Radioactive elements found in rocks, soil, water, air, and in food from the earth get to human bodies through breathing in air or eating foods which contain them. These naturally occurring radionuclides such as carbon-14, potassium-40, thorium-232, uranium-238, polonium-218 and tritium expose humans to radiation from within our bodies. Figure 2.1 gives a summary of radiation exposure sources and their respective percentages. Natural sources, including radon gas, rocks, cosmic and inside human body contribute about 82% of the total radiation source while the remaining 18% comes from human activities such as medical, nuclear medicine, consumer products and other human activity sources as can be seen from figure 2.1.

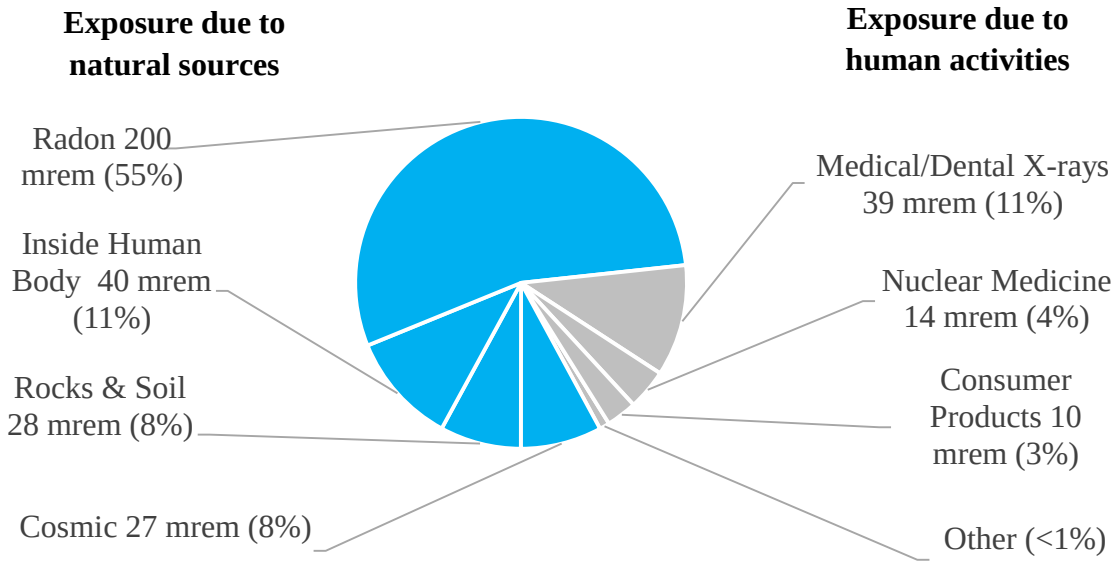

Figure 2.1: Average Annual Exposures to Ionizing Radiation (Audeen *et al.*, 2012)

Nationwide surveys have been carried out to ascertain radium equivalent activity of soil samples in many countries (Sing *et al.*, 2003; Ibrahim., 1999; Ibrahim *et al.*, 1993). To evaluate terrestrial gamma dose rate for outdoor occupation, it is of importance to estimate natural radioactivity level for geological samples, normally determined from

^{226}Ra, ^{232}Th and ^{40}K contents (UNSCEAR, 2000). The collected soil samples activity concentrations of ^{226}Ra, ^{232}Th and ^{40}K have been mainly estimated using gamma ray spectrometry, although the fission track registration technique has also been used for the analysis of uranium concentration of these samples (Sing *et al.*, 2005). They found that absorbed dose rate in air, calculated gamma dose rate from radionuclides concentration of ^{226}Ra, ^{232}Th and ^{40}K, from which they deduced that annual effective dose the inhabitants receive.

By far, the largest contributor to our daily exposure of radiation is the natural world, and the major form of natural radiation is radon gas. Radon-222 is an odorless, colorless, tasteless, chemically non-reactive gas and a naturally occurring decay product of uranium-238 commonly found in soils and rocks. As radon gas escapes from rocks and soils of which it is trapped, it enters the air we breathe and the water we drink (Okeyode and Akanni, 2009).

The daughter products of radon are present in air either as attached with the aerosols or as free atoms (unattached) Tufail *et al.,* 1992. The radon and its progeny attached to aerosols present in the ambient air constitute significant radioactive hazards to human lungs. The radon gas has a radioactive half-life of 4-days, and when radon decays, it divides the radiation part and the daughter. The daughter is a metal and can easily attach to dust and other particles in the air. It is thus easy for radon and its daughter to be carried by air currents and to become attached to aerosols, droplets, dust, or other surfaces, thus they can be inhaled and deposited in the lungs. When inhaled by human, these products irradiate lung tissues as the process of radioactive decay continues.

Although radioisotopes occur naturally in the environment, activities of humans have brought this radiation closer to us all. For example, the bricks, stones, cements and drywalls that we use for the building of our homes, schools, offices frequently contain uranium ores and are thus sources of radon. Uranium and thorium relationship can be considered as a Thorium/Uranium (Th/U) ratio. Theoretical values of the elemental ratios of Thorium/Uranium are expected to be approximately 3.0 for normal continental crust. A low or high value of Thorium/Uranium ratio as measured in studied areas may be an indication of depletion of uranium or an enrichment of

thorium due to natural processes alteration in those areas (Tzortzis and Tsertos, 2004, Al-Hamarneh and Awadallah, 2009).

Cosmic radiation, from the sun and from the outer space, varies with altitude and latitude. Cosmic rays are extremely energetic particles, primarily protons, which originate in the sun, other stars, and from violent cataclysms in the far reaches of space. At sea level, cosmic radiation is composed mainly of muons, with some gamma rays, neutrons and electrons. The exposure of an individual to cosmic rays is greater at higher elevations than at sea level. Cosmic radiation dose increases with altitude, roughly doubling every 6000 feet (Fact Sheet no. 10, 2002).

Small traces of many NORMs are present in the human body. These come mainly from naturally occurring radioactive nuclides present in the food we eat and in the air we breathe. These isotopes include tritium (^{3}H), carbon-14 (^{14}C) and potassium-40 (^{40}K). About 11% (40mrem) of our radiation dose comes from NORMs in the body. Radioactive potassium-40, as well as other radioactive materials (such as carbon-14) which occur naturally in air, water and soil are incorporated into the food we eat and then into our body tissues.

The human production of tobacco products introduces another way for us to get exposure to radiation. Smokers receive a dose of radiation from polonium-210 which is naturally present in tobacco. Smokers also receive an additional dose of radiation from the decay product of radon gas, polonium-218. Polonium-218 clings to aerosols such as tobacco smoke, and eventually winds up in the lungs. Once in the lungs, polonium decays by alpha particle emission and in the process may damage cells (EHDORP, 2006).

Although medical field does not contribute radiation on a daily basis, it has several ways of causing exposure to an individual. This exposure results from the attempt to diagnose fractures or cavities using x-rays, or to diagnose or treat cancer using injected radioisotopes. Patients are exposed to nuclear radiation in the diagnosis and treatment of cancer. Additionally, radiologists routinely use radioisotopes of technetium or thorium to diagnose heart disease (Updedegraff and Hoedl, 2013).

Depending on one's occupation, the risk of exposure can be greater than that of the average person. These higher risk occupations include underground miners, radiologists, medical technologists, nuclear plant operators, research scientists and pilots. An outdoor concentration of 47.65 pCi/L (1763.05Bq/m^3) is very high and may be hazardous to human health since it implies a Working Level (WL) of 0.48 and Working Level Month (WLM) of 9.79 using the conversions 1WL = 100 Ci/L, and 1 WLM ≡Exposure to 180 Bq/m^3 (Bochicchio *et al.*, 1995).

An average person receives a radiation dose of about 300 mrem per year from natural sources compared to a dose of about 50 mrem from produced material source of radioactive materials such as medical x-ray (UNSCEAR, 1988).

The UNSCEAR established that the world mean dose from natural radiation sources of normal area is estimated to be 2.4 $mSvy^{-1}$, while for all man-made sources including exposure, is about 0.8 $mSvy^{-1}$ (UNSCEAR, 2008).

Measurement of natural radioactivity is crucial in implementing pre-cautionary measures whenever the source is found to exceed recommended limit. (UNSCEAR, 2000) reports 400 Bq kg^{-1}, 35 Bq kg^{-1} and 30 Bq kg^{-1} as the worldwide average activity concentrations of ^{40}K, ^{226}Ra and ^{232}Th respectively. According to Aziz *et al.*, (2014), the average world acceptable excess lifetime cancer risk is 1.45×10^{-3}.

Shenber, (1996) carried out measurement of radioactivity levels in soil in Tripoli by use of low level gamma counting system consisting of a high resolution HPGe detector coupled to a 8192 channel analyzer with built in microprocessor and found concentrations of 10.5 $Bqkg^{-1}$, 9.5 $Bqkg^{-1}$ and 270 $Bqkg^{-1}$ from ^{238}U, ^{232}Th and ^{40}K respectively. The above found values were from photo peaks produced by the machine.

Activity concentrations measurement of ^{40}K, ^{232}Th, ^{226}Ra and exposure levels in Tabaka quarries, Kisii region using a germanium (HPGe) detector showed that ^{40}K had the highest activity concentration within this area. All the average values were found higher than worldwide average activity concentrations of ^{40}K, ^{226}Ra and ^{232}Th (Kinyua *et al.*, 2011).

Aguko *et al.,* (2013) carried out a research of radiation exposure levels in a gold mine in Bondo district. Their findings revealed that activity concentrations for the area was high than the world average. An excess life-time cancer risk of 0.02 % was achieved.

Nnenesi *et al.,* (2009) observed that meteorological parameters like wind speed, wind direction and relative humidity had very little or no effect on the concentration levels of radon. The study was conducted for two different locations – Midvaal water and Botshabelo community health centre within the Klerksdorp gold mining areas of the north west province of South Africa. It was concluded that the area had the highest radon concentration, build-up and exposure in Southern Africa.

Radium concentrations were also measured in other southern African countries like Swaziland. Mahlobo *et al.,* (1995) observed that the levels of concentration of radium for indoor are low during summer than in winter, due to the openings of windows for allowing ventilation. The study was conducted in different locations in Swaziland – Kwaluseni where radon concentrations were found.

Avwiri *et al.,* (2014) carried out research in Port Harcourt, River state in Nigeria to find out radiation hazard indices and excess cancer risk in water and soil from the area. Their values were below the internationally recommended values.

Concentrations of radionuclide in soil together with lifetime cancer risk due to gamma radioactivity in Kirklareli, Turkey were also investigated by Taskin *et al.,* (2009) and found that annual gamma doses and the excess lifetime risks of cancer were higher than the world's average.

In their work of evaluating excessive lifetime cancer risk in the rivers sediments of Nothern Pakistandue to natural radioactivity, found a total excess lifetime cancer risk higher than the world recommended value and attributed the numerous cancer deaths in this area to high radioactivity.

Other meteorological parameters like temperature, relative humidity and rainfall may affect the concentration of radon gas. These parameters are crucial because normally after sunrise, as temperature increases, the humidity decreases. This causes increased vertical mixing which results in lower concentration of radon and its progeny at the

ground level. As a consequence, the aerosol to which radon and its daughters are attached will be present at higher concentrations during night and in the early morning hours at ground level, which in turn increases the ionization rate in the atmosphere (Sannappa *et al.,* 1999; Debaje *et al.,* 1996; Nagaraja *et al.,* 2003). Also, solar heating during the day tends to induce some turbulence, so that radon is more readily transported upwards and away from the ground. Radon exhaled from the soil accumulates near the ground leading to gradual increase in the concentration.

2.2 Theory of Natural Radioactivity

The world is naturally radioactive, and around 90% of human radiation exposure arises from natural sources such as cosmic radiations, exposure to radon gas and terrestrial radiations. Every day, we ingest and inhale radionuclides in air, food and water.

Uranium and thorium decay to other radioactive atoms, including radium, which then decays to radon gas. Average number of radioactive decays per unit time (rate) or - change in number of radioactive nuclei present depends on number of nuclei present (N) as given by a general decay equation shown below.

$$A = -\frac{dN}{dt} \quad \text{.....1}$$

During decay of a given sample, *A* will decrease with time. Since radon is an inert (that is, chemically stable) gas, it moves from the soil, where it is produced, and into the air. The amount of uranium and radium in soil varies greatly with geographic location and soil type, thus the radiation levels appear at different levels in the soil of each region in the world (UNSCEAR, 2000).

2.2.1 Radioactivity in Minerals

Radioactivity in minerals is caused by the inclusion of NORMs in the mineral's composition. The degree of radioactivity is dependent on the concentration and isotope present in the mineral. For the most part, minerals that contain potassium (K), Uranium (U) and Thorium (Th) are radioactive.

Mineral radioactivity is due to α, β and γ radiation from the unstable isotopes in the composition. α-decay is due to the ejection of a helium nucleus (2 protons and 2 neutrons) from the parent isotope. This α-particle is accompanied by γ-radiation and

a daughter isotope which is 2 protons and 2 neutrons lighter than the parent isotope. β decay is due to the ejection of an electron from a neutron in the parent nucleus. This particle is accompanied by γ-radiation and a daughter isotope which is one proton heavier and one neutron lighter than the parent isotope. Electron capture (EC) decay is very rare and is the result of the nucleus capturing one of the atom's orbital electrons. This decay is accompanied by gamma radiation and a daughter isotope which is one neutron heavier and one proton lighter than the parent isotope. Of the three main types of radioactive decay, γ-radiation causes the most damage because it has a greater effect on biological materials and is neutralized only by heavy shielding. The next most damaging type of radiation is β-particles which are absorbed by a few feet of air. The least damaging is α-particles which have a range of 6 inches or less in air (Radioactivity in minerals. https://webmineral.com/help/Radioactivity.shtml#:~:text=This%20table%20lists%20all%20of,neutrons)%20from%20the%20parent%20isotope. Retrieved on 12th February, 2019).

2.2.1.1 NORM Decay Series

Uranium and thorium are not stable; they decay mainly by α-particle emission to nuclides that themselves are radioactive. Natural uranium is composed of three long lived isotopes, ^{238}U, a smaller proportion of ^{235}U and an even smaller proportion of ^{234}U, the decay-series daughter of ^{238}U. Natural thorium has one isotope, ^{232}Th. Each of these nuclide's decays to an unstable daughter leading, in turn, to a whole series of nuclides that terminate in one or other of the stable isotopes of lead. Under normal circumstances, in a natural material, the $^{235}U/^{238}U$ ratio will be fixed and all nuclides in each of the series will be in equilibrium.

Gamma spectrometry of materials containing these nuclides can only be effectively done with a detailed understanding of the decay chains of the nuclides involved.

i. Uranium Series

The products of decay are called radioactivity series. This series starts with the Uranium-^{238}isotope, which has a half-life of $4.5x10^{10}$ years (Henery & John, 1972, Littlefield *et al*., 1974). Since nuclides have very long half-life, this chain is still present today. The radionuclide ^{238}U decays into ^{234}Th emitting an α-particle, the newly formed nuclide is also unstable and decay further (equation 2). Finally, after total of 14 such steps, emitting 8 α-particles and 6 β-particles, accompanied by γ-

radiation, stable lead is formed. This series is said to be in secular equilibrium because all their daughters following ^{238}U have shorter half-life than the parent nuclide ^{238}U.

$$^{238}_{92}U \rightarrow ^{234}_{90}Th + ^{4}_{2}\alpha \quad \text{.....2}$$

This decay series includes ^{226}Ra which has half-lives of 1600 years and chemical properties clearly different from those of uranium. ^{226}Ra decay into ^{222}Rn which is an inert noble gas that do not form any chemical bonds and can escape into the atmosphere and attacks rapidly to aerosols and dust particles in the air deposited. The radiation emitted at the decay of these products, can cause the damage to the deep lungs.

ii. Actinium Series

It is also known as Uranium-235 series and starts with ^{235}U and by successive transformations, end up in a stable lead ^{207}Pb. It comprises 0.72% of natural uranium. Although only a small proportion of the element, its shorter half-life means that, in terms of radiations emitted, its spectrometric significance is comparable to ^{238}U. Equation 3 gives decay series equation for actinium series. The series involves 12 nuclides in 11 decay stages and the emission of 7 α-particles (ignoring a number of minor decay branches). Since its abundance is very small, it is not taken into account in the measurements.

$$^{235}_{92}U \rightarrow ^{231}_{90}Th + ^{4}_{2}He \text{ .....3}$$

Within this series, only ^{235}U itself can readily be measured, although ^{227}Th, ^{223}Ra and ^{219}Rn can be measured with more difficulty. Even though the uncertainties may be high, measurement of the daughter nuclides can provide useful support information confirming the direct ^{235}U measurement or giving insight into the disruption of the decay series.

iii. Thorium Series

Natural thorium is 100% ^{232}Th. The decay series is given by equation 4. 6 α-particles are emitted during 10 decay stages. Four nuclides can be measured easily by gamma spectrometry: ^{228}Ac, ^{212}Pb, ^{212}Bi and ^{208}Tl. The decay of ^{212}Bi is branched – only 35.94% of decay produces ^{208}Tl by α-decay. The β-decay branch produces ^{212}Po that

cannot be measured by gamma spectrometry. If a ^{208}Tl measurement is to be used to estimate the thorium activity, it must be divided by 0.3594 to correct for the branching.

$$^{232}_{90}Th \rightarrow ^{228}_{88}Ra + ^{4}_{2}He \quad \text{....} \quad (4)$$

iv. Potassium Radionuclide

^{40}K is what makes everybody radioactive and is present in body tissue. This radionuclide can be decayed by three general modes:

a. Positron emission: β+ decay is the emission of a positron from the nucleus. ^{40}K radionuclide disintegrates directly into the ground state of ^{40}Ca by the emission of β-particle of energy 1321 keV in probability of 88.8% of the decays and no γ emission is associated with this type of formation (Obid and Hamza 2011).

$$^{40}_{19}K + ^{0}_{+1}e \rightarrow ^{40}_{18}Ar \quad \text{.....} \quad (5)$$

b. K-electron capture: Occurs when one of the inner electrons in an atom is captured by the atom's nucleus. For example, potassium-40 undergoes electron capture.

$$^{40}_{19}K + ^{0}_{-1}e \rightarrow ^{40}_{18}Ar \quad \text{.....} \quad (6)$$

^{40}K nuclide can be transformed into stable state (ground state) of ^{40}Ar by two ways, in the first one, ^{40}K disintegrates directly with one jump into ground state of ^{40}Ar with sixteen hundredths of the decays go by electron capture. In the second way, ^{40}K nuclide can be decayed indirectly into the ground state of ^{40}Ar by two stages. Firstly, ^{40}K decay into the first excited state of ^{40}Ar. Secondly, the excited nuclide ^{40}Ar, decayed into ground state, accompanied by γ-radiation of 1460keV energy in probability of 11% of the ^{40}K atoms undergo this change.

c. Beta emission: β-emission, a proton will be decayed into positron and ^{40}K changed into ^{40}Ar by probability of 0.0011%.

2.2.2 Radiation Detection

Radiation can be detected using a variety of instruments and methods that read out in exposure or count rate. The measuring device used is dependent upon the type of radiation and the measurement needed. The three basic methods employed involve use of survey instruments, liquid scintillation counters and dosimetry. Some of these methods include radiation survey meter, liquid scintillation counting and gamma-ray spectrometry. Survey meters are portable radiation detection and measurement instruments used to check personnel, equipment and facilities for radioactive contamination, or to measure external or ambient ionizing radiation fields (to evaluate the direct exposure hazard). Liquid Scintillation Counting is a standard laboratory method in the life-sciences for measuring radiation from beta-emitting nuclides. Scintillating materials are also used in differently constructed "counters" in many other fields. Samples are dissolved or suspended in a "cocktail" containing an aromatic solvent and small amounts of other additives known as fluors, *i.e.*, scintillants or scintillators. Beta particles emitted from the sample transfer energy to the solvent molecules, which in turn transfer their energy to the fluors; the excited fluor molecules dissipate the energy by emitting light. In this way, each beta emission results in a pulse of light. Scintillation cocktails often contain additives that shift the wavelength of the emitted light to make it more easily detected. Gamma-ray spectrometry using hyper pure germanium (HPGe) detectors has been an essential and principal spectroscopy technique in almost all radioactivity measurements laboratories worldwide. Its major advantages are being non-destructive, multi-elements analysis, simplified regarding sample preparation, i.e. mostly no need for any chemical separation processes, and its applicability for all types of samples, etc. Low energy gamma emitters are used in many scientific studies in a wide range of applications.

2.2.3 Effects of Ionizing Radiation on Cells

Radiation may come from either an external source, such as an x-ray machine, or an internal source, such as an injected radioisotope. It is known that even a small amount of a radiation substance may produce damaging biological effects and that ingested and inhaled radiation can be a serious health risk (Rowland, 1993). The radiological impact of natural radionuclides is due to the gamma ray exposure of the body and irradiation of lung tissue from inhalation of radon and its daughters. In general,

exposure to ionizing radiation often comes from medical diagnosis and therapy application in just food, air and environmental sources.

Harm to people from radiation exposure starts with damage to cells in the body. The functions of living tissue (collection of cells) are carried out by molecules, that is, combination of different types of atoms united by chemical bonds. The proper functioning of these molecules depends upon their composition and also their structure (shape). Altering chemical bonds may change composition or structure. Ionizing radiation is powerful enough to do this, for example, a typical ionization releases six to seven times the energy needed to break the chemical bond between two carbon atoms. Of all the molecules in the body, the most crucial is the DNA (deoxyribose nucleic acid), the fundamental blueprint for all the body's structures.

2.2.3.1 Harm from Small Radiation Doses

Radiation Effects in Somatic and Germ Cells, Genetic Effects and Late Somatic Effects are some of the harms resulting from small radiation doses.

For radiation effects in somatic and germ cells, most of the cells in the body are somatic cells. Somatic cells are cells other than the germ cells. Germ cells are involved in reproduction. Skin and lung cells are examples of somatic cells and are not involved in reproduction. Small radiation doses can affect cells biologically. The effects depend on the type and amount of radiation, and include cell killing, altered genes, damaged chromosomes, and cells temporarily held (arrested) at specific places in the cell cycle called checkpoints.

Misrepair (incorrect repair) of DNA damage can lead to unstable DNA in the cell nucleus. Unstable DNA in living cells is called genomic instability. Cells that survive with genomic instability can, over time, cause big problems for people. Two such problems are Cancer – arising from genomic instability in somatic cells in the irradiated persons and Genetic effects in children – arising from genomic instability in gem cells of irradiated parents.

Another harm from small radiation doses is the genetic effect where small doses of ionizing radiation can permanently damage DNA in germ cell. One type of permanent damage is gene mutation (modification). Gene modifications may result such conditions and diseases as asthma, diabetes, anemia. Genetic changes are passed on

from one generation to another. Two specific germ cell stages are considered important in evaluating the effects of radiation on the heredity of germ cell. These are the stem (cell spermatogonia in males) and the oocytes (primarily in the immature ones, in females). Spermatogonia continue to multiply throughout the reproductive lifespan of an individual. However, oocytes are not replaced during adult life.

Late somatic effects of irradiation are those effects that occur in somatic cells years after brief exposure. Cancer is the somatic effect of most concern in radiation risk assessment. Cancer does not appear immediately after brief radiation exposure, but appears only after a delay (latent period). For humans, the latent period may be many years for some cancers, e.g. lung cancer. Other factors such as cigarette smoking can also influence the cancer risk from radiation exposure.

2.2.3.2 Harm from Large Radiation Doses

Acute and chronic harms, sometimes called harm from short-time exposure originate from large radiation dose harms. In acute type of harm, large radiation doses can destroy millions or more cells in tissues of the body. Because tissues of the body have important functions, destroying large numbers of cells in the tissue can lead to impairment of organ function, morbidity and death from organ failure. Deterministic (non-stochastic) effects of irradiation are those health effects that arise only when large numbers of cells are destroyed by radiation. These health effects usually appear within a few months after brief (short-term) exposure to large radiation doses e.g. from a nuclear weapon or nuclear accident.

For chronic exposure, deterministic effects also include radiation effects (other than cancer and genetic effects) that continue to occur after an extended period e.g. years of chronic (long-term) exposure. Such chronic exposure can arise from long-lived radionuclides ingested via contaminated food or inhaled via contaminated air.

2.2.4 Gamma Ray Production and Detection

Gamma rays are often produced alongside other forms of radiation such as α and β-particles. When a nucleus emits an α-particle or β-particle, the daughter nucleus is sometimes left in an excited state. It can then jump down to a lower energy state by emitting a gamma ray as illustrated in Figure 2.2, in much the same way that an atomic electron can jump to a lower energy state by emitting infrared, visible, or ultraviolet

light. Detecting the produced gamma-rays can be done using detectors. For detection, the kinds of detectors commonly used can be categorized as gas-filled detectors, scintillation detectors and semiconductor detectors. The choice of a particular detector type for an application depends upon the gamma energy range of interest and the application's resolution and efficiency requirements. Additional considerations include count rate performance, the suitability of the detector for timing experiments, and of course, the price.

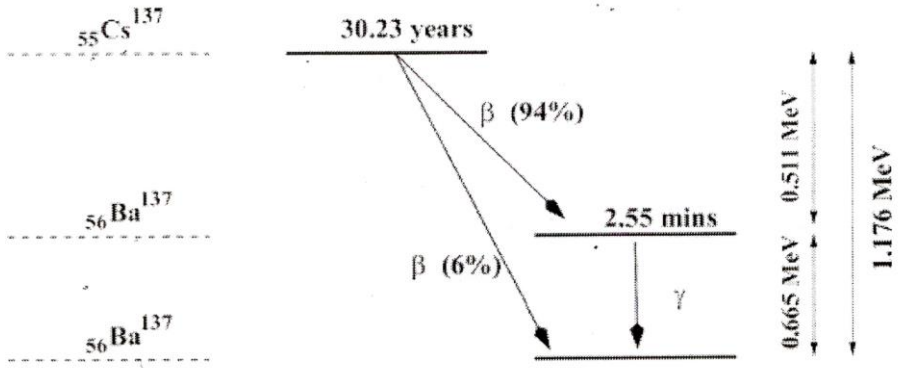

Figure 2.2: Illustration of a Decay Scheme of ^{137}Cs (Helmut F., 2003)

Gamma rays, x-rays, visible light and radio waves are all forms of electromagnetic radiation. The difference is the frequency and hence the energy of the photons. Gamma rays are the most energetic.

2.2.5 Interactions of Gamma Radiation with Detector Crystal

Gamma-ray detection is based on the effect of a γ-ray interacting with matter. There are three important types of interaction of a γ-ray with matter. These are called:

i. The Photoelectric Effect

Figure 2.3 (a) shows how photoelectric process occurs. In this process, the γ- or X-ray gives all of its energy to the recoil electron. As a result, the recoil electrons ejected from the shell of atoms and hence produces the electron-hole pairs in the detector that yield the output pulse. This output pulse from the detector is proportional to the energy of the γ-ray or X-ray that made the interaction. In the spectrum, these events will show up as full-energy photo-peaks.

The Photo electric effect is significant for the incident gamma energy of 0-150 keV**.**

ii. The Compton Effect

The Compton Effect too contributes strongly to full energy peak by multiple Compton scattering under the condition that the last interaction is a photoelectric one and that all the preceding Compton interactions take place in the Ge crystal. This is shown in figure 2.3 (b). In large-volume detectors the probability of multiple Compton scattering increases. If the last interaction does not occur by the photoelectric effect or if one of the multiple Compton interactions takes place outside the sensitive volume of the detector, the pulse will contribute to the Compton continuum.

The Compton cross section is the dominant one for all energies except the very lowest ($E_\gamma \leq$ 150 keV) and the very highest (E_γ=8.5 MeV).

iii. The Pair-Production

The pair-production process can also provide a total absorption of the γ-ray energy. Figure 2.3 (c) illustrates the pair-production process. The gamma enters in the detector and creates an electron-positron pair. From the law of conservation of mass and energy, it follows that the initial gamma must have energy of at least 1.02 MeV because it takes that much energy to create both the negative and positive electrons.

The characteristics of these effects are important in detector design *(*Miglierini, 2004). The primary γ-ray interactions are as shown in figure 2.3 (a), (b) and (c).

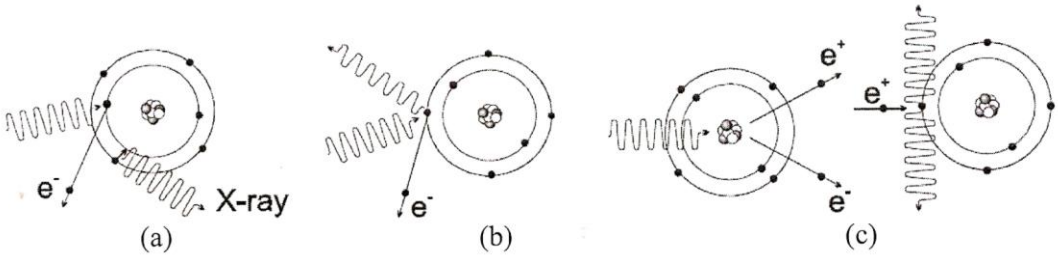

Figure 2.3: Primary γ-Ray Interactions: (a). Photoelectric Effect (b). Compton Scattering (c). Pair Production and Annihilation *(*Miglierini, 2004)

2.2.6 Gamma-Ray Spectrometry

Gamma-ray spectrometry using hyper pure germanium (HpGe) detectors has been an essential and principal spectroscopy technique in almost all radioactivity measurements laboratories worldwide. Its major advantages are being non-destructive, multi-elements analysis, simplified regarding sample preparation, i.e. mostly no need for any chemical separation processes, and its applicability for all types of samples, etc. Low energy gamma emitters are used in many scientific studies in a wide range of applications. The precise determination of the activity concentration of each radionuclide requires the determination of full energy efficiency calibration for a given geometry. Therefore, a detection efficiency curve, known as efficiency calibration, over the energy region of interest must be established precisely in advance. The detection efficiency at certain gamma-ray energy and sample geometry is given by;

$$\varepsilon(E,n) = \frac{C(E,n)}{t.f(E,n).A} \quad \ldots\ldots\ldots\ldots\ldots\ldots\ldots\ldots\ldots\ldots\ldots\ldots\ldots\ldots\ldots\ldots\ldots\ldots\ldots\ldots\ldots\ldots\ldots\ldots 7$$

Where:

C(E,n): net photo-peak count of gamma-ray transition with energy E of radionuclide n, f(E,n) : branching ratio, number of photon with energy E per hundred disintegration of radionuclide n,

Gamma-ray photons are known to be attenuated through the material according to the following relation;

$$I = I_o.e^{(\mu_m.x)} \quad \ldots\ldots\ldots\ldots\ldots\ldots\ldots\ldots\ldots\ldots\ldots\ldots\ldots\ldots\ldots\ldots 8$$

Where:

I_o: the photons, with energy E, intensity without attenuation,

I: the photons, with energy E, intensity after attenuation,

μ: the linear attenuation coefficient, cm^{-1},

μ_m: the mass attenuation coefficient, $\mu_m = \mu/\rho$, cm^{-2}/g,

x: the sample thickness (or effective thickness)

Germanium detectors are considered semiconductor diodes with a p-i-n structure from which the intrinsic region (I) is sensitive to ionizing radiation, more so x-rays and gamma rays. Under reverse bias, an electric field extends across intrinsic or depleted region. Photons interaction with the material within the depleted volume of a detector produces charge carriers, holes and electrons, and are swept by the electric field to the P and N electrodes. This charge, which is in proportion to the energy deposited in the detector by the incoming photon, is converted to a voltage pulse by an integral charge sensitive pre-amplifier. Germanium detectors must be cooled in order to reduce the thermal generation of charge carriers (hence reverse leakage current) to an acceptable level because germanium has relatively low band gap. The common cooling medium for such germanium detectors are liquid nitrogen with a temperature 77 K. Otherwise, leakage current induced noise destroys the energy resolution of the detector. Germanium detector is mounted in a vacuum chamber attached to or inserted into an LN_2 Dewar. The sensitive detector surfaces are protected from moisture and condensable contaminants (John & Paolo, 1970).

2.2.7 Radiological Parameters

These include Radium equivalent activity, absorbed gamma dose rate, Annual effective dose rate, Annual Gonadal Equivalent Dose, etc.

2.2.7.1 Radium Equivalent Activity (Ra_{eq})

Radium equivalent (Ra_{eq}) activity is a representation of a weighted sum of activities of ^{238}U, ^{232}Th and ^{40}K. Its estimation is on the fact that 1 Bq $kg^{-1}$of ^{238}U, 0.7 Bq kg^{-1}

of ^{232}Th and 13 Bq kg^{-1} of ^{40}K produce the same radiation dose rates. Avwiri *et al.*, 2013 estimates radium equivalent activity as:

$$Ra_{eq}(Bqkg^{1}) = C_U + 143C_{Th} + 0.077C_K \quad \ldots\ldots 9$$

Where,

C_U, $143C_{Th}$ and $0.077C_K$ are the activity concentrations in Bqkg^{-1} or Bql^{-1} of ^{238}U, ^{232}Th and ^{40}K.

All the Ra_{eq} values should be below the international accepted value of 370 Bqkg^{-1}.

2.2.7.2 Absorbed Gamma Dose Rate (D)

Absorbed dose rates (D), due to gamma radiations in air as measured 1 m above ground surface for uniform distribution of naturally occurring radionuclides (^{40}K, ^{232}Th, and ^{226}Ra) was computed as per guidelines provided by UNSCEAR 2000. Assuming that contributions from other naturally occurring radionuclides to be insignificant, then D can be calculated from:

$$D\left(nGyh^{-1}\right) = \left(0.467C_{Ra} + 0.662C_{Th} + 0.043C_K\right) \quad \ldots\ldots 10$$

Where,

C_{Ra}, C_{Th} and C_k are respectively average activity concentrations of radium, thorium and potassium in the sample and nGyh^{-1} (nano Gray per hour) is the unit of the absorbed dose rates (D).

2.2.7.3 Annual Effective Dose Rate (De)

Effective dose in radiation protection and radiology is a measure of the cancer risk to a whole organism due to ionizing radiation delivered non-uniformly to part(s) of its body. It is a calculated value, measured in mSv, that takes three factors into account:

i. The absorbed dose to all organs of the body.
ii. The relative harm level of the radiation, and
iii. The sensitivities of each organ to radiation.

The quantity of effective dose helps us to take into account sensitivity. Different body parts have different sensitivities to radiation e.g. the head is less sensitive than the chest.

To estimate the annual effective dose rates, the conversion coefficient from absorbed dose in air to effective dose (0.7 $Sv.Gy^{-1}$) and outdoor occupancy factor (0.2) proposed by UNSCEAR 2000 are used. In Kenya, the average of time spent indoor and outdoor (occupancy factors) are 0.6 and 0.4 respectively (Mustapha, 1999). The world average indoor and outdoor occupancy factors are 0.8 and 0.2 respectively (UNSCEAR, 2000). Therefore, the effective dose rate in units of $mSvy^{-1}$ was estimated using the formula (Mustapha, 1999).

$$De(mSv.y^{-1}) = D\left(nGyh^{-1}\right) \times 8760h.y^{-1} \times 0.4 \times 0.7\, Sv.Gy^{-1} \times 10^{-6} \ldots 11$$

Where,

De is $Effective\ dose\ rate$, D is the dose rate, $mSvy^{-1}$ (millisieverts per year) is the unit for annual effective dose rate (De), $nGyh^{-1}$ (nano Gray per hour) is the unit of the absorbed dose rates (D), hyr^{-1} (hour per year) given by 24 hours (in a day) X 365days (in a year)

For water,

Annual effective doses were computed according to equation 12. (EPA, 1999; Meltem and Gursel, 2010).

$$DR_W = A_W \times IR_W \times ID_F \ldots\ldots\ldots\ldots\ldots\ldots\ldots\ldots\ldots\ldots\ldots\ldots\ldots\ldots\ldots\ldots\ldots\ldots 12$$

Where,

DR_W = effective dose ($mSvyr^{-1}$), A_W = activity (Bql^{-1}), IR_W = water intake per person, in a year, and ID_F = conversion factor for effective dose equivalent ($mSvBql^{-1}$).

(WHO, 2008) estimates dose consumption rates for infants, children and adults as 0.5, 1.0 and 2.0 ld^{-1} respectively. Conversion factors for ^{226}Ra, ^{232}Th and ^{40}K for infants, children and adults are 1.4×10^{-7}, 1.6×10^{-6} and 5.2×10^{-8}

$SvBq^{-1}$, 6.8 × 10^{-8}, 2.9 × 10^{-7} and 1.3 × 10^{-8} $SvBq^{-1}$, 4.5 × 10^{-8}, 2.3 × 10^{-7} and 6.2 × 10^{-9} $SvBq^{-1}$ respectively (ICRP, 2012).

2.2.7.4 Annual Gonadal Equivalent Dose (AGED)

UNCEAR (2000) considers bone surface cells, bone marrow and gonads as organs of interest because of their sensitivity to radiation. A fatal disease of the blood known as leukemia is caused by destruction of red blood cells due to an increase in AGED which has been known to affect the bone marrow. AGED for the resident using such material for building may be evaluated by the following equation (Avwiri *et al.*, 2012):

$$AGED(\mu Svy^{-1})C = 3.09C_U + 4.18C_{Th} + 0.314C_K \quad \text{.....13}$$

Potential carcinogenic effects that are characterized by estimating the probability of cancer incidence in a population of individuals for a specific lifetime from projected intakes and exposures is called Excess Lifetime Cancer Risk (ELCR). Taskin *et al.*, 2009 calculates ELCR as:

$$ELCR = AEDE \times DL \times RF \quad \text{.....14}$$

For stachostic effect(s), RF of 0.5 for public is used by ICRP (Taskin *et al.*, 2009).

2.2.8 Hazard Indices

2.2.8.1 Hazard Indices for External Gamma Radiation (H_{ex} and I_γ)

It is important to assess the gamma radiation hazards to humans associated with soils used for buildings. A widely used hazard index, reflecting the external exposure, called the external hazard index, H_{ex}, is defined in equation 15. This index is used to evaluate the indoor radiation dose rate due to the external exposure to gamma radiation from the natural radionuclides in the construction building materials of dwellings. For assessment of excess gamma radiation from building materials to ensure of safety of building materials, two indices were used. A hazard index for the external gamma radiation dose from building materials is as given below (Berekta and Mathew, 1985, Raghu *et al.*, 2017).

$$H_{ex} = \frac{A_{Ra}}{370\ Bq\ kg^{-1}} + \frac{A_{Th}}{259\ Bq\ kg^{-1}} + \frac{A_K}{4810\ Bq\ kg^{-1}} \quad \text{.....15}$$

The value of H_{ex} should be below 1 to ensure the safe use of building materials, which corresponds to the upper limit of Ra_{eq} (370 $Bqkg^{-1}$). The European Commission (EC) proposed an index (I_γ) to verify whether the guidelines of EC for building material usage are met.

$$I_\gamma = \frac{A_{Ra}}{300} + \frac{A_{Th}}{200} + \frac{A_K}{3000} \leq 1 \quad \text{.....16}$$

The European Commission (EC) introduced a two-dose criteria for gamma dose of building materials:

i. an exception criterion of 0.3 $mSvy^{-1}$ and
ii. an upper limit of 1 $mSvy^{-1}$.

Many countries apply their control on the upper limit (1 $mSvy^{-1}$). If exemption level of 0.3 $mSvy^{-1}$ is taken into consideration, then I_γ values should be below 0.5 for materials used in large quantities (i.e. cement and brick); however, considering upper level of 1 $mSvy^{-1}$, then I_γ values of should be below unity for such materials. For building materials considered as superficial with restricted use (tiles and board), I_γ value should be below 2 and 6, supposing that control values of 0.3 and 1 mSv y^{-1}, respectively.

2.2.8.2 Hazard Indices for Internal Alpha Radiation (H_{in} and I_α)

In addition to external hazard index, radon and its short-lived products are also hazardous to the respiratory organs. The assessment of excess α-radiation due to radon gas from the building materials can be calculated by some indices. Two indices, called the internal hazard index (H_{in}) and the alpha index (I_α), were studied. The internal exposure to radon and its daughter products is quantified by the internal hazard index, H_{in}, which is given by the equation 17. H_{in} can be used for considering the excess internal radiation due to inhalation of ^{222}Rn and its short lived decay products from building materials, (Raghu *et al*., 2017) which is defined as.

$$H_{in} = \frac{A_{Ra}}{185\ Bq\ kg^{-1}} + \frac{A_{Th}}{259\ Bq\ kg^{-1}} + \frac{A_K}{4810\ Bq\ kg^{-1}} \quad \text{.....17}$$

For safe use of materials in the construction of buildings, this quantity should be less than one.

For radiation hazard indices to be negligible, the (H_{ex}, H_{in}) indices values must be less than one (Harb *et al.,* 2010).

The quantity I_{α} is given by:

$$I_{\alpha} = \frac{A_{Ra}}{200} \leq 0.5 \quad \text{.....18}$$

The recommended values of $I_{\alpha}$and I_{γ} are below 0.5 and 1, respectively (Raghu *et al*., 2017).

2.2.9 Elemental Concentration of ^{238}U, ^{232}Th and ^{40}K

According to Avwiri *et al*., 2014 and IAEA Technical Report No. 1363, the elemental concentrations of Uranium-238 (ppm), Thorium-232 (ppm) and potassium (%) can be computed from measured activity concentrations of ^{238}U, ^{232}Th and ^{40}K in Bq kg^{-1} using the following conversion factors:

For K, 1 % K ≡ 313 Bq kg^{-1} of ^{40}K

For U, 1 ppm U ≡ 12.35 Bq kg^{-1} of ^{238}U

For Th, 1 ppm Th ≡ 4.06 Bq kg^{-1} of ^{232}Th

2.2.10 Health Effects of Gamma Rays

Gamma radiation, also known as gamma rays refers to electromagnetic radiation of high frequency and therefore high energy per photon. Gamma rays are ionizing radiation, and are thus biologically hazardous. They are classically produced by the decay from high energy states of atomic nuclei (gamma decay), but are also created by other processes.

All ionizing radiation causes similar damage at a cellular level, but because rays of alpha particles and beta particles are relatively non-penetrating, external exposure to them causes only localized damage, e.g. radiation burns to the skin. Gamma rays and neutrons are more penetrating, causing diffuse damage throughout the body (e.g. radiation sickness, cell's DNA damage, cell death due to damaged DNA, increasing incidence of cancer) rather than burns. External radiation exposure should also be distinguished from internal exposure, due to ingested or inhaled radioactive

substances, which, depending on the substance's chemical nature, can produce both diffuse and localized internal damage. The most biological damaging forms of gamma radiation occur in the gamma ray window, between 3 and 10 MeV.

Gamma radiation is often used to kill living organisms, in a process called irradiation. Applications of this include sterilizing medical equipment (as an alternative to autoclaves or chemical means), removing decay-causing bacteria from many foods or preventing fruit and vegetables from sprouting to maintain freshness and flavor.

Despite their cancer-causing properties, gamma rays are also used to treat some types of cancer, since the rays kill cancer cells also. In the procedure called gamma-knife surgery, multiple concentrated beams of gamma rays are directed on the growth in order to kill the cancerous cells. The beams are aimed from different angles to concentrate the radiation on the growth while minimizing damage to surrounding tissues.

Gamma rays are also used for diagnostic purposes in nuclear medicine in imaging techniques. A number of different gamma-emitting radioisotopes are used. For example, in a PET scan a radiolabeled sugar called fludeoxyglucose emits positrons that are converted to pairs of gamma rays that localize cancer (which often takes up more sugar than other surrounding tissues). The most common gamma emitter used in medical applications is the nuclear isomer technetium-99 m which emits gamma rays in the same energy range as diagnostic X-rays. When this radionuclide tracer is administered to a patient, a gamma camera can be used to form an image of the radioisotope's distribution by detecting the gamma radiation emitted. Depending on what molecule has been labeled with the tracer, such techniques can be employed to diagnose a wide range of conditions e.g. the spread of cancer to the bones in a bone scan.

2.3 Theory of Magnetic Method

The magnetic field of the earth originates from its core all the way to space, where a flow of charged particles coming out of the sun exist (Lowrie, 2007). Magnetic anomalies caused by an underlying resource within the Earth’s sub-surface are

obtained during magnetic survey. Bodies found within the earth's sub-surface give rise to magnetic anomalies because of their effects on the geomagnetic field. By putting in corrections to the noticed magnetic values, we obtain magnetic anomalies. A freely swaying material of magnetic in nature tends to rest towards ambient geomagnetic field direction at some place on the surface of the earth, usually at some vertical angle and geographic north. The geomagnetic elements as seen in figure 2.4 are usually used to depict magnetic field vector (Kearey *et al*., 2002).

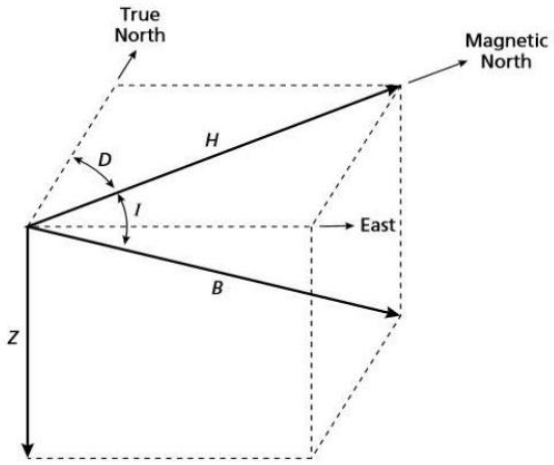

Figure 2.4: Geomagnetic Elements

Where,

B is total geomagnetic field, Z is vertical geomagnetic component, H is horizontal geomagnetic element, I is the dip of B and D as horizontal angle between geographic and magnetic north.

Vector B, considered the total geomagnetic field has geomagnetic component Z and geomagnetic component H in vertical and horizontal axes respectively in the direction of magnetic north. The field inclination I and declination D are respectively considered the dip of B and the horizontal angle between geographic and magnetic north (Kearey et al., 2002). Below expression gives the force between two magnetic poles.

$$F = \frac{m_1 m_2}{4\pi\mu r^2} m \quad \text{.....19}$$

Where μ is the magnetic permeability of the medium separating the poles, m_1 and m_2 are the pole strengths and r is the distance parting the poles.

The magnetic flux density B is as given in equation 20 (Parasnis, 1986).

$$B = kH \quad \ldots\ldots 20$$

Where k and H are the magnetic susceptibility and the magnetizing force respectively. Magnetic susceptibility, a parameter used in interpreting magnetic data is the ease in which materials within the earth's crust get magnetized by the earth's magnetic field (Parasnis, 1986).

2.3.1 Magnetics Surveying

The magnitude as well as orientation of the earth's magnetic field is measured by magnetics survey. Magnetic field at Earth's surface relies on generated field in earth's core, surface materials' magnetic mineral content together with remnant magnetisation of surface rocks. A physical parameter, magnetic susceptibility, κ, is that parameter to which magnetic surveys are sensitive.

Applications of magnetic surveying include some of the following:

i. Metal objects' location including pipes, cables, military ordnance.
ii. Near-surface mapping e.g. archeological sites, hidden mine shafts, igneous intrusions.
iii. Mineral exploration to help identify metalliferous deposits, e.g. massive sulphides
iv. Mapping of Geological Bedrock to identify faults together with geological boundaries, especially underneath sediment cover.

2.3.1.1 Geomagnetic Field

A field will exist if an object placed in that field experiences a force. Total Magnetic Field, B represents the summation of the magnetising field strength and the magnetisation of the medium. Magnetic fields in Geophysics are small and measured in nano-teslas (nT). earth's magnetic field tends to vary between 20,000 to 60,000 nT.

Two types of magnetisation are:

i. Induced magnetisation which is generated within a rock in response to an applied external magnetic field.
ii. Remnant or permanent magnetisation where a field may exist within rock even in absence of external field because of permanent magnetic particles.

Interpretation of magnetic data is complicated as magnetic field due to a subsurface body result from combined effect of two vector magnetisations that may have different magnitudes and directions.

For magnetic susceptibilities of rocks and minerals, rocks with significant concentrations of ferri/ferro-magnetic minerals have highest susceptibilities as given table 1.1.

Table 2.1: Magnetic Susceptibilities of Rocks and Minerals

Type of rock	susceptibility range	susceptibility ranking
Ultramafic	95,000 – 200,000	highest
Mafic	550 – 122,000	high
Felsic	40 – 52,000	low
Metamorphic	0 – 73,000	low
Sedimentary	0 – 36,000	very low

Source (Abdelhady, 2020)

2.3.1.2 Earth's Magnetic Field

The earth's surface position intersected by the dipole axis that best fits the magnetic field of the earth is called Geomagnetic Pole while the position where the magnetic field is vertical is Magnetic Pole or Dip Pole. Geomagnetic and Magnetic Poles slightly diverge because earth's magnetic field is not quite a dipole.

Geomagnetic field can be represented mathematically, and international standard is called International Geomagnetic Reference Field (IGRF). It is noted that IGRF excludes effects of near-surface rocks. Total field recalculation is done every 5 years because of secular variation with epoch being the year of calculation.

The difference between International Geomagnetic Reference Field (IGRF) and the diurnal corrected value gives geomagnetic correction and is applied to obtain the magnetic anomaly as expressed in equation 21. (Lowrie, 2007). Magnetic anomaly is

because of variations in the magnetic content of the underlying rocks within the earth's subsurface.

$$Magnetic\ anomaly\ =\ Diurnal\ corrected\ value\ -\ Geomagnetic\ correction \quad ...21$$

2.3.1.3 Variations in Earth's Magnetic Field

This includes changes in the magnetic field of the earth and can be caused by the following:

i. Geomagnetic Reversals: Earth's magnetic field rolls over polarity unpredictably on geological time scale owing to sudden changes in fluid motions in core.
    a. Secular Variations which could be due to: Observations of Earth's magnetic field made over 400 years show a gradual change in position of the magnetic pole.
    b. Owing to slow movement of eddy currents in Earth's core.

ii. Diurnal Variations due to

    a. Changes are smooth and average around 50 nT.
    b. Daily changes in field owing to changes in currents of charged particles in ionosphere.

Diurnal corrections take consideration the effect of everyday variation in the Earth's geomagnetic field. It comes from the discrepancies in the geomagnetic field strength during the field collection of magnetic data. These discrepancies occur because of the ionosphere as well as solar wind interactions, considered a constant stream of ionized gas with a frail magnetic field (Lowrie, 2007). This correction is done by:

a. having one magnetometer stationed at the base station throughout the data collection day. This is suitable if one has two magnetometers.
b. by recording time and magnetometer readings at the base station and occasionally returning to the base station and taking and recording time

and magnetometer readings. This process is repeated until each data collection day ends.

These values ascertain diurnal correction by assessing the difference between the magnetic readings at a given time together with the day's first reading (Kearey *et al*., 2002). To correct a station's diurnal variation, the reading time is used to record the corresponding diurnal correction and then subtracted from the observed station magnetic reading and is expressed as in equation 22.

$$Corrected\ value = Observed\ value - Diurnal\ correction \ldots\ldots\ldots 22$$

iii. Magnetic Storms:

a. Disturbances in magnetic field, considered short term are associated with sun spot activity together with streams of charged particles from sun.
b. May go up to 1000 nT in magnitude, making magnetic surveying impossible.

2.3.1.4 Magnetic Field Measurements

Magnetometers measure the total magnetic field F_T or the horizontal and/or vertical components of magnetic field, F_H and F_Z respectively. A number of magnetometers exist and use different principles in carrying out measurements. A Proton Precession Magnetometer was used. It uses sensor consisting of bottle 15 cm long, of proton-rich liquid, usually kerosene or water, with wire coil wrapped, reduced measurement accuracy in areas of high magnetic field gradient. Unlike fluxgate, it measures total field strength, so instrument orientation not important.

2.3.2 Instrumentation

Different instruments were used during the research work. A hoe was used for soil digging during soil sample collection, a proton precession magnetometer, model G-856 was used for magnetic field measurements, GPS was used to locate station coordinates for soil and magnetic field stations, measurements method of gamma spectrometry employing a high purity germanium (HPGe) detector was employed

basically to evaluate the radiological hazard of radioactivities. Surfer 10 and Geosoft^{R} Oasis Montaj software were used to process magnetic data. A hand-held radiation, Wilnos type of model X5Cplus survey meter was used for background radiation measurements.

2.3.2.1 Semiconductor Detectors

A material that can act as a conductor or as an insulator is referred to as a semiconductor. “Solid state” term in electronics is often used interchangeably with semiconductor, but can obviously be applied to solid scintillators in the detector field. Therefore, semiconductor is the favorable term for those detectors assembled from either compound or elemental single crystal materials with a band gap in the range of roughly 1 to 5eV. Germanium together with Silicon are by far the most widely-used semiconductors in group IV elements with band gaps of 1.12 and 0.74eV respectively.

Semiconductor detectors have a P-I-N diode structure in which the intrinsic (I) region is created by depletion of charge carriers when a reverse bias is applied across the diode. When photons interact in the depletion region, charge carriers (holes and electrons) are freed and are swept away to their respective collecting electrode by the electric field. The resultant charge is integrated by a charge sensitive preamplifier and converted to a voltage pulse with amplitude proportional to the original photon energy. Since the depletion depth is inversely proportional to net electrical impurity concentration, and since counting efficiency is also dependent on the purity of the material, large volumes of very pure material are needed to ensure high counting efficiency for high energy photons.

The band gaps signify the temperature sensitivity of the materials and practical ways in which these materials can be put to use as detectors. Just as transistors of GE origin have much lower maximum operating temperatures than Si devices, so are Ge detectors. Practically, both Si together with Ge detectors must be cooled so as to reduce the thermal charge carrier production (noise) to some allowable level.

The most common medium method for detector cooling is liquid nitrogen (LN_2). In these detectors, the detector element (and in some cases pre-amplifier components), are housed in a clean vacuum chamber which is attached to or inserted in a LN_2 Dewar.

The detector is in thermal contact with the liquid nitrogen which makes it cools to around 77 K or 200 °C. At these temperatures, reverse leakage currents are in the range of 10^{-9} to 10^{-12} amperes. Figure 2.5 gives a cross-sectional view of a typical liquid nitrogen cryostat.

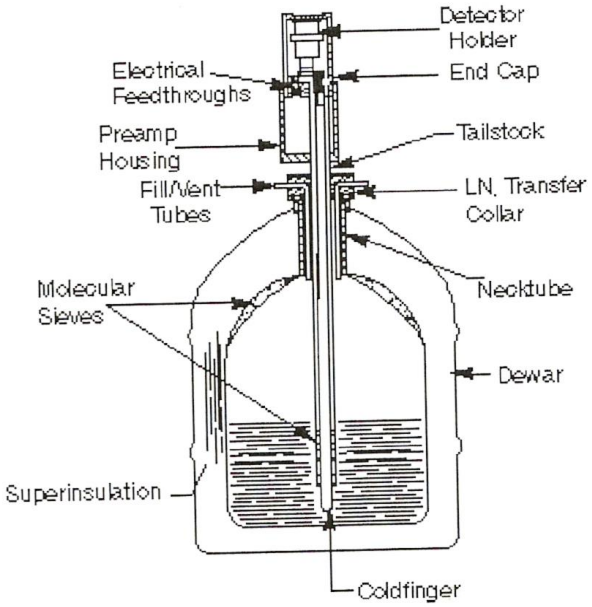

Figure 2.5: Germanium Detectors in Liquid Nitrogen Dewars (Canberra, 2013)

A typical HPGe detector-based gamma spectroscopy system consists of a high voltage power supply, HPGe detector, pre-amplifier (usually supplied differently as part of the detector), amplifier, analog-to-digital (ADC) and multichannel analyzer (MCA). Figure 2.6 illustrates a simplified system of gamma spectroscopy.

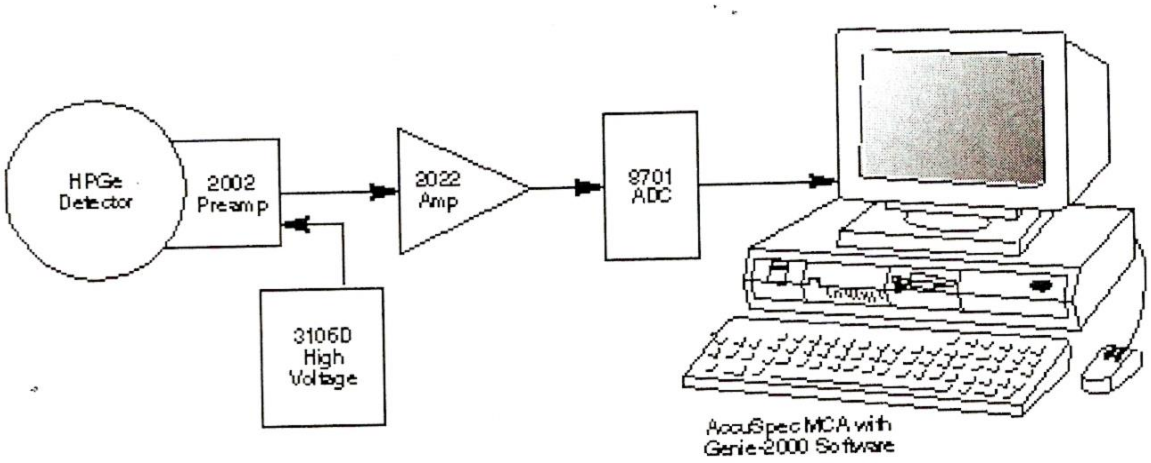

Figure 2.6: HPGe Detector and MCA (Canberra, 2013)

The HPGe detector should be positioned in the shelter of the shield so as to minimize scatter from the walls. In this position, the shield must accommodate the largest sample that is anticipated.

The precise determination of the activity concentration of each radionuclide requires the determination of full energy efficiency calibration for a given geometry. Therefore, a detection efficiency curve, also called efficiency calibration, over the energy region of interest must be precisely confirmed in advance. The detection efficiency at certain gamma-ray energy together with sample geometry is given by equation 7. Gamma-ray photons are known to be attenuated through the material according to equation 8.

Detector Resolution

Resolution is a measure of the width (full width half maximum) of a single energy peak at a specific energy, either expressed in absolute keV (as with Germanium Detectors), or as a percentage of the energy at that point (Sodium Iodide Detectors). HPGe detector resolutions at 1332 keV usually ranges between 1.6 - 2.0 keV. ^{137}Cs and ^{60}Co sources are usually used in spectrum energy peak calibration. By acquiring spectrum from these two sources with atleast 10000 counts in the full energy peak, energy resolutions of 662 keV from ^{137}Cs and 1173 keV and 1332 keV from ^{60}Co are achieved and used in spectrum peak calibration. Generally, the superior resolution of

a HPGe detector is sufficient enough to avoid problem of peak convolution, (i.e. all peaks are separate and distinct) as witnessed with the NaI(TI) spectrum.

Detector Efficiency

This is a measure is a measure of the number of pulses occurring for a given number of gamma rays. Clearly, to be useful, the detector must be capable of absorbing a large fraction of the gamma ray energy. Various kinds of efficiency definitions are in common use for gamma ray detectors:

i. **Absolute Efficiency:** Ratio of the number of detectors produced counts to the number of gamma rays emitted by the source in (all directions).
ii. **Intrinsic Efficiency:** Ratio of the number of detector pulses to the number of gamma rays striking the detector.
iii. **Relative Efficiency:** Efficiency of one detector relative to another; commonly that of a germanium detector relative to a 3inches diameter by 3 inches long NaI crystal, each at 25cm from a point of source, and specified at 1.33 MeV only.
iv. **Full-Energy Peak (or Photopeak) Efficiency:** The efficiency for producing full-energy peak pulses only, rather than a pulse of any size for the gamma ray.

2.3.2.2 Proton Precession Magnetometer

This type of magnetometer measures the size of the Earth's magnetic field and bases its work on a sensor that contains hydrogen atoms like kerosene and water covered in a coil, as shown in figure 2.7. The protons within the hydrogen atom's function have small dipoles and appear parallel to the ambient geomagnetic field B_e figure 2.7 (b). A current is passed through the coil figure 2.7 (a) to generate a magnetic field B_p figure 2.7 (c) should be $50 - 100$ times larger than the geomagnetic field and in a different direction, causing the protons to realign in this new direction. The current to the coil is then cut to remove the polarizing field very fast. The protons return to their original alignment with Be by spiraling figure 2.7 (d) in phase around this direction with about 0.5 ms, taking one to three seconds to achieve their original orientation (Kearey *et al*., 2002).

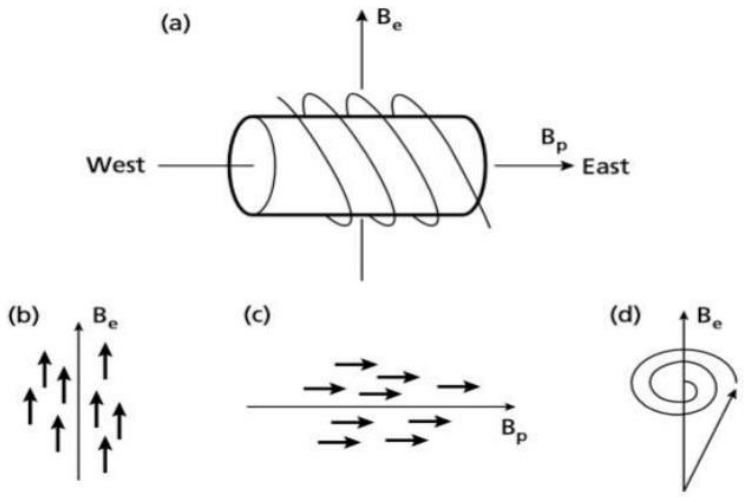

Figure 2.7: Proton Precession Magnetometer

Kearey *et al.*, 2002 gives the formula for the frequency f of this spiralling as in the expression equation 23.

$$f = \frac{\gamma_p B_e}{2\pi} \quad \text{.....23}$$

Where γ_p is a constant accurate value representing the proton's gyromagnetic ration. The value of f, around 2 kHz, is acquired by taking measurement of the alternating voltage of similar frequency prompted to flow in the coil by precessing protons. As a result, the correct measuring of the magnetic field is given by f (Kearey *et al.*, 2002). 0.1 nT is the accuracy to which the total field's strength can be measured. The cylindrical sensor is affected by speedy changes measuring over 600 nT/m in the magnetic field resulting in low value readings (Telford *et al.*, 1990). This tends to happen when the sensor is positioned near a magnetic material.

2.3.3 Euler Deconvolution

Euler's method furnishes depth and location estimates of anomaly sources within the earth's sub-surface, unearths the causative body and finds out its depth from the observation level as well as generating a map that manifests the depths and positions of the perceived gravity anomaly sources. No geologic model is adopted by this method, thus the method can be put in for the interpretation of gridded gravity together

with data from magnetic source even when the geology of the area under study cannot be represented by a specific model such as a prism (Nyakundi *et al.,* 2017; Pawan *et al.,* 2007).

2.3.3.1 Theory of Euler Deconvolution

Euler deconvolution is considered a probable field data analysis technique for approximating position and depth of a causative body (Hong *et al*., 2017). The technique blends the probable field together with its gradient components to unearth the probable anomalous source, with the strength of homogeneity indicated as a structural index, and it is a worthy method for featuring anomalies resulting from isolated and multiple sources (Dawi et al.,2004). The technique relates the probable field, for example, magnetic field or gravity together with its gradient components, to the location of the source of an anomaly with a degree of homogeneity indicated as a structural index (Nyakundi *et al*., 2017).

The basis of Euler deconvolution is Euler's equation of homogeneity (Reid & Thurston, 2014) as given in equation 24;

$$(x - x_0)T_{zx} + (y - y_0)T_{zy} + (z - z_0)T_{zz} = n(B_z - T_z) \quad \text{.....24}$$

Where T_z is a vertical component of potential field anomaly source with the degree of homogeneity n, (x_0, y_0, z_0) is the coordinate of the field anomaly source in the Earth's crust to be determined while (x, y, z) is the measured co-ordinate.

Parameters (T_{zx}, T_{zy}, T_{zz}) are gradients as determined in the x, y and z directions respectively, n taken as the structural index and B_z taken as the regional probable field value to be estimated (Melo & Barbosa, 2018). First, the method determines the analytic signal, it then finds peaks in the analytic signal and applies these peak locations for Euler deconvolution with estimate window size (Castro *et al.,* 2019). The analytic signal grid is computed and put on view from derivative grids. Equation 25 expresses analytic signal grid and is the square root of the sum of the squares of the derivatives in the x, y and z directions (Thompson, 1982).

$$A = \sqrt{(\partial x \times \partial x) + (\partial y \times \partial y) + (\partial z \times \partial z)} \text{.....25}$$

where A is the analytic signal grid.

This technique is preferred as solutions are only determined over-identified analytic signal peaks, the window size differs according to anomaly size and the final solution involves only a few more accurate depth estimates (Beard & Szidarovszky, 2018).

An appropriate structural index is put in use when working with Euler deconvolution analysis (Castro *et al.,* 2019). In the regional interpretation of data from gravity source, structural indices of 2.0, 1.0 and 0.5 are said to be common for contact, fault, dyke, sphere and sill location (Felipe & Valeria, 2017) while structural indices of 3.0, 2.0, 1.0 and 0.5 are common for sphere, pipe, dyke or sill and thick step respectively for magnetic data interpretation (Beard & Szidarovszky, 2018). A measure of the rate of change of potential field with distance is what we call structural index. The basic principle of the structural index is Euler's homogeneity equation (Reid *et al*., 1990) expressed in equation 26.

$$x\frac{\partial f}{\partial x} + y\frac{\partial f}{\partial y} + z\frac{\partial f}{\partial z} = nf \text{.....26}$$

For potential field data analysis, the expression in equation 10 is rewritten as equation 27 (Melo & Barbosa, 2018).

$$(x - x_0)\frac{\partial T}{\partial x} + (y - y_0)\frac{\partial T}{\partial y} + (z - z_0)\frac{\partial T}{\partial z} = n(B - T) \text{.....27}$$

where (x_0, y_0, z_0) is the position of anomaly source whose vertical component of potential field T is measured at (x, y, z). n is the structural index, and B is the regional value of the potential field (Reid & Thurston, 2014).

A structural index is calculated by determining how many infinite dimensions are present in a geologic representation (Thompson, 1982). representation index is the infinite dimension number taken away from the maximum structural index for the field. The maximum structural index for gravity field is two because the gravity field

from a point source dies off as $\frac{1}{r^2}$ (Kearey *et al.*, 2002) while it is three for a magnetic field because the magnetic field from a point dipole falls off as $\frac{1}{r^3}$. In real life experience, it is not true that probable field does not vary with distance from the anomaly source as suggested by zero structural index.

2.3.4 Spectral Analysis of Ground Magnetic Data

This technique is based on Fast Fourier Transform (FFT) which changes the space domain grid data to Fourier wavenumber domain (Fedi & Mastro, 2018, Nyakundi *et al.*, 2022). Oasis Montaj magmap software creates a radially averaged energy spectrum. Magmap applies filters in the Fourier wavenumber domain. Mathematically, the Fourier transform of space domain function $f(x, y)$ is defined as in equation 28:

$$\bar{f}(\mu, v) = \int_{-\infty}^{\infty}\int_{-\infty}^{\infty} (x, y) \, . \, e^{-i(\mu x + vy)} dxdy \ldots\ldots\ldots\ldots\ldots\ldots\ldots\ldots\ldots\ldots\ldots 28$$

And the space domain function is expressed as in equation 29 below:

$$f(x, y) = \frac{1}{4\pi^2}\int_{-\infty}^{\infty}\int_{-\infty}^{\infty} \bar{f}(\mu, v) \, . \, e^{-i(\mu x + vy)} d\mu dv \ldots\ldots\ldots\ldots\ldots\ldots\ldots\ldots\ldots\ldots 29$$

Where μ together with v are wavenumbers in the x and y directions respectively, measured in cycles per metre.

A given probable field function in the space domain has a unique and single wavenumber domain function and vice versa. The 2-D function of energy against wavenumber and direction is referred to as the energy spectrum. Spectra tries to explain the variation of energy as a function of wavenumber. The power spectrum $\left|\bar{f}(\mu, v)\right|^2$ and its total energy E_T are related by the expression in equation 30:

$$E_T = \frac{1}{2\pi}\int_{-\infty}^{\infty}\left|\bar{f}(\mu, v)\right|^2 d\mu dv \ldots\ldots\ldots\ldots\ldots\ldots\ldots\ldots\ldots\ldots\ldots\ldots\ldots\ldots\ldots\ldots 30$$

Where μ, v are wavenumbers in x, y directions.

Collection of geophysical probable data is done with defined boundaries within the study area, unlike the infinite area assumed in mathematical equations 30, 31, and 32. Radially averaged energy spectrum is a function of wavenumber only and is determined by getting the mean of the energy for all directions for similar wavenumber. The Nyquist wavenumber N is the largest wavenumber that has been sampled by the grid which is the highest frequency that it is possible to measure given a fixed sample interval as expressed in equation 31 (Fedi & Mastro, 2018; Nyakundi *et al*., 2022). The spatial frequency of a wave measured in cycles per unit distance is its wavenumber, k.

$$N = \frac{1}{2d} \quad \text{.....31}$$

Where d is the sample interval.

The expression used in determining the depth of a statistical ensemble of sources is given in 32 as

$$h = \frac{-s}{4\pi} \quad \text{.....32}$$

Where h is depth and s is the five-point average of the slope of the energy spectrum (Spector & Grant, 1970, Nyakundi *et al*., 2022).

Electrons orbiting around the nucleus and their revolving causes magnetic moments in atoms (Parasnis, 1986). From quantum theory, two electrons revolving in different directions can be in similar electron state, and such two electrons are known as paired electrons. The paired electrons give rise to zero magnetic moments since individual magnetic moment contributions cancel out. When an external magnetic field such as the Earth's geomagnetic field exists, the spin magnetic moments of neighborhood atoms are uniformly aligned, thus giving rise to overall magnetisation. There are no unpaired electrons in diamagnetic minerals such as halite hence all the electron shells are complete (Kearey *et al.,* 2002). The magnetization is induced when an external magnetic field is introduced, for example, the Earth's geomagnetic field. Negative magnetic susceptibility arises because electrons spin in a manner that produces a magnetic field that resists the applied field. There are unpaired electrons in

paramagnetic minerals for example fayerite, amphiboles, pyroxenes, olivines, garnets and biotite (Reynolds, 1998). This results in incomplete electron shells that generate unbalanced spin magnetic moments among atoms of paramagnetic minerals. When an external magnetic field such as the Earth's geomagnetic field is introduced, the magnetic moments re-arrange themselves in line with the direction of an applied magnetic field. This produces a weak positive anomaly that reduces as the materials' temperature increases (Reynolds, 1998). During spectral analysis of magnetic data, paramagnetic materials generate a bigger anomaly than diamagnetic rocks.

The temperature together with the strength of the applied magnetic field affect the magnetic susceptibility of ferromagnetic minerals. Interaction among the neighbouring atoms together with overlap of electron shells makes the spin moments of unpaired electrons stick magnetically. The magnetic coupling can be in such a way that the magnetic moments are lined up either parallel or antiparallel.

Ferromagnetic minerals like iron, nickel and cobalt (Reynolds, 1998) are not commonly occurring, though can be found in some areas. These minerals do have a parallel arrangement of magnetic moments. When ferromagnetic mineral's temperature rises above some curie temperature T_C, the dipoles are dis-organised and the mineral ceases to manifest ferromagnetic properties thereby showing Paramagnetic behaviour.

The magnetic moments of antiferromagnetic minerals are antiparallel to each other, for example hematite (Telford *et al.*, 1990). The overall magnetic moment of antiferromagnetic mineral is zero since the magnetism of dipoles in different directions cancel one another. The dipoles in ferrimagnetic minerals are antiparallel as well as unequal, generating a resultant magnetisation. Common ferrimagnetic minerals are Ilmenite, magnetite and titanomagnetite (Parasnis, 1986). Ferrimagnetic minerals are characterised by spontaneous magnetisation as well as large magnetic susceptibilities, for example, pyrrhotite (Jiao & Lei, 2019). Common magnetic rocks occurring within the earth's crust are either ferrimagnetic or antiferromagnetic.

CHAPTER THREE

METHODOLOGY

3.1 Study Area

Figure 3.1 shows the area under study, Kargi. Kargi is in Marsabit county, Laisamis constituency, Loiyangalani sub-county and approximately 72 km from Marsabit town to the west. It borders Gabra, Samburu and Chalbi.

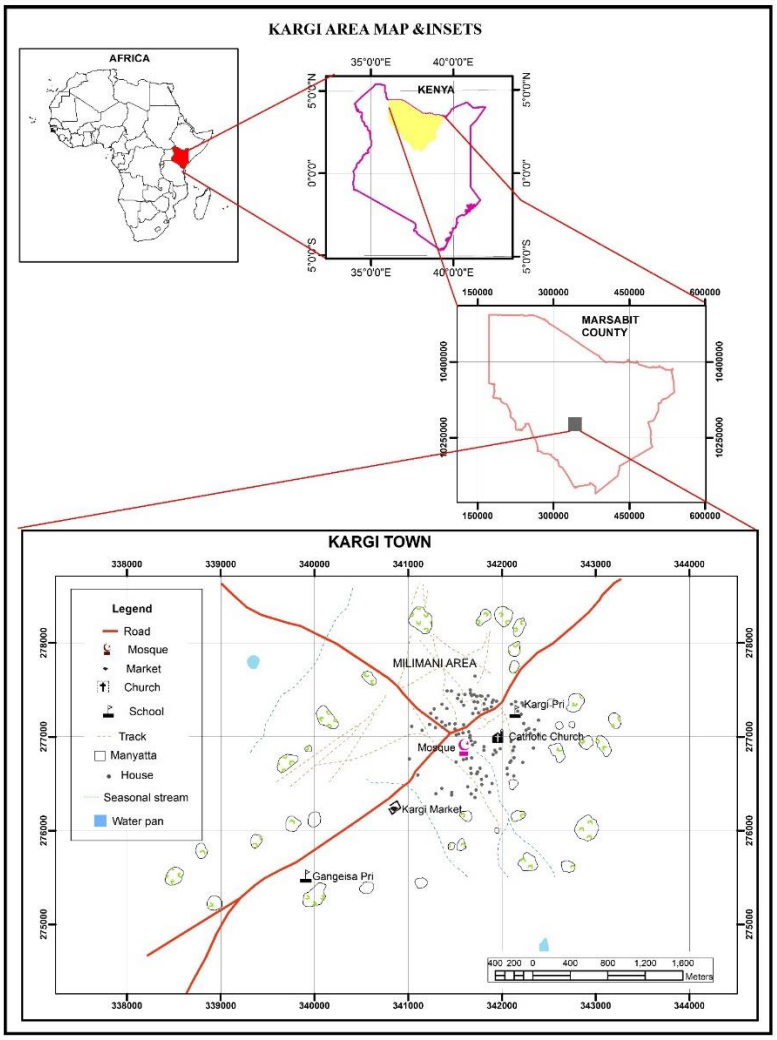

Figure 3.1. Map Showing Kargi Area (Survey of Kenya, 2017, Modified)

The area under study, approximately 6.54 km by 4.78 km is located between latitudes 2°28´37´´ and 2°31´15´´ N and longitudes 37°32´34´´ and 37°36´07´´ E as seen from figure 3.0.

3.2 Methodology

In order to find the surface distribution of ionizing radiation dose in Kargi area, water and soil samples were collected in this area and used to establish the distribution and levels of natural ^{238}U, ^{235}U, ^{232}Th, ^{40}K and ^{82}Rb radionuclide activities and their respective annual effective dose rates.

3.2.1 Samples Collection

Figure 3.1 below gives samples plan for Kargi area. Soil or rock samples, background radiation level measurements together with magnetic radiation measurements were taken from the stations marked A_1, A_2, A_3, A_4, etc with spacing between the stations as 500 m for the entire region. This spacing was to give better representative samples for final analysis. Water samples were however taken from water sources/points as distributed in Kargi area. Radiation background measurements were also done at these water sources/points. Appendix VI gives block name, sampling area size, sample number and location of soil, magnetic readings and radiation samples collection.

3.2.1.1 Soil Sampling

Samples were collected according to the internationally established experience (Tzortzis, M. and Tsertos, H., 2004). Systematic grid sampling, considered as the most commonly employed sampling method was employed as shown in figure 3.2 and tabulated in appendix VI. It is generally unbiased as long as the starting point is randomly selected. The area was divided by use of a square grid, and samples were collected from nodes (intersections of grid lines) (IAEA TECDOC 486, 2019).

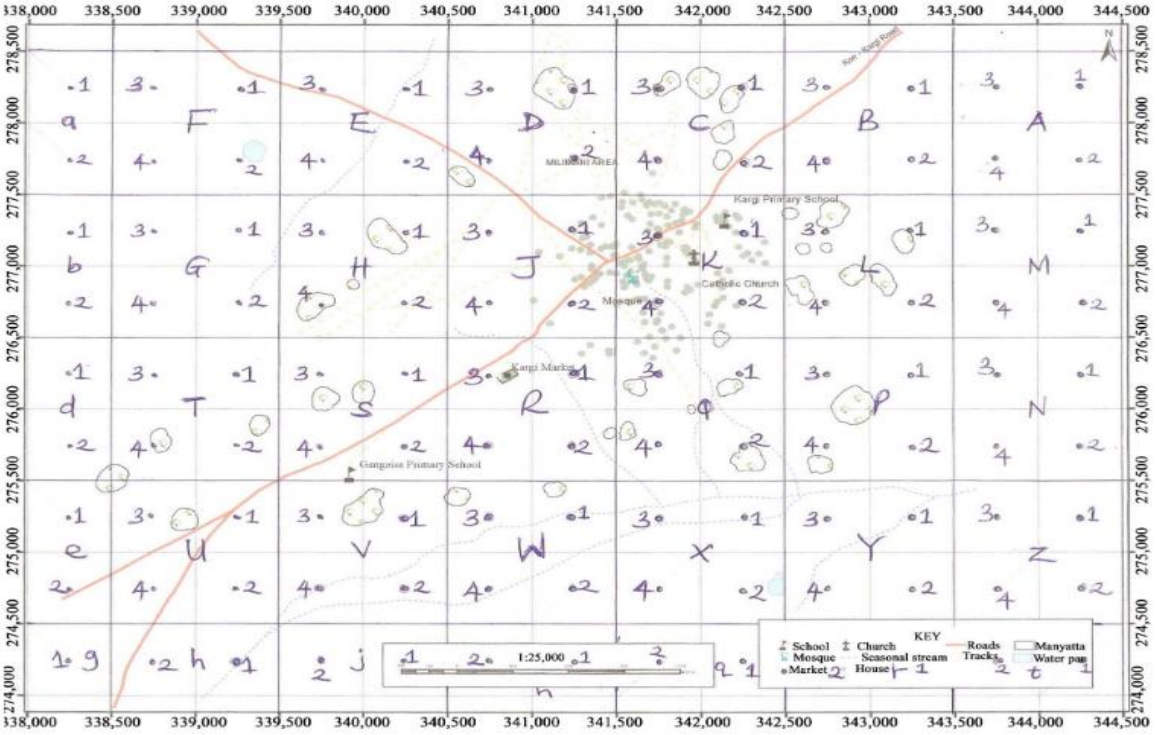

Figure 3.2: Systematic Grid Sampling of Kargi Area

The EPA, 1995 describes factors which determine sampling distance between sampling locations in the grid as the size of the area to be sampled and the total number of samples. For each sample collection, an area of about 0.5 km x 0.5 km was marked to help get a good representation of the area giving a total of 117 samples from the entire area. An area of 1 km x 1 km would have given less samples hence poor sample representation of the area. These samples were collected in batches of 3 as the area is big. To avoid samples contamination from top soil containing leaves and other contaminations, samples were collected 10 centimetres from the surface (Monika *et al.*, 2010), packed and clearly marked before transporting to Nairobi.

3.2.1.2 Water Sampling

Water sources/ points including boreholes and water points were located within the area using GPS device, recorded and sampling done. Table 3.1 gives water source, water sample number and location of water samples collection. Sampling of water samples from these points done in standard (0.5 litre) polyethylene Marinelli beakers

as shown in appendix III (b), which were also used as measuring containers (Hany, E. and Abdallah, I. A., 2014).

3.3.2 Sample Preparation

After samples collection, rock and soil samples were sun dried and then crushed separately into powder form to homogenize them. Sieving of the crushed powder was done through a 0.6 mm mesh sieve, oven dried at 100°C for 24 hours, completely removing water from the samples. Appendix II shows each sample (crushed powder and water) being weighed and packed in special plastic containers and tightly closed for about 4 weeks, a sufficient time required to attain a state of secular radioactive equilibrium after their progeny (Hassan *et al.,* 2016, Kinyua *et al.,* 2011, Karahan & Bayolken, 2000).

Collected water samples were allowed to settle before decanting. Before use, the containers were washed with dilute hydrochloric acid and rinsed with distilled water to avoid any contamination which might give wrong results. Each beaker will be filled to brim, acidified by adding 0.5 ml of concentrated HNO_3 per litre as shown in appendix III (a), to prevent any loss of radium isotopes around the container walls and to avoid growth of micro-organisms. A tight cap was then pressed on so that no air allowed (See appendix III (b)). Water samples were well kept in the laboratory at the Institute of Nuclear Science, University of Nairobi for a minimum of 1 month to allow daughter products to come into radioactive equilibrium with their parents ^{226}Ra and ^{232}Th before radiometric analysis (Hany, E. and Abdallah, I. A., 2014).

After the one-month period, the samples were run for spectroscopic analysis. Sealed samples placed in marinelli beakers were put in the detector one at a time then counted for between 22000 – 179000 seconds. Before these counts, background counts were recorded first under similar factors of those of the samples measured. These were subtracted at the end of the counts of all the samples in order to find net counts for the samples. Displayed spectrum recorded on MCA screen is displayed where the horizontal and vertical axes representing the photon energy or channel number and photons recorded per channel or intensity at the end of each counting session. Both the field and laboratory aspect of this project were carried out between February, 2018 and March, 2020.

3.3.3 Safety in Samples Collection and Preparation

Since we were involved with sampling of materials suspected to be radioactive, our safety was paramount. In this case, the film badge dosimeter was used. Film badge, or film badge dosimeter, is an instrument used for checking cumulative exposure to ionizing radiation. Two main parts of this badge are: dental X-ray film or photographic film together with and a holder. The film is removed from the holder and then developed to measure recorded radiation exposure due to gamma rays, X-rays and beta particles. Typically, the badge is worn around the chest or torso outside of clothing. This location helps monitor exposure of most vital organs and represents the bulk of body mass. The badge is worn over the protection to observe the dose literally received to non-protected parts (uncovered parts with lead). Under special cases, where an operator may receive a high dose to one area of the body (e.g. the hands of a radio pharmacist) then additional monitoring of the area is required. For monitoring of hands, a miniature Thermoluminescent Dosimeter worn as a finger ring is usually used.

3.3.4 Measurement of Gamma Radiation from Collected Samples

To determine the distribution and levels of naturally occurring radionuclide ^{226}Ra, ^{232}Th and ^{40}K in samples of soil and water from Kargi area, a germanium (HPGe) detector of EG&G ORTEC type coupled with a computer based high resolution multi-channel analyzer available from Institute of Nuclear Science was used (appendix V). The detector's relative efficiency is 31.6 % and full width at half maximum (FWHM) of 1.8 keV energy resolution for 1332 keV gamma ray line of ^{60}Co. See attached data sheet on appendix VI.

Two approaches were used in determining the radiation absorbed dose rate in Kargi area and include measurement of absorbed dose rates in air, 1 m above surface at each sampling area using a personal portable survey meter with a reading span of up to 100 μSvh^{-1} and calculation of absorbed dose rates from measured activity concentrations were done with the help of equation 10 while annual effective dose rate were computed by use of the formula in equation 11 and 12 for soil and water respectively.

3.3.5 Analysis of Radionuclides from Collected Samples

Activity concentration from ^{226}Ra, ^{232}Th and ^{40}K in collected samples were analysed using gamma-ray spectrum and a graph of Activity ($Bqkg^{-1}$) versus Energy (keV) plotted. The ^{226}Ra activities for samples presumed to be in radioactive equilibrium were approximated from ^{214}Pb (351.92 keV) as well as ^{214}Bi (609.31 keV). The gamma-ray energies of ^{212}Bi, ^{212}Pb as well as ^{228}Ac were employed to estimating activity of ^{232}Th. The activity concentrations of ^{40}K were computed directly by its own gamma rays (1460.81 keV) (Kinyua *et al.*, 2011, Aguko *et al.*, 2013, Hassan *et al.*, 2016). Obtained activity concentrations were also used to calculate External and Internal hazard indices, where values computed need to be less than unity ($1mSvy^{-1}$) for the radiation hazard to have negligible hazardous effects to respiratory organs of the public. To get these indices, equations 15 and 17 are used. The calculated indices were recorded in a tabular form as in appendices XI and XII.

3.3.6 Background Radiation Measurements

Survey meters are transportable radiation detection and measurement instruments employed to check facilities, equipment and personnel for radioactive contamination, or to compute external or ambient ionizing radiation fields (to assess the direct exposure hazard). The hand-held survey meter is probably the most familiar radiation measuring equipment to society owing to its wide as well as highly visible use (Meisenhelder & Bursik, 2018). Background radiation measurements were done in all the soil/rock samples collection points as in figure 3.1 together with the water sources/ points by use of hand-held survey meter(s) as in appendix I (a) and appendix IV (a) and (b). A total of 131 measurements for soil/rock areas and water points were done. Hand held survey meters were used to give direct reading of the absorbed dose rate in the air, in Gyh^{-1}. These readings were then converted to $SvGyh^{-1}$ by a conversion factor of 0.7S $vGyh^{-1}$ as recommended by UNSCEAR 2000 and given in a table form.

3.3.7 Magnetic Measurements

A proton magnetometer was used for this exercise (see appendix I (b)). 115 magnetic measurements were expected from the area under study. These measurements were taken alongside soil sample collection points, making the measurement number to be

the same as those of soil samples. Magnetic measurements helped us understand the rock structure in the area and any possible association of the rocks and radiation contribution. It also helped us understand possible sources of radiation in Kargi.

Because of few resources, we used one magnetometer in our measurements. A base station was carefully selected, away from buildings. First, time and magnetometer readings at the base station were taken and recorded. The time and magnetometer readings were then taken from the soil sample collection points as discussed earlier and recorded. After a number of measurements, we occasionally (averagely 3 hours) returned to the base station taking and recording time and magnetometer readings. This process is repeated until the day ends.

Table 3.1: Water Source, Water Sample Number and Location of Water Samples Collection

WATER SOURCE	WATER SAMPLE NUMBER	LOCATION	
		Easting, E	Northing, N
Tap	W_1	343456	278365
Burst pipe	W_2	343910	276824
Tap/Kiosk	W_3	342509	275896
Dam	W_4	342459	274767
Kiosk	W_5	338724	274937
Bore hole	W_6	339131	275587
Bore hole	W_7	340833	277452
Shallow well	W_8	340923	276614
Shallow well	W_9	340925	276634
Shallow well	W_{10}	341063	275587
Shallow well	W_{11}	341076	276374
Shallow well	W_{12}	341078	276381
Shallow well	W_{13}	341695	276846
Shallow well	W_{14}	341673	276821

3.4 Activity Concentration Measurements

Measurement of activity concentrations was performed with high-purity germanium (HPGe) gamma-ray detector with 144 mm^3 active volume and 57.4 mm external diameter. The detector has an efficiency of 31.6% with a resolution of 1.8 keV. Each sample was put in a marinelli beaker of 500 cm^3 and filled up to the same level as the certified reference standard soil (IAEA-375, IAEA-RGTh-1, IAEA-RGU-1 and IAEA

–RGK-1 soil) then placed in a lead shielded detector. A counting time of between 22000 – 179000 seconds was adopted to ensure that all nuclides due to ^{232}Th and ^{238}U were visible in gamma spectrum. A soil sample (IAEA-375, IAEA-RGTh-1, IAEA-RGU-1 and IAEA –RGK-1 soil) was analyzed for the method of spectrometer validation and calibration. At the start of every measurement session energy calibration was carried out to cater for the weather condition variation, vibrations as well as heating up of the detector. RGK-1, RGU-1, and RGTH-1 for potassium, uranium, and thorium respectively are the standard samples (IAEA, 1987). Calibration is done so that the channels are provided with relevant energy values. The peak positions were then used to deduce the Energy-Channel relationship. By using a second order polynomial as in Equation 33, the photon energy is represented as a function of channel number (Oborah *et al.*, 2024).

$$E=Y_0+C_1B+C_2B^2 \quad \text{.....33}$$

Where B represents channel number, while Y_0, C_1 as well as C_2 are constants and the fitted values are 13.867±0.693, 3.513±0.176 and 0.001±00005.

The activity concentration of each radionuclide was then computed using the method of comparison of equation 34 (Oborah, *et al.*, 2024)

$$A = \frac{I_i}{\sum M_i} \quad (Bqkg^{-1}) \text{.....34}$$

Where;

Σ represents the summation of the masses,

A represents the activity concentration of the actual sample,

M_i represents the mass of the sample,

I_i represents the intensity and

i is the sample number

For each sample, five significant gamma lines existed, ^{40}K line, $^{214}P_b$ and $^{214}B_i$ lines from ^{238}U and $^{212}P_b$ and $^{228}A_c$ lines from ^{232}Th. The activity of ^{40}K was assessed from 1461 keV gamma line while the activity of ^{238}U from 352 keV and 609 keV gamma

lines of $^{214}P_b$ and $^{214}B_i$ respectively and that of ^{232}Th from 238 keV and 911 keV gamma lines of $^{212}P_b$ and $^{228}A_c$ respectively.

3.5 Absorbed Dose

Absorbed dose is the concentration of energy deposited in tissue (energy absorbed by human tissue) as a result of an exposure to ionizing radiation. It is used to assess the potential for biochemical changes in specific tissues. Two approaches were employed to approximate the external doses that result from deposition of radionuclides in soil surfaces: direct measurement and computations based on radionuclide deposition densities

3.5.1 Measurement of Absorbed Dose Rates in Air

The absorbed dose rates in air at 1 m above the ground surface were measured for each point using a hand-held survey meter Thermo Scientific, FH 40G-L10 Radiameter and Wilnos X5Cplus (appendix IVa and 4b respectively) with a reading range of 10 $nSvh^{-1}$ – 100 $mSvh^{-1}$ and 1 μSvh^{-1} – 20 $mSvh^{-1}$ respectively. The absorbed dose rates in air in $nGyh^{-1}$ were computed from the dose rates in $nSvh^{-1}$ as measured in the field using the conversion

Activity concentration from ^{226}Ra, ^{232}Th and ^{40}K in the collected soil and rock samples were analysed by use of gamma-ray spectrum and photo peaks as plotted from a graph of Activity ($Bqkg^{-1}$) versus Energy (keV). Since uranium and thorium are not gamma emitters, they are measured indirectly through the gamma-ray photons emitted from their daughters, ^{234}Th ranging between 81 keV – 108 keV for ^{238}U, ^{212}Pb ranging between 221 keV – 273 keV for ^{232}Th and radium is to be measured from the gamma-ray photon emitted by ^{214}Pb ranging between 327 keV – 390 keV whereas potassium is measured directly from the gamma-ray photon emitted by ^{40}K ranging from 1319 keV – 1471 keV.

CHAPTER FOUR

RESULTS AND DISCUSSION

4.1 Activity Concentrations of Radionuclides in the Samples

The activity concentration of each radionuclide was computed using the method of comparison and values of appendix VIII of nuclide identification report. The calculated values are presented in appendix X. For each sample, five significant gamma lines existed, ^{40}K line, ^{214}Pb and ^{214}Bi lines from ^{238}U and $^{212}P_b$ and ^{228}Ac lines from ^{232}Th. The activity of ^{40}K was evaluated from 1461 keV gamma line while the activity of ^{238}U from 352 keV and 609 keV gamma lines of ^{214}Pb and $^{214}B_i$ respectively and that of ^{232}Th from 238 keV and 911 keV gamma lines of ^{212}Pb and ^{228}Ac respectively.

Table 4.1: Calculated Activity Concentrations in Bqkg^{-1} of ^{226}Ra, ^{232}Th and ^{40}K for Water Samples from Kargi Area, Marsabit - Kenya

WATER SOURCE	WATER SAMPLE NUMBER	Average Activity, Bq/kg		
		^{232}Th	^{238}U	^{40}K
Tap	W_1	0.12	3.63	71.33
Burst pipe	W_2	2.64	4.55	54.63
Tap/Kiosk	W_3	1.71	7.84	36.01
Dam	W_4	0.98	2.08	68.92
Kiosk	W_5	7.99	3.39	57.72
Bore hole	W_6	3.94	6.04	77.16
Bore hole	W_7	Undetected	5.66	45.68
Shallow well	W_8	1.90	6.41	64.45
Shallow well	W_9	4.37	7.66	60.49
Shallow well	W_{10}	3.12	0.58	42.33
Shallow well	W_{11}	0.19	3.59	72.53
Shallow well	W_{12}	0.54	0.27	Undetected
Shallow well	W_{13}	6.09	Undetected	81.22
Shallow well	W_{14}	Undetected	Undetected	7.61
Average		**2.80±2.45**	**4.31±2.52**	**56.93±20.16**

Appendix X and table 4.1 give all the calculated activities for soil and water samples respectively. Minimum and maximum concentrations at particular collection points could easily be seen from the tables. The values were averaged and compared with other areas of the world. The comparisons are as in tables 4.2 and 4.3 for soil and water respectively.

Also, from appendix X that the calculated activities for ^{226}Ra ranged from 3.30 – 18.12 Bq.kg^{-1} with a mean and standard deviation of 7.40±2.61 Bq.kg^{-1}, for ^{232}Th ranged from 0.00 – 27.45 Bq.kg^{-1} with a mean and standard deviation of 7.98±4.01 Bq.kg^{-1}

and for ^{40}K ranged from 119.17 – 667.77 $Bq.kg^{-1}$ with a mean and standard deviation of 352.51±108.30 $Bq.kg^{-1}$.

Table 4.1 were results for calculated activities of water samples ranging from 0.00 – 7.84 $Bq.kg^{-1}$, 0.12 – 7.99 $Bq.kg^{-1}$ and 0.00 – 81.22 $Bq.kg^{-1}$ with means and standard deviations of 4.31±2.52 $Bq.kg^{-1}$, 2.80±2.45 $Bq.kg^{-1}$ and 56.93±20.16 $Bq.kg^{-1}$ for ^{226}Ra, ^{232}Th and ^{40}K respectively. The maximum allowed world average concentrations of ^{226}Ra, ^{232}Th and ^{40}K for both water and soil are 37±4, 33±3 and 400±24 $Bq.kg^{-1}$ (UNSCEAR, 2008). These activities lie within the maximum allowable limits making the waters here safe.

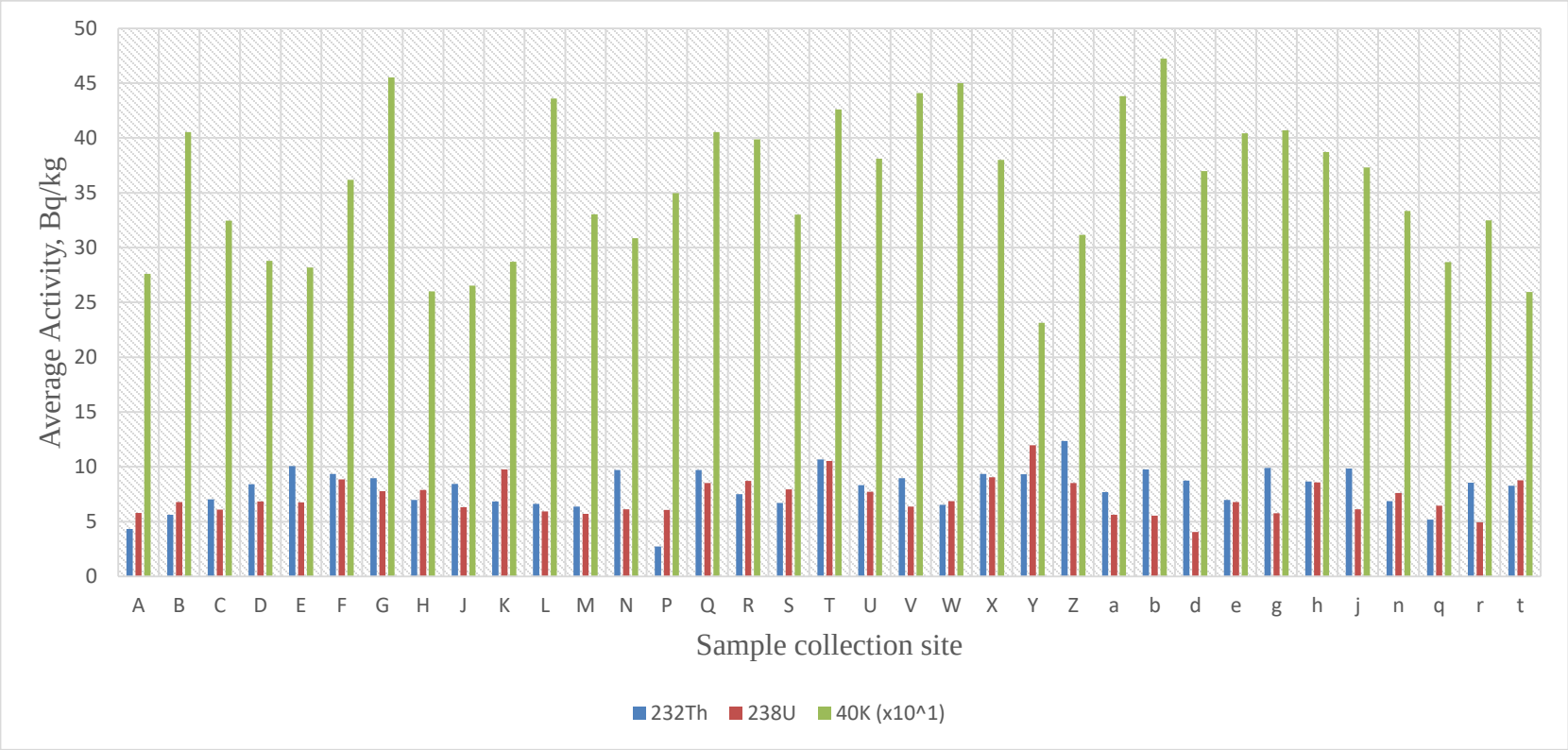

Figure 4.1: Average Values of Calculated Activities for Soil Samples due to ^{226}Ra, ^{232}Th and ^{40}K in all Area under Investigation

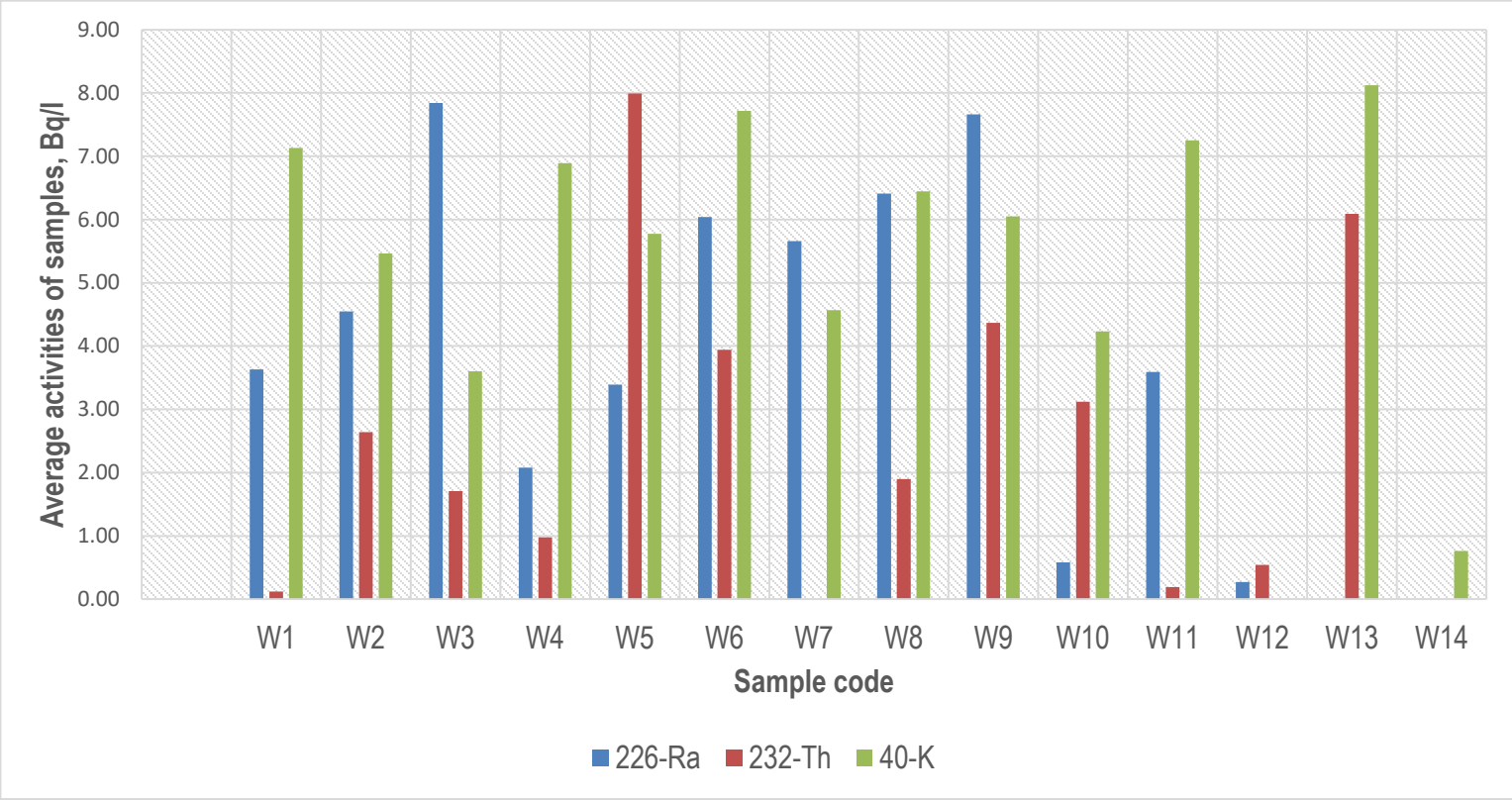

Figure 4.2: Average Values of Calculated Activities for Water Samples due to ^{226}Ra, ^{232}Th and ^{40}K in all Area Under Investigation

Table 4.2: Comparison of Natural Radioactivity Levels in Soil Samples under Investigation with Those in Other Countries

Country	Activity concentration ($Bqkg^{-1}$)				References
	^{226}Ra	^{232}Th	^{40}K	Ra_{eq}	
Kargi, Kenya	7.4±2.6	7.8±4.0	353.0±110.1	45.9±12.7	current work
Sakwa Wagusu, Kenya	40.7±12.0	35.8±15.4	639.6±192.1	140.7±54.3	Aguko *et al.*, 2013
Destroyed fuel facility, Iraq	15.8±1.2	14.1±1.5	306.4±18.1	28.9±2.12	Abdulla *et al.*, 2016
Tamilnadu, India	116.0	44.0	300.0	201.0	Raghu *et al.*, 2017
Kirklareli, Turkey	37.0±18.0	40.0±18.0	667.0±280.0	-	Taskin *et al.*, 2009
World average	37.0±4.0	33.0±3.0	400.0±24.0	370.0	UNSCEAR, 2008, Lu & Zhang, 2006

Table 4.3: Comparison of Results of Activity Concentration in Bql^{-1} of ^{226}Ra, ^{232}Th and ^{40}K of Water Tested Samples with Other Countries

Country		Activity concentration (Bql^{-1})			References
		^{226}Ra	^{232}Th	^{40}K	
Kargi, Kenya		4.31±2.52	2.80±2.45	56.93±20.18	Current work
Egypt		0.20±0.11 (average)	0.13±0.08 (average)	5.29±2.41 (average)	Hany, E and Abdallah, I. A. E., 2014
Nigeria, oilfield of River state	Tap water	4.20±0.12	4.44±0.14	37.85±2.15	Ononugbo *et al*., 2013
	Well water	9.22±0.82	8.46±0.61	44.27±2.34	
	River water	6.57±0.24	6.85±0.36	29.48±1.98	
World average		37.0±4.0	33.0±3.0	400.0±24.0	UNSCEAR, 2008, Lu & Zhang, 2006

The elemental abundance of original Th, U and K concentrations may vary in soils and rocks due to alteration in metamorphic processes and the elemental abundance of $\frac{Th}{U}$, $\frac{K}{U}$ and $\frac{K}{Th}$ ratios help us study the enrichment or depletion processes as a result of complexity in environmental degradation or pollution history, metamorphic history, alteration together with/or weathering that affected investigating the rocks/soil. Hence, the ratios of $\frac{Th}{U}$, $\frac{K}{U}$ and $\frac{K}{Th}$ provides an indication whether relative depletion or enrichment of radioisotopes had occurred in an environment (Irunkwor and Abanjo, 2022). Elemental radionuclide concentrations in soil and water samples were computed from the activity concentrations in $Bq{\cdot}kg^{-1}$ by application of conversion factors covered under section 2.2.9 on elemental concentration of ^{238}U, ^{232}Th and ^{40}K. These results are presented in appendices XIII and XIV and table 4.4. From appendix XIII, the computed elemental concentrations for soil ranged from 0.12% to 2.13%, 0.27 to 1.47 ppm and 0.00 to 6.76 ppm for potassium, uranium and thorium respectively with respective arithmetic mean and standard deviation of 1.13± 0.21%, 0.60 ± 0.21 ppm, 1.97 ± 0.99 ppm. For water samples, the computed elemental concentrations for ranged from 0 % to 0.247 %, 0.000 to 0.635 ppm and 0.000 to 1.968 ppm for potassium, uranium and thorium respectively with respective arithmetic mean and standard deviation of 0.167± 0.082 %, 0.299 ± 0.227 ppm, 0.591 ± 0.609 ppm as seen from table 4.4. Tzortzis & Tsertos (2004) and Al-Hamarneh & Awadalla (2009) took note that a low or high value of $\boldsymbol{\frac{Th}{U}}$ ratios as measured in some studied locations may be a clear indication of thorium enrichment or a uranium depletion owing to natural processes alteration in that area.

Table 4.4: Elemental Concentration of Specific Activity of ^{238}U (ppm), ^{232}Th (ppm) and ^{40}K (%) in Water Samples with Their Ratios

Sample code	^{238}U	^{232}Th	^{40}K	$\frac{Th}{U}$	$\frac{K}{U}$	$\frac{K}{Th}$
W_1	0.294	0.030	0.228	0.101	0.775	7.710
W_2	0.368	0.650	0.175	0.176	0.474	0.268
W_3	0.635	0.421	0.115	0.663	0.181	0.273
W_4	0.168	0.241	0.220	1.433	1.307	0.912
W_5	0.274	1.968	0.184	7.169	0.672	0.094
W_6	0.489	0.970	0.247	1.984	0.504	0.254
W_7	0.458	undetected	0.146	0.000	0.318	undetected
W_8	0.519	0.468	0.206	0.902	0.397	0.440
W_9	0.620	1.076	0.193	1.735	0.312	0.180
W_{10}	0.047	0.768	0.135	16.363	2.880	0.176
W_{11}	0.291	0.047	0.232	0.161	0.797	4.952
W_{12}	0.022	0.133	undetected	6.084	undetected	undetected
W_{13}	undetected	1.500	0.259	undetected	undetected	0.173
W_{14}	undetected	undetected	undetected	10.364	undetected	undetected
Mean	**0.349±0.204**	**0.689±0.204**	**0.195±0.046**	**3.928±5.123**	**0.783±0.762**	**1.403±2.523**

They estimated the theoretical normal continental crust values of $\frac{Th}{U}$ elemental ratios to be 3.0. From appendix XIV for soil samples, our $\frac{Th}{U}$ results were from 1.19±0.85 to 6.35±1.72 with mean and standard deviation of 3.42±1.63. Other correlation ratios of $\frac{K}{U}$ together with $\frac{K}{Th}$ varied from 0.84±0.46 to 3.89±2.13 as well as 0.34±0.09 to 1.94±2.42 with mean and standard deviations of 2.07±0.89 and 0.70±0.61 respectively. For water samples, table 4.4 gives the $\frac{Th}{U}$ mean and standard deviation of 3.928±5.123. Other correlation ratios of $\frac{K}{U}$ together with $\frac{K}{Th}$ mean and standard deviation are 0.783±0.762 and 1.403±2.523 respectively. Figures 4.3 a and 4.3 b represents correlations for soil and water respectively.

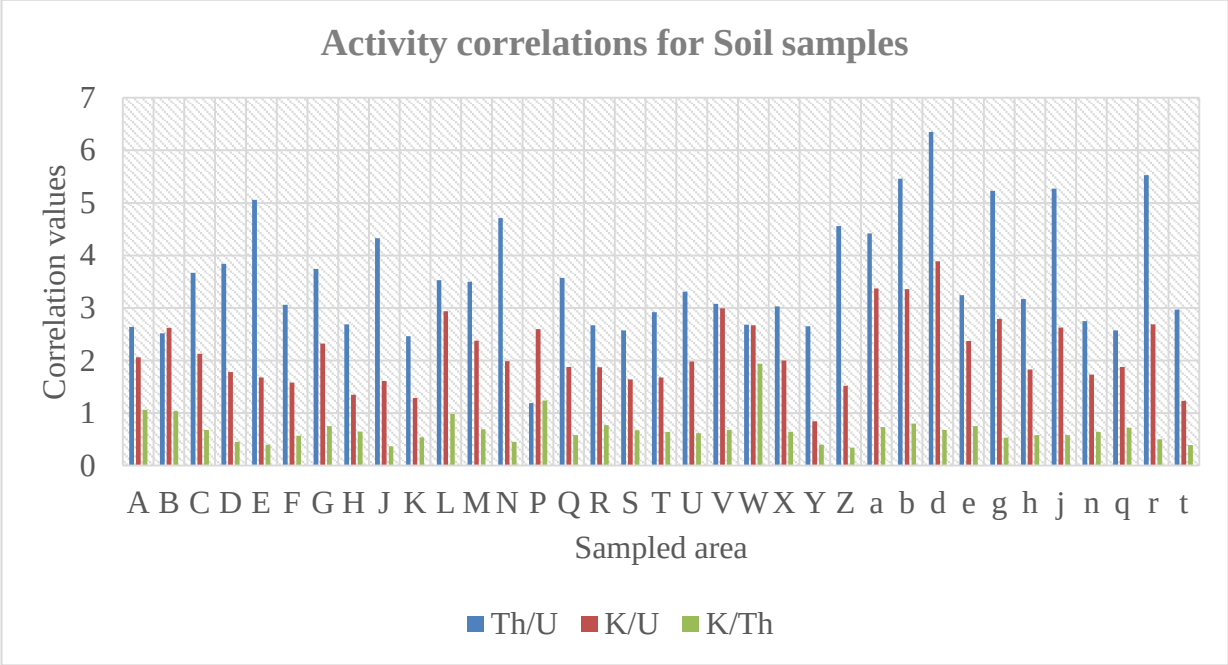

Figure 4.3 a: Average Soil Sample Values of Activity Correlations for Soil Samples

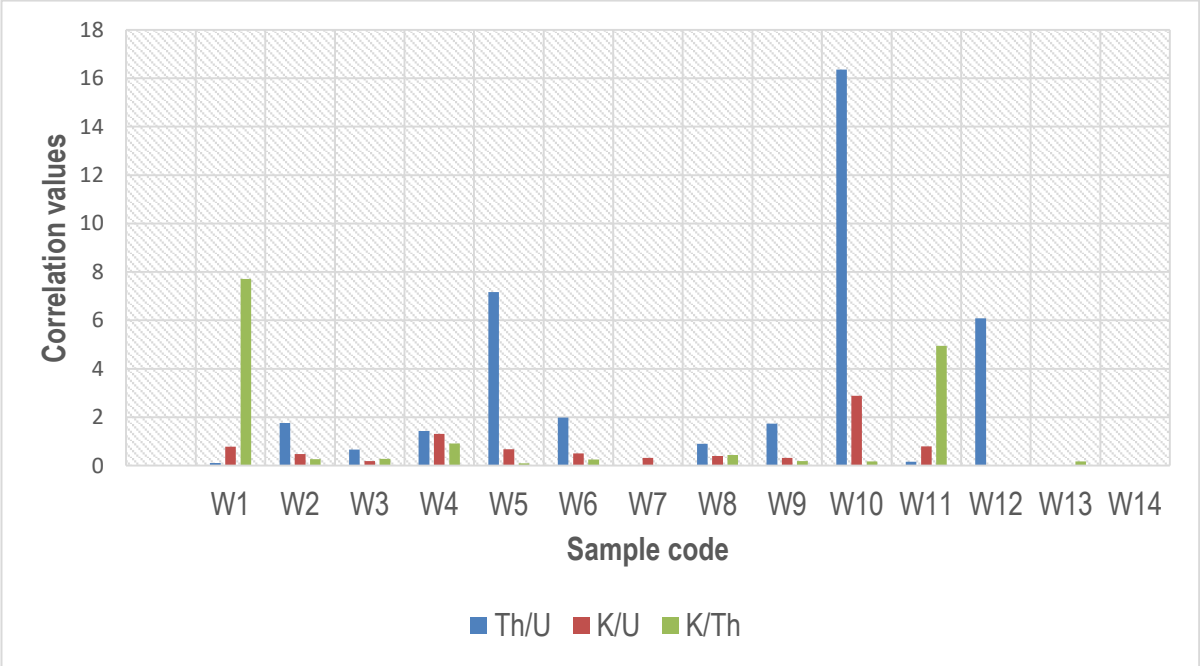

Figure 4.3 b: Average Water Sample Values of Activity Correlations for Water Samples

4.2 Absorbed Dose Rates

4.2.1 Measured Absorbed Dose Rates

The measured absorbed dose rates in air measured 1 m above the surface at each soil sample location are presented in appendix XV and ranges from 42.86 – 170.00 $nGyh^{-1}$. The mean measured absorbed dose rate for the area was 82.64 $nGyh^{-1}$ comparing to the world average value of 60 $nGyh^{-1}$ (UNSCEAR, 2000). This average is about 1.4 times higher than the worldwide limit. The lowest value of the measured absorbed dose rate was at A_1 site, Site V_3 had a value of 170.00 n Gyh^{-1}, considered highest.

For water sample locations, table 4.5 gives data for measured absorbed dose rates. These rates ranged from 44.29 to 130.00 $nGyh^{-1}$ with lowest and highest at Kisima (shallow wells) and tap respectively. Arithmetic mean of the water sources absorbed dose rate was 77.76 $nGyh^{-1}$ comparing to the world average value of 60 $nGyh^{-1}$ (UNSCEAR, 2000). This average is about 1.3 times higher than the worldwide limit.

Table 4.5: Absorbed Dose Rates as Measured 1 m above the Surface at Each Water Point

WATER SOURCE	WATER SAMPLE NUMBER	Average measured absorbed dose rate	Average calculated absorbed dose rate	UNSCEAR, 2000 RECOMMENDATION, nGy/h	
				As measured	As calculated
Tap	W_1	130.00	4.84		
Burst pipe	W_2	107.14	6.22		
Tap/Kiosk	W_3	75.71	6.34		
Dam	W_4	58.57	4.58		
Kiosk	W_5	85.71	9.35		
Bore hole	W_6	61.43	8.75		
Bore hole	W_7	108.57	4.61		
Kisima (shallow well)	W_8	45.71	7.02	**60**	**54**
Kisima (shallow well)	W_9	95.71	9.07		
Kisima (shallow well)	W_{10}	61.43	4.16		
Kisima (shallow well)	W_{11}	44.29	4.92		
Kisima (shallow well)	W_{12}	64.29	0.48		
Kisima (shallow well)	W_{13}	44.29	7.52		
Kisima (shallow well)	W_{14}	105.71	0.33		
Mean		**77.76±27.82**	**5.59±2.80**		

4.2.2 Calculated Absorbed Dose Rates

The calculated absorbed dose rates due to ^{226}Ra, ^{232}Th and ^{40}K and the total average calculated absorbed dose rates are presented in appendix XVI and table 4.7 for soil and water respectively. Equation 10 was used to calculate the absorbed dose rate for soil samples. From appendix XVI, the absorbed dose rates due to ^{226}Ra ranged from 1.85 to 8.46 $nGyh^{-1}$ with mean and standard deviation of 3.46±1.21 $nGyh^{-1}$, the absorbed dose rates due to ^{232}Th ranged from 0.00 to 18.17 $nGyh^{-1}$ with mean and standard deviation of 5.29±2.65 $nGyh^{-1}$ and the absorbed dose rates due to ^{40}K ranged from 1.59 to 28.75 $nGyh^{-1}$ with a mean and standard deviation of 15.12±4.74 $nGyh^{-1}$. The total average absorbed dose rate ranged from 8.67 to 52.34 $nGyh^{-1}$ with mean and standard deviation of 23.87±6.57 $nGyh^{-1}$. Again, equation 10 was used to calculate the

absorbed dose rate for water samples. From table 4.5, the total mean and standard deviation absorbed dose rates was 5.59±2.80 $nGyh^{-1}$.

Figures 4.4 and 4.5 shows bar-graphs of both measured absorbed dose rate and computed absorbed dose rates together with their averages for soil and water samples. These are summaries of table 4.6 and 4.7 together with appendix XVI.

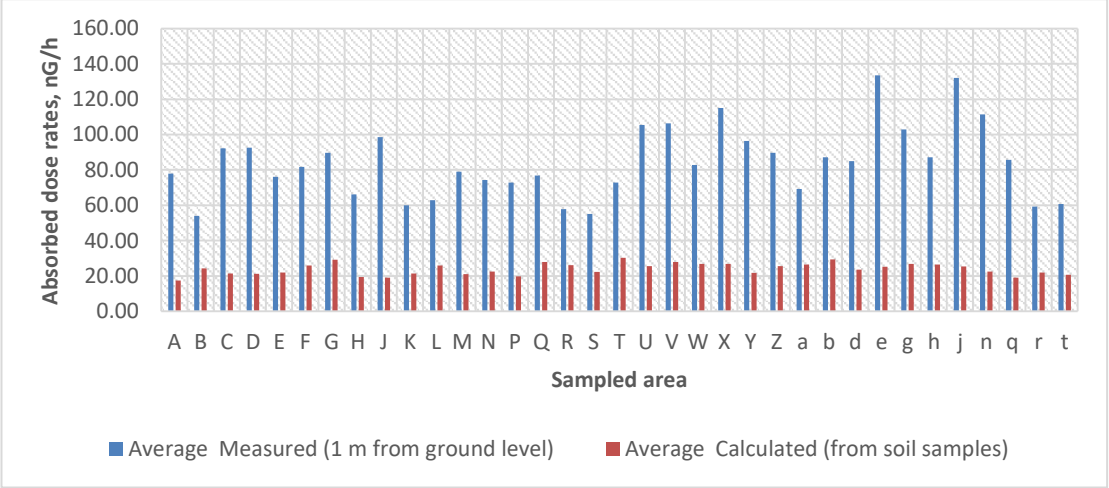

Figure 4.4: Average Computed and Measured (1 m over Ground) Absorbed Dose of Samples from Soil

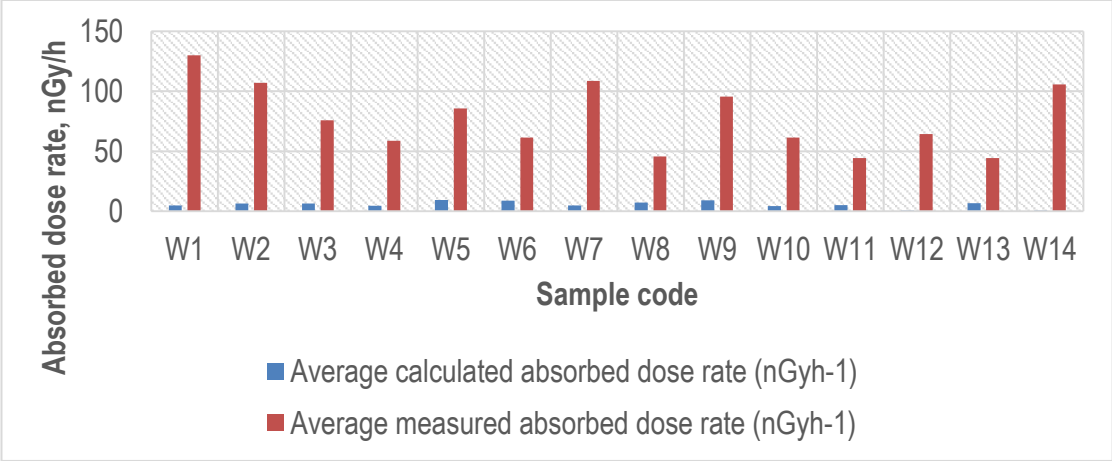

Figure 4.5: Mean Computed and Measured (1 m over Ground) Absorbed Dose of Samples from Water and its Sources

Table 4.6 and appendix XVIII compares both computed and measured dose rates respectively for water and soil sample locations.

Table 4.6: Average Calculated and Measured (1 m above Ground) Absorbed Dose of Samples from Water and its Sources

WATER SAMPLE NUMBER	Average absorbed dose, $nGyh^{-1}$	
	Calculated (from water samples)	Measured 1 m above ground (from sampling area)
W_1	4.84	130.00
W_2	6.22	107.14
W_3	6.34	75.71
W_4	4.58	58.57
W_5	9.35	85.71
W_6	8.75	61.43
W_7	4.61	108.57
W_8	7.02	45.71
W_9	9.07	95.71
W_{10}	4.16	61.43
W_{11}	4.92	44.29
W_{12}	0.48	64.29
W_{13}	7.52	44.29
W_{14}	0.33	105.71
Mean	**5.59±2.80**	**77.76±27.82**

Table 4.7: Calculated Absorbed Dose Rates ($nGyh^{-1}$) of the Water Samples

WATER SOURCE	SAMPLE NUMBER	Dose rates due to			Total average absorbed dose rate	UNSCEAR, 2000 RECOMMENDATION, nGy/h
		^{232}Th	^{226}Ra	^{40}K		
Tap	W_1	0.08	1.70	3.07	4.84	54
Burst pipe	W_2	1.75	2.12	2.35	6.22	
Tap/Kiosk	W_3	1.13	3.66	1.55	6.34	
Dam	W_4	0.65	0.97	2.96	4.58	
Kiosk	W_5	5.29	1.58	2.48	9.35	
Bore hole	W_6	2.61	2.82	3.32	8.75	
Bore hole	W_7	undetected	2.64	1.96	4.61	
Shallow well	W_8	1.26	2.99	2.77	7.02	
Shallow well	W_9	2.89	3.58	2.60	9.07	
Shallow well	W_{10}	2.07	0.27	1.82	4.16	
Shallow well	W_{11}	0.13	1.68	3.12	4.92	
Shallow well	W_{12}	0.36	0.13	undetected	0.48	
Shallow well	W_{13}	4.03	undetected	3.49	7.52	
Shallow well	W_{14}	undetected	undetected	0.33	0.33	
Average		**1.85±1.62**	**2.01±1.18**	**2.45±0.87**	**5.59±2.80**	

Appendix XVI gives values of absorbed dose rates as calculated for soil samples for each sampled area computed from equation 10. Table 4.7 and appendix XVII summerises calculated absorbed dose rates for water and soil samples in area of study. From table 4.7, the average calculated absorbed dose rates for analysed water samples due to ^{226}Ra ranged from 0.27 to 3.66 nGyh^{-1} with arithmetic mean and standard deviation of 2.01±1.18 nGyh^{-1}, the average absorbed dose rates due to ^{232}Th ranged from 0.08 to 5.29 nGyh^{-1} with arithmetic mean and standard deviation of 1.85±1.62 nGyh^{-1} and the average absorbed dose rates due to ^{40}K were from 0.33 to 3.49 nGyh^{-1} with arithmetic mean and standard deviation of 2.45±0.87 nGyh^{-1}. The total average calculated absorbed dose rate ranged from 0.33 to 9.35 nGyh^{-1}. The mean value of the calculated average dose rate for all the sampled area of Kargi was 5.59 nGyh^{-1}. This value was 10 times lower than the world average limit of 54 nGyh^{-1} (UNSCEAR, 2000).

From appendix XVII, the average calculated absorbed dose rates for analysed soil samples due to ^{226}Ra ranged from 0.22 to 8.46 nGyh^{-1} with a mean range of 0.30 to 5.5 nGyh^{-1}, the average absorbed dose rates due to ^{232}Th ranged from 0.00 to 18.17 nGyh^{-1} with a mean range of 1.82 to 7.05 nGyh^{-1} and the average absorbed dose rates due to ^{40}K ranged from 1.59 to 28.74 nGyh^{-1} with a mean range of 9.94 to 20.32 nGyh^{-1}. The total average calculated absorbed dose rate ranged from 8.67 to 52.34 nGyh^{-1}. The mean value of the computed average dose rate for all the sampled area of Kargi was 23.87 nGyh^{-1}. This value was 2.26 times lower than the world average limit of 54 nGyh^{-1} (UNSCEAR, 2000).

Appendix XVIII compares the measured and calculated absorbed dose rates. From this appendix, it is evident that the measured absorbed dose rates are higher that the calculated absorbed dose rates, a fact that could be attributed that the calculated dose rate does not include cosmic rays.

4.3 Hazard Indices

Appendix VIII gives calculations for external (H_{ex}) and internal (H_{in}) hazard indices, representative gamma ($I\gamma$) and representative alpha ($I\alpha$) indices for soil samples for the area under study. Equations 15, 16, 17 and 18 were used in these. Ranges and mean

of external (H_{ex}) and internal (H_{in}) hazard indices, representative gamma ($I\gamma$) and representative alpha ($I\alpha$) indices for soil are given in appendix XII. Respective mean values as well as their standard deviations of representative alpha (I_{α}), representative gamma (I_{γ}), internal hazard (H_{in}) and external hazard (H_{ex}) indices values, as seen from appendix VIII are 0.04 ± 0.01, 0.18 ± 0.04, 0.14 ± 0.04 and 0.12 ± 0.03 with ranges from 0.02 ± 0.01 to 0.05 ± 0.02, 0.13 ± 0.01 to 0.23 ± 0.07, 0.11 ± 0.01 to 0.17 ± 0.05 and 0.09 ± 0.01 to 0.16 ± 0.05 respectively. Ranges can be seen in appendix IX with

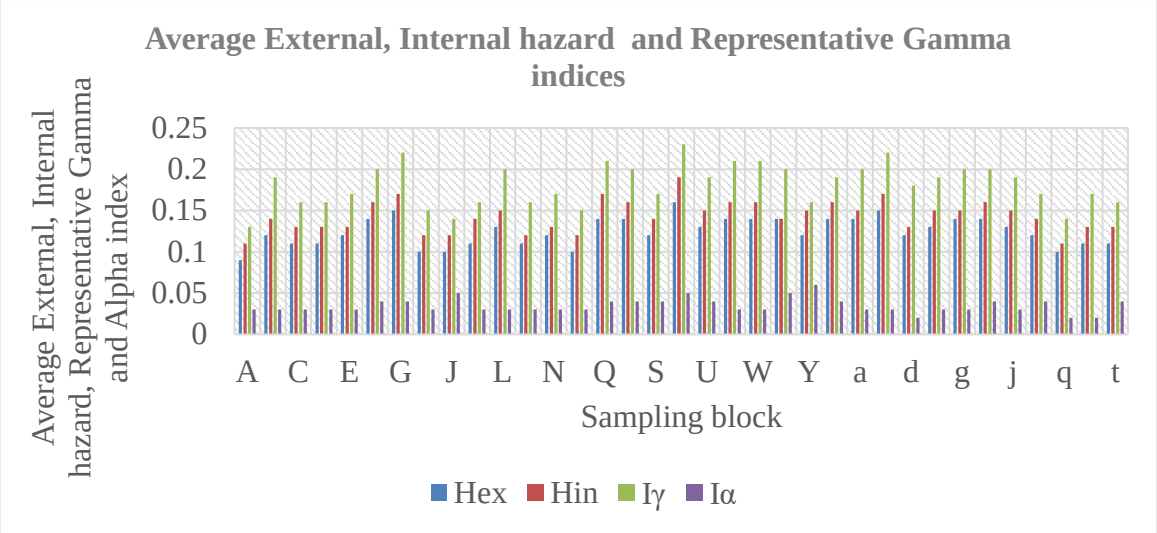

a pictorial representation of hazard indices shown in figure 4.6.

Figure 4.6: Average Soil Sample Values of External and Internal Hazard Index

4.4 Radium Equivalent and Annual Gonadal Equivalent Dose for Soil Samples

Bricks, blocks, sand, stones and soils are considered building materials. Water is used as a mixture to help in binding processes and dries after a short period. The ultimate application of the measured activities in building materials is to give estimates the radiation dose expected to be delivered externally if a building is constructed using these materials. Again, a fatal disease of the blood known as leukemia is caused by destruction of red blood cells due to an increase in Annual Gonadal Equivalent Dose (AGED) which has been known to interfere with the bone marrow. AGED for the resident using such material for building was evaluated using equation 13 and presented in appendix XIX together with radium equivalent dose. From appendix XIX,

the calculated radium equivalent and Annual Gonadal Equivalent Dose (AGED) are shown. Appendix XX gives ranges and averages of the entire researched area. Figure 4.7 gives a pictorial representation of radium equivalent summery of the area for analysed soil samples.

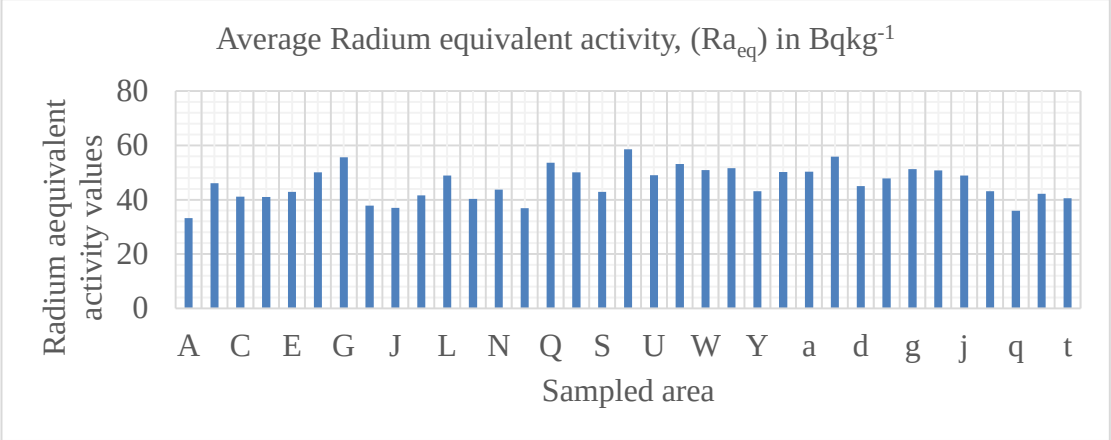

Figure 4.7: Average Soil Sample Values of Radium Equivalent Activity

Table 4.8: Annual Effective Doses ($mSvy^{-1}$) Caused by Water Ingestion of ^{226}Ra, ^{232}Th and ^{40}K for Different Age Groups

Sample code	^{226}Ra ($x10^{-6}$)			^{232}Th ($x10^{-6}$)			^{40}K ($x10^{-6}$)			Total dose ($x10^{-6}$)		
	Infants	Children	Adults	Infants	Children	Adults	Infants	Children	Adults	Infants	Children	Adults
W_1	92.75	90.10	119.25	3.50	12.70	20.15	676.92	338.46	322.84	773.17	441.26	462.023
W_2	116.25	112.93	149.47	77.09	279.44	443.26	518.44	259.22	247.26	711.78	651.59	839.98
W_3	200.31	194.59	257.54	49.93	181.00	287.11	341.73	170.87	162.98	591.98	546.46	707.63
W_4	53.14	51.63	68.33	28.62	103.73	164.54	654.05	327.03	311.93	735.81	482.38	544.80
W_5	86.61	84.14	111.36	233.31	845.74	1341.52	547.76	273.88	261.24	867.69	1203.76	1714.12
W_6	154.32	149.91	198.41	115.05	417.05	661.53	732.25	366.12	349.23	1001.62	933.09	1209.17
W_7	144.61	140.48	185.93	0.00	0.00	0.00	433.50	216.75	206.75	578.12	357.53	392.68
W_8	163.78	159.10	210.57	55.48	201.12	319.01	611.63	305.82	291.70	830.89	666.03	821.28
W_9	195.71	190.12	251.63	127.60	462.56	733.72	574.05	287.03	273.78	897.37	939.71	1259.13
W_{10}	14.82	14.40	19.05	91.10	330.25	523.85	401.72	200.86	191.59	507.63	545.50	734.49
W_{11}	91.72	89.10	117.93	5.55	20.11	31.90	688.31	344.15	328.27	785.58	453.37	478.10
W_{12}	6.90	6.70	8.87	15.77	57.16	90.67	0.00	0.00	0.00	22.67	63.86	99.54
W_{13}	0.00	0.00	0.00	177.83	644.63	1022.51	770.78	385.39	367.76	948.61	1030.02	1390.11
W_{14}	0.00	0.00	0.00	0.00	0.00	0.00	72.22	36.11	34.44	72.22	36.11	34.44
Average	**94.35**	**91.66**	**121.31**	**70.06**	**253.96**	**402.84**	**501.67**	**250.83**	**239.26**	**666.08**	**596.46**	**763.41**
								Global Limit		**0.26**	**0.20**	**0.10**

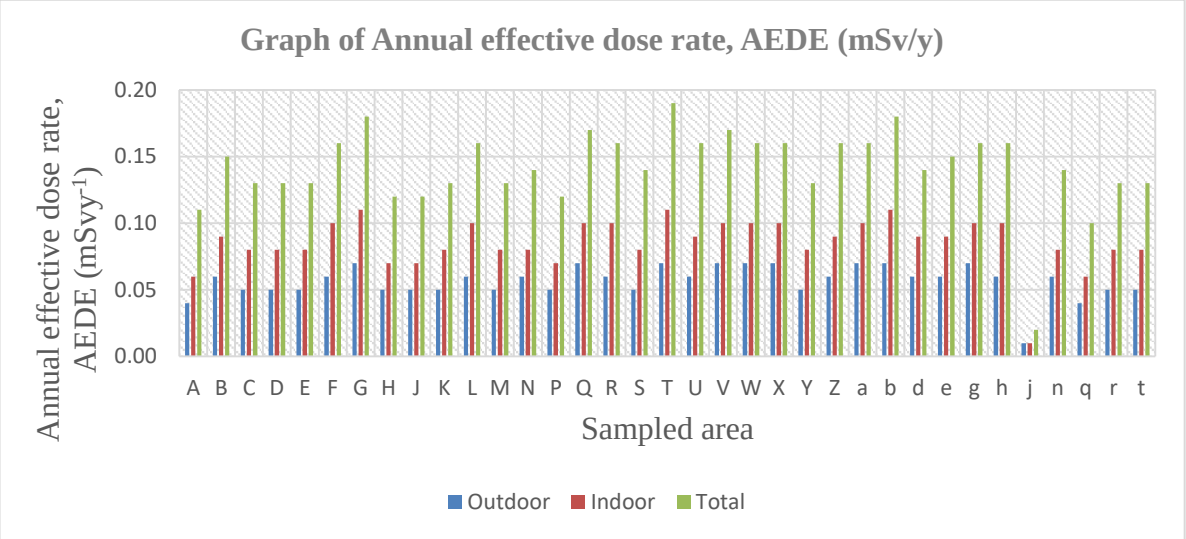

Figure 4.8: Annual Effective Dose Rate Associated with Soil Radio-Activities in the Area under Study

Figures 4.6, 4.7 and 4.8 show bar-graphs of the average values of external and internal hazard index, annual effective dose rate and radium equivalent activity in all the area under investigation. From the figures, it is easy to conclude which location has the least and highest values.

4.5 Annual Effective Dose Rate

Calculations of Annual Effective dose rate from soil sample analysis was done using equations 11 and 12 and presented in appendix XXI and table 4.8, appendix XXII also gives Annual effective dose rates and excess lifetime cancer risk but in a summarized form. These summaries can be seen pictorially in figure 4.8. For excess lifetime cancer risk in soils, equation 14 was used. Annual effective doses ($mSvy^{-1}$) caused by water ingestion of ^{226}Ra, ^{232}Th and ^{40}K for different age groups was calculated using equation 12 and is represented in table 4.8. Figure 4.8 graphically shows outdoor, indoor and total annual effective dose rate associated with soil radio-activities in the area under study.

From appendices XXI and XXII, the annual effective dose rate was from 0.01 to 0.24 $mSvy^{-1}$ (average range: 0.02 to 0.19) $mSvy^{-1}$. All these values (for the sites and areas under study) were less than the recommended value of 1 $mSvy^{-1}$.

4.6 Excess Lifetime Cancer Risk

Assuming that the miners work in mines for 30 years, the risk factor is 0.04 per Sv (ICRP, 2008) and the mean annual effective dose rate is 0.17 $mSvy^{-1}$, then the computed excess lifetime cancer risk is 0.02%. Excess lifetime cancer risk from soil sample analysis was done using equation 14 and presented in appendix XXI, appendix XXII also gives Annual effective dose rates and excess lifetime cancer risk but in a summarized form. A graphical representation of this is given in figure 4.9. The calculated excess lifetime cancer risk for this work is compared with other computed results from different regions and are represented in table 4.9.

Table 4.9: Comparison of Excess Lifetime Cancer Risk from Different Locations

Country	Total Excess Lifetime Cancer Risk (ELCR), %	Reference
Kenya, Kargi	0.050	Current
Kenya, Wagusu	0.020	Aguko *et al.*, (2013)
Nigeria, Delta region	0.004	Agbalagba *et al.*, (2021)
Pakistan, Northern	0.320	Aziz *et al.*, (2014)
Iran, Neyriz	0.490	Azhdarpoor *et al*., (2021)
Global recommendation	0.031	WHO, UNCEAR 2000

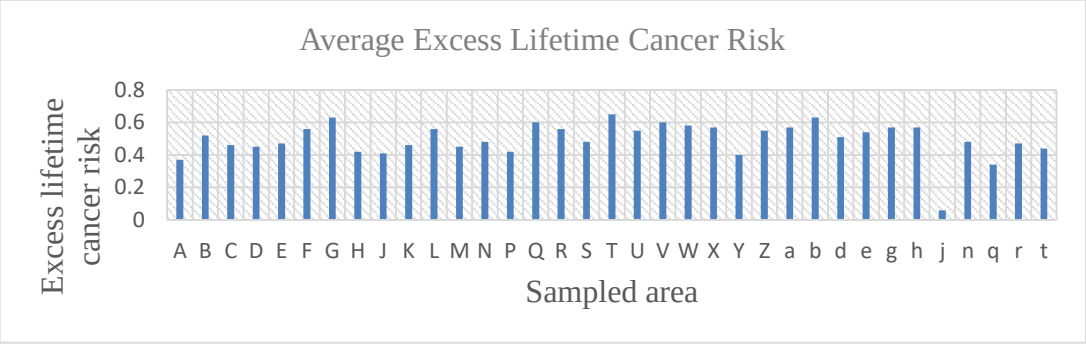

Figure 4.9: Excess Cancer Risk Associated with Soil Radio-Activities in the Area under Study

Excess cancer risk, computed from soil samples showed smaller values hence minimal chance of getting cancer disease.

4.7 Magnetic Data

52 collected magnetic data were corrected using equation 21, together with appendices XXVI, XXVII, XXVIII, XXIX and XXX which were then used to generate appendix XXXI for use in drawing a magnetic anomaly for area under study as shown in figure 4.10. Base station values in appendix XXVIII were used to plot graphs of appendices XXVII, XXVIII, XXIX and XXX for correction purposes of the said appendices. Appendix XXVI is the computed values for IGRF correction. By applying surfer 10 software, kriging technique was used. Values of appendix XXVI were used together with values of appendix XXVIII to draw a magnetic anomaly map for studied area.

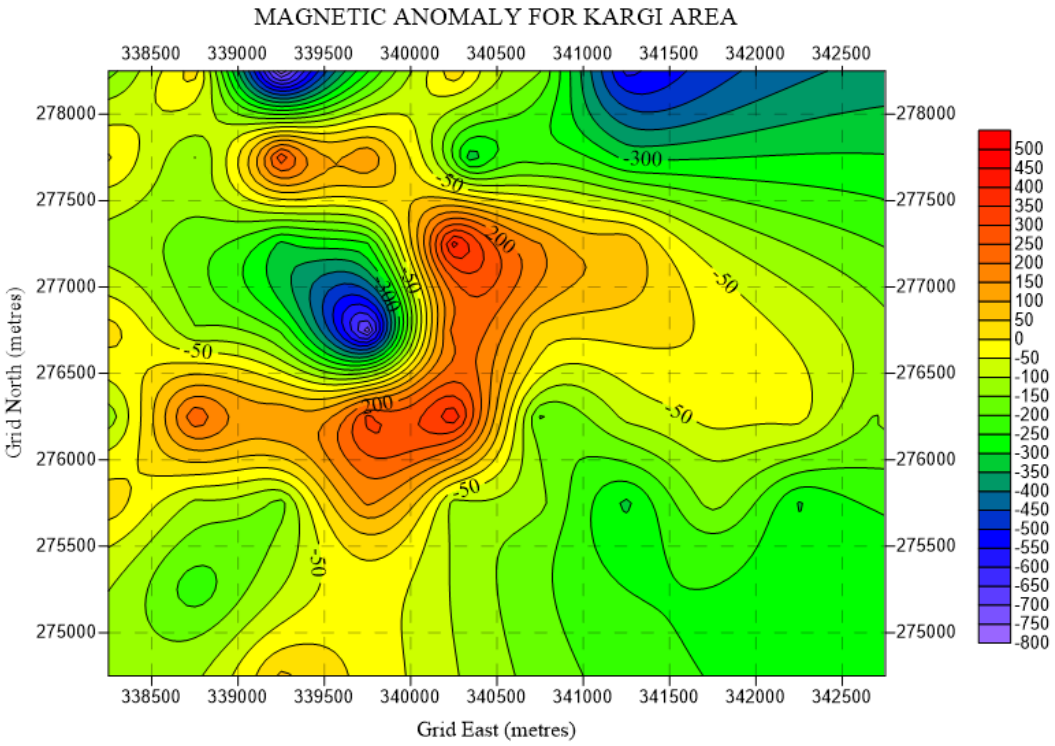

Figure 4.10: Magnetic Anomaly for Kargi

Magnetic anomaly maps shown above showed anomalies between the lows and the highs. It is noted that zero contours give locations of sudden changes in magnetic susceptibility values. Higher amplitude in magnetic intensity suggests the existence of the basement rocks occurring at shallow depth below the surface as seen from the magnetic anomaly map above. Low negative amplitude in magnetic intensity are areas indicating the zones of weakness that suggest existence of geologic structures like faults, fractures and lineaments. Cross-sectioning the area under study with anomalies (figure 4.10) together with equation 29 gave the cross section of the areas as seen in figure 4.11. From the cross-sectioned figure 4.11, Euler Deconvolution diagrams (figures 4.12, 4.13, 4.14 and 4.15) were developed.

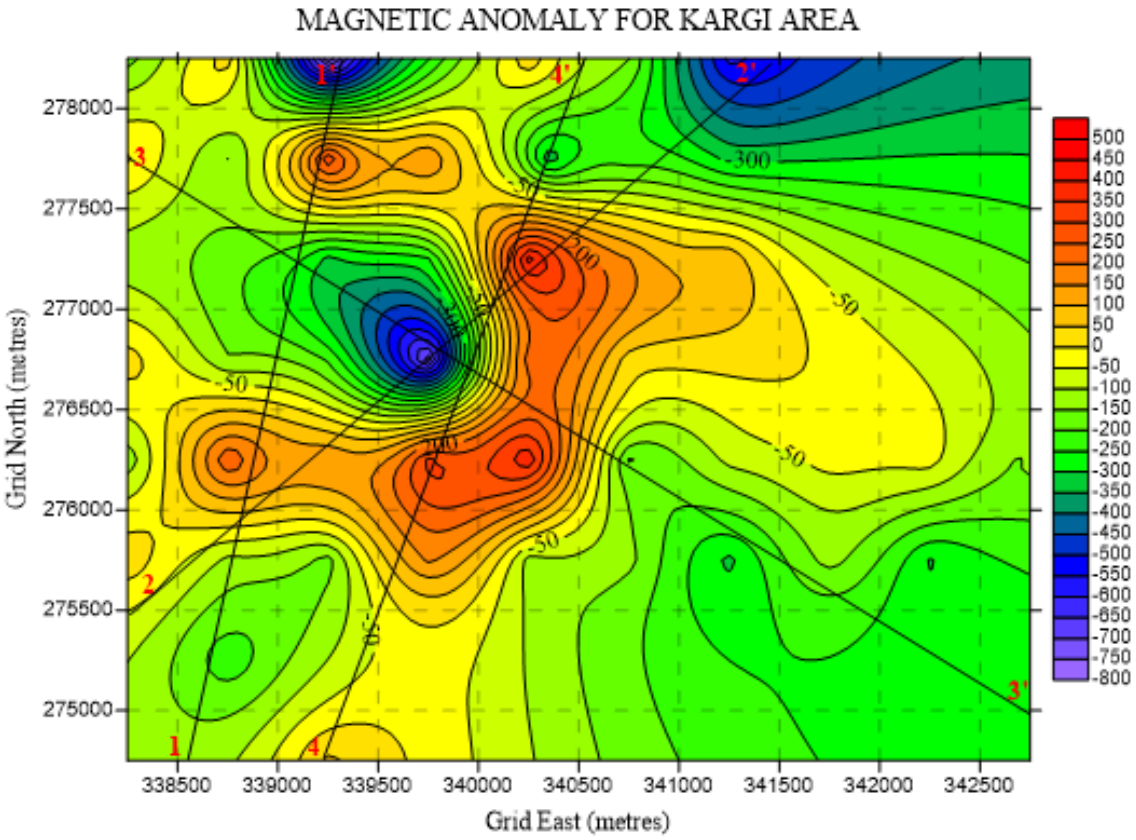

Figure 4.11: Cross-Sectioning of Magnetic Anomaly Map for Kargi

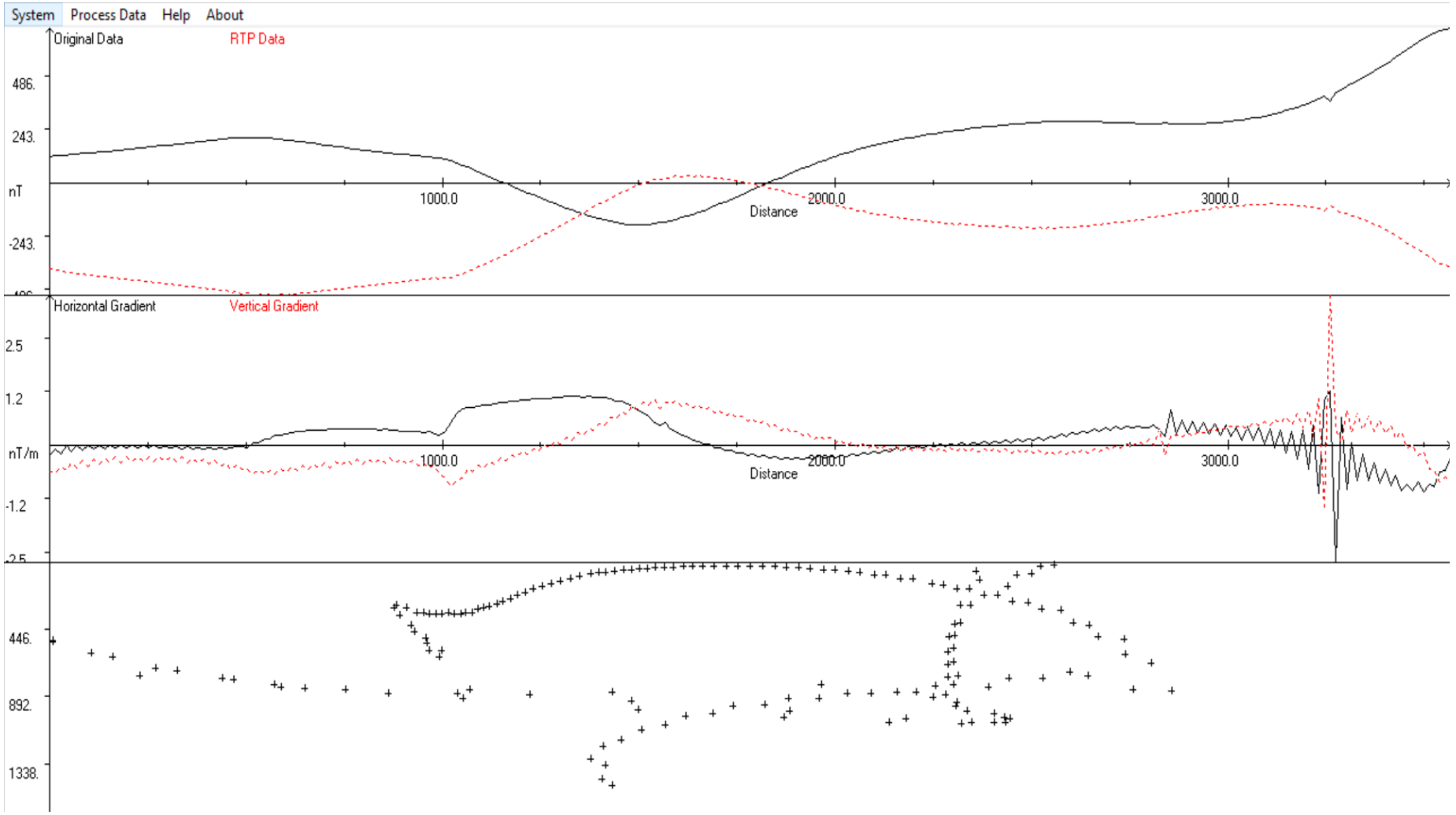

Figure 4.12: Euler Diagram for Section 1-1'

From magnetic profile 1-1'' in figure 4.12, computed solutions map the depth to the subsurface structure. 1.0 structural index was used since it best represents sill edge, dike, or fault with limited throw. The vertical and horizontal gradients highly vary over entire distance along the profile, with an abrupt change between 2.8 km to 3.5 km. Magnetic anomaly source can be seen to be seen all the way from 0 m to about 3 km at depths ranging from subsurface to about 1.5 km.

From magnetic profile 2-2'' in figure 4.13, the vertical and horizontal gradients highly vary over entire distance along the profile, with an abrupt change between 2.3 km to 4.3 km with peaks noticed 3.8 km and 4.1 km. The depth to the magnetic structure is shallowest from 0.5 km to 1.5 km and 3.3 km at a the subsurface. The deepest part of the profile is 1.7 km. The shoulder of the reduction to the pole (RTP) outlines the probable edges of causative structure located at profile distances 0.5 km, 1.3 km, 1.8 km and 2.8 km.

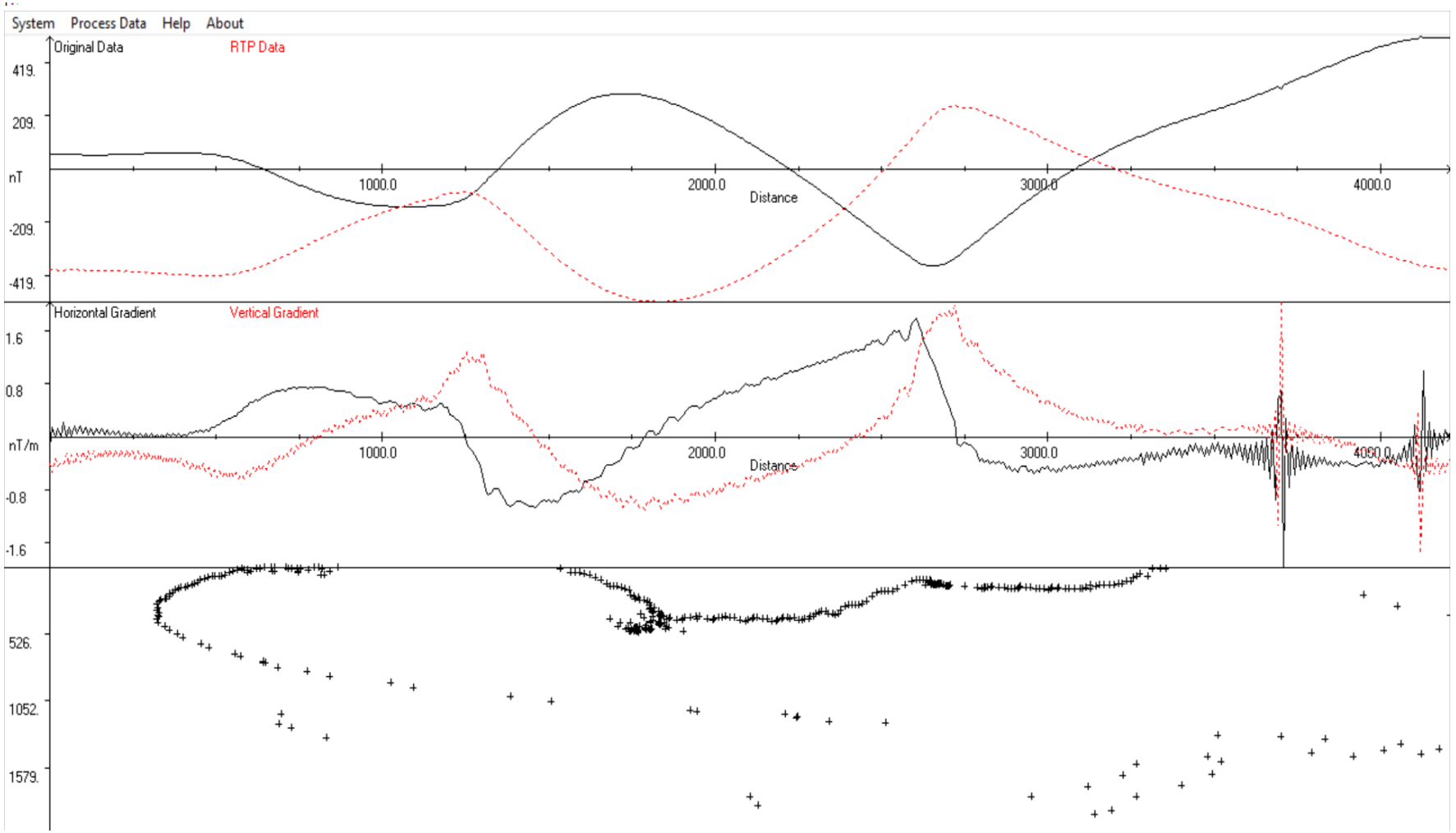

Figure 4.13: Euler Diagram for Section 2-2'

Figure 4.14 gives magnetic profile 3-3'', the horizontal and vertical gradients have no fluctuations over entire distance along the profile. The depth to the magnetic structure is shallowest from 2.3 km to 4.1 km at a subsurface depth. The deepest part of the profile is 2.0 km. The shoulder of the reduction to the pole (RTP) outlines the probable edges of causative structure located at profile distances 0.1 km, 1.3 km, 2.5 km and 4.1 km.

From magnetic profile 4-4'' in figure 4.15, the horizontal and vertical gradients highly fluctuate between 1.0 km to 2.0 km with abrupt changes at the same range with peak at 1.5 km. This may represent sudden lateral change in magnetization over the distance range. The depth to the magnetic structure is at the subsurface from a distance of 1.5 km. The deepest part of the profile is 2.0 km. Fault line/shear noticed between 1.5 km – 2 km surface distance. The shoulder of the reduction to the pole (RTP) outlines the probable edges of causative structure located at profile distances 0.5 km, 1.1 km, 1.6 km, 2.8 km and 3.1 km. The main advantage of using RTP proficiency is that it provided a fast method for imaging approximate depths to subsurface bodies. The approximate source depth locations acquired will be used later for start models in generating forward models.

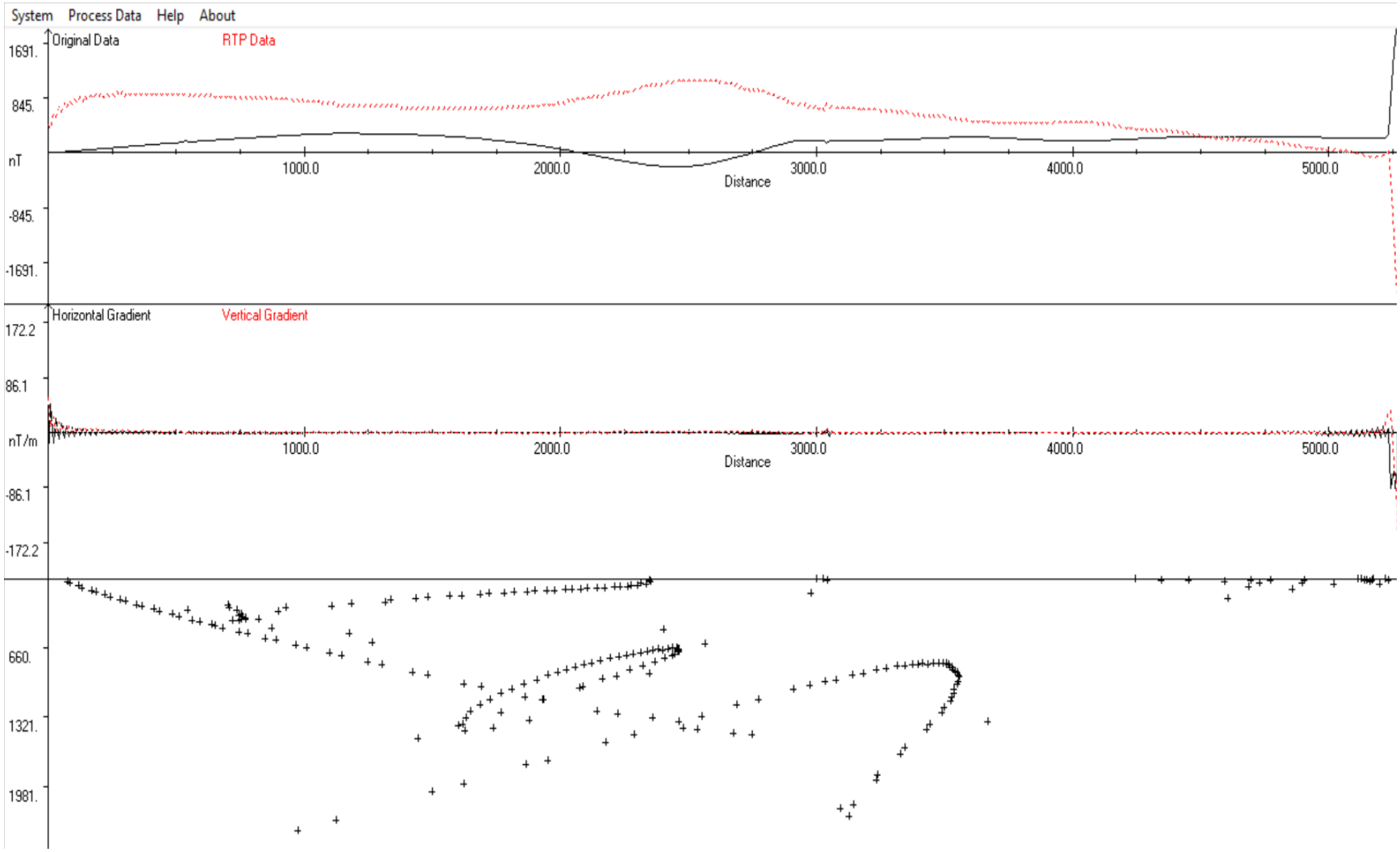

Figure 4.14: Euler Diagram for Section 3-3'

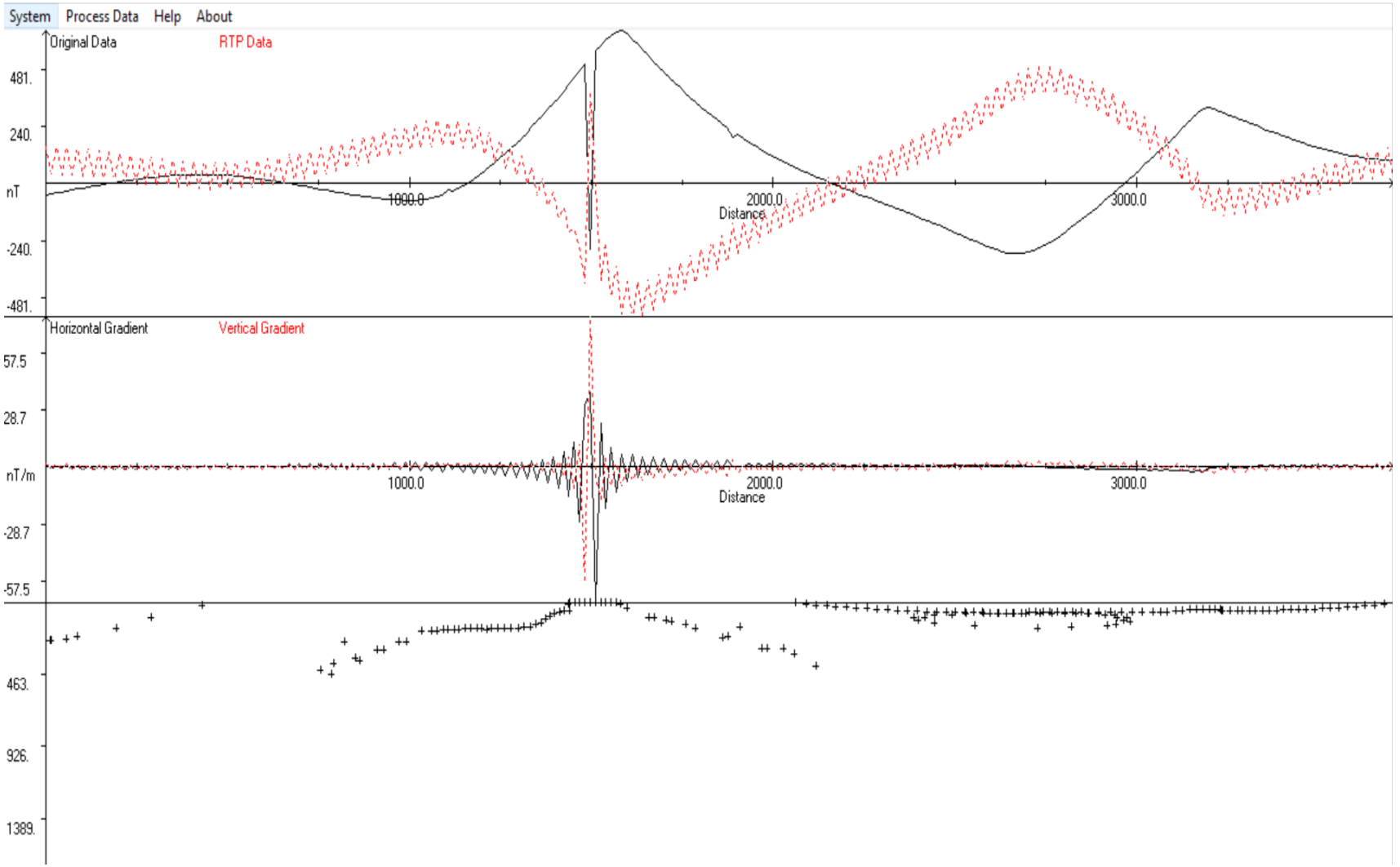

Figure 4.15: Euler Diagram for Section 4-4'

4.8 Magnetic Maps

Obtained magnetometer data along traverses of the eastern side of Kargi was used to come up with Total magnetic intensity (TMI) map. In order to know magnetic intensity ranges of rocks with geologic structures as well as susceptible areas, TMI is used. From appendix XXIV, an amplitude variation betwixt -791.4 nT and 419.9 nT for the Total magnetic intensity map can be seen. In a basement complex, these values have been researched and found not uncommon (Telford *et al*., 1990). The total magnetic intensity varies from one location to another, and this is attributed to the mineral content in the surface and subsurface rocks and its structural mapping. Figure 4.16 shows maps the Total magnetic intensity (TMI) for area studied. A, B and C denoted areas are areas seen as having high amplitude of magnetic intensity; meaning there exist basement rocks at shallow depth below the surface. Low negative amplitude areas marked D in magnetic intensity is an area showing zones of weaknesses and thus suggesting existence of geologic structures like faults, lineaments and fractures.

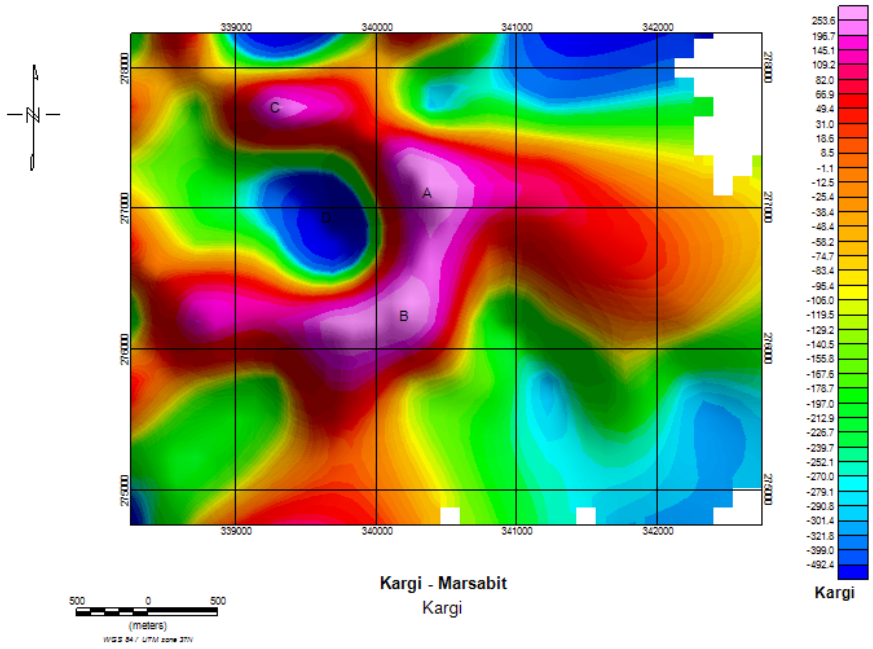

Figure 4.16: Total Magnetic Intensity (TMI) Map of Kargi Area

The varying magnetic intensity suggests varying magnetic materials associated with the rock types in the area. Gunn *et al.*, 1997a notes magnetic anomaly amplitude is

directly proportional to magnetization which is dependent on magnetic susceptibility of the rocks.

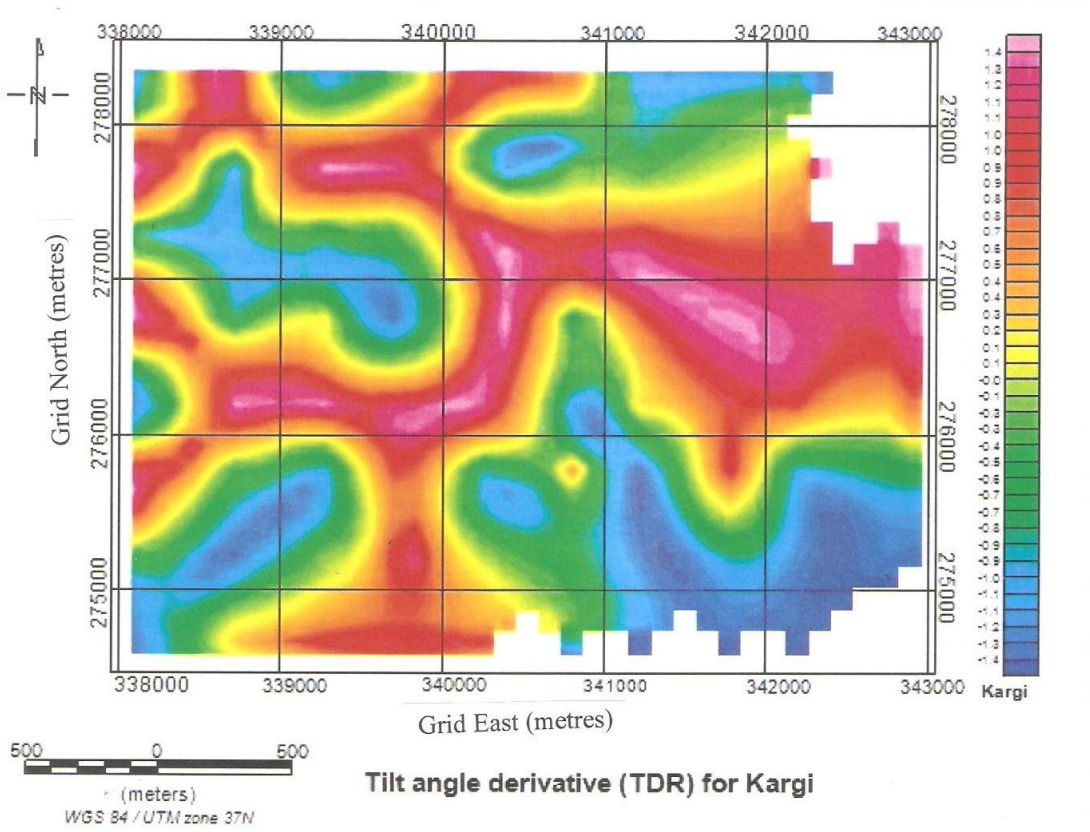

Figure 4.17: Tilt Angle Derivative (TDR) Derived from TMI of the Study Area

Tilt Derivative (TDR) and its Horizontal component (HD_TDR) maps for studied area were got from the tilt derivative filter applied to the TMI grids to determine fault as well as folds, the contacts and edges or magnetic sources' boundary as in figures 4.17 and 4.18, and to enhance both weak as well as strong magnetic anomalies of the area positioning an anomaly directly over its source. TDR of TMI locates the edges of formations and especially at shallow depths by applying the theory that the zero contours are the edges of the formation (Salem *et al.*, 2007). Observation has it that the zero contours approximate locations of sudden changes in magnetic susceptibility values. Yellow colour contours represent zero contour lines, blue colour are areas with lineaments, while red colours are the un-weathered or un-deformed basement. Figure 4.17 shows the resolution of the tilt angle derivative (TDR) in the vertical direction

while figure 4.18 shows the resolution of the TDR in the horizontal direction of the study area. Comparing Figure 4.16 together with Figure 4.18, the TDR image shows different contacts and lineaments in the area.

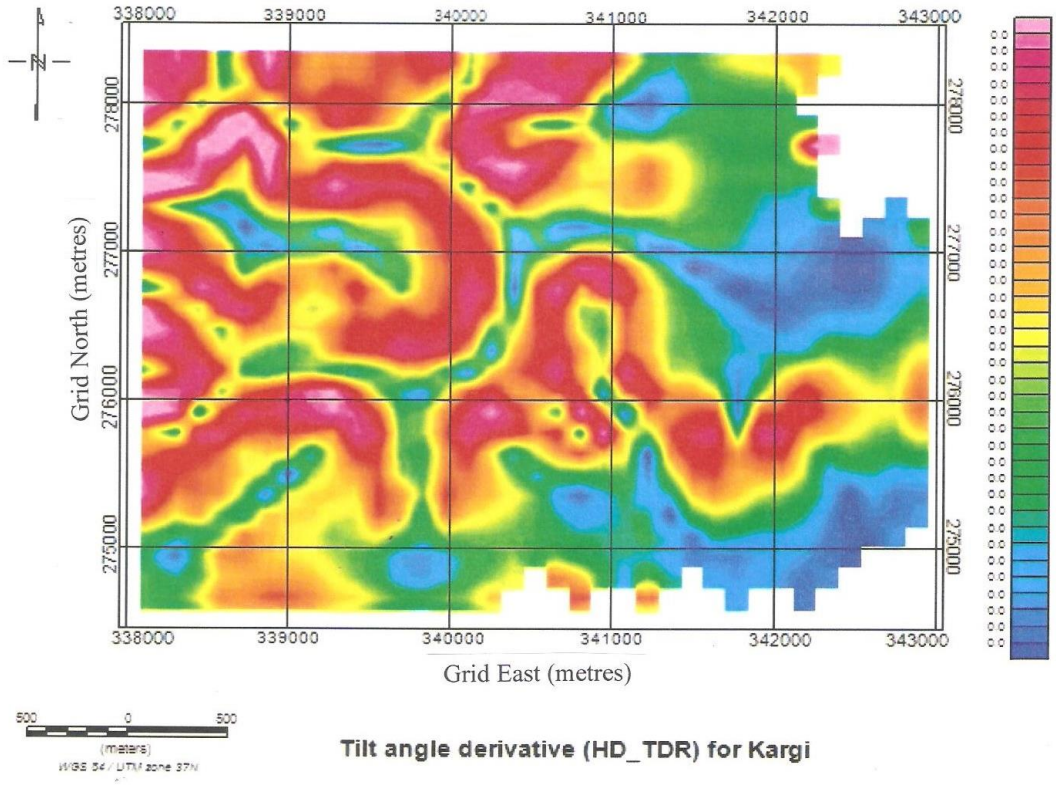

Figure 4.18: Tilt Angle Derivative (HD_TDR) in the Horizontal Direction Derived from TMI of the Study Area

Figure 4.19 shows the Radial Average Power Spectrum (RAPS) for studied area with the total depth estimate to the top of geologic sources that produced the observed anomalies in the magnetic map and were determined using spectral analysis. For the studied area, the depths to the magnetic sources ranges from 100 m to 480 m. These anomalous bodies depths in the area showed that the bodies are closer to the surface since power spectrum depth estimations indicates near surface of the bodies.

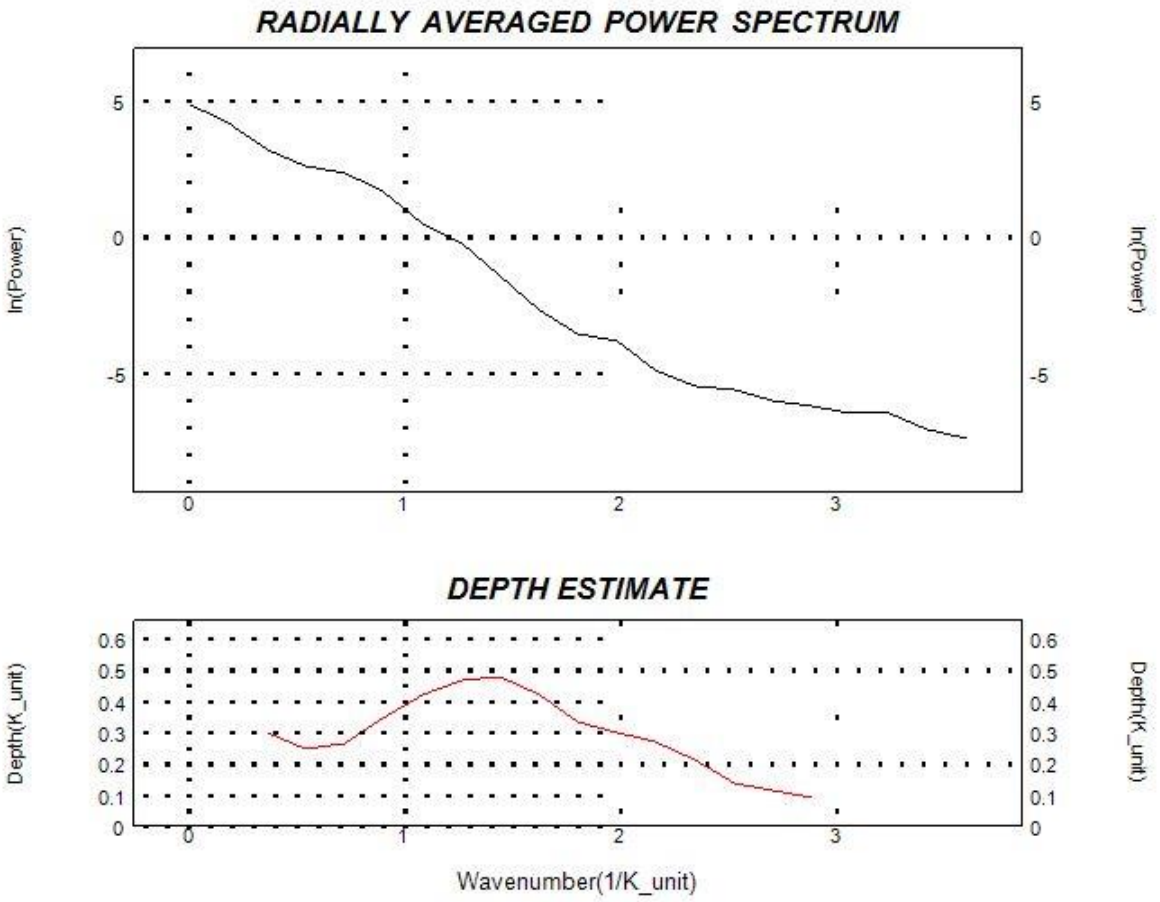

Figure 4.19: Radially Averaged Power Spectrum (RAPS) and Depth Estimate

CHAPTER FIVE

CONCLUSIONS AND RECOMMENDATIONS

5.1 Conclusions

Results from the soil samples study give the arithmetic mean and standard deviation of activities for the area as 354.81 ± 67.06, 7.23 ± 1.67, 8.03 ± 1.91 and 45.90 ± 12.65 $Bq \cdot kg^{-1}$ against the world standard values of 400, 35, 30 and 370 $Bq \cdot kg^{-1}$ for ^{40}K, ^{226}Ra, ^{232}Th together with Ra_{eq} (Lu & Zhang, 2006) respectively. All mean activities for ^{226}Ra, ^{232}Th, ^{40}K as well as Ra_{eq} were less than the recommended global values limits. For water samples tested, the specific activities of ^{40}K, ^{232}Th series (^{232}Th) as well as ^{238}U series (^{226}Ra), expressed in Bql^{-1}. The mean activities for the water source areas were 4.31±2.52, 2.80±2.45, 56.93±2.16 and 11.19±5.74 for ^{226}Ra, ^{232}Th, ^{40}K and Ra_{eq} respectively. 10.0 Bql^{-1}, 1.0 Bql^{-1}, 10.0 Bql^{-1} and 370 $Bqkg^{-1}$ are respectively the worldwide allowable limits for activities. Except for ^{232}Th and ^{40}K average activity values, all other average activity values for ^{226}Ra and Ra_{eq} were less than the worldwide recommended values. For water samples, mean activities for the area studied is 5 times high, low and 2 times high against the worldwide accepted limit for ^{40}K, ^{226}Ra and ^{232}Th respectively. The area generally cannot be classified as a High Background Radiation Area (HBRA) except for the water sources which showed some high elements of the activities.

Mean calculated and measured absorbed dose rates for all soil samples were 23.87 and 82.64 $nGy \cdot h^{-1}$ against the global median value of 54 and 60 $nGy \cdot h^{-1}$ respectively. These evaluated mean values for absorbed dose rates were below recommended values by almost half (for calculated) and about 1.4 times higher (for measured) than the worldwide limit. The ambient dose rate is obtained by measuring γ-ray doses in the air by use of a hand-held radiation survey meter. γ-rays from radioactive materials suspended in the air and from radioactive materials fallen on the ground are both detected, hence, the elevated measured absorbed dose rates. All these soil study values (for the sites and areas under study) were less than the recommended value of 1 $mSvy^{-1}$.

The annual effective dose rate from soil study ranged from 0.01 to 0.24 $mSvy^{-1}$ (average range: 0.02 to 0.19) $mSvy^{-1}$. Annual effective doses ($mSvy^{-1}$) caused by water ingestion of ^{226}Ra, ^{232}Th and ^{40}K for different age groups shows lower levels as given by the global body. that the water is safe for use for all age groups.

For soil samples, Hazard indices (H_{ex}, H_{in}, I_{α} and I_{γ}) values for the studied area were smaller than values recommended of 1 (H_{ex}, H_{in} and I_{γ}) and 0.5 (I_{α}). Radiation risk linked to these soils can be considered negligible making the rocks and soils in the area safe for construction causing no important radiological threat to populace. Because Th/U value in soil samples was higher than the recommended while the mean elemental ratio for Th/U for water sources was lower than 3. The study can therefore conclude that there could have been a fractionation during weathering or involvement of metasomatic activity of the radioelements for the larger area. The elevated radiation level of ^{40}K in some parts of the western side of Kargi, with some ^{238}U and ^{232}Th, suggests that the geologic formation of the area is richer in potassium-bearing minerals, Uranium-bearing-minerals and Thorium bearing-minerals respectively.

Excess cancer risk, computed from soil samples showed smaller values hence minimal chance of getting cancer disease.

The study has shown the importance of radiometric and magnetics methods in effective mapping out of lithologies, characterizing magnetic intensities and radionuclides, delineating subsurface structures¸ anomalous zo magnetic sources. Inspection of the individual Total (TMI) maps revealed the range of the magnetic intensity of the rocks with the infilled geologic materials, geologic structures and areas that are susceptible of intensity with amplitude variation between -791.4 nT and 419.9 nT. The derivative (TDR) with the horizontal component (HD_TDR) showed that the lineament structures to be trending approximately in dipping, vertical and horizontal directions with break in subtle as seen from the shape of the structures. It is evident that the TMI map has similar trends of NE-SW, NW-SE and some perpendicular to the strike direction with those on the TDR and HD_TDR maps. The ranging magnetic intensity suggests ranging magnetic materials associated with the rock types in the area. The radiometric profiles found evidences from the geologic formations about the radiation levels of the area under investigation. Geologic events like intensive

weathering of the feldspar-bearing-minerals in parent rocks into clay particles have been eroded from their source and low enrichment of the parent rocks in potassic feldspar in relation to other feldspar minerals must have caused the radioactivity level K, U and Th in area. Gamma rays among the other radiations have the highest energy and will penetrate several hundred feet in the atmosphere but a few inches of earth attenuate them. Radiation elements must occur in outcrop or sediments to be detected. The concentration and spatial distribution of radioactive elements such as uranium thorium and potassium from the upper 10-60 cm layer of earth's surface having no vegetation may be measured in radiometric surveys.

The elevated radiation level of ^{40}K in some parts of the western side of Kargi as evidenced from the study, with some ^{238}U and ^{232}Th, suggests that the geologic formation of the area is richer in potassium-bearing minerals, Uranium-bearing-minerals and Thorium bearing-minerals respectively. Weathering rate of the parent rocks, terrestrial gamma radiation enrichment in parent rocks, and low fracturing density system of the parent rocks that would have accumulated materials that are non-radioactive could all have accounted for the radioactivity level of the area. Because Th/U value was higher than the recommended, the study can therefore conclude that there could have been a fractionation during weathering or involvement of metasomatic activity of the radioelements. This study also reveals that the mining activities in the nearby study area could have affected the geologic formation causing more fracturing in rocks and pronounced subsurface structures as a result of mining that could have served as passage for leachates from pollutants as well as the level of radiation in the study area.

Nevertheless, the study found that results from analyzed soil and water samples from the study area when compared with international standard show that the area is safe to humans for agricultural practices, drinking, mining and domestic purposes.

5.2 Recommendations

Based on the outcome of this study and conclusions made, it is recommended that:

1. Since Internal, External and Radium Equivalent indices values are lower than the worldwide acceptable limits, these soils and/or rocks are safe to be used in building materials. This is because the inhalation of radon gas coming from these soils together with radiation doses cannot have effect on human health. However, proper ventilation is required as any amount of radiation is still harmful.
2. More research on soil together with waters samples in Kargi area need to be done at different times of the year to check how the concentrations are affected by different weather seasons (metrological parameters) of the year. An example is during rainy season when the waters could be coming from an area with high radionuclides and deposited in the area due to erosion. These waters could also be used by livestock in drinking.
3. It is recommended for similar research to be extended to other counties or other nearby towns to ascertain the level of activity concentration and other radiological parameters.
4. The radiological parameters that have been achieved during the study will be of great value to both the County Government of Marsabit as well as the National Government. Both the county and national governments can use these research findings to sensitive the area residents on safety of staying in the area.

REFERENCES

Aguko, W., Kinyua, R., & Ongeri, R. (2013). Assessment of Radiation Exposure Levels Associated with Gold Mining in Sakwa Wagusu, Bondo District, Kenya. Proceedings of the 8th JKUAT Scientific, Technological and Industrialization Conference, Juja-Kenya, 14- 15 November, 221-228.

Abdelhady, E. (20202). Lecture notes. Retrieved from *http://www.svu.edu.eg › sci › uploads › 2020/03*.

Abdulla, A. R., Nada, F. K., & Nadhim, K. I. (2016). Natural Radioactivity and Associated Dose Rates in Soil Samples in the Destroyed Fuel Fabrication Facility, Iraq. International Journal of Physics, **4**, 50-54.

Agbalagba, E.O., Egarievwe, S.U., Odesiri-Eruteyan, E.A. and Drabo, M.L. (2021) Evaluation of Gross Alpha and Gross Beta Radioactivity in Crude Oil Polluted Soil, Sediment and Water in the Niger Delta Region of Nigeria. Journal of Environmental Protection, **12**, 526-546. https://doi.org/10.4236/jep.2021.128033.

Al-Hamarne, I. F., & Awadallah, M. I. (2009). Soil Radioactivity Levels and Radiation Hazard Assessment in the Highlands of Northern JORDAN. Radiation Measurements, **44**, 102-110. https://doi.org/10.1016/j.radmeas.2008.11.005.

Alpen, (1988). Electromagnetic Radiation. *Principles of Radiation Interactions,* 22.

Arogunjo, A. M., Farai, I. P., & Fuwape, I. A. (2004). Impact of oil and gas industry on the natural radioactivity distribution in the Delta region of Nigeria. Nigeria Journal of Physics **16** (131), 136.

Aviation, Space and Environment Medicine (2003). Medical Guidelines for Airline Travel, 2nd Edition, Section II, supplement. **5** (74), A_1-A_{19}.

Audeen, W. Fentiman, Brian K. Hajek and Joyce E. Meredith (2012). "What are the sources of ionizing radiation"? Retrieved from http://ohioline.osu.edu/rer-fact/rer 22.html.

Avwiri, G. O., & Agbalagba, E. O. (2007). Survey of gross alpha and gross beta radionuclide activity in Okpare–Creek, Delta State, Nigeria. Asian Journal of Applied Science, **7** (22), 3542–3542.

Avwiri, G. O., Osimobi, J. C., Agbalagba, E. O. (2012). Evaluation of radiation hazard indices and excess lifetime cancer risk due to natural radioactivity in soil profile of Udi and Ezeagu local government areas of Enugu State, Nigeria, Comprehensive Journal of Environmental and Earth Sciences. **1**, 1-10.

Avwiri, G.O., Ononugbo, C.P., & Egieya, J. M. (2013). Evaluation of natural radionuclide content in surface and ground water and excess lifetime cancer risk due to gamma radioactivity. Academic Research International, **4** (6), 636-647.

Avwiri, G. O., Ononugbo, C. P., & Nwokeoji, I. E. (2014). Radiation Hazard Indices and Excess Lifetime cancer risk in soil, sediment and water around mini-okoro/oginigba creek, Port Harcourt, Rivers State, Nigeria. *Comprehensive Journal of Environment and Earth Sciences*, **3** (1), 38–50.

Azhdarpoor, A., Hoseini, M., Shahsavani, S., Shamsedini, N and Garehchachi, E (2021). Assessment of excess lifetime cancer risk and risk of lung cancer due to exposure to radon in a middle eastern city in Iran. *Journal of Radiation Medicine and Protection,* **2** (3), 112-116

Aziz, A. Q., Shahina, T, Kamal, U. D., Shahid, M, Chiara, C; Abdul, W (2014). Evaluation of excessive lifetime cancer risk due to natural radioactivity in the rivers sediments of Northern Pakistan. *Journal of Radiation Research Applied Sciences*, **7**, 438-447.

Aziz, F., Miller, R., Giraldo, C., & Carigali, P. (2019, September 17th). Improving deep crustal structure depth interpretation by integrating 2D gravity-magnetic modelling and structural restoration: Offshore Borneo. *Paper presented at the SEG International Exposition and 89th Annual Meeting, San Antonio, USA.*

Beard, L., & Szidarovszky, A. (2018). Estimating depths of magnetic bodies under volcanic cover using Euler deconvolution. *Paper presented at the SEG International Exposition and 88th annual Meeting.*

Beretka, J. & Mathew, P.J., 1985. Natural radioactivity of Australian building materials, industrial wastes and by-products. *Health Physics.* **48**, pp 87 – 95.

Bochicchio, F., Mc Laughlin, J.P. and Piermattei, S. (1995). Radon in Indoor Air European Collaborative Action on Indoor Air Quality. European Commission, Luxembourg, Report EUR 16123 EN.

Canberra, 2013 http://www.canberra.com/default.asp. Accessed 14th March, 2013.

Castro, F., Oliveira, S., deSouza, J., & Ferreira, F. (2019). Constraining Euler deconvolution solutions through combined tilt derivative filters. *Paper presented at the SEG International Exposition and 89th Annual Meeting.*

Cember, H. (1996). Introduction to Health Physics (3rd ed.). New York: McGraw-Hill.

Cherry, Simon R., James A. Sorenson, Michael E. Phelps. *Physics in Nuclear Medicine*. Third edition. Philadelphia, PA: Saunders 2003.Print.

Chikasawa, K., Ishii T., and Sugiyama H, (2001). Terrestrial Gamma Radiation in Kochi Prefecture, Japan. *Journal of Health Sciences.* **47** (4), 362 – 372.

Cristina., R. and Forte, M. (2012). Radioactivity in drinking water: regulations, monitoring results and radiation protection issues. Annali dell'Instituto superior di sanita, **48** (4), 362–373.

Daily Radiation Reports, (2012). Alaskan Red Salmon Results 2011-2013. Retrieved from https://www.radcast.org/category/lab-tests/page/2/.

Dawi, E. L., Tianyou, M. G., Hui, L., & Dapeny, L. (2004). Depth estimation of 2-D magnetic anomalous sources by using Euler deconvolution method. American Journal of Applied Sciences.

Debaje, S. B., Vernekar, K. G., & Ramachandran, T. V. (1996). Study of atmospheric radon-222 concentrations at Pune. Indian Journal of Environmental Protection, **16** (10), 755–760.

EHDORP. (2006). Polonium-210 Fact-sheet 320-091. Washington State Department of Health.

EPA (1995). Representative Sampling Guidance, Vol. 1: Soil, EPA/540/R-95/141, EPA, Washington, DC.

EPA (1999). Final draft for the drinking water criteria document on radium. US Environmental Protection Agency, Washington DC. Tr-1241-85.

EPA (2007). Environmental Protection Agency, United States. Ionizing Radiation Fact book. Office of Radiation and Indoor Air. EPA-402-F-06-061

Factsheet no. 10 (2002). Background Radiation: Natural versus Man-Made. *Washington State department of health.* Pages 1-7.

Fedi, M., & Mastro, S. (2018). Bounded-Region Wavelet spectrum: a new tool for depth estimation of gravity and magnetic data. Paper presented at the SEG International Exposition and 88th annual Meeting, Napoli, Italy.

Felipe, F., & Valeria, C. (2017). What to expect from Euler deconvolution estimates for isolated sources. Paper presented at the 15th International Congress of the Brazilian Geophysical Society, Rio de Janeiro, Brazil.

Girigisu S., Ibeanu I.G.E., Adeyemo D.J., and Oko S. (2012). Determination of Heavy Metals and Other Elements in Artisanal Gold Mining Soils. *American Journal of Applied Sciences.* **9** (7), 1014-1019.

Girigisu S., Ibeanu I.G.E., Adeyemo D.J., Onoja R.A., Bappah I.A. and Oko S. (2013). Assessment of radiological levels in soils from Bagega artisanal gold mining exercises at Bagega Zamfara State, Nigeria. *Archives of Applied Science Research*. **5** (3), 204-210.

Githiri, J. G., Patel, J. P., Barongo, J. O. and Karanja, P. K. (2011). Application of euler deconvolution technique in determining depths to magnetic structures in Magadi area, southern Kenya rift. *Journal of Agriculture, Science and Technology*. **13** (1), 142-156.

Gandhi S.M. and Sarkar B. C. Essentials of Mineral Exploration and Evaluation, 2016

Gunn, P., Maidment, D. and Milligan, P. 1997a. Interpreting aeromagnetic data in areas of limited outcrop. *AGSO Journal of Australian Geology & Geophysics*. **17** (2), 175-185.

Hany, E. and Abdallah, I. A. E. (2014). Natural Radioactivity in Water samples from Assiut city, Egypt. International Journal of Pure and Applied Sciences and Technology, **22** (1), 44-52.

Harb S. (2004). *On the Human Radiation Exposure as Derived From the Analysis of Natural and Man-made Radionuclides in Soil,* Ph.D. Thesis, Hannover University.

Harb, S., Salehel K. Din, Aaady A. and Mostaf. M. (2010). *Activity concentration for surface soil samples collected from Armant, Qema, Egypt*. Proceedings of the 4th Environmental Physics Conference 49-57.

Hassan, S. F., Mahmoud, M. A. M., & El-Rahman, M. A. (2016). Effect of Radioactive Minerals Potentiality and Primordial Nuclei Distribution on Radiation Exposure Levels within Muscovite Granite, Wadi Nugrus, Southeastern Desert, Egypt. Journal of Geoscience and Environment Protection, **4**, 62-78. Retrieved from https://doi.org/10.4236/gep.2016.43006.

Helmut Fischer (2003). "Radioisotopes in Soil". Retrieved from http://www.physics.purdue.edu/~sergei/classes/phys3421/compton.pdf.

Hennery S. and John R.A. (1972). *Introduction to Atomic and Nuclear Physics,* Fifth edition, Holt, Rineart and Winston INC.

Hong, L., Jianbao, Y., Hui, L., Pengfei, X., & Sinopec Geophysical Research Institute, C. (2017). Gravity and aeromagnetic data interpretation of the Xiongxian geothermal system, China. Paper presented at the SEG International Exposition and 87th Annual Meeting.

Manyattas of death. Retrieved from https://www.standardmedia.co.ke/article/2000095804/up-to-500-deadand-counting-as-mystery-cancer-devastates-marsabit.

IAEA TECDOC 1363 (2003). Guidelines for Radioelement Mapping Using Gamma Ray Spectrometry Data. Vienna: International Atomic Energy Agency.

IAEA-TECDOC-1660. (2011). Exposure of the Public from Large Deposits of Mineral Residues. *International Atomic Energy Agency.*

IAEA TECDOC 486 (2019). Guidelines on Soil and Vegetation Sampling for Radiological Monitoring. Vienna: International Atomic Energy Agency.

Ibrahim N.M., Abdel-Ghani A.H., Shawky S.M., Ashraf E.M., Farouk M.A. (1993). Measurement of radioactity levels in soil in the Nile delta and middle Egypt. *Health Physics* 64.

Ibrahim N.M. (1999). Natural activities of ^{238}U, ^{232}Th and ^{40}K in building materials. *Journal on Environmental Radioactivity* 43.

ICRP (2008). The 2008 Recommendations of the International Commission on Radiological Protection. ICRP Publication 107. Annals of the ICRP, 38 (3).

ICRP (2012). Compendium of Dose Coefficients based on ICRP Publication 60. ICRP Publication 119. Ann. ICRP 41(Suppl.).

Irunkwor, T. C. and Abanjo, N. (2022). Determination of Elemental Concentration of Natural Radionuclide in Soils of Industrial Communities, South-South Nigeria. *United International Journal for Research & Technology*. **11**(3), 60-74.

Jackson S.A (1992). Estimating radon potential from an Aerial radiometric survey, *Health Physics, The radiation protection journal,* 62.

Jiao, L., & Lei, Y. (2019). Curie point depth inversion and its potential application to geothermal resource exploration. Paper presented at the International Workshop on Gravity, Electrical & Magnetic Methods and Their Applications, Xi'an, China.

John, S. A., & Paolo, G. (1970). Gamma-Ray Spectrometry of Rocks: Methods in Geochemistry and Geophysics. 1-57.

Karahan G. and Bayulken A. (2000). Assesment of gamma dose rates around Istanbul (Turkey). *J. Environmental Radioactivity*, **47**, 221-231.

Kearey, P., Brooks, M., & Hill, I. (2002). An introduction to geophysical exploration. Iowa, USA: Iowa state university press.

Kinyua R. Atambo V. and Ongeri R.M.(2011). Activity concentrations of ^{40}K, ^{232}Th, ^{226}Ra and radiation exposure levels in Tabaka soapstone quarries of the Kisii region, Kenya. *African Journal of Environmental Science and Technology* **5**, 682-688.

Kiss, J.J., E. de Jong and J.R. Bettany (1988). The distribution of natural radionuclides in native soils of Southern Saskatchewan, Canada. *Journal of Environmental Quality.* **17**, 437-445.

Littlefield T.A. and Thorley N. (1974). *Atomic and Nuclear Physics,* Third edition. Van Nostrand Reinhold Company, London, UK.

Lowrie, W. (2007). Fundamentals of Geophysics (Second ed.). Newyork: Cambridge University Press.

Lu, X. W., & Zhang, X. L. (2006). Measurement of Natural Radioactivity in Sand Samples Collected from the Baoji Weihe Sands Park, China. Environmental Geology, **50**, 977-982. https://doi.org/10.1007/s00254-006-0266-5.

Maher O. El-Ghossain and Raed M. Abu Saleh (2007). Radiation Measurements in Soil in the Middle of Gaza-Strip Using Different Type of Detectors, *The Islamic University Journal (Series of Natural Studies and Engineering)*, **15**, 23-37.

Mahlobo M.J. (1995). Radon measurement in Swaziland with the Solid State Nuclear Track Detector. *Environmental Radioactivity* **27**, 265-268.

Medical News Today, Newsletter. (2016). Cancer Oncology. Retrieved from http://www.medicalnewstoday.com/info/cancer-oncology.

Melo, F., & Barbosa, V. (2018). Correct structural index in Euler deconvolution via baselevel estimates. Geophysics, 83(6), J87-J98. doi: 10.1190/GEO2017-0774.1

Meltem, D. and Gursel, K (2010). Natural radioactivity in various surface waters in Adana, Turkey, Desalination, **261**, 126-130.

Meisenhelder, J. and S. Bursik. (2018). Radiation Safety and Measurement. Current Protocols Essential Laboratory Techniques 16, e22.

Miglierini, Marcel. "Detectors of Radiation". E. Wigner Course on Reactor Physics Experiments. Bratislava, Slovakia. 27th April – 15th May, 2004. Retrieved from http://www.reak.bme.hu/nti/Education/Wigner_Course/2004/WignerManuals/Bratislava/detectors.pdf.

Monika, S., Leszek, P., & Marcin, Z. (2010). Natural Radioactivity of Soil and Sediment Samples Collected from Postindustrial Area, Poland. Polish Journal of Environmental Studies, **19**, 1095-1099.

Mustapha A.O. Narayana D.G.S. Patel J. P. and Otwoma D. (1997). *Natural radioactivity in some building materials in Kenya and Contributions to the indoor external doses*. Radiation protection dosimetry 71:

Mustapha, A. O. (1999). Assessment of Human Exposures to Natural Sources of Radiation in Kenya. PhD Thesis, Nairobi: University of Nairobi. https://doi.org/10.1093/oxfordjournals.rpd.a032637.

Nagaraja, K., Prasad, B. S. N., Madhava, M. S., Chandrashekara, M. S., Paramesh, L., Sannappa, J. & Kamra, A. K. (2003). Radon and its short-lived progeny: variations near the ground. Radiation measurements, **36** (1-6), 413–417.

Nazaroff W. W. (1992). Radon transport from soil to air. *Reviews of Geophisics.* **30** (2), 137-160.

Njinga, R., Ibrahim, V., & Ishoryiyi, I. (2015). Radioactivity analysis in underground drinking water sources in Niger State University of Nigeria. Pollution, **1** (3), 315–324.

Nnenesi A. Kgabi, Sipho A. Mokgethi and Amanda Bubu (2009). Atmospheric Radioactivity Associated with Gold Mining Activities in the North West Province of South Africa. *European Journal of Scientific Research* **33** (4) 594-605.

Nyakundi, E. R., Githiri, J., & Ambuso, W. (2017). Geophysical investigation of geothermal potential of the Gilgil area, Nakuru county, Kenya using gravity. *Journal of geology and geophysics,* **6** (2).

doi:10.4172/2381-8719.1000278.

Nyakundi, E. R., Githiri, J., & K'Orowe, M. (2022). Geothermal heat sources characterization and mapping using heat flow, gravity, and magnetics in Eburru, Kenya. Ph.D. Thesis, Jomo Kenyatta University of Agriculture and Technology.

Obed, R. I., Farai, I. P., & Jibiri, N. N. (2005). Population Dose Distribution Due to Soil Radioactivity Concentration Levels in 18 Cities across Nigeria. *Journal of Radiological Protection*, 25, 305. https://doi.org/10.1088/0952-4746/25/3/007.

Oborah, K. A., Hashim, N. O., Migwi, C. M. and Rotich, C (2024). Assessment of radioactivity concentration for building materials used in Babadogo Estate, Nairobi City County, Kenya. *Radiation Protection Dosimetry*, **200** (2), 201–205. https://doi.org/10.1093/rpd/ncad293.

OECD (1979). Organisation for Economic Coorporation and Development. Exposure to Radiation from the natural radioactivity in building materials. Nuclear Energy Agency; Paris France.

Okeyode, I. C. and Akanni, A. O. (2009). Determination of some physical parameters of Olumo rock, Abeokuta Ogun-State, Nigeria. *Indian Journal of Science and Technology*, **2** (7), 6–10.

Okpoli, C.C. and Akingboye, A.S. 2016. Magnetic, Radiometric and Geochemical Survey of Quarry Sites in Ondo State, Southwestern, Nigeria. International Basic and Applied Research Journal, Volume 2, Issue no. 8, pp. 16-30.

Otton, J. K. (1994). National Radioactivity in Environment. Retrieved from http://energy.usgs.gov/factsheets/radioactivity.

Parasnis, D. S. (1986). Principles of applied geophysics. Newyork, USA: Chapman and Hall Ltd.

Pawan, D., Ramprasad, T., Ramana, M. V., Desa, M., & Shailaja, B. (2007). Automatic interpretation of magnetic data using Euler deconvolution with nonlinear background. Pure and Applied Geophysics, **164**, 2359-2372.

Obid, R. Hussain, & Hamza, H. Hussain. 2011. Natural Occurring Radionuclide Materials. Radioisotopes - Applications in Physical Sciences, 1. Https://Doi.Org/10.5772/20562

Radioactivity in minerals. Retrieved from https://webmineral.com/help/Radioactivity.shtml#:~:text=This%20table%20lists%20all%20of,neutrons)%20from%20the%20parent%20isotope.

Raghu, Y., Ravisankar, A., Chandrasekaran, P. (2017). Assessment of Natural Radioactivity and Radiological Hazards in Building Materials Used in the Tiruvannamalai District, Tamilnadu, India, Using Statistical Approach. Journal of Taiban University for Science, **11**, 523-533. https://doi.org/10.1016/j.jtusci. 2015.08.004.

Reid, A. B., Allsop, J. M., Granser, H., Millett, A. J., & Somerton, W. I. (1990). Magnetic interpretation in three dimensions using Euler deconvolution. Geophysics, **55**, 80-91.

Reid, A. B., & Thurston, J. B. (2014). The structural index in gravity and magnetic interpretation: Errors, uses, and abuses. Geophysics, **79**, J61-J66.

Reconnaissance, 1987. Ministry of Environment and Natural Resources, Mines and Geological department, Republic of Kenya, Report 108.

Reynolds, J. M. (1998). An introduction to applied and environmental geophysics. Chichester, England: John Wiley & sons Ltd.

Rodgers, D.W.O and A.F. Bielajew, Monte Carlo Techniques of Electron and Photon Transport for Radiation Dosimetry, in Vol. III of "Dosimetry of Ionization Radiation" editors: K. Kase, B Bjarngard and F.H. Attix. Academic press, New York. 1990: 427-539

Rowland R.E. (1993). Low-Level Radium Retention by the Human Body; A Modification of the ICRP publication20 Retention Equation, *Health physics*, **65**:507 – 513.

Salam A.M., Said A.F., Hassan S.F., and Mahamed W.S.M (2010). *Assessment of the Environmental Impacts and Health Hazards Indices at Wadi Sahu Area, Sinai, Egypt.* In: Nasr City. Proceedings of Tenth Radiation Physics & Protection Conference, Cairo, Egypt. Pp. 145-158.

Salem, A., Williams, S., Fairhead, J., Ravat, D. and Smith, R. 2007. Tilt-depth method: a simple depth estimation method using first-order magnetic derivatives. The Leading Edge, **26**, 1502-1505.

Sannappa J., Paramesh L. and Venkataramaiah P (1997). Seasonal variation in the rate of radon exhalation from soil in Mysore. *Indian Journal of Physics* **71B** (5), 613-618.

Sannappa J., Paramesh L. and Venkataramaiah P (1999). Study of radon exhalation in soil and air concentrations. *Indian Journal of Physics* **73B**: 629-639.

Schery S.D. and Wasiolok M.A. (1998). Modeling Radon Flux from the Earth's surface. In: *Radon and Thoron in the Human Environment.* World Scientific Publishing, Singapore, pp. 207-217.

Schubert M. and Schulz H., (2002). Diurnal radon variations in the upper soil layers and at the soil-air interface related to meteorological parameters. *Health Physics* **83** (1), 91-96.

Sing S., Sing B. and Kumar A. (2003). Natural Radioactivity measurements in soil samples from Hamirpur district. *Radiation Measurement* 36.

Sing S., Mehra R. and Sing K. (2005). *Atmospheric Environment* **39** (40), 7761-7767.

Shenber M.A. 1996. "Measurement of Natural Radioactivity Levels in Soil in Tripoli". *Journal on Application Radiation* **48** (1) 147-148.

Spector, A., & Grant, F. S. (1970). Statistical models for interpreting aeromagnetic data. Geophysics, **35** (2), 293-302.

Survey of Kenya (2017). Retrieved from https://lands.go.ke

Taskin, H., Karavus, M., Ay, P., Topuzoglu, A., Hidiroglu, S., & Karahan, G. (2009). Radionuclide Concentrations in Soil and Lifetime Cancer Risk Due to Gamma Radioactivity in Kirklareli, Turkey. Journal of Environmental Radioactivity, **100**, 49-53. https://doi.org/10.1016/j.jenvrad.2008.10.012.

Telford, W.M., Geldart, L.P. and Sheriff, R.E. 1990. Applied Geophysics (Second edition). Cambridge University Press.

Tzortzis, M., E. Svoukis and H. Tsertos (2004). A comprehensive study of natural gamma radioactivity levels and associated dose rates from surface soils in Cyprus. *Radiation Protection Dosimetry Journal.* **109**, 217-224.

Tufail M., Ahmad N., Khan M.A., Zafar M.S. and Khan H.A., (1992). Effective dose equivalent rate for the respiratory tract from daughter products of radon, *Journal of Islamic Academy of Sciences* **5** (2), 136-141.

Tzortzis, M., & Tsertos, H. (2004). Determination of Thorium, Uranium and Potassium Elemental Concentrations in Surface Soils in Cyprus. Journal of Environmental Radioactivity, **77**, 325-338. https://doi.org/10.1016/j.jenvrad.2004.03.014.

UNSCEAR 1988. Effects and Risks of Ionizing Radiation. *The United Nation Scientific Committee on the Effects of Atomic Radiation Sources to the General Assembly with Annexes,* United Nations publication, New York.

UNSCEAR (1993). Sources and Effects of Ionizing Radiation. *United Nation Scientific Committee on the Effects of Atomic Radiation Sources to the General Assembly with Annexes, Effects and Risks of Ionizing Radiation,* United Nations publication, New York.

UNSCEAR (2000). Sources and Effects of Ionizing Radiation. *United Nation Scientific Committee on the Effects of Atomic Radiation Sources to the General Assembly with Annexes, Effects and Risks of Ionizing Radiation,* United Nations publication, New York.

UNSCEAR (2008). Sources and Effects of Ionizing Radiation. *United Nation Scientific Committee on the Effects of Atomic Radiation Sources to the General Assembly with Annexes, Effects and Risks of Ionizing Radiation,* United Nations publication, New York.

Updegraff, D. and Hoedl, S. A. Nuclear Medicine without Nuclear Reactors or Uranium Enrichment. Centre for Science, Technology and Security Policy, American Association for the Advancement of Science, 2013. Print.

USEPA. (2010). Exposure Pathways. Retrieved February 2, 2017, from http://www.epa.gov/rpdweb00/understand/pathways WHO, World Health Organisation (2004). Guidelines for Drinking Water Quality: Radiological aspects, at http://www.who.int/water_sanitation_health/dwq/gdwq3rev/en/S.

Vallyathan, V. V. Castraova, D. Pack, S. Leonard and J. Shumaker (1995). Freshly fractured quartz inhalation leads to enhanced lung injury and inflammation. Potential role of free radicals. Am. J. Respir. Crit. Care Med., **152,** 1003-1009. PMID: 7663775.

WHO, World Health Organisation (2006). Guidelines for Drinking Water Quality: 3rd edition. Chapter 9; Radiological aspects. at http://www.who.int/water_ sanitation_health/dwq/gdwq3rev/en/index.

WHO, World Health Organisation (2008). Guidelines for Drinking Water Quality, 3rd edition in cooperating the 1st Agenda vol. 1 Recommendations; Radiological aspect Geneva: WHO Geneva.

WHO, World Health Organisation (2011). Guidelines for Drinking Water Quality. Fourth edition in cooperating the 1st and 2nd Agenda vol. 1 Recommendations; WHO Geneva.

Whicker F. W., and Schults V. (1982). Radioecology: Nuclear Energy and the Environment. CRC Press, Boca Raton.

WR. (1998). Heavy metals and healthy. World Resources Institute, Washington, D.C.

Y.I. Zakari, R. Nasiru and M.A. Abdullahi (2013). Determination of Absorbed and Annual Effective Doses around Birnin Gwari Artisanal Goldmine, Kaduna State, Nigeria. *Journal of Environmental and Earth Sciences.* **5** (5): 252-255.

APPENDICES

Appendix I: Samples Collection

a). Collection of soil/rock samples and background radiation measurements

b). Magnetic readings

Appendix II: Sample Preparation Processes

a). Sun drying of soil and rock samples

b). Manual grinder and wire mesh sieve

c). Labelling of sieved soil samples

d). Prepared soil samples ready for oven drying

f). Sieved soil samples being dried in an oven

g). Dried soil samples cooled in air at room temperature

e). Sieved soil samples in an oven

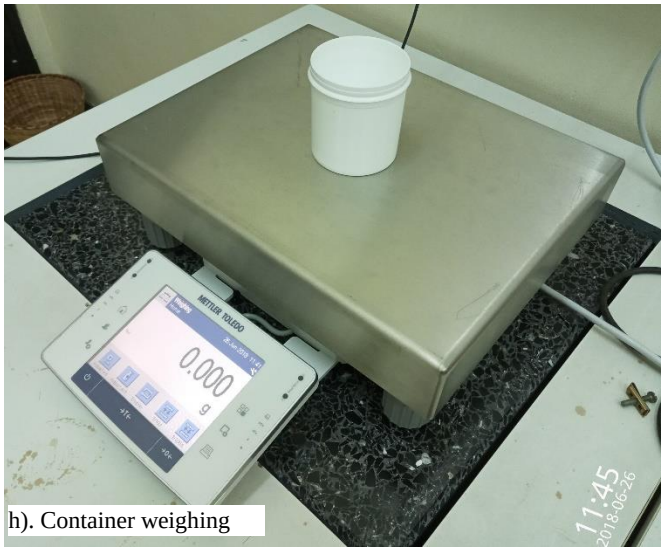

h). Container weighing

i). Dried cooled soil samples weighed, closed and labelled

i). Weighed, closed and labelled soil samples to be kept for 30 days

Appendix III: Samples Collection and Preservation

a). Nitric acid for water sample preserving

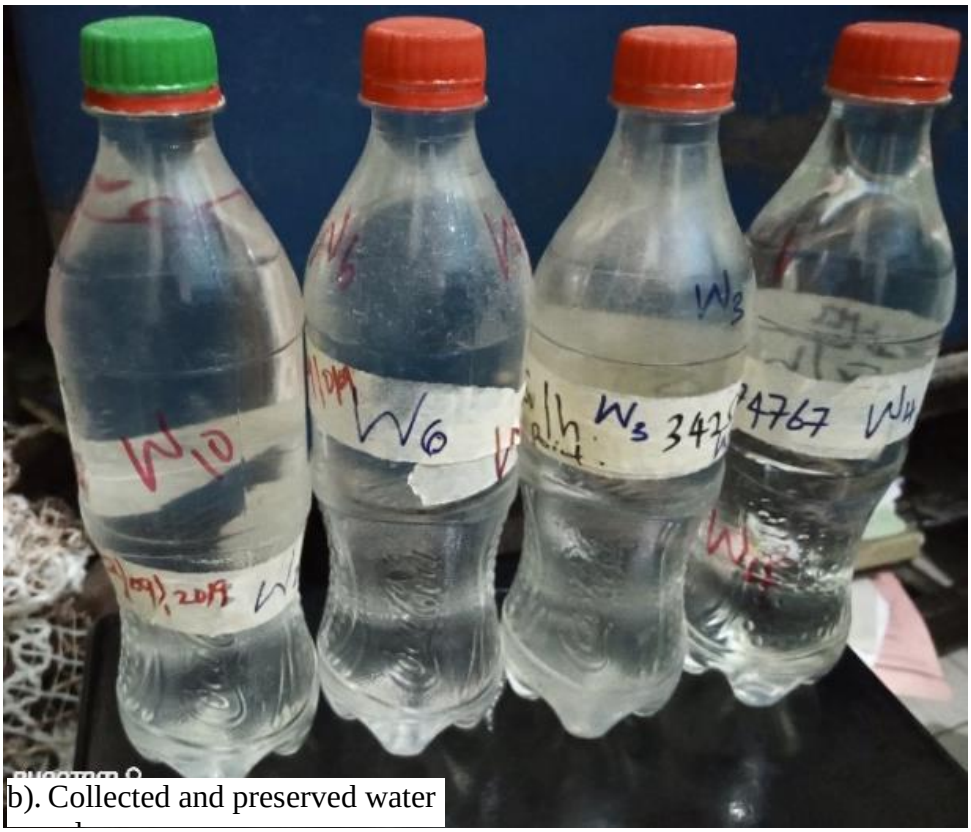

b). Collected and preserved water

Appendix IV: Absorbed Dose Rate Measuring Equipment (a). Thermo Scientific Radiameter, Model FH 40G-L10 (b). Wilnos NDT Radiameter, Model X5Cplus

(a)

(b)

Appendix V: Germanium Detector of EG&G ORTEC Type Together with a Computer Based High Resolution Multi-Channel Analyzer from Institute of Nuclear Science

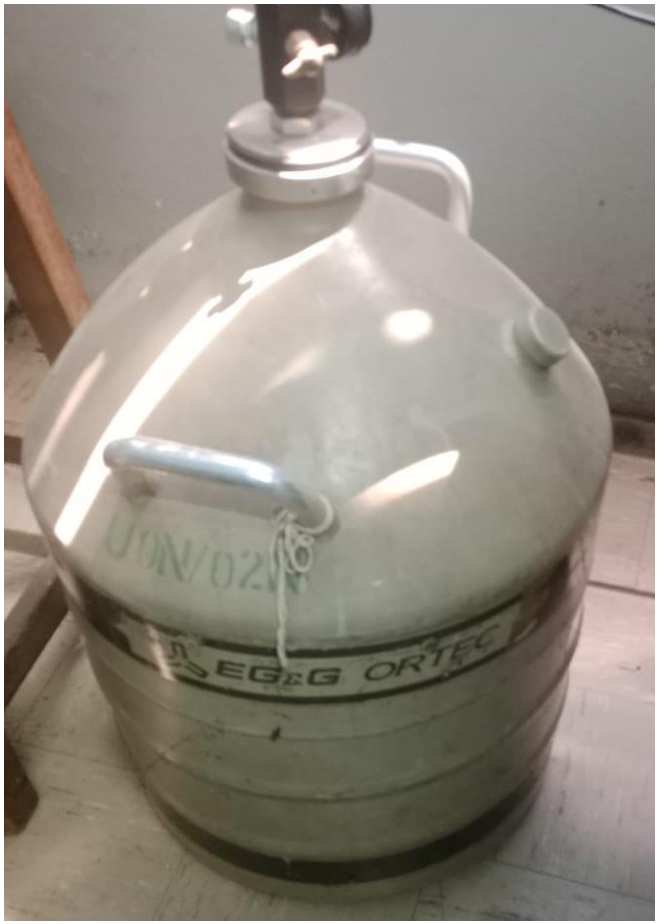

Appendix VI: Germanium Detector Data Sheet

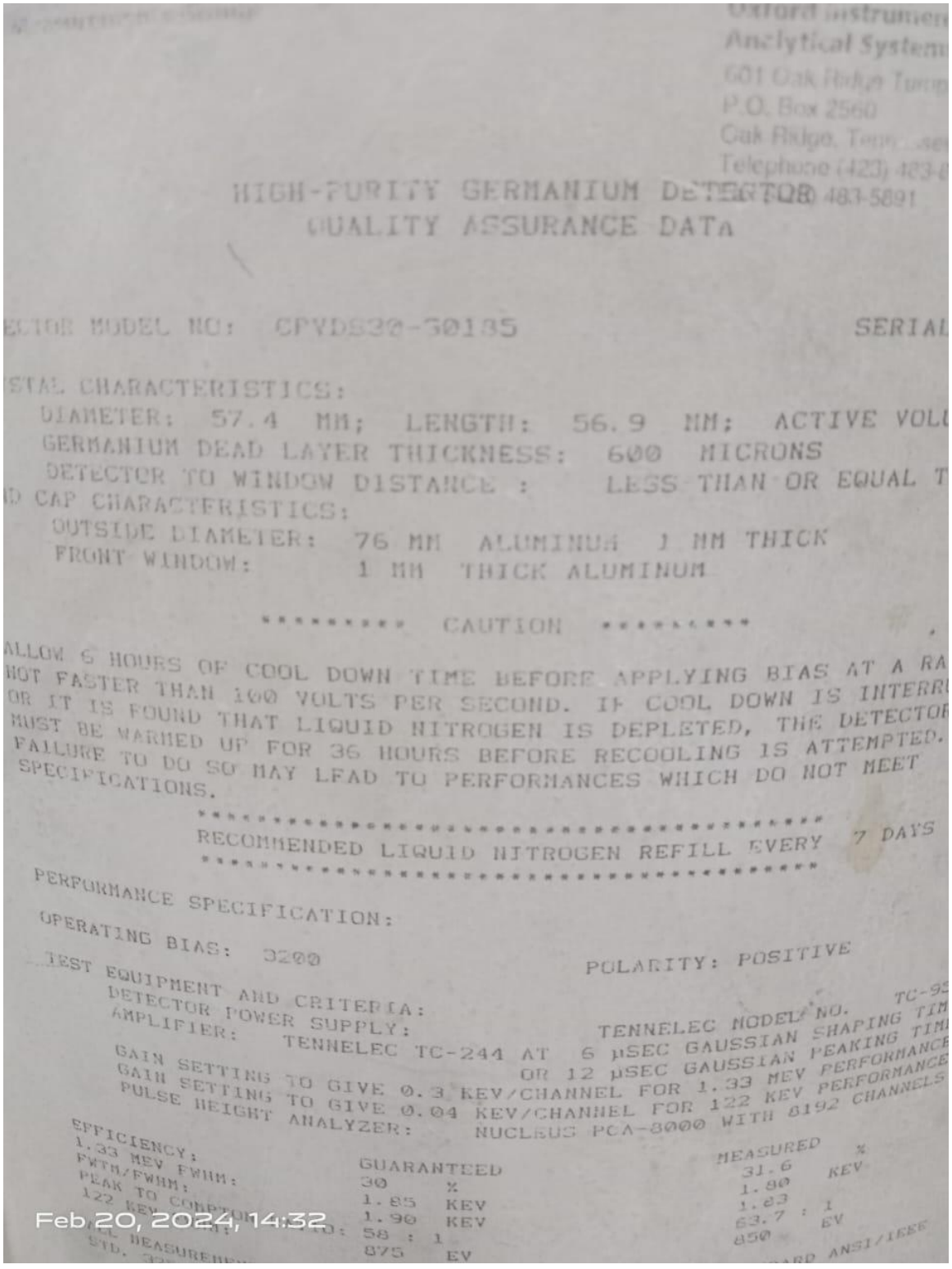

Oxford Instruments
Analytical Systems
601 Oak Ridge Turnpike
P.O. Box 2560
Oak Ridge, Tennessee
Telephone (423) 483-6
(800) 483-5891

HIGH-PURITY GERMANIUM DETECTOR
QUALITY ASSURANCE DATA

ECTOR MODEL NO: CPVDS20-30185 SERIAL

STAL CHARACTERISTICS:
DIAMETER: 57.4 MM; LENGTH: 56.9 MM; ACTIVE VOLU
GERMANIUM DEAD LAYER THICKNESS: 600 MICRONS
DETECTOR TO WINDOW DISTANCE : LESS THAN OR EQUAL T
D CAP CHARACTERISTICS:
OUTSIDE DIAMETER: 76 MM ALUMINUM 1 MM THICK
FRONT WINDOW: 1 MM THICK ALUMINUM

********* CAUTION *********

ALLOW 6 HOURS OF COOL DOWN TIME BEFORE APPLYING BIAS AT A RA
NOT FASTER THAN 100 VOLTS PER SECOND. IF COOL DOWN IS INTERR
OR IT IS FOUND THAT LIQUID NITROGEN IS DEPLETED, THE DETECTOR
MUST BE WARMED UP FOR 36 HOURS BEFORE RECOOLING IS ATTEMPTED.
FAILURE TO DO SO MAY LEAD TO PERFORMANCES WHICH DO NOT MEET
SPECIFICATIONS.

****
RECOMMENDED LIQUID NITROGEN REFILL EVERY 7 DAYS
****

PERFORMANCE SPECIFICATION:

OPERATING BIAS: 3200 POLARITY: POSITIVE

TEST EQUIPMENT AND CRITERIA:
DETECTOR POWER SUPPLY:
AMPLIFIER: TENNELEC TC-244 AT 6 µSEC GAUSSIAN SHAPING TIM
OR 12 µSEC GAUSSIAN PEAKING TIM
GAIN SETTING TO GIVE 0.3 KEV/CHANNEL FOR 1.33 MEV PERFORMANCE
GAIN SETTING TO GIVE 0.04 KEV/CHANNEL FOR 122 KEV PERFORMANCE
PULSE HEIGHT ANALYZER: NUCLEUS PCA-8000 WITH 8192 CHANNELS

	GUARANTEED	MEASURED
EFFICIENCY:	30 %	31.6 %
1.33 MEV FWHM:	1.85 KEV	1.80 KEV
FWTM/FWHM:	1.90	1.83 : 1
PEAK TO COMPTON:	58 : 1	63.7 : 1
122 KEV FWHM:	875 EV	850 EV

TEST MEASUREMENTS STD. ANSI/IEEE

Feb 20, 2024, 14:32

Appendix VII: Soil and Water Spectra

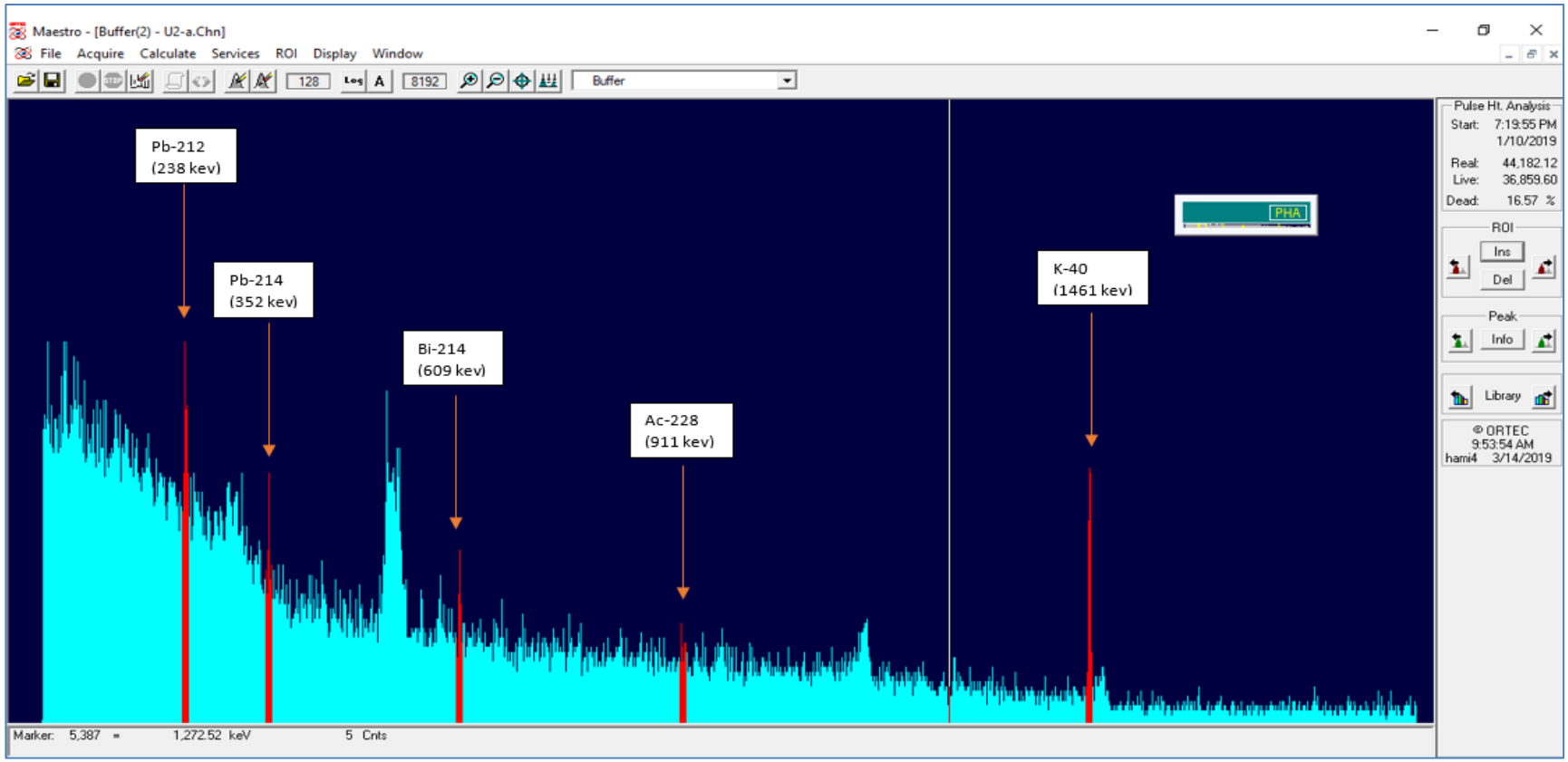

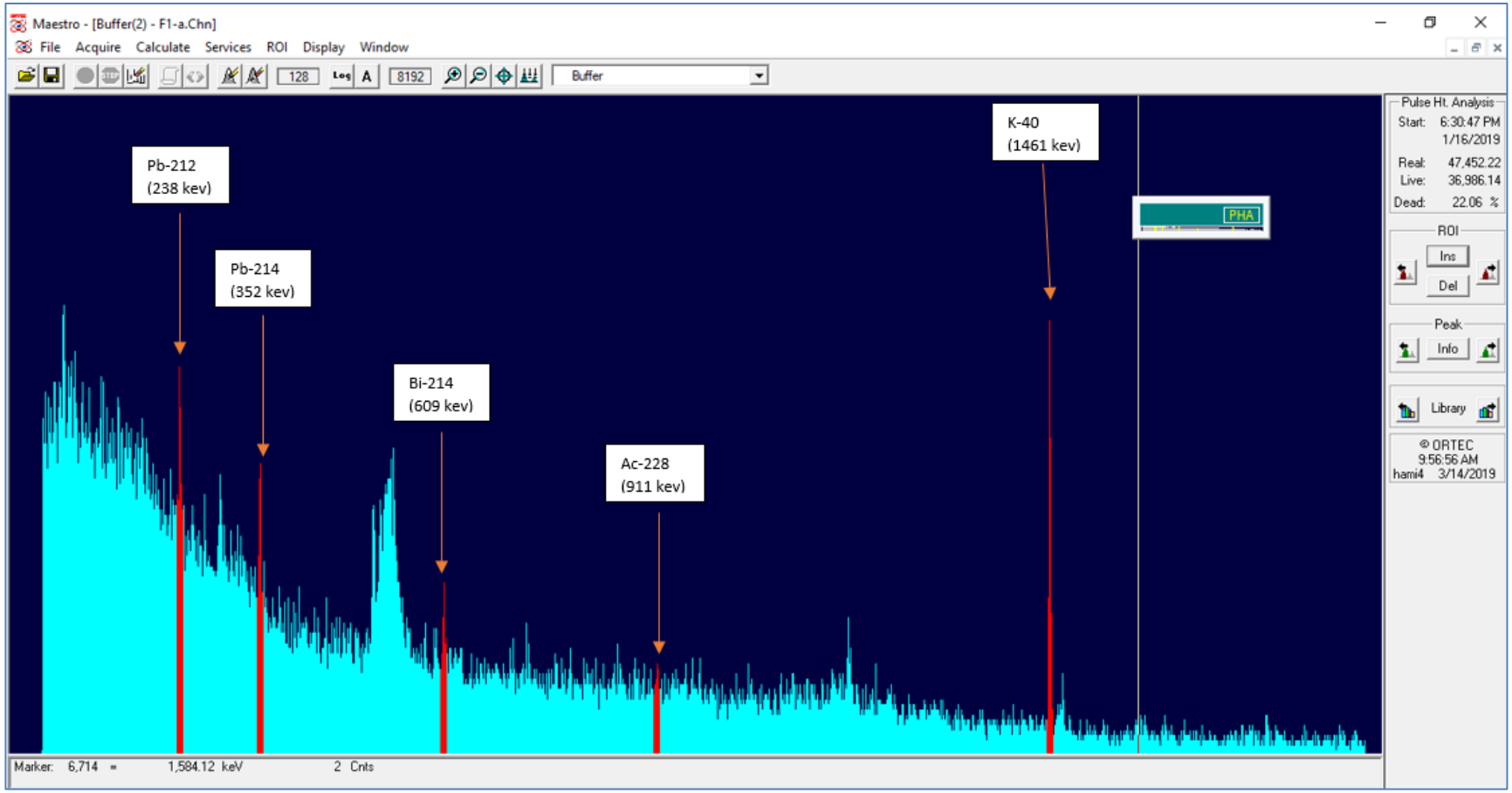
Maestro - [Buffer(2) - F1-a.Chn]
File Acquire Calculate Services ROI Display Window
Buffer
Pb-212
(238 kev)
Pb-214
(352 kev)
Bi-214
(609 kev)
Ac-228
(911 kev)
K-40
(1461 kev)
PHA
Pulse Ht. Analysis
Start: 6:30:47 PM
1/16/2019
Real: 47,452.22
Live: 36,986.14
Dead: 22.06 %
ROI
Ins
Del
Peak
Info
Library
© ORTEC
9:56:56 AM
hami4 3/14/2019
Marker: 6,714 = 1,584.12 keV 2 Cnts

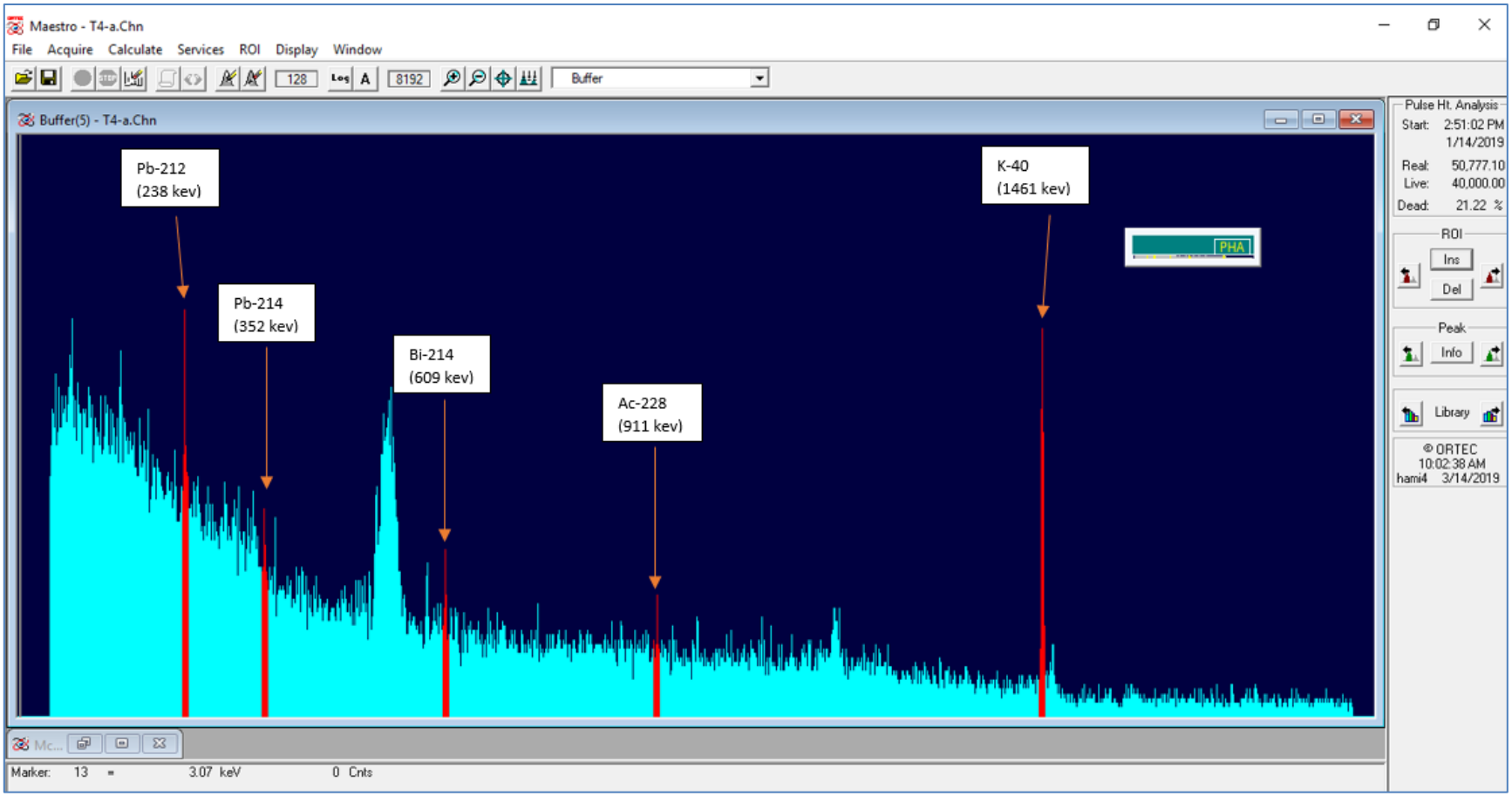
Maestro - T4-a.Chn
File Acquire Calculate Services ROI Display Window
Buffer
Buffer(5) - T4-a.Chn
Pb-212
(238 kev)
Pb-214
(352 kev)
Bi-214
(609 kev)
Ac-228
(911 kev)
K-40
(1461 kev)
PHA
Pulse Ht. Analysis
Start: 2:51:02 PM
1/14/2019
Real: 50,777.10
Live: 40,000.00
Dead: 21.22 %
ROI
Ins
Del
Peak
Info
Library
© ORTEC
10:02:38 AM
hami4 3/14/2019
Marker: 13 = 3.07 keV 0 Cnts

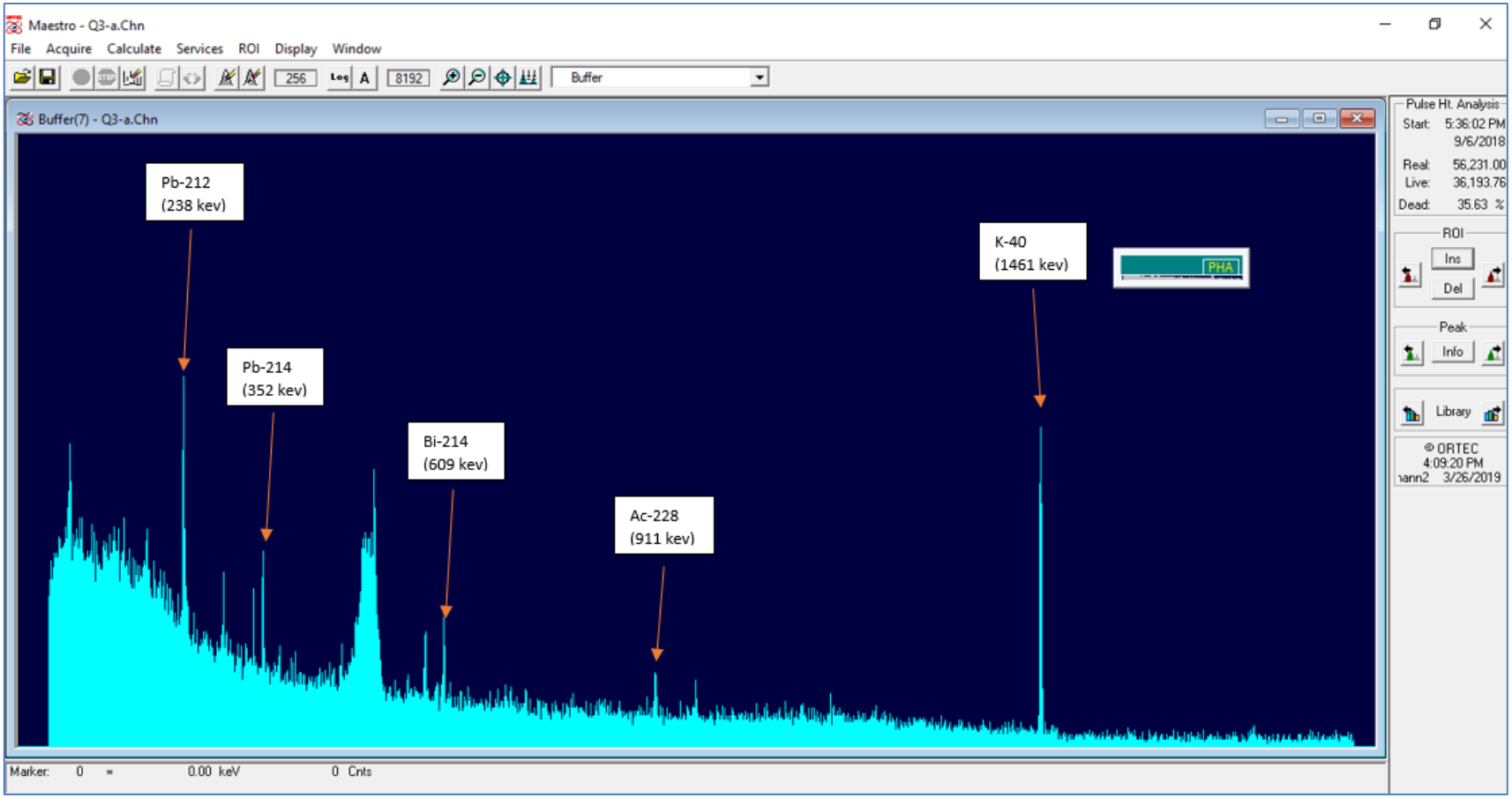
Maestro - Q3-a.Chn
File Acquire Calculate Services ROI Display Window
256
Log
A
8192
Buffer
Buffer(7) - Q3-a.Chn
Pb-212
(238 kev)
Pb-214
(352 kev)
Bi-214
(609 kev)
Ac-228
(911 kev)
K-40
(1461 kev)
PHA
Pulse Ht. Analysis
Start: 5:36:02 PM
9/6/2018
Real: 56,231.00
Live: 36,193.76
Dead: 35.63 %
ROI
Ins
Del
Peak
Info
Library
ORTEC
4:09:20 PM
3/26/2019
Marker: 0 0.00 keV 0 Cnts

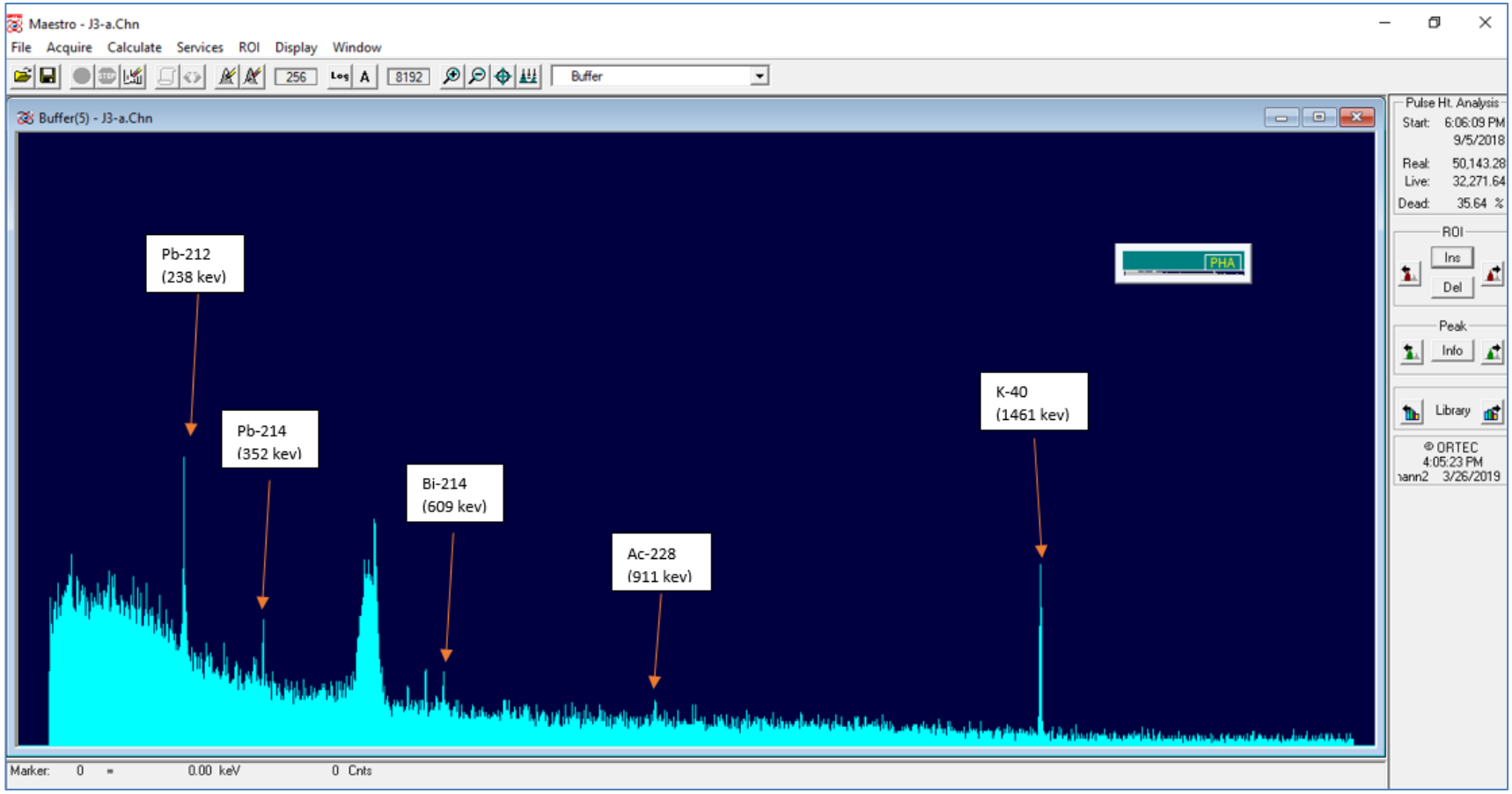
Maestro - J3-a.Chn
File Acquire Calculate Services ROI Display Window
256
Log
A
8192
Buffer
Buffer(5) - J3-a.Chn
Pb-212
(238 kev)
Pb-214
(352 kev)
Bi-214
(609 kev)
Ac-228
(911 kev)
K-40
(1461 kev)
PHA
Pulse Ht. Analysis
Start: 6:06:09 PM
9/5/2018
Real: 50,143.28
Live: 32,271.64
Dead: 35.64 %
ROI
Ins
Del
Peak
Info
Library
© ORTEC
4:05:23 PM
3/26/2019
Marker: 0 = 0.00 keV 0 Cnts

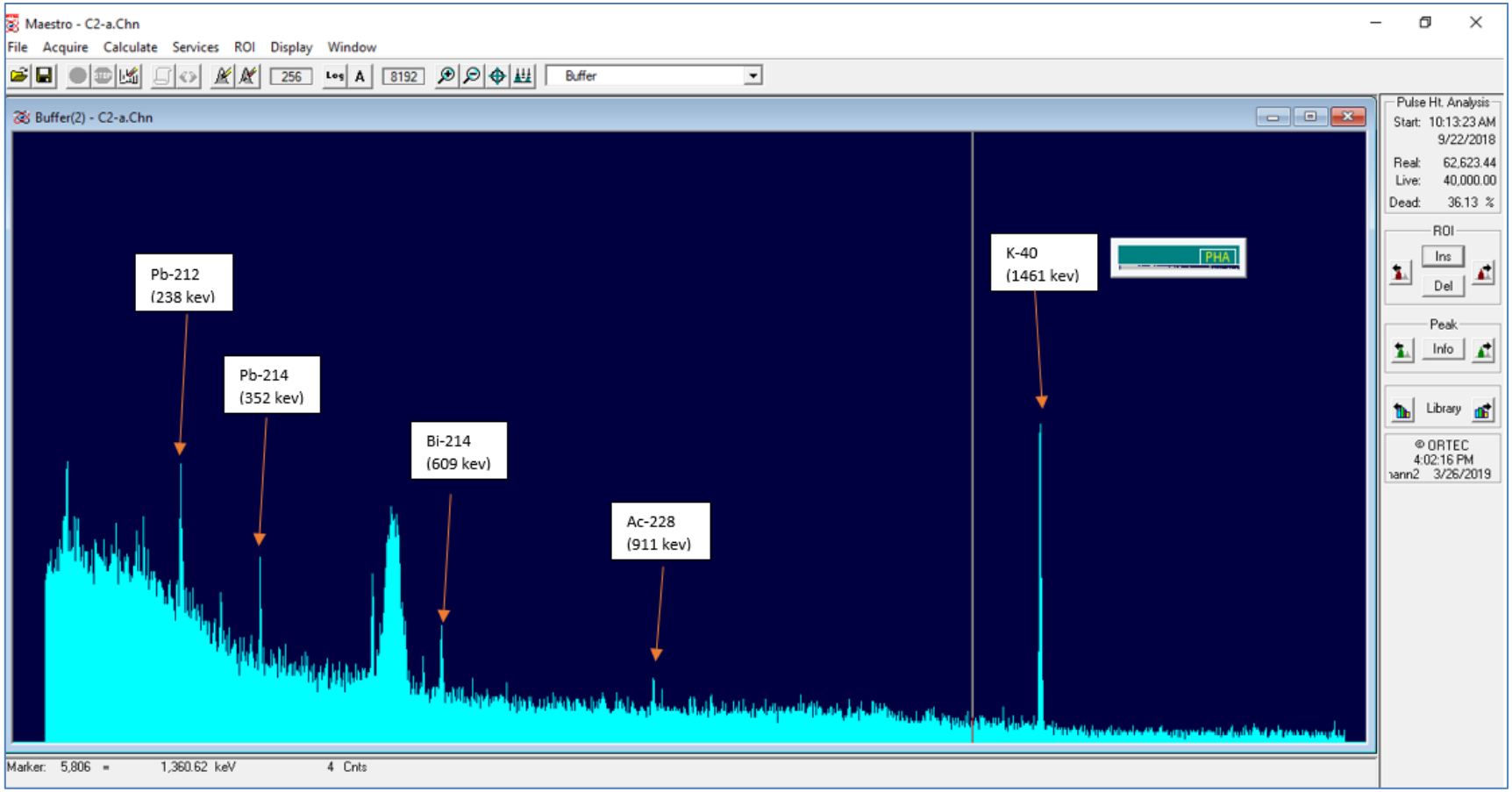
Maestro - C2-a.Chn
File Acquire Calculate Services ROI Display Window
Buffer
Buffer(2) - C2-a.Chn
Pb-212
(238 kev)
Pb-214
(352 kev)
Bi-214
(609 kev)
Ac-228
(911 kev)
K-40
(1461 kev)
PHA
Pulse Ht. Analysis
Start: 10:13:23 AM
9/22/2018
Real: 62,623.44
Live: 40,000.00
Dead: 36.13 %
ROI
Ins
Del
Peak
Info
Library
ORTEC
4:02:16 PM
3/26/2019
Marker: 5,806 = 1,360.62 keV 4 Cnts

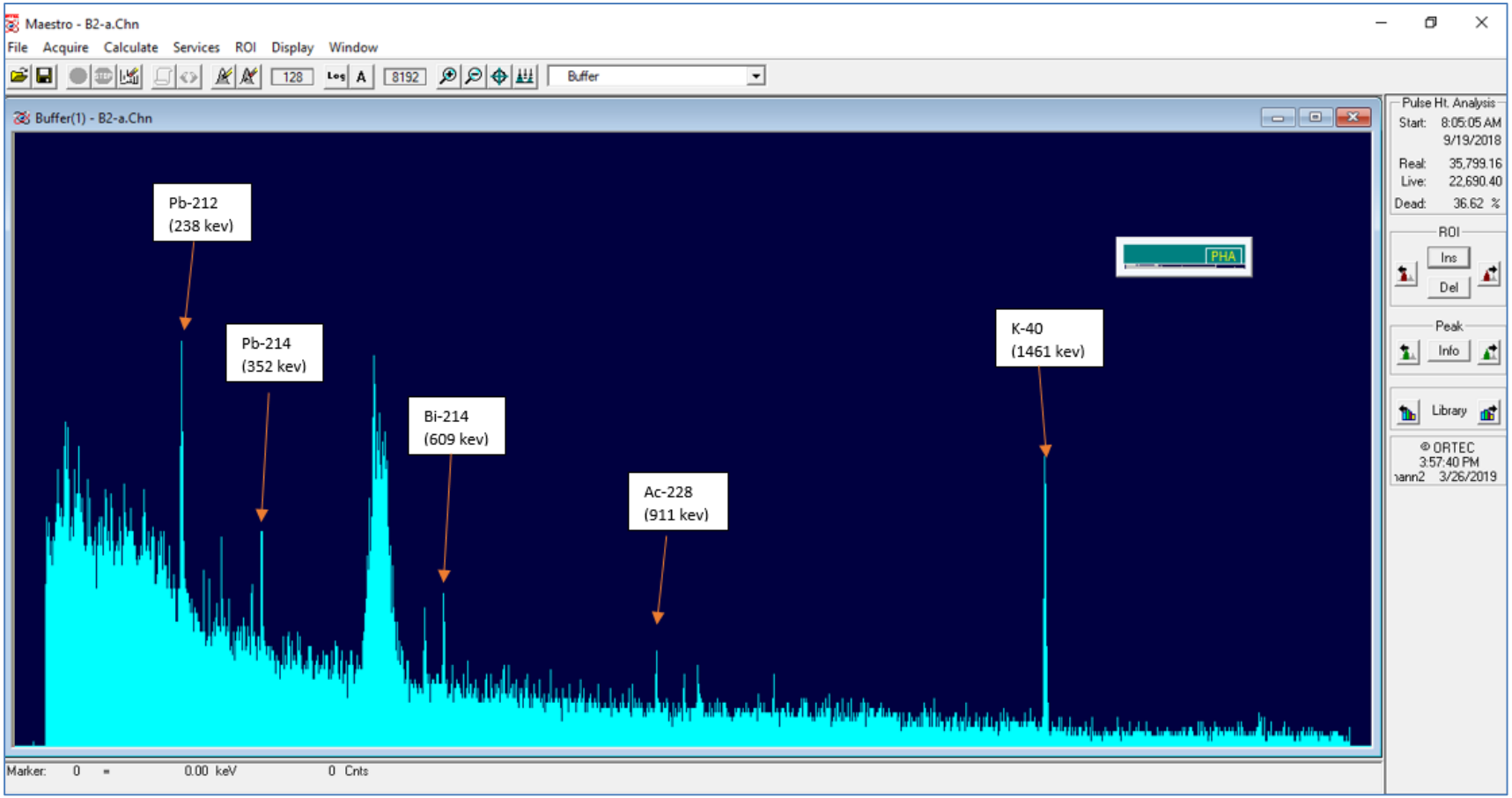
Maestro - B2-a.Chn
File Acquire Calculate Services ROI Display Window
128
Log
A
8192
Buffer
Buffer(1) - B2-a.Chn
Pb-212
(238 kev)
Pb-214
(352 kev)
Bi-214
(609 kev)
Ac-228
(911 kev)
K-40
(1461 kev)
PHA
Pulse Ht. Analysis
Start: 8:05:05 AM
9/19/2018
Real: 35,799.16
Live: 22,690.40
Dead: 36.62 %
ROI
Ins
Del
Peak
Info
Library
ORTEC
3:57:40 PM
3/26/2019
Marker: 0 0.00 keV 0 Cnts

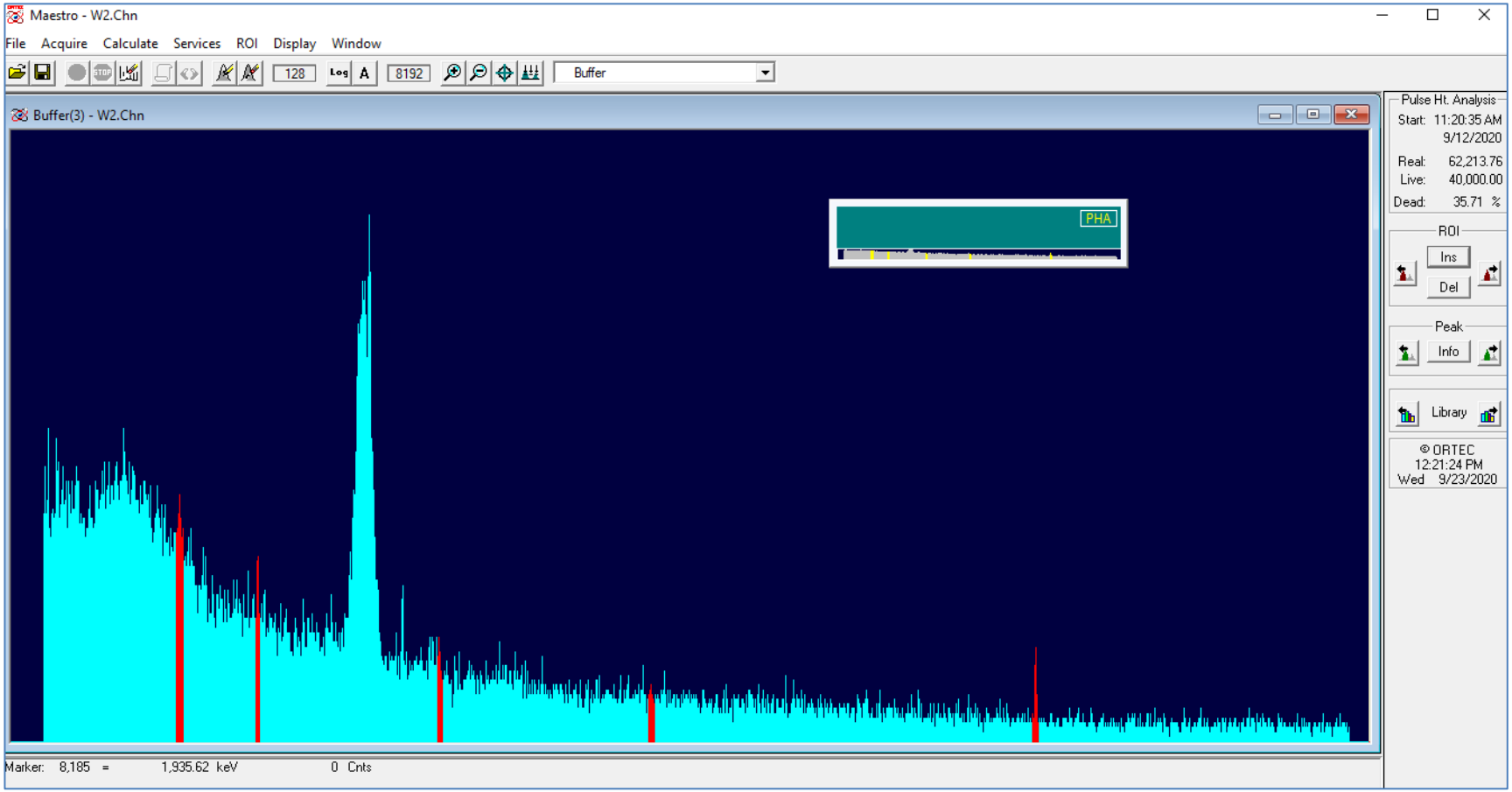
Maestro - W2.Chn
File Acquire Calculate Services ROI Display Window
128
Log A
8192
Buffer
Buffer(3) - W2.Chn
PHA
Pulse Ht. Analysis
Start: 11:20:35 AM
9/12/2020
Real: 62,213.76
Live: 40,000.00
Dead: 35.71 %
ROI
Ins
Del
Peak
Info
Library
© ORTEC
12:21:24 PM
Wed 9/23/2020
Marker: 8,185 = 1,935.62 keV 0 Cnts

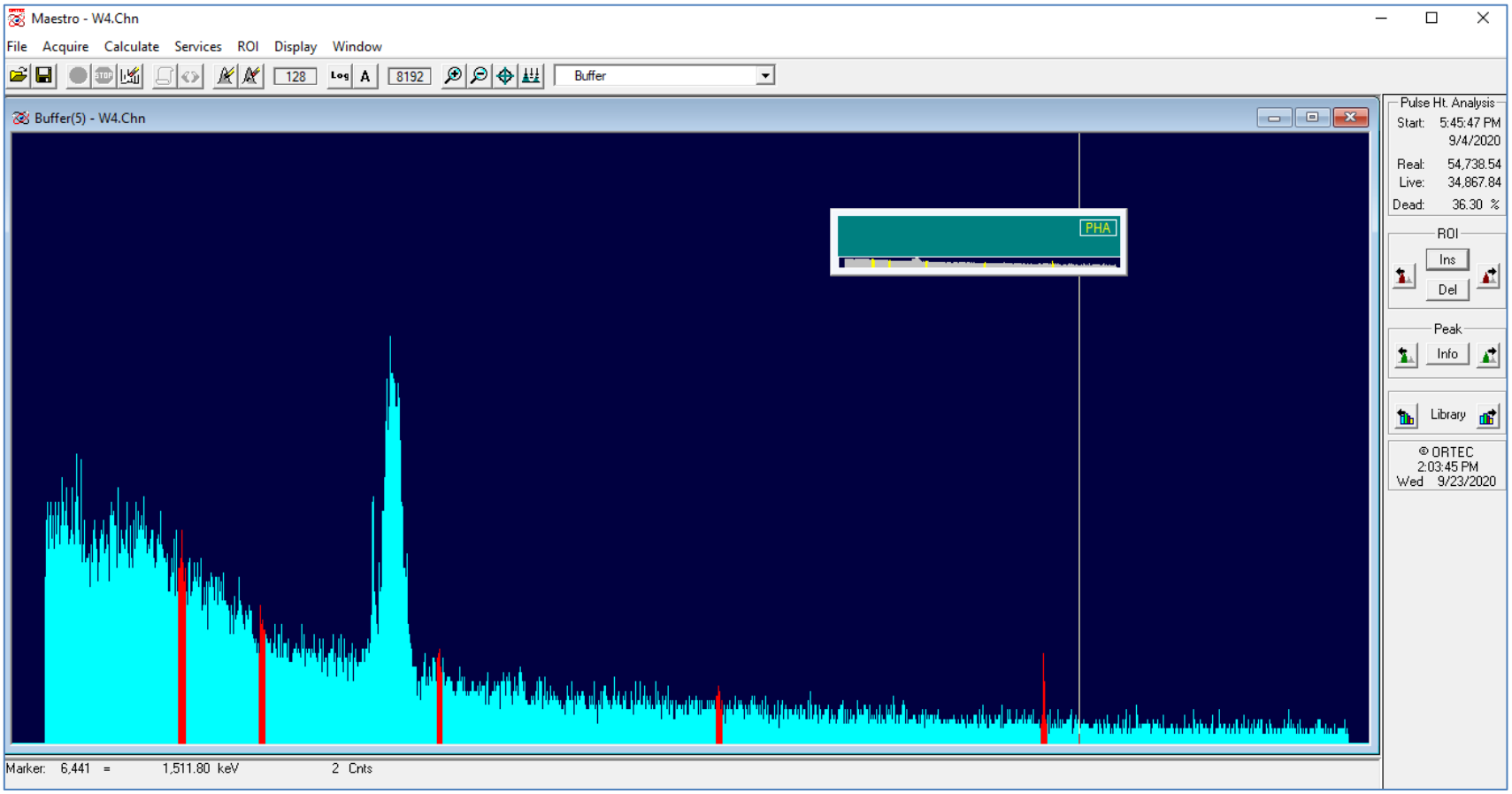
Maestro - W4.Chn
File Acquire Calculate Services ROI Display Window
128
Log
A
8192
Buffer
Buffer(5) - W4.Chn
PHA
Pulse Ht. Analysis
Start: 5:45:47 PM
9/4/2020
Real: 54,738.54
Live: 34,867.84
Dead: 36.30 %
ROI
Ins
Del
Peak
Info
Library
© ORTEC
2:03:45 PM
Wed 9/23/2020
Marker: 6,441 = 1,511.80 keV 2 Cnts

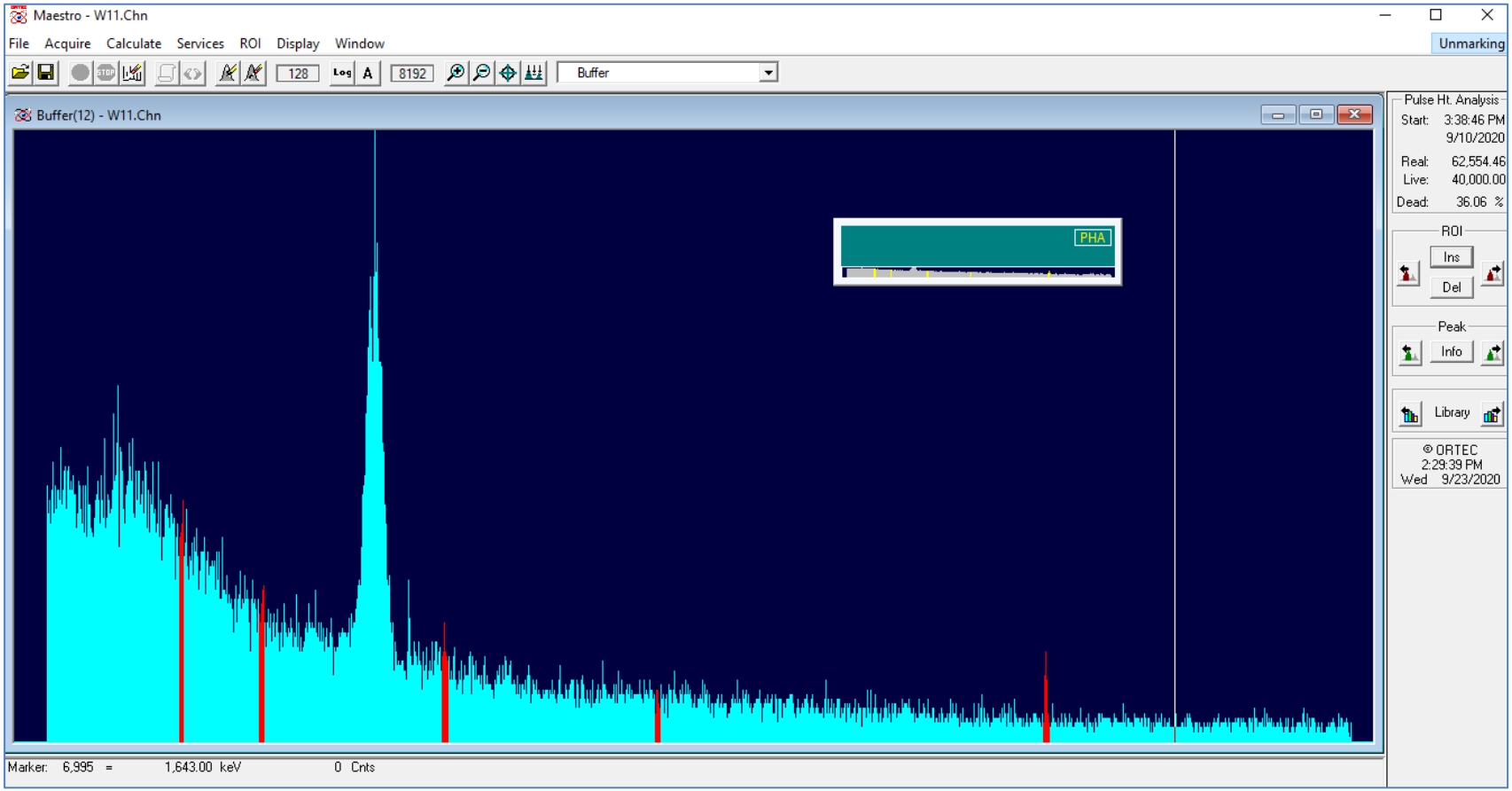
Maestro - W11.Chn
File Acquire Calculate Services ROI Display Window
Unmarking
128
8192
Buffer
Buffer(12) - W11.Chn
PHA
Pulse Ht. Analysis
Start: 3:38:46 PM
9/10/2020
Real: 62,554.46
Live: 40,000.00
Dead: 36.06 %
ROI
Ins
Del
Peak
Info
Library
© ORTEC
2:29:39 PM
Wed 9/23/2020
Marker: 6,995 = 1,643.00 keV 0 Cnts

Appendix VIII: Nuclide Identification Reports Table

BLOCK	Sampling area, km^2	Sample no.	Nuclide name	Energy±0.005 (keV)	Activity ±0.005 ($Bqkg^{-1}$)
A	1.0	A_1	^{40}K	1461	335.43
			^{214}Bi	609	5.91
			^{212}Pb	238	4.61
			^{214}Pb	352	2.02
			^{228}Ac	911	1.54
	1.0	A_2	^{40}K	1461	283.16
			^{214}Bi	609	9.34
			^{212}Pb	238	4.33
			^{214}Pb	352	6.44
			^{228}Ac	911	1.83
	1.0	A_3	^{40}K	1461	262.72
			^{214}Bi	609	5.24
			^{212}Pb	238	1.69
			^{214}Pb	352	8.66
			^{228}Ac	911	0.00
	1.0	A_4	^{40}K	1461	223.25
			^{214}Bi	609	4.38
			^{212}Pb	238	6.66
			^{214}Pb	352	4.39
			^{228}Ac	911	2.93
B	1.0	B_1	^{40}K	1461	513.24
			^{214}Bi	609	6.18
			^{212}Pb	238	5.49
			^{214}Pb	352	5.34

			^{228}Ac	911	5.56
		B_2	^{40}K	1461	502.42
			^{214}Bi	609	11.04
			^{212}Pb	238	8.10
			^{214}Pb	352	6.40
			^{228}Ac	911	14.12
		B_3	^{40}K	1458	373.73
			^{214}Bi	609	7.12
			^{212}Pb	238	6.47
			^{214}Pb	351	8.36
			^{228}Ac	909	8.69
		B_4	^{40}K	1458	320.96
			^{214}Bi	609	8.49
			^{212}Pb	238	10.89
			^{214}Pb	351	0.51
			^{228}Ac	909	2.54
C	1.0	C_1	^{40}K	1458	361.704
			^{214}Bi	609	3.44
			^{212}Pb	238	2.61
			^{214}Pb	351	7.44
			^{228}Ac	909	5.48
		C_2	^{40}K	1461	322.56
			^{214}Bi	609	6.89
			^{212}Pb	238	4.46
			^{214}Pb	352	8.29
			^{228}Ac	911	9.36
		C_3	^{40}K	1458	226.60

			^{214}Bi	609	5.20
			^{212}Pb	238	4.26
			^{214}Pb	351	4.37
			^{228}Ac	909	13.35
		C_4	^{40}K	1458	386.81
			^{214}Bi	609	6.42
			^{212}Pb	238	5.93
			^{214}Pb	351	6.60
			^{228}Ac	909	9.15
D	1.0	D_1	^{40}K	1461	451.25
			^{214}Bi	609	3.12
			^{212}Pb	238	5.58
			^{214}Pb	352	3.49
			^{228}Ac	911	2.59
		D_2	^{40}K	1458	308.34
			^{214}Bi	609	6.63
			^{212}Pb	238	7.52
			^{214}Pb	351	7.99
			^{228}Ac	909	15.36
		D_3	^{40}K	1458	346.42
			^{214}Bi	609	8.59
			^{212}Pb	238	8.90
			^{214}Pb	351	7.63
			^{228}Ac	909	8.64
		D_4	^{40}K	1458	320.96
			^{214}Bi	609	8.49
			^{212}Pb	238	10.89

			^{214}Pb	351	0.51
			^{228}Ac	909	2.54
E	1.0	E_1	^{40}K	1461	387.08
			^{214}Bi	609	11.57
			^{212}Pb	238	6.78
			^{214}Pb	352	10.33
			^{228}Ac	911	7.97
		E_2	^{40}K	1461	141.10
			^{214}Bi	609	2.52
			^{212}Pb	238	3.48
			^{214}Pb	352	4.71
			^{228}Ac	911	10.07
		E_3	^{40}K	1461	375.51
			^{214}Bi	609	6.60
			^{212}Pb	238	7.25
			^{214}Pb	352	7.32
			^{228}Ac	911	16.15
		E_4	^{40}K	1461	223.25
			^{214}Bi	609	4.38
			^{212}Pb	238	6.66
			^{214}Pb	352	4.39
			^{228}Ac	911	2.93
F	1.0	F_1	^{40}K	1461	283.16
			^{214}Bi	609	9.34
			^{212}Pb	238	4.33
			^{214}Pb	352	6.44
			^{228}Ac	911	1.83

		F_2	^{40}K	1461	534.22
			^{214}Bi	609	11.91
			^{212}Pb	238	7.97
			^{214}Pb	352	10.59
			^{228}Ac	911	17.20
		F_3	^{40}K	1461	290.92
			^{214}Bi	609	7.76
			^{212}Pb	238	5.86
			^{214}Pb	352	8.24
			^{228}Ac	911	10.37
		F_4	^{40}K	1461	338.49
			^{214}Bi	609	8.04
			^{212}Pb	238	6.07
			^{214}Pb	352	8.54
			^{228}Ac	911	9.42
G	1.0	G_1	^{40}K	1461	318.92
			^{214}Bi	609	5.41
			^{212}Pb	238	8.33
			^{214}Pb	352	6.14
			^{228}Ac	911	16.12
		G_2	^{40}K	1461	444.67
			^{214}Bi	609	8.84
			^{212}Pb	238	4.21
			^{214}Pb	352	8.95
			^{228}Ac	911	6.85
		G_3	^{40}K	1461	555.03
			^{214}Bi	609	7.97

			^{212}Pb	238	8.97
			^{214}Pb	352	7.42
			^{228}Ac	911	5.01
		G_4	^{40}K	1461	502.42
			^{214}Bi	609	11.04
			^{212}Pb	238	8.10
			^{214}Pb	352	6.40
			^{228}Ac	911	14.12
H	1.0	H_1	^{40}K	1461	243.36
			^{214}Bi	609	4.05
			^{212}Pb	238	4.65
			^{214}Pb	352	8.04
			^{228}Ac	911	11.36
		H_2	^{40}K	1461	338.42
			^{214}Bi	609	2.92
			^{212}Pb	238	7.90
			^{214}Pb	352	6.76
			^{228}Ac	911	6.86
		H_3	^{40}K	1461	246.36
			^{214}Bi	609	6.58
			^{212}Pb	238	2.81
			^{214}Pb	352	7.62
			^{228}Ac	911	2.11
		H_4	^{40}K	1461	211.41
			^{214}Bi	609	11.09
			^{212}Pb	238	6.67
			^{214}Pb	352	8.24

			^{228}Ac	911	2.06
J	1.0	J_1	^{40}K	1458	325.76
			^{214}Bi	609	4.38
			^{212}Pb	238	8.59
			^{214}Pb	351	6.32
			^{228}Ac	909	8.97
		J_2	^{40}K	1458	291.38
			^{214}Bi	609	7.80
			^{212}Pb	238	6.45
			^{214}Pb	351	9.65
			^{228}Ac	909	10.40
		J_3	^{40}K	1461	231.42
			^{214}Bi	609	4.45
			^{212}Pb	238	6.15
			^{214}Pb	352	4.66
			^{228}Ac	911	10.87
		J_4	^{40}K	1458	212.67
			^{214}Bi	609	6.57
			^{212}Pb	238	5.82
			^{214}Pb	351	6.56
			^{228}Ac	909	10.16
K	1.0	K_1	^{40}K	1458	373.73
			^{214}Bi	609	7.12
			^{212}Pb	238	6.47
			^{214}Pb	351	8.36
			^{228}Ac	909	8.69
		K_2	^{40}K	1458	202.30

			^{214}Bi	609	8.30
			^{212}Pb	238	2.94
			^{214}Pb	351	5.50
			^{228}Ac	909	10.51
		K_3	^{40}K	1458	200.51
			^{214}Bi	609	6.77
			^{212}Pb	238	4.59
			^{214}Pb	351	5.69
			^{228}Ac	909	6.00
		K_4	^{40}K	1458	371.96
			^{214}Bi	609	20.57
			^{212}Pb	238	7.66
			^{214}Pb	351	15.68
			^{228}Ac	909	7.82
L	1.0	L_1	^{40}K	1458	427.95
			^{214}Bi	609	4.49
			^{212}Pb	238	4.94
			^{214}Pb	351	5.72
			^{228}Ac	909	4.49
		L_2	^{40}K	1458	383.17
			^{214}Bi	609	6.79
			^{212}Pb	238	5.20
			^{214}Pb	351	6.77
			^{228}Ac	909	0.96
		L_3	^{40}K	1458	478.54
			^{214}Bi	609	5.02
			^{212}Pb	238	6.48

			^{214}Pb	351	6.41
			^{228}Ac	909	11.41
		L_4	^{40}K	1458	454.36
			^{214}Bi	609	6.76
			^{212}Pb	238	6.14
			^{214}Pb	351	5.51
			^{228}Ac	909	6.76
M	1.0	M_1	^{40}K	1461	367.51
			^{214}Bi	609	6.62
			^{212}Pb	238	1.92
			^{214}Pb	352	3.60
			^{228}Ac	911	5.21
		M_2	^{40}K	1458	322.56
			^{214}Bi	609	6.89
			^{212}Pb	238	4.46
			^{214}Pb	351	8.29
			^{228}Ac	909	9.36
		M_3	^{40}K	1461	310.53
			^{214}Bi	609	6.07
			^{212}Pb	238	1.13
			^{214}Pb	352	5.18
			^{228}Ac	911	6.63
		M_4	^{40}K	1458	320.96
			^{214}Bi	609	8.49
			^{212}Pb	238	10.89
			^{214}Pb	351	0.51
			^{228}Ac	909	2.54

N	1.0	N_1	^{40}K	1461	283.91
			^{214}Bi	609	0.92
			^{212}Pb	238	3.79
			^{214}Pb	352	5.17
			^{228}Ac	911	7.98
		N_2	^{40}K	1461	260.64
			^{214}Bi	609	5.67
			^{212}Pb	238	5.87
			^{214}Pb	352	6.54
			^{228}Ac	911	8.40
		N_3	^{40}K	1458	212.67
			^{214}Bi	609	6.57
			^{212}Pb	238	5.82
			^{214}Pb	351	6.56
			^{228}Ac	909	10.16
		N_4	^{40}K	1461	160.71
			^{214}Bi	609	8.03
			^{212}Pb	238	5.74
			^{214}Pb	352	4.72
			^{228}Ac	911	0.88
P	1.0	P_1	^{40}K	1461	301.50
			^{214}Bi	609	6.25
			^{212}Pb	238	1.70
			^{214}Pb	352	2.63
			^{228}Ac	911	1.93
		P_2	^{40}K	1461	243.93
			^{214}Bi	609	11.87

			^{212}Pb	238	5.44
			^{214}Pb	352	7.18
			^{228}Ac	911	6.89
		P_3	^{40}K	1458	382.04
			^{214}Bi	609	4.28
			^{212}Pb	238	-0.19
			^{214}Pb	351	4.59
			^{228}Ac	909	-1.08
		P_4	^{40}K	1458	392.05
			^{214}Bi	609	6.09
			^{212}Pb	238	3.25
			^{214}Pb	351	5.70
			^{228}Ac	909	2.73
Q	1.0	Q_1	^{40}K	1461	295.09
			^{214}Bi	609	7.75
			^{212}Pb	238	6.88
			^{214}Pb	352	8.78
			^{228}Ac	911	4.48
		Q_2	^{40}K	1458	208.26
			^{214}Bi	609	5.27
			^{212}Pb	238	4.89
			^{214}Pb	351	3.61
			^{228}Ac	909	7.83
		Q_3	^{40}K	1461	508.11
			^{214}Bi	609	11.79
			^{212}Pb	238	12.55
			^{214}Pb	352	8.85

			^{228}Ac	911	15.57
		Q_4	^{40}K	1458	554.20
			^{214}Bi	609	10.48
			^{212}Pb	238	11.55
			^{214}Pb	351	9.22
			^{228}Ac	909	1.81
R	1.0	R_1	^{40}K	1461	332.23
			^{214}Bi	609	1.82
			^{212}Pb	238	7.27
			^{214}Pb	352	4.08
			^{228}Ac	911	11.71
		R_2	^{40}K	1461	317.26
			^{214}Bi	609	2.97
			^{212}Pb	238	7.59
			^{214}Pb	352	8.61
			^{228}Ac	911	2.28
		R_3	^{40}K	1461	434.74
			^{214}Bi	609	11.12
			^{212}Pb	238	10.00
			^{214}Pb	352	8.58
			^{228}Ac	911	-0.10
		R_4	^{40}K	1461	389.04
			^{214}Bi	609	7.02
			^{212}Pb	238	4.18
			^{214}Pb	352	6.83
			^{228}Ac	911	7.21
S	1.0	S_1	^{40}K	1461	286.72

			^{214}Bi	609	5.83
			^{212}Pb	238	4.34
			^{214}Pb	352	9.78
			^{228}Ac	911	6.28
		S_2	^{40}K	1461	356.26
			^{214}Bi	609	7.21
			^{212}Pb	238	7.28
			^{214}Pb	352	8.12
			^{228}Ac	911	5.47
		S_3	^{40}K	1461	290.23
			^{214}Bi	609	8.25
			^{212}Pb	238	3.08
			^{214}Pb	352	8.00
			^{228}Ac	911	9.06
		S_4	^{40}K	1461	387.28
			^{214}Bi	609	4.89
			^{212}Pb	238	6.63
			^{214}Pb	352	5.16
			^{228}Ac	911	5.51
T	1.0	T_1	^{40}K	1461	365.85
			^{214}Bi	609	15.07
			^{212}Pb	238	7.27
			^{214}Pb	352	8.22
			^{228}Ac	911	15.30
		T_2	^{40}K	1461	532.94
			^{214}Bi	609	10.62
			^{212}Pb	238	7.44

			^{214}Pb	352	11.49
			^{228}Ac	911	15.82
		T_3	^{40}K	1461	536.55
			^{214}Bi	609	11.85
			^{212}Pb	238	7.72
			^{214}Pb	352	6.66
			^{228}Ac	911	3.59
		T_4	^{40}K	1461	268.58
			^{214}Bi	609	6.74
			^{212}Pb	238	3.51
			^{214}Pb	352	2.42
			^{228}Ac	911	4.04
U	1.0	U_1	^{40}K	1461	432.33
			^{214}Bi	609	0.79
			^{212}Pb	238	6.61
			^{214}Pb	352	6.35
			^{228}Ac	911	4.26
		U_2	^{40}K	1461	160.71
			^{214}Bi	609	8.03
			^{212}Pb	238	5.74
			^{214}Pb	352	4.72
			^{228}Ac	911	0.88
		U_3	^{40}K	1461	367.11
			^{214}Bi	609	6.18
			^{212}Pb	238	4.91
			^{214}Pb	352	6.71
			^{228}Ac	911	10.49

		U_4	^{40}K	1461	563.75
			^{214}Bi	609	11.58
			^{212}Pb	238	11.17
			^{214}Pb	352	8.60
			^{228}Ac	911	12.13
V	1.0	V_1	^{40}K	1461	350.66
			^{214}Bi	609	5.62
			^{212}Pb	238	3.84
			^{214}Pb	352	5.66
			^{228}Ac	911	6.41
		V_2	^{40}K	1461	667.77
			^{214}Bi	609	13.61
			^{212}Pb	238	20.59
			^{214}Pb	352	9.72
			^{228}Ac	911	34.31
		V_3	^{40}K	1461	369.72
			^{214}Bi	609	5.85
			^{212}Pb	238	-0.13
			^{214}Pb	352	2.19
			^{228}Ac	911	0.00
		V_4	^{40}K	1461	375.46
			^{214}Bi	609	4.43
			^{212}Pb	238	3.25
			^{214}Pb	352	3.79
			^{228}Ac	911	0.28
W	1.0	W_1	^{40}K	1461	389.04
			^{214}Bi	609	7.02

			^{212}Pb	238	4.18
			^{214}Pb	352	6.83
			^{228}Ac	911	7.21
		W_2	^{40}K	1460	516.10
			^{214}Bi	609	8.14
			^{212}Pb	238	7.88
			^{214}Pb	352	6.71
			^{228}Ac	912	9.01
		W_3	^{40}K	1460	441.52
			^{214}Bi	609	5.29
			^{212}Pb	238	3.26
			^{214}Pb	352	4.67
			^{228}Ac	912	-1.20
		W_4	^{40}K	1461	453.81
			^{214}Bi	609	9.71
			^{212}Pb	238	8.47
			^{214}Pb	352	6.42
			^{228}Ac	911	13.51
X	1.0	X_1	^{40}K	1461	592.73
			^{214}Bi	609	14.50
			^{212}Pb	238	11.82
			^{214}Pb	352	9.06
			^{228}Ac	911	3.94
	1.0	X_2	^{40}K	1461	369.90
			^{214}Bi	609	3.42
			^{212}Pb	238	2.23
			^{214}Pb	352	3.34

			^{228}Ac	911	4.53
		X_3	^{40}K	1461	520.81
			^{214}Bi	609	13.76
			^{212}Pb	238	19.42
			^{214}Pb	352	13.76
			^{228}Ac	911	13.67
		X_4	^{40}K	1461	36.87
			^{214}Bi	609	0.20
			^{212}Pb	238	5.63
			^{214}Pb	352	7.20
			^{228}Ac	911	0.00
Y	1.0	Y_1	^{40}K	1461	312.38
			^{214}Bi	609	8.36
			^{212}Pb	238	12.91
			^{214}Pb	352	9.53
			^{228}Ac	911	10.34
		Y_2	^{40}K	1461	119.17
			^{214}Bi	609	16.24
			^{212}Pb	238	2.13
			^{214}Pb	352	15.01
			^{228}Ac	911	2.35
		Y_3	^{40}K	1461	284.89
			^{214}Bi	609	11.09
			^{212}Pb	238	13.81
			^{214}Pb	352	10.78
			^{228}Ac	911	14.51
		Y_4	^{40}K	1461	208.63

			^{214}Bi	609	12.37
			^{212}Pb	238	1.59
			^{214}Pb	352	12.22
			^{228}Ac	911	9.19
Z	1.0	Z_1	^{40}K	1461	281.68
			^{214}Bi	609	10.25
			^{212}Pb	238	14.65
			^{214}Pb	352	10.83
			^{228}Ac	911	18.55
		Z_2	^{40}K	1461	290.23
			^{214}Bi	609	8.25
			^{212}Pb	238	3.08
			^{214}Pb	609	8.00
			^{228}Ac	911	9.06
		Z_3	^{40}K	1461	295.09
			^{214}Bi	609	7.75
			^{212}Pb	238	6.88
			^{214}Pb	352	8.78
			^{228}Ac	911	4.48
		Z_4	^{40}K	1461	318.92
			^{214}Bi	609	5.41
			^{212}Pb	238	8.33
			^{214}Pb	352	6.14
			^{228}Ac	911	16.12
a	0.5	a_1	^{40}K	1461	336.44
			^{214}Bi	609	5.80
			^{212}Pb	238	3.97

			^{214}Pb	352	7.68
			^{228}Ac	911	7.09
	0.5	a_2	^{40}K	1461	539.67
			^{214}Bi	609	4.48
			^{212}Pb	238	4.81
			^{214}Pb	352	2.64
			^{228}Ac	911	11.80
b	0.5	b_1	^{40}K	1461	513.24
			^{214}Bi	609	6.18
			^{212}Pb	238	5.49
			^{214}Pb	352	5.34
			^{228}Ac	911	5.56
	0.5	b_2	^{40}K	1461	431.72
			^{214}Bi	609	5.31
			^{212}Pb	238	3.83
			^{214}Pb	352	-0.21
			^{228}Ac	911	13.96
d	0.5	d_1	^{40}K	1461	451.25
			^{214}Bi	609	3.12
			^{212}Pb	238	5.57
			^{214}Pb	352	3.49
			^{228}Ac	911	2.59
	0.5	d_2	^{40}K	1461	288.26
			^{214}Bi	609	5.21
			^{212}Pb	238	3.32
			^{214}Pb	352	4.35
			^{228}Ac	911	11.90

e	0.5	e_1	^{40}K	1461	462.76
			^{214}Bi	609	7.29
			^{212}Pb	238	6.35
			^{214}Pb	352	8.78
			^{228}Ac	911	7.72
	0.5	e_2	^{40}K	1461	345.79
			^{214}Bi	609	1.26
			^{212}Pb	238	6.58
			^{214}Pb	352	5.52
			^{228}Ac	911	7.27
g	0.25	g_1	^{40}K	1461	407.13
			^{214}Bi	609	8.02
			^{212}Pb	238	7.95
			^{214}Pb	352	3.48
			^{228}Ac	911	11.83
h	0.5	h_1	^{40}K	1461	417.54
			^{214}Bi	609	7.71
			^{212}Pb	238	9.22
			^{214}Pb	352	13.07
			^{228}Ac	911	8.97
		h_2	^{40}K	1461	332.23
			^{214}Bi	609	1.82
			^{212}Pb	238	7.27
			^{214}Pb	352	4.08
			^{228}Ac	911	11.71
j	0.5	j_1	^{40}K	1461	395.64
			^{214}Bi	609	-1.19

			^{212}Pb	238	8.90
			^{214}Pb	352	4.51
			^{228}Ac	911	10.95
		j_2	^{40}K	1461	350.31
			^{214}Bi	609	7.97
			^{212}Pb	238	11.66
			^{214}Pb	352	7.48
n	0.5	n_1	^{40}K	1461	310.29
			^{214}Bi	609	9.34
			^{212}Pb	238	7.27
			^{214}Pb	352	5.76
			^{228}Ac	911	7.45
		n_2	^{40}K	1461	301.50
			^{214}Bi	609	6.25
			^{212}Pb	238	1.70
			^{214}Pb	352	2.63
			^{228}Ac	911	1.93
q	0.5	q_1	^{40}K	1461	278.68
			^{214}Bi	609	1.46
			^{212}Pb	238	0.00
			^{214}Pb	352	4.66
			^{228}Ac	911	4.67
		q_2	^{40}K	1461	295.09
			^{214}Bi	609	7.75
			^{212}Pb	238	6.88
			^{214}Pb	352	8.78
			^{228}Ac	911	4.48

r	0.5	r_1	^{40}K	1461	332.23
			^{214}Bi	609	1.82
			^{212}Pb	238	7.27
			^{214}Pb	352	4.08
			^{228}Ac	911	11.72
		r_2	^{40}K	1461	317.26
			^{214}Bi	609	2.97
			^{212}Pb	238	7.59
			^{214}Pb	352	8.61
			^{228}Ac	911	2.28
t	0.5	t_1	^{40}K	1461	168.83
			^{214}Bi	609	10.97
			^{212}Pb	238	8.92
			^{214}Pb	352	8.70
			^{228}Ac	911	4.68
		t_2	^{40}K	1461	350.31
			^{214}Bi	609	7.97
			^{212}Pb	238	11.66
			^{214}Pb	352	7.48
			^{228}Ac	911	7.80

Appendix IX: Block, Sampling area, Sample Number and Location of Soil And Radiation Samples Collection

BLOCK	Sampling area, km^2	Sample no.	Sampling area, km^2	LOCATION	
				Easting, E	Northing, N
A	1.0	A_1	0.25	344250	278250
		A_2	0.25	344250	277750
		A_3	0.25	343750	278250
		A_4	0.25	343750	277750
B	1.0	B_1	0.25	343250	278250
		B_2	0.25	343250	277250
		B_3	0.25	342750	278250
		B_4	0.25	342750	277250
C	1.0	C_1	0.25	342250	278250
		C_2	0.25	342250	277250
		C_3	0.25	341750	278250
		C_4	0.25	341750	277250
D	1.0	D_1	0.25	341250	278250
		D_2	0.25	341250	277250
		D_3	0.25	340750	278250
		D_4	0.25	340750	277250
E	1.0	E_1	0.25	340250	278250
		E_2	0.25	340350	278250
		E_3	0.25	339750	278250
		E_4	0.25	339750	278250
F	1.0	F_1	0.25	339256	278250
		F_2	0.25	339250	277750
		F_3	0.25	338750	278250
		F_4	0.25	338750	277750
G	1.0	G_1	0.25	339250	277250
		G_2	0.25	339250	276750
		G_3	0.25	338750	277250
		G_4	0.25	338750	276750
H	1.0	H_1	0.25	340250	277250
		H_2	0.25	340250	276750
		H_3	0.25	339750	277250
		H_4	0.25	339750	276750

J	1.0	J_1	0.25	341250	277250
		J_2	0.25	341250	276750
		J_3	0.25	340750	277250
		J_4	0.25	340750	276750
K	1.0	K_1	0.25	342250	277250
		K_2	0.25	342250	276750
		K_3	0.25	341750	277250
		K_4	0.25	341750	276750
L	1.0	L_1	0.25	343250	277250
		L_2	0.25	343250	276750
		L_3	0.25	342750	277250
		L_4	0.25	342750	276750
M	1.0	M_1	0.25	344250	277250
		M_2	0.25	344250	276750
		M_3	0.25	343750	277250
		M_4	0.25	343750	276750
N	1.0	N_1	0.25	344250	276250
		N_2	0.25	344250	275750
		N_3	0.25	343750	276250
		N_4	0.25	343750	275750
P	1.0	P_1	0.25	343250	276250
		P_2	0.25	343250	275750
		P_3	0.25	342750	276250
		P_4	0.25	342750	275750
Q	1.0	Q_1	0.25	342250	276250
		Q_2	0.25	342250	275750
		Q_3	0.25	341750	276250
		Q_4	0.25	341750	275750
R	1.0	R_1	0.25	341250	276250
		R_2	0.25	341250	275750
		R_3	0.25	340750	276250
		R_4	0.25	340750	275750
S	1.0	S_1	0.25	340250	276250
		S_2	0.25	340250	275750
		S_3	0.25	339710	276250
		S_4	0.25	339750	275750
T	1.0	T_1	0.25	339250	276250

		T_2	0.25	339250	275750
		T_3	0.25	338890	276250
		T_4	0.25	338750	275750
U	1.0	U_1	0.25	339250	275250
		U_2	0.25	339250	274750
		U_3	0.25	338750	275250
		U_4	0.25	338750	274750
V	1.0	V_1	0.25	340280	275250
		V_2	0.25	340250	274750
		V_3	0.25	339750	275250
		V_4	0.25	339750	274750
W	1.0	W_1	0.25	341250	275250
		W_2	0.25	341250	274750
		W_3	0.25	340750	275250
		W_4	0.25	340750	274750
X	1.0	X_1	0.25	340250	277250
		X_2	0.25	342250	275250
		X_3	0.25	342250	274750
		X_4	0.25	341750	275250
Y	1.0	Y_1	0.25	341750	274750
		Y_2	0.25	343250	275250
		Y_3	0.25	343250	274750
		Y_4	0.25	342750	275250
Z	1.0	Z_1	0.25	344250	275250
		Z_2	0.25	344250	274750
		Z_3	0.25	343750	275250
		Z_4	0.25	343750	274750
a	0.5	a_1	0.25	338250	278250
		a_2	0.25	338250	277750
b	0.5	b_1	0.25	338250	277250
		b_2	0.25	338250	276750
d	0.5	d_1	0.25	338250	276250
		d_2	0.25	338250	275750
e	0.5	e_1	0.25	338250	275250
		e_2	0.25	338250	274750
g	0.5	g_1	0.25	338250	278250
h	0.5	h_1	0.25	339250	274250

		h_2	0.25	338750	274250
j	0.5	j_1	0.25	340250	274250
		j_2	0.25	339750	274250
n	0.5	n_1	0.25	341250	274250
		n_2	0.25	340750	274250
q	0.5	q_1	0.25	342250	274250
		q_2	0.25	341750	274250
r	0.5	r_1	0.25	343250	274250
		r_2	0.25	342750	274250
t	0.5	t_1	0.25	344250	274250
		t_2	0.25	343750	274250

Appendix X: Calculated Activity Concentrations in Bqkg^{-1} of ^{226}Ra, ^{232}Th and ^{40}K for Soil and Rock Samples from Kargi Area, Marsabit – Kenya

BLOCK	Sample no.	Activity, Bq/kg			Average activity, Bg/kg		
		^{232}Th	^{238}U	^{40}K	^{232}Th	^{238}U	^{40}K
A	A_1	4.61	3.97	335.43	4.32±2.04	5.80±1.92	276.14±46.70
	A_2	4.33	7.89	283.16			
	A_3	1.69	6.95	262.72			
	A_4	6.66	4.39	223.25			
B	B_1	5.52	5.76	513.23	5.63±1.86	6.78±2.25	405.39±84.53
	B_2	7.87	9.81	306.76			
	B_3	3.32	4.56	396.59			
	B_4	5.79	6.99	404.98			
C	C_1	4.05	5.44	361.70	7.03±2.29	6.08±1.23	324.42±70.37
	C_2	6.91	7.59	322.56			
	C_3	9.60	4.78	226.59			
	C_4	7.54	6.51	386.81			
D	D_1	6.76	7.38	176.00	8.42±2.23	6.83±1.59	287.93±76.28
	D_2	11.44	7.31	308.34			
	D_3	8.77	8.11	346.42			
	D_4	6.72	4.50	320.96			
E	E_1	7.38	10.95	387.08	10.07±4.31	6.75±3.02	281.74±119.85
	E_2	10.07	4.71	141.10			
	E_3	16.15	6.96	375.51			
	E_4	6.66	4.39	223.25			
F	F_1	4.33	7.89	283.16	9.35±5.51	8.86±1.60	361.70±117.59
	F_2	17.2	11.25	534.22			
	F_3	8.11	8	290.92			
	F_4	7.75	8.29	338.49			
G	G_1	12.22	5.77	318.92	8.96±3.21	7.77±1.44	455.26±101.45
	G_2	5.53	8.90	444.67			
	G_3	6.99	7.69	555.03			
	G_4	11.11	8.72	502.42			
H	H_1	11.36	8.04	243.36	6.97±3.65	7.89±1.30	259.89±54.69
	H_2	7.38	6.76	338.42			
	H_3	2.46	7.10	246.36			
	H_4	6.67	9.66	211.41			

J	J_1	8.78	5.35	325.76	8.43±0.33	6.30±1.82	265.31±55.45
	J_2	8.43	8.73	291.38			
	J_3	8.51	4.56	231.42			
	J_4	7.99	6.56	212.67			
K	K_1	7.58	7.74	373.73	6.84±1.12	9.75±5.62	287.13±98.99
	K_2	6.72	6.90	202.30			
	K_3	5.30	6.23	200.51			
	K_4	7.74	18.12	371.96			
L	L_1	8.16	5.11	427.95	6.62±2.61	5.93±0.70	436.01±40.84
	L_2	3.08	6.78	383.17			
	L_3	8.94	5.71	478.54			
	L_4	6.28	6.13	454.36			
M	M_1	5.21	5.11	367.51	6.37±0.78	5.71±1.34	330.39±25.32
	M_2	6.91	7.59	322.56			
	M_3	6.63	5.62	310.53			
	M_4	6.72	4.5	320.96			
N	N_1	5.88	5.17	283.91	9.70±5.47	6.13±0.68	308.68±116.39
	N_2	7.13	6.11	260.64			
	N_3	7.99	6.56	212.67			
	N_4	17.80	6.66	477.50			
P	P_1	1.81	4.43	382.04	2.74±2.59	6.07±2.40	349.51±70.58
	P_2	6.17	9.52	243.93			
	P_3	0.00	4.45	380.00			
	P_4	2.99	5.89	392.05			
Q	Q_1	11.48	9.69	355.52	9.70±3.70	8.51±2.73	405.47±155.79
	Q_2	6.36	4.44	208.26			
	Q_3	14.06	10.32	508.11			
	Q_4	6.90	9.60	550.00			
R	R_1	8.19	6.76	357.01	7.49±2.78	8.72±2.26	398.65±33.46
	R_2	11.11	11.36	413.80			
	R_3	4.95	9.85	434.74			
	R_4	5.70	6.92	389.04			
S	S_1	5.31	7.81	286.72	6.71±1.63	7.93±0.24	330.12±49.75
	S_2	6.38	7.66	356.26			
	S_3	9.06	8.13	290.23			
	S_4	6.07	8.13	387.28			
T	T_1	15.30	15.07	365.85	10.66±5.89	10.53±3.51	425.98±131.73

	T_2	15.82	11.06	532.94			
	T_3	7.72	9.26	536.55			
	T_4	3.78	6.74	268.58			
U	U_1	5.43	6.35	432.33	8.33±3.20	7.73±1.75	380.98±168.08
	U_2	5.74	8.03	160.71			
	U_3	10.49	6.45	367.11			
	U_4	11.65	10.09	563.75			
V	V_1	5.13	5.64	350.66	8.96±12.51	6.36±3.62	440.90±151.52
	V_2	27.45	11.67	667.77			
	V_3	0.00	4.02	369.72			
	V_4	3.25	4.11	375.46			
W	W_1	5.70	6.92	389.04	6.54±4.26	6.85±1.33	450.12±52.19
	W_2	8.45	7.43	516.10			
	W_3	1.03	4.98	441.51			
	W_4	10.99	8.07	453.81			
X	X_1	11.82	11.78	592.73	9.34±5.98	9.05±4.68	380.08±246.93
	X_2	3.38	3.38	369.90			
	X_3	16.54	13.82	520.81			
	X_4	5.63	7.20	36.87			
Y	Y_1	11.63	8.95	312.38	9.31±5.13	11.96±2.81	231.27±86.67
	Y_2	2.24	15.63	119.17			
	Y_3	14.16	10.94	284.89			
	Y_4	9.19	12.30	208.63			
Z	Z_1	16.60	10.54	281.68	12.34±3.14	8.53±2.09	311.59±33.34
	Z_2	9.06	8.13	290.23			
	Z_3	11.48	9.69	355.52			
	Z_4	12.22	5.77	318.92			
a	a_1	7.09	6.74	336.44	7.70±0.86	5.61±1.61	438.06±143.71
	a_2	8.30	4.47	539.67			
b	b_1	5.53	5.76	513.24	9.75±5.96	5.54±0.32	472.49±57.64
	b_2	13.96	5.31	431.73			
d	d_1	5.57	3.30	451.25	8.73±4.47	4.04±1.05	369.76±115.25
	d_2	11.89	4.78	288.26			
e	e_1	7.03	8.03	462.76	6.98±0.07	6.78±1.77	404.28±82.71
	e_2	6.93	5.52	345.79			
g	g_1	9.89	5.75	407.13	9.89±0.00	5.75±0.00	407.13±0.00
h	h_1	9.10	10.39	417.54	8.65±0.64	8.58±2.57	387.28±42.80

	h_2	8.19	6.76	357.01			
j	j_1	9.93	4.51	395.64	9.83±0.14	6.12±2.27	372.98±32.05
	j_2	9.73	7.72	350.31			
n	n_1	6.38	7.66	356.26	6.87±0.69	7.61±0.08	333.28±32.51
	n_2	7.36	7.55	310.29			
q	q_1	4.67	4.66	278.68	5.18±0.71	6.46±2.55	286.89±11.60
	q_2	5.68	8.26	295.09			
r	r_1	9.49	4.08	332.23	8.54±1.34	4.94±1.21	324.75±10.59
	r_2	7.59	5.79	317.26			
t	t_1	6.80	9.83	168.83	8.27±2.07	8.78±1.49	259.57±128.33
	t_2	9.73	7.72	350.31			

Appendix XI: External (H_{ex}) and Internal (H_{in}) Hazard Indices, Representative Gamma ($I\gamma$) and Representative Alpha ($I\alpha$) Indices and Activity Correlations for Soil Samples

BLOCK	Sample no.	External hazard index, (H_{ex})	Internal hazard index, (H_{in})	Representative Gamma Index, $I\gamma$	Representative Alpha Index, $I\alpha$
A	A_1	0.10	0.11	0.15	0.02
	A_2	0.10	0.12	0.14	0.04
	A_3	0.08	0.10	0.12	0.03
	A_4	0.08	0.10	0.12	0.02
B	B_1	0.14	0.16	0.22	0.03
	B_2	0.12	0.15	0.17	0.05
	B_3	0.11	0.12	0.16	0.02
	B_4	0.13	0.14	0.19	0.03
C	C_1	0.11	0.10	0.16	0.03
	C_2	0.11	0.15	0.17	0.04
	C_3	0.10	0.15	0.14	0.02
	C_4	0.13	0.12	0.19	0.03
D	D_1	0.08	0.10	0.12	0.04
	D_2	0.13	0.15	0.18	0.04
	D_3	0.13	0.15	0.19	0.04
	D_4	0.10	0.12	0.16	0.02
E	E_1	0.14	0.17	0.20	0.05
	E_2	0.08	0.09	0.11	0.02
	E_3	0.16	0.18	0.23	0.03
	E_4	0.08	0.10	0.12	0.02
F	F_1	0.10	0.12	0.14	0.04
	F_2	0.21	0.24	0.30	0.06
	F_3	0.11	0.14	0.16	0.04
	F_4	0.12	0.15	0.18	0.04
G	G_1	0.13	0.14	0.19	0.03
	G_2	0.14	0.16	0.21	0.04
	G_3	0.16	0.18	0.25	0.04
	G_4	0.17	0.19	0.25	0.04
H	H_1	0.12	0.13	0.16	0.04
	H_2	0.12	0.14	0.17	0.03

	H_3	0.09	0.11	0.12	0.04
	H_4	0.07	0.09	0.14	0.05
J	J_1	0.12	0.13	0.17	0.03
	J_2	0.12	0.14	0.17	0.04
	J_3	0.09	0.11	0.13	0.02
	J_4	0.07	0.09	0.10	0.03
K	K_1	0.13	0.15	0.19	0.04
	K_2	0.09	0.11	0.12	0.03
	K_3	0.08	0.10	0.11	0.03
	K_4	0.16	0.21	0.22	0.09
L	L_1	0.13	0.15	0.20	0.03
	L_2	0.11	0.13	0.17	0.03
	L_3	0.15	0.16	0.22	0.03
	L_4	0.14	0.15	0.20	0.03
M	M_1	0.11	0.12	0.17	0.03
	M_2	0.11	0.13	0.17	0.04
	M_3	0.11	0.12	0.16	0.03
	M_4	0.10	0.12	0.16	0.02
N	N_1	0.10	0.11	0.14	0.03
	N_2	0.10	0.11	0.14	0.03
	N_3	0.09	0.11	0.13	0.03
	N_4	0.19	0.20	0.27	0.03
P	P_1	0.10	0.11	0.15	0.02
	P_2	0.10	0.13	0.14	0.05
	P_3	0.09	0.10	0.14	0.02
	P_4	0.11	0.12	0.17	0.03
Q	Q_1	0.14	0.17	0.21	0.05
	Q_2	0.08	0.09	0.12	0.02
	Q_3	0.19	0.22	0.27	0.05
	Q_4	0.17	0.19	0.25	0.05
R	R_1	0.12	0.14	0.18	0.03
	R_2	0.16	0.19	0.23	0.06
	R_3	0.14	0.16	0.20	0.05
	R_4	0.12	0.14	0.18	0.03
S	S_1	0.10	0.12	0.15	0.04
	S_2	0.12	0.14	0.18	0.04
	S_3	0.12	0.14	0.17	0.04

	S_4	0.13	0.15	0.19	0.04
T	T_1	0.18	0.22	0.25	0.08
	T_2	0.20	0.23	0.29	0.06
	T_3	0.17	0.19	0.25	0.05
	T_4	0.09	0.11	0.13	0.03
U	U_1	0.13	0.15	0.19	0.03
	U_2	0.08	0.10	0.11	0.04
	U_3	0.13	0.15	0.20	0.03
	U_4	0.19	0.22	0.28	0.05
V	V_1	0.11	0.12	0.16	0.03
	V_2	0.28	0.31	0.40	0.06
	V_3	0.09	0.10	0.14	0.02
	V_4	0.10	0.11	0.16	0.02
W	W_1	0.12	0.14	0.18	0.03
	W_2	0.16	0.18	0.24	0.04
	W_3	0.11	0.12	0.17	0.02
	W_4	0.16	0.18	0.23	0.04
X	X_1	0.20	0.23	0.30	0.06
	X_2	0.10	0.11	0.15	0.02
	X_3	0.21	0.25	0.30	0.07
	X_4	0.05	0.07	0.06	0.04
Y	Y_1	0.13	0.16	0.19	0.04
	Y_2	0.08	0.12	0.10	0.08
	Y_3	0.14	0.17	0.20	0.05
	Y_4	0.11	0.15	0.16	0.06
Z	Z_1	0.15	0.18	0.21	0.05
	Z_2	0.12	0.14	0.17	0.04
	Z_3	0.14	0.17	0.21	0.05
	Z_4	0.13	0.14	0.19	0.03
a	a_1	0.12	0.13	0.17	0.03
	a_2	0.16	0.17	0.24	0.02
b	b_1	0.14	0.16	0.22	0.03
	b_2	0.16	0.17	0.23	0.03
d	d_1	0.12	0.13	0.19	0.02
	d_2	0.12	0.13	0.17	0.02
e	e_1	0.15	0.17	0.22	0.04
	e_2	0.11	0.13	0.17	0.03

g	g_1	0.14	0.15	0.20	0.03
h	h_1	0.15	0.18	0.22	0.05
	h_2	0.12	0.14	0.18	0.03
j	j_1	0.13	0.14	0.20	0.02
	j_2	0.13	0.15	0.19	0.04
n	n_1	0.12	0.14	0.18	0.04
	n_2	0.11	0.13	0.17	0.04
q	q_1	0.09	0.10	0.13	0.02
	q_2	0.11	0.13	0.15	0.04
r	r_1	0.12	0.13	0.17	0.02
	r_2	0.11	0.13	0.16	0.03
t	t_1	0.09	0.11	0.12	0.05
	t_2	0.13	0.15	0.19	0.00
Mean		**0.12±0.03**	**0.14±0.04**	**0.18±0.05**	**0.04±0.01**

Appendix XII: Ranges and Averages for External (H_{ex}) and Internal (H_{in}) Hazard Indices, Representative Gamma Index (Iγ) and Representative Alpha Index (Iα) for Soil Samples

BLOCK	External hazard index, (H_{ex})		Internal hazard index, (H_{in})		Representative Gamma Index, Iγ		Representative Alpha Index, Iα	
	Range	Average	Range	Average	Range	Average	Range	Average
A	0.08 – 0.11	0.09±0.01	0.10 – 0.12	0.11±0.01	0.12 – 0.15	0.13±0.01	0.02 – 0.04	0.03±0.01
B	0.11 – 0.14	0.12±0.01	0.12 – 0.16	0.14±0.02	0.16 – 0.22	0.19±0.02	0.02 – 0.05	0.03±0.01
C	0.10 – 0.13	0.11±0.01	0.11 – 0.14	0.13±0.02	0.14 – 0.19	0.16±0.02	0.02 – 0.04	0.03±0.01
D	0.08 – 0.13	0.11±0.02	0.10 – 0.15	0.13±0.02	0.12 – 0.19	0.16±0.03	0.02 – 0.04	0.03±0.01
E	0.08 – 0.16	0.12±0.04	0.09 – 0.18	0.13±0.05	0.11 – 0.23	0.17±0.06	0.02 – 0.05	0.03±0.02
F	0.10 – 0.21	0.14±0.05	0.14 – 0.19	0.17±0.02	0.14 – 0.30	0.20±0.07	0.04 – 0.06	0.04±0.01
G	0.13 – 0.17	0.15±0.02	0.10 – 0.14	0.12±0.02	0.19 – 0.25	0.22±0.03	0.03 – 0.04	0.04±0.01
H	0.08 – 0.12	0.10±0.02	0.09 – 0.14	0.12±0.02	0.12 – 0.17	0.15±0.03	0.03 – 0.05	0.04±0.01
J	0.07 – 0.12	0.10±0.02	0.10 – 0.21	0.14±0.05	0.10 – 0.17	0.14±0.03	0.02 – 0.04	0.03±0.01
K	0.08 – 0.16	0.11±0.04	0.13 – 0.16	0.15±0.02	0.11 – 0.19	0.16±0.05	0.03 – 0.09	0.05±0.03
L	0.11 – 0.15	0.13±0.02	0.12 – 0.13	0.12±0.01	0.17 – 0.22	0.20±0.02	0.03 – 0.03	0.03±0.00
M	0.10 – 0.11	0.11±0.00	0.12 – 0.13	0.12±0.01	0.16 – 0.17	0.16±0.01	0.02 – 0.04	0.03±0.01
N	0.09 – 0.10	0.12±0.05	0.11 – 0.20	0.13±0.05	0.13 – 0.27	0.17±0.07	0.03 – 0.03	0.03±0.00
P	0.09 – 0.11	0.10±0.01	0.10 – 0.13	0.12±0.01	0.14 – 0.17	0.15±0.01	0.02 – 0.05	0.03±0.01
Q	0.08 – 0.17	0.14±0.05	0.09 – 0.22	0.17±0.05	0.12 – 0.27	0.21±0.07	0.02 – 0.05	0.04±0.01
R	0.12 – 0.16	0.14±0.02	0.14 – 0.19	0.16±0.02	0.18 – 0.23	0.20±0.02	0.03 – 0.06	0.04±0.01
S	0.10 – 0.13	0.12±0.01	0.12 – 0.15	0.14±0.01	0.15 – 0.19	0.17±0.02	0.04 – 0.04	0.04±0.00
T	0.09 – 0.20	0.16±0.05	0.11 – 0.23	0.19±0.06	0.13 – 0.29	0.23±0.07	0.03 – 0.08	0.05±0.02
U	0.08 – 0.19	0.13±0.05	0.10 – 0.22	0.15±0.05	0.11 – 0.28	0.19±0.07	0.03 – 0.05	0.04±0.01
V	0.09 – 0.28	0.14±0.09	0.10 – 0.31	0.16±0.10	0.14 – 0.40	0.21±0.12	0.02 – 0.06	0.03±0.02

W	0.11 – 0.16	0.14±0.03	0.12 – 0.18	0.16±0.03	0.17 – 0.24	0.21±0.04	0.02 – 0.04	0.03±0.01
X	0.05 – 0.21	0.14±0.08	0.07 – 0.25	0.14±0.02	0.06 – 0.30	0.20±0.12	0.02 – 0.07	0.05±0.02
Y	0.08 – 0.14	0.12±0.03	0.12 – 0.17	0.15±0.02	0.10 – 0.20	0.16±0.04	0.04 – 0.08	0.06±0.01
Z	0.12 – 0.15	0.14±0.02	0.14 – 0.18	0.16±0.02	0.17 – 0.21	0.19±0.02	0.03 – 0.05	0.04±0.01
a	0.12 – 0.16	0.14±0.03	0.13 – 0.17	0.15±0.02	0.17 – 0.24	0.20±0.05	0.02 – 0.03	0.03±0.01
b	0.14 – 0.16	0.15±0.01	0.16 – 0.17	0.17±0.01	0.22 – 0.23	0.22±0.01	0.03 – 0. 03	0.03±0.00
d	0.12 – 0.12	0.12±0.00	0.13 – 0.13	0.13±0.00	0.17 – 0.19	0.18±0.01	0.02 – 0.02	0.02±0.01
e	0.11 – 0.15	0.13±0.02	0.13 – 0.17	0.15±0.03	0.17 – 0.22	0.19±0.03	0.03 – 0.04	0.03±0.01
g	0.14	0.14±0.00	0.15	0.15±0.00	0.2	0.20±0.00	0.03	0.03±0.00
h	0.12 – 0.15	0.14±0.02	0.14 – 0.18	0.16±0.03	0.18 – 0.22	0.20±0.03	0.03 – 0.05	0.04±0.01
j	0.13 – 0.13	0.13±0.00	0.14 – 0.15	0.15±0.01	0.19 – 0.20	0.19±0.00	0.02 – 0.04	0.02±0.01
n	0.11 – 0.12	0.12±0.00	0.13 – 0.14	0.14±0.00	0.17 – 0.18	0.17±0.01	0.04 – 0.04	0.04±0.00
q	0.09 – 0.11	0.10±0.01	0.10 – 0.13	0.11±0.02	0.13 – 0.15	0.14±0.02	0.02 – 0.04	0.03±0.01
r	0.11 – 0.12	0.11±0.00	0.13 – 0.13	0.13±0.00	0.16 – 0.17	0.17±0.01	0.02 – 0.03	0.02±0.01
t	0.09 – 0.13	0.11±0.03	0.11 – 0.15	0.13±0.03	0.12 – 0.19	0.16±0.05	0.04 – 0.05	0.04±0.01

Appendix XIII: Elemental Concentration of Specific Activity of ^{238}U (ppm), ^{232}Th (ppm) and ^{40}K (%) in Soil Samples with their Ratios

BLOCK	Sample no.	Elemental concentration			Correlation		
		^{232}Th (ppm)	^{238}U (ppm)	^{40}K (%)	Th/U	K/U	K/Th
A	A_1	1.14	0.32	1.07	3.53	3.33	0.94
	A_2	1.07	0.64	0.90	1.67	1.42	0.85
	A_3	0.42	0.56	0.84	0.74	1.49	2.02
	A_4	1.64	0.36	0.71	4.61	2.01	0.43
B	B_1	1.36	0.47	1.64	2.92	3.52	1.21
	B_2	1.94	0.79	0.98	2.44	1.23	0.51
	B_3	0.82	0.37	1.27	2.21	3.43	1.55
	B_4	1.43	0.57	1.29	2.52	2.29	0.91
C	C_1	1.00	0.44	1.16	2.26	2.62	1.16
	C_2	1.70	0.61	1.03	2.77	1.68	0.61
	C_3	2.36	0.39	0.72	6.11	1.87	0.31
	C_4	1.86	0.53	1.24	3.52	2.34	0.67
D	D_1	1.67	0.60	0.56	2.79	0.94	0.34
	D_2	2.82	0.59	0.99	4.76	1.66	0.35
	D_3	2.16	0.66	1.11	3.29	1.69	0.51
	D_4	1.66	0.36	1.03	4.54	2.81	0.62
E	E_1	1.82	0.89	1.24	2.05	1.39	0.68
	E_2	2.48	0.38	0.45	6.50	1.18	0.18
	E_3	3.98	0.56	1.20	7.06	2.13	0.30
	E_4	1.64	0.36	0.71	4.61	2.01	0.43
F	F_1	1.07	0.64	0.90	1.67	1.42	0.85
	F_2	4.24	0.91	1.71	4.65	1.87	0.40
	F_3	2.00	0.65	0.93	3.08	1.43	0.47
	F_4	1.91	0.67	1.08	2.84	1.61	0.57
G	G_1	3.01	0.47	1.02	6.44	2.18	0.34
	G_2	1.36	0.72	1.42	1.89	1.97	1.04
	G_3	1.72	0.62	1.77	2.76	2.85	1.03
	G_4	2.74	0.71	1.61	3.88	2.27	0.59
H	H_1	2.80	0.65	0.78	4.30	1.19	0.28
	H_2	1.82	0.55	1.08	3.32	1.98	0.59
	H_3	0.61	0.57	0.79	1.05	1.37	1.30
	H_4	1.64	0.78	0.68	2.10	0.86	0.41

J	J_1	2.16	0.43	1.04	4.99	2.40	0.48
	J_2	2.08	0.71	0.93	2.94	1.32	0.41
	J_3	2.10	0.37	0.74	5.68	2.00	0.35
	J_4	1.97	0.53	0.68	3.70	0.73	0.20
K	K_1	1.87	0.56	0.65	2.98	1.91	0.64
	K_2	1.66	0.56	0.65	2.96	1.16	0.39
	K_3	1.31	0.50	0.64	2.59	1.27	0.49
	K_4	1.91	1.47	1.19	1.30	0.81	0.62
L	L_1	2.01	0.41	1.37	4.86	3.30	0.68
	L_2	0.76	0.55	1.22	1.38	2.23	1.61
	L_3	2.20	0.46	1.53	4.76	3.31	0.69
	L_4	1.55	0.50	1.45	3.12	2.92	0.94
M	M_1	1.28	0.41	1.17	3.10	2.84	0.91
	M_2	1.70	0.61	1.03	2.77	1.68	0.61
	M_3	1.63	0.46	0.99	3.59	2.18	0.61
	M_4	1.66	0.36	1.03	4.54	2.81	0.62
N	N_1	1.45	0.42	0.91	3.46	2.17	0.63
	N_2	1.76	0.53	0.68	3.55	1.68	0.47
	N_3	1.97	0.53	0.68	3.70	1.28	0.35
	N_4	4.38	0.54	1.53	8.13	2.83	0.35
P	P_1	0.45	0.36	1.22	1.24	3.40	2.74
	P_2	1.52	0.77	0.78	1.97	1.01	0.51
	P_3	0.00	0.36	1.21	0.00	3.37	0.00
	P_4	0.74	0.48	1.25	1.54	2.63	1.70
Q	Q_1	2.83	0.78	1.14	3.60	1.45	0.40
	Q_2	1.57	0.36	0.67	4.36	1.85	0.42
	Q_3	3.46	0.84	1.62	4.14	1.94	0.47
	Q_4	1.70	0.78	1.76	2.19	2.26	1.03
R	R_1	2.02	0.55	1.14	3.69	2.08	0.57
	R_2	2.74	0.92	1.32	2.97	1.44	0.48
	R_3	1.22	0.80	1.39	1.53	1.74	1.14
	R_4	1.40	0.56	1.24	2.51	2.22	0.89
S	S_1	1.31	0.63	0.92	2.07	1.45	0.70
	S_2	1.57	0.62	1.14	2.53	1.84	0.72
	S_3	2.23	0.66	0.93	3.39	1.41	0.42
	S_4	1.50	0.66	1.24	2.27	1.88	0.83
T	T_1	3.77	1.22	1.17	3.09	0.96	0.31

	T_2	3.90	0.90	1.70	4.35	1.90	0.44
	T_3	1.90	0.75	1.71	2.54	2.29	0.90
	T_4	0.93	0.55	0.86	1.71	1.57	0.92
U	U_1	1.34	0.51	1.38	2.60	2.69	1.03
	U_2	1.41	0.65	0.51	2.17	0.79	0.36
	U_3	2.58	0.52	1.17	4.95	2.25	0.45
	U_4	2.87	0.82	1.80	3.51	2.20	0.63
V	V_1	1.26	0.46	1.12	2.77	2.45	0.89
	V_2	6.76	0.94	2.13	7.16	2.26	0.32
	V_3	0.00	0.33	1.18	0.00	3.63	0.00
	V_4	0.80	0.33	1.20	2.41	3.60	1.50
W	W_1	1.40	0.56	1.24	2.51	2.22	0.89
	W_2	2.08	0.60	1.65	3.46	2.74	0.79
	W_3	0.25	0.40	1.41	0.63	3.50	5.56
	W_4	2.71	0.65	1.45	4.14	2.22	0.54
X	X_1	2.91	0.95	1.89	3.05	1.99	0.65
	X_2	0.83	0.27	1.18	3.04	4.32	1.42
	X_3	4.07	1.12	1.66	3.64	1.49	0.41
	X_4	1.37	0.58	0.12	2.38	0.20	0.08
Y	Y_1	2.86	0.72	1.00	3.95	1.38	0.35
	Y_2	0.55	1.27	0.38	0.44	0.30	0.69
	Y_3	3.49	0.89	0.91	3.94	1.03	0.26
	Y_4	2.26	1.00	0.67	2.27	0.67	0.29
Z	Z_1	4.09	0.85	0.90	4.79	1.05	0.22
	Z_2	2.23	0.66	0.93	3.39	1.41	0.42
	Z_3	2.83	0.78	1.14	3.60	1.45	0.40
	Z_4	3.01	0.47	1.02	6.44	2.18	0.34
a	a_1	1.75	0.55	1.07	3.20	1.97	0.62
	a_2	2.04	0.36	1.72	5.65	4.76	0.84
b	b_1	1.36	0.47	1.64	2.92	3.52	1.20
	b_2	3.44	0.43	1.38	8.00	3.21	0.40
d	d_1	1.37	0.27	1.44	5.13	5.40	1.05
	d_2	2.93	0.39	0.92	7.57	2.38	0.31
e	e_1	1.73	0.65	1.48	2.66	2.27	0.85
	e_2	1.71	0.45	1.10	3.82	2.47	0.65
g	g_1	2.44	0.47	1.30	5.23	2.79	0.53
h	h_1	2.24	0.84	1.33	2.66	1.59	0.60

	h_2	2.02	0.55	1.14	3.69	2.08	0.57
j	j_1	2.45	0.37	1.26	6.70	3.46	0.52
	j_2	2.40	0.63	1.12	3.83	1.79	0.47
n	n_1	1.57	0.62	1.14	2.53	1.84	0.72
	n_2	1.81	0.61	0.99	2.97	1.62	0.55
q	q_1	1.15	0.38	0.89	3.05	2.36	0.77
	q_2	1.40	0.67	0.94	2.09	1.41	0.67
r	r_1	2.34	0.33	1.06	7.08	3.21	0.45
	r_2	1.87	0.47	1.01	3.99	2.16	0.54
t	t_1	1.67	0.80	0.54	2.10	0.68	0.32
	t_2	2.40	0.63	1.12	3.83	1.79	0.47
Mean and standard deviation		**1.97±0.99**	**0.60±0.21**	**1.13±0.35**	**3.42±1.63**	**2.07±0.89**	**0.70±0.61**

Appendix XIV: Range and Mean for Correlation Between ^{232}Th, ^{238}U and ^{40}K Activities as Calculated from Soil Samples

BLOCK	Th/U		K/U		K/Th	
	Range	Average	Range	Average	Range	Average
A	0.74 – 4.61	2.64±1.76	1.42 – 3.33	2.06±0.89	0.85 – 2.02	1.06±0.67
B	2.21 – 2.92	2.52±0.29	1.23 – 3.52	2.62±1.08	0.51 – 1.55	1.04±0.44
C	2.26 – 6.11	3.67±1.71	1.68 – 2.62	2.13±0.43	0.31 – 1.16	0.68±0.35
D	2.79 – 4.76	3.84±0.96	0.94 – 2.81	1.78±0.77	0.34 – 0.62	0.45±0.14
E	2.05 – 7.06	5.06±2.26	1.39 – 2.13	1.68±0.46	0.18 – 0.68	0.40±0.21
F	1.67 – 4.65	3.06±1.23	1.42 – 1.61	1.58±0.21	0.40 – 0.85	0.57±0.20
G	1.89 – 6.44	3.74±1.97	1.97 – 2.85	2.32±0.37	0.34 – 1.04	0.75±0.35
H	1.05 – 4.30	2.69±1.42	0.86 – 1.98	1.35±0.47	0.28 – 1.30	0.65±0.35
J	2.94 – 4.99	4.33±1.24	0.73 – 2.40	1.61±0.74	0.20 – 0.48	0.37±0.13
K	1.30 – 2.98	2.46±0.79	0.81 – 1.91	1.29±0.46	0.39 – 0.64	0.54±0.12
L	1.38 – 4.86	3.53±1.64	2.23 – 3.30	2.94±0.51	0.68 – 1.61	0.98±0.44
M	2.77 – 4.54	3.50±0.77	1.68 – 2.84	2.38±0.56	0.61 – 0.91	0.69±0.15
N	3.46 – 8.13	4.71±2.28	1.28 – 2.83	1.99±0.67	0.35 – 0.63	0.45±0.13
P	0.00 – 1.97	1.19±0.85	1.01 – 3.40	2.60±1.12	0.00 – 2.74	1.24±1.24
Q	2.19 – 4.36	3.57±0.98	1.45 – 2.26	1.88±0.33	0.40 – 1.03	0.58±0.30
R	1.53 – 3.69	2.67±0.90	1.44 – 2.22	1.87±0.35	0.48 – 1.14	0.77±0.30
S	2.07 – 3.39	2.57±0.58	1.41 – 1.88	1.64±0.25	0.42 – 0.83	0.67±0.18
T	1.71 – 4.35	2.92±1.11	0.96 – 2.29	1.68±0.56	0.31 – 0.92	0.64±0.32
U	2.60 – 4.95	3.31±1.23	0.79 – 2.69	1.98±0.82	0.36 – 1.03	0.62±0.30
V	0.00 – 7.16	3.08±2.98	2.26 – 3.63	2.99±0.73	0.00 – 1.50	0.68±0.66
W	0.63 – 4.14	2.68±1.53	2.22 – 3.50	2.67±0.61	0.54 – 5.56	1.94±2.42
X	2.38 – 3.64	3.03±0.52	0.20 – 4.32	2.00 ±1.72	0.08 – 1.42	0.64±0.57
Y	0.44 – 3.95	2.65±1.67	0.30 – 1.38	0.84±0.46	0.26 – 0.69	0.40±0.20
Z	3.39 – 6.44	4.56±1.40	1.05 – 2.18	1.52±0.47	0.22 – 0.42	0.34±0.09
a	3.20 – 5.65	4.42±1.73	1.97 – 4.76	3.37±1.98	0.62 – 0.84	0.73±0.16
b	2.92 – 8.00	5.46±3.59	3.21 – 3.52	3.36±0.22	0.40 – 1.20	0.80±0.57
d	5.13 – 7.57	6.35±1.72	2.38 – 5.40	3.89±2.13	0.31±1.05	0.68±0.52
e	2.66 – 3.82	3.24±0.82	2.27 – 2.47	2.37±0.14	0.65 – 0.85	0.75±0.15
g	5.23	5.23±0.00	2.79	2.79±0.00	0.53	0.53±0.00
h	2.66 – 3.69	3.17±0.72	1.59 – 2.08	1.83±0.35	0.57 – 0.60	0.58±0.02
j	3.83 – 6.70	5.27±2.20	1.79 – 3.46	2.63±1.18	0.47 – 0.52	0.58±0.04
n	2.53 – 2.97	2.75±0.31	1.62 – 1.84	1.73±0.15	0.55 – 0.72	0.64±0.13
q	2.09 – 3.05	2.57±0.68	1.41 – 2.36	1.88±0.67	0.67 – 0.77	0.72±0.07
r	3.99 – 7.08	5.53±2.18	2.16 – 3.21	2.69±0.74	0.45 – 0.54	0.50±0.06
t	2.10 – 3.83	2.97±1.22	0.68 – 1.79	1.23±0.79	0.45 – 0.54	0.39±0.10

Appendix XV: Absorbed Dose Rates as Measured 1 m Above the Surface at Each Sapling Point for Soil samples

BLOCK	Sample no.	Average site absorbed dose rate ($nGyh^{-1}$)	Average absorbed dose rate ($nGyh^{-1}$)	UNSCEAR, 2000 RECOMMENDATION, nGy/h
A	A_1	42.86	77.86±34.84	60.00
	A_2	98.57		
	A_3	115.71		
	A_4	54.29		
B	B_1	58.57	53.93±4.72	
	B_2	51.43		
	B_3	48.57		
	B_4	57.14		
C	C_1	94.29	92.14±5.28	
	C_2	98.57		
	C_3	87.14		
	C_4	88.57		
D	D_1	102.86	92.50±11.03	
	D_2	77.14		
	D_3	97.14		
	D_4	92.86		
E	E_1	88.57	76.07±19.98	
	E_2	74.29		
	E_3	48.57		
	E_4	92.86		
F	F_1	91.43	81.79±18.34	
	F_2	90.00		
	F_3	54.29		
	F_4	91.43		
G	G_1	80.00	89.64±23.42	
	G_2	98.57		
	G_3	62.86		
	G_4	117.14		
H	H_1	95.71	66.07±21.23	
	H_2	45.71		
	H_3	58.57		

	H_4	64.29		
J	J_1	132.86	98.57±31.90	
	J_2	90.00		
	J_3	112.86		
	J_4	58.57		
K	K_1	51.43	60.00±7.90	
	K_2	67.14		
	K_3	57.14		
	K_4	64.29		
L	L_1	64.29	62.86±3.09	
	L_2	58.57		
	L_3	62.86		
	L_4	65.71		
M	M_1	87.14	78.93±16.76	
	M_2	65.71		
	M_3	64.29		
	M_4	98.57		
N	N_1	67.14	74.25±15.66	
	N_2	55.57		
	N_3	85.71		
	N_4	88.57		
P	P_1	70.00	72.86±21.73	
	P_2	71.43		
	P_3	101.43		
	P_4	48.57		
Q	Q_1	60.00	76.79±12.90	
	Q_2	82.86		
	Q_3	90.00		
	Q_4	74.29		
R	R_1	57.14	57.86±5.28	
	R_2	64.29		
	R_3	58.57		
	R_4	51.43		
S	S_1	48.57	55.00±4.29	
	S_2	57.14		
	S_3	57.14		
	S_4	57.14		

T	T_1	70.00	72.86±21.73	
	T_2	71.43		
	T_3	101.43		
	T_4	48.57		
U	U_1	101.43	105.36±9.14	
	U_2	112.86		
	U_3	112.86		
	U_4	94.29		
V	V_1	58.57	106.43±54.79	
	V_2	62.86		
	V_3	170.00		
	V_4	134.29		
W	W_1	90.00	82.86±11.01	
	W_2	94.29		
	W_3	75.71		
	W_4	71.43		
X	X_1	128.57	115.00±21.43	
	X_2	91.43		
	X_3	102.86		
	X_4	137.14		
Y	Y_1	84.29	96.43±31.35	
	Y_2	132.86		
	Y_3	108.57		
	Y_4	60.00		
Z	Z_1	82.86	89.65±15.88	
	Z_2	90.00		
	Z_3	74.29		
	Z_4	111.43		
a	a_1	81.43	69.29±17.18	
	a_2	57.14		
b	b_1	80.00	87.15±10.10	
	b_2	94.29		
d	d_1	97.14	85.00±17.17	
	d_2	72.86		
e	e_1	148.57	133.57±21.21	
	e_2	118.57		
g	g_1	102.86	102.86±0.00	

h	h_1	77.14	87.14±14.14	
	h_2	97.14		
j	j_1	145.71	132.14±19.19	
	j_2	118.57		
n	n_1	132.86	111.43±30.31	
	n_2	90.00		
q	q_1	112.86	85.72±38.39	
	q_2	58.57		
r	r_1	51.43	59.29±11.11	
	r_2	67.14		
t	t_1	57.14	60.72±5.06	
	t_2	64.29		

Appendix XVI: Calculated Absorbed Dose Rates ($nGyh^{-1}$) of the Soil Samples from Sites

BLOCK	Sample no.	Dose rates due to ^{232}Th ($nGyh^{-1}$)	Dose rates due to ^{226}Ra ($nGyh^{-1}$)	Dose rates due to ^{40}K ($nGyh^{-1}$)	Total average absorbed dose rate ($nGyh^{-1}$)	Total average absorbed dose rate ($nGyh^{-1}$)	UNSCEAR 2000 RECOMMENDATION, nGy/h
A	A_1	3.05	1.85	14.42	19.33	17.45±1.85	54
	A_2	2.87	3.68	12.18	18.73		
	A_3	1.12	3.25	11.30	15.66		
	A_4	4.41	2.05	9.60	16.06		
B	B_1	3.65	2.69	22.07	28.41	24.32±3.01	
	B_2	5.21	4.58	13.19	22.98		
	B_3	2.20	2.13	17.05	21.38		
	B_4	3.83	3.26	17.41	24.51		
C	C_1	2.68	2.54	15.55	20.77	21.44±2.63	
	C_2	4.57	3.54	13.87	21.99		
	C_3	6.36	2.23	9.74	18.33		
	C_4	4.99	3.04	16.63	24.66		
D	D_1	4.48	3.45	7.57	15.49	21.15±4.22	
	D_2	7.57	3.41	13.26	24.25		
	D_3	5.81	3.79	14.90	24.49		
	D_4	4.45	2.10	13.80	20.35		
E	E_1	4.89	5.11	16.64	26.64	21.93±7.58	
	E_2	6.67	2.20	6.07	14.93		

	E_3	10.69	3.25	16.15	30.09		
	E_4	4.41	2.05	9.60	16.06		
F	F_1	2.87	3.68	12.18	18.73	25.88±9.37	
	F_2	11.39	5.25	22.97	39.61		
	F_3	5.37	3.74	12.51	21.61		
	F_4	5.13	3.87	14.56	23.56		
G	G_1	8.09	2.69	13.71	24.50	29.14±4.09	
	G_2	3.66	4.16	19.12	26.94		
	G_3	4.63	3.59	23.87	32.08		
	G_4	7.35	4.07	21.60	33.03		
H	H_1	7.52	3.75	10.46	21.74	19.47±3.29	
	H_2	4.89	3.16	14.55	22.59		
	H_3	1.63	3.32	10.59	15.54		
	H_4	4.42	4.51	9.09	18.02		
J	J_1	5.81	2.50	14.01	22.32	18.95±4.17	
	J_2	5.58	4.08	12.53	22.19		
	J_3	5.63	2.13	9.95	17.71		
	J_4	5.29	3.06	5.23	13.58		
K	K_1	5.02	3.61	16.07	24.70	21.42±6.92	
	K_2	4.45	3.22	8.70	16.37		
	K_3	3.51	2.91	8.62	15.04		
	K_4	5.12	8.46	15.99	29.58		
L	L_1	5.40	2.39	18.40	26.19	25.90±3.11	

	L_2	2.04	3.17	16.48	21.68		
	L_3	5.92	2.67	20.58	29.16		
	L_4	4.16	2.86	19.54	26.56		
M	M_1	3.45	2.39	15.80	21.64	21.09±0.85	
	M_2	4.57	3.54	13.87	21.99		
	M_3	4.39	2.62	13.35	20.37		
	M_4	4.45	2.10	13.80	20.35		
N	N_1	3.89	2.41	12.21	18.52	22.56±8.60	
	N_2	4.72	2.85	11.21	18.78		
	N_3	5.29	3.06	9.14	17.50		
	N_4	11.78	3.11	20.53	35.43		
P	P_1	1.20	2.07	16.43	19.69	19.68±1.37	
	P_2	4.08	4.45	10.49	19.02		
	P_3	0.00	2.08	16.34	18.42		
	P_4	1.98	2.75	16.86	21.59		
Q	Q_1	7.60	4.53	15.29	27.41	27.83±9.11	
	Q_2	4.21	2.07	8.96	15.24		
	Q_3	9.31	4.82	21.85	35.98		
	Q_4	4.57	4.48	23.65	32.70		
R	R_1	5.42	3.16	15.35	23.93	26.17±3.13	
	R_2	7.35	5.31	17.79	30.45		
	R_3	3.28	4.60	18.69	26.57		
	R_4	3.77	3.23	16.73	23.73		

S	S_1	3.52	3.65	12.33	19.49	22.34±2.10	
	S_2	4.22	3.58	15.32	23.12		
	S_3	6.00	3.80	12.48	22.27		
	S_4	4.02	3.80	16.65	24.47		
T	T_1	10.13	7.04	15.73	32.90	30.29±9.15	
	T_2	10.47	5.17	22.92	38.55		
	T_3	5.11	4.32	23.07	32.51		
	T_4	2.50	3.15	11.55	17.20		
U	U_1	3.59	2.97	18.59	25.15	25.51±9.07	
	U_2	3.80	3.75	6.91	14.46		
	U_3	6.94	3.01	15.79	25.74		
	U_4	7.71	4.71	24.24	36.67		
V	V_1	3.40	2.63	15.08	21.11	27.86±16.38	
	V_2	18.17	5.45	28.71	52.34		
	V_3	0.00	1.88	15.90	17.78		
	V_4	2.15	1.92	16.14	20.22		
W	W_1	3.77	3.23	16.73	23.73	26.89±4.71	
	W_2	5.59	3.47	22.19	31.26		
	W_3	0.68	2.33	18.98	21.99		
	W_4	7.28	3.77	19.51	30.56		
X	X_1	7.82	5.50	25.49	38.81	26.75±15.19	
	X_2	2.24	1.58	15.91	19.72		
	X_3	10.95	6.45	22.39	39.80		

	X_4	3.73	3.36	1.59	8.67		
Y	Y_1	7.70	4.18	13.43	25.31	21.69±5.77	
	Y_2	1.48	7.30	5.12	13.91		
	Y_3	9.37	5.11	12.25	26.73		
	Y_4	6.08	5.74	8.97	20.80		
Z	Z_1	10.99	4.92	12.11	28.02	25.55±2.67	
	Z_2	6.00	3.80	12.48	22.27		
	Z_3	7.60	4.53	15.29	27.41		
	Z_4	8.09	2.69	13.71	24.50		
a	a_1	4.69	3.15	14.47	22.31	26.55±6.00	
	a_2	5.49	2.09	23.21	30.79		
b	b_1	3.66	2.69	22.07	28.42	29.36±1.32	
	b_2	9.24	2.48	18.56	30.29		
d	d_1	3.72	1.54	19.40	24.66	23.61±1.48	
	d_2	7.93	2.23	12.40	22.56		
e	e_1	4.65	3.75	19.90	28.30	25.17±4.43	
	e_2	4.59	2.58	14.87	22.03		
g	g_1	6.55	2.69	17.51	26.74	26.74±0.00	
h	h_1	6.02	4.85	17.95	28.83	26.38±3.46	
	h_2	5.42	3.16	15.35	23.93		
j	j_1	6.57	2.11	17.01	25.69	25.40±0.41	
	j_2	6.44	3.61	15.06	25.11		
n	n_1	4.22	3.58	15.32	23.12	22.43±0.98	

	n_2	4.87	3.53	13.34	21.74		
q	q_1	4.22	3.58	15.32	23.12	19.09±5.71	
	q_2	3.51	2.91	8.62	15.04		
r	r_1	6.28	1.91	14.29	22.47	21.92±0.78	
	r_2	5.02	2.70	13.64	21.37		
t	t_1	4.50	4.59	7.26	16.37	20.74±6.18	
	t_2	6.44	3.61	15.09	25.11		
Mean		**5.29±2.65**	**3.46±1.21**	**15.12±4.74**	**23.87±6.57**		

Appendix XVII: Range and Mean Calculated Absorbed Dose Rates ($nGyh^{-1}$) of the Samples from Locations

BLOCK	Dose rates due to ^{232}Th ($nGyh^{-1}$)		Dose rates due to ^{226}Ra ($nGyh^{-1}$)		Dose rates due to ^{40}K ($nGyh^{-1}$)		Total average absorbed dose rate ($nGyh^{-1}$)	
	Range	Average	Range	Average	Range	Average	Range	Average
A	1.12 – 4.41	2.86±1.35	1.85 – 3.68	2.71±0.90	9.60 – 14.42	11.87±2.01	15.66 – 19.33	17.45±1.85
B	2.20 – 5.21	3.72±1.23	2.13 – 4.58	3.17±1.05	13.19 – 22.07	17.43±3.63	21.38 – 28.41	24.32±3.01
C	2.68 – 6.36	4.65±1.52	2.23 – 3.54	2.84±0.58	9.74 – 16.63	13.95±3.03	18.33 – 24.66	21.44±2.63
D	4.45 – 7.57	5.58±1.47	2.10 – 3.79	3.19±0.74	7.57 – 14.90	12.38±3.28	15.49 – 24.49	21.14±4.22
E	4.41 – 10.69	6.66±2.86	2.05 – 5.11	3.15±1.41	6.07 – 16.64	12.11±5.15	14.93 – 30.09	21.93±7.58
F	2.87 – 11.39	6.19±3.64	3.68 – 5.25	4.14±0.75	12.18 – 22.97	15.55±5.06	18.73 – 39.61	25.88±9.37
G	3.66 – 8.09	5.93±2.12	2.69 – 4.16	3.63±0.67	13.71 – 23.87	19.58±4.36	24.50 – 33.03	29.14±4.09
H	1.63 – 7.52	4.61±2.41	3.16 – 4.51	3.68±0.61	9.09 – 14.55	11.18±2.35	15.54 – 22.59	19.47±3.29
J	5.29 – 5.81	5.58±0.22	2.13 – 4.08	2.94±0.61	5.23 – 14.01	10.43±3.85	13.58 – 22.32	18.95±4.17
K	3.51 – 5.12	4.52±0.74	2.91 – 8.46	4.55±2.62	8.62 – 16.07	12.35±4.26	15.04 – 29.58	21.42±6.92
L	2.04 – 5.92	4.38±1.73	2.39 – 3.17	2.77±0.33	16.48 – 20.58	18.75±1.76	21.68 – 29.16	25.90±3.11
M	3.45 – 4.57	4.22±0.45	2.10 – 3.54	2.66±0.54	13.35 – 15.80	14.21±0.94	20.35 – 21.99	21.09±0.74
N	3.89 – 11.78	6.42±3.62	2.41 – 3.11	2.86±0.32	9.14 – 20.53	13.27±5.00	17.50 – 35.43	22.56±8.60
P	0.00 – 4.45	1.82±1.72	2.07 – 4.45	2.84±1.12	10.49 – 16.86	15.03±3.03	18.42 – 21.59	19.68±1.37
Q	4.21 – 9.31	6.42±2.45	2.07 – 4.82	3.98±1.28	8.96 – 23.65	17.44±6.70	15.24 – 35.98	27.83±9.11
R	3.28 – 7.35	4.96±1.84	3.16 – 5.31	4.07±1.06	15.35 – 18.69	17.14±1.44	23.73 – 30.45	26.17±3.13
S	3.52 – 6.00	4.44±1.08	3.58 – 3.80	3.70±0.11	12.33 – 16.65	14.20±2.14	19.49 – 24.47	22.34±2.10
T	2.50 – 10.47	7.05±3.90	3.15 – 7.04	4.92±1.64	11.55 – 23.07	18.32±5.66	17.20 – 38.55	30.29±9.15
U	3.80 – 7.71	5.51±2.12	2.97 – 4.71	3.61±0.82	6.91 – 24.24	16.38±7.23	14.46 – 36.67	25.50±9.07
V	0.00 – 18.17	5.93±8.28	1.88 – 5.45	2.97±1.69	15.08 – 28.71	18.96±6.52	17.78 – 52.34	27.86±16.38
W	0.68 – 7.28	4.33±2.82	2.33 – 3.77	3.20±0.62	16.73 – 22.19	19.35±2.24	21.99 – 30.56	26.89±4.71

X	2.24 – 10.95	6.18±3.96	1.58 – 6.45	4.22±2.19	1.59 – 25.49	16.34±10.62	8.67 – 39.80	26.75±15.19
Y	1.48 – 9.37	6.16±3.40	4.18 – 7.30	5.58±1.31	5.12 – 13.43	9.94±3.73	13.91 – 26.73	21.69±5.77
Z	6.00 – 10.99	8.17±2.08	2.69 – 4.92	3.98±0.98	12.11 – 15.29	13.40±1.43	22.27 – 28.02	25.55±2.67
a	4.69 – 5.49	5.09±0.57	2.09 – 3.15	2.62±0.75	14.47 – 23.21	18.84±6.18	23.31 – 30.79	26.55±6.00
b	3.66 – 9.24	6.45±3.95	2.48 – 2.69	2.58±0.15	18.56 – 22.07	20.32±2.48	28.42 – 30.29	29.35±1.32
d	3.72 – 7.93	5.82±2.98	1.54 – 2.23	1.89±0.49	12.40 – 19.40	15.90±4.96	22.56 – 24.66	23.61±1.49
e	4.59 – 4.65	4.62±0.05	2.58 – 3.75	3.16±0.83	14.87 – 19.90	17.38±3.56	22.03 – 28.30	25.17±4.43
g	6.55	6.55±0.00	2.69	2.69±0.00	17.51	17.51±0.00	26.74	26.74±0.00
h	5.42 – 6.02	5.72±0.43	3.16 – 4.85	4.00±1.20	15.35 – 17.95	16.65±1.84	23.93 – 28.83	26.38±3.47
j	6.44 – 6.57	6.51±0.09	2.11 – 3.61	2.86±1.06	15.06 – 17.01	16.04±1.38	25.11 – 25.69	25.40±0.41
n	4.22 – 4.87	4.55±0.46	3.58 – 3.53	3.55±0.04	13.3 – 15.34	14.33±1.40	21.74 – 23.12	22.43±0.98
q	3.09 – 3.76	3.43±0.47	0.22 – 0.39	0.30±0.12	11.98 – 12.69	12.34±0.50	15.29±16.83	16.06±1.09
r	5.02 – 6.28	5.65±0.89	1.91 – 2.70	2.30±0.56	13.64 – 14.29	13.96±0.46	21.37 – 22.47	21.92±0.78
t	4.50 – 6.44	5.47±1.37	3.61 – 4.59	4.10±0.70	7.26 – 15.06	11.16±5.52	16.35 – 25.11	20.73±6.19

Appendix XVIII: Comparison of Calculated Absorbed Dose Rates and Measured Absorbed Dose Rates, in $nGyh^{-}$

BLOCK	Average Measured Absorbed dose rate	UNSCEAR, 2000 RECOMMENDATION, nGy/h	Average Calculated Absorbed dose rate	UNSCEAR, 2000 RECOMMENDATION, nGy/h
A	77.86±34.84	60	17.45±1.85	54
B	53.93±4.72		24.32±3.01	
C	92.14±5.28		21.44±2.63	
D	92.50±11.03		21.14±4.22	
E	76.07±19.98		21.93±7.58	
F	81.79±18.34		25.88±9.37	
G	89.64±23.42		29.14±4.09	
H	66.07±21.23		19.47±3.29	
J	98.57±31.90		18.95±4.17	
K	60.00±7.90		21.42±6.92	
L	62.86±3.09		25.90±3.11	
M	78.93±16.76		21.09±0.74	
N	74.25±15.66		22.56±8.60	
P	72.86±21.73		19.68±1.37	
Q	76.79±12.90		27.83±9.11	
R	57.86±5.28		26.17±3.13	
S	55.00±4.29		22.34±2.10	
T	72.86±21.73		30.29±9.15	
U	105.36±9.14		25.50±9.07	
V	106.43±54.79		27.86±16.38	
W	82.86±11.01		26.89±4.71	
X	115.00±21.43		26.75±15.19	
Y	96.43±31.35		21.69±5.77	
Z	89.65±15.88		25.55±2.67	
a	69.29±17.18		26.55±6.00	
b	87.15±10.10		29.35±1.32	
d	85.00±17.17		23.61±1.49	
e	133.57±21.21		25.17±4.43	
g	102.86±0.00		26.74±0.00	
h	87.14±14.14		26.38±3.47	
j	132.14±19.19		25.40±0.41	
n	111.43±30.31		22.43±0.98	
q	85.72±38.39		16.06±1.09	
r	59.29±11.11		21.92±0.78	
t	60.72±5.06		20.73±6.19	

Appendix XIX: Calculated Annual Gonadal Equivalent Dose (AGED) and Radium Equivalent Activity, (Ra_{eq}) in $Bqkg^{-1}$ for Soil Samples

BLOCK	Sample no.	Annual Gonadal Equivalent Dose (AGED)	Radium equivalent activity, (Ra_{eq})
A	A_1	136.86	36.39
	A_2	131.39	35.89
	A_3	111.03	29.60
	A_4	111.50	31.10
B	B_1	202.03	53.17
	B_2	159.53	44.68
	B_3	152.50	39.85
	B_4	172.97	46.45
C	C_1	147.31	39.09
	C_2	153.62	42.31
	C_3	126.05	35.96
	C_4	173.09	47.08
D	D_1	106.33	30.60
	D_2	167.23	47.41
	D_3	170.49	47.33
	D_4	142.78	38.82
E	E_1	186.23	51.31
	E_2	100.95	29.97
	E_3	206.92	58.97
	E_4	111.50	31.10
F	F_1	131.39	35.89
	F_2	274.40	76.98
	F_3	149.97	42.00
	F_4	164.30	45.44
G	G_1	169.05	47.80
	G_2	190.24	51.05
	G_3	227.26	60.42
	G_4	231.14	63.29
H	H_1	148.74	43.02
	H_2	158.00	43.37
	H_3	109.58	29.59
	H_4	124.11	35.48

J	J_1	155.52	42.99
	J_2	153.71	43.22
	J_3	122.33	34.55
	J_4	91.87	27.35
K	K_1	172.95	47.36
	K_2	112.93	32.09
	K_3	104.36	29.25
	K_4	205.14	57.83
L	L_1	184.28	49.73
	L_2	154.14	40.69
	L_3	205.27	55.34
	L_4	187.86	50.10
M	M_1	152.97	40.86
	M_2	153.62	42.31
	M_3	142.59	39.01
	M_4	142.78	38.82
N	N_1	129.70	35.44
	N_2	130.52	36.38
	N_3	120.45	34.36
	N_4	244.92	68.68
P	P_1	141.22	36.44
	P_2	131.80	33.71
	P_3	133.07	37.13
	P_4	153.80	40.35
Q	Q_1	189.56	53.48
	Q_2	105.70	29.57
	Q_3	250.21	69.55
	Q_4	231.21	61.82
R	R_1	167.22	45.96
	R_2	211.42	59.11
	R_3	187.64	50.40
	R_4	167.37	45.03
S	S_1	136.36	37.48
	S_2	162.20	44.22
	S_3	154.12	43.43
	S_4	172.10	46.63
T	T_1	225.40	65.12

	T_2	267.65	74.72
	T_3	229.36	61.61
	T_4	120.96	32.83
U	U_1	178.07	47.40
	U_2	99.27	28.61
	U_3	179.05	49.72
	U_4	256.89	70.16
V	V_1	148.98	39.98
	V_2	360.48	102.34
	V_3	128.51	32.49
	V_4	144.18	37.67
W	W_1	167.37	45.03
	W_2	220.34	59.25
	W_3	158.33	40.25
	W_4	213.37	58.73
X	X_1	271.93	74.32
	X_2	140.72	36.70
	X_3	275.38	77.57
	X_4	57.36	18.09
Y	Y_1	174.36	49.63
	Y_2	95.08	28.01
	Y_3	182.45	53.13
	Y_4	141.93	41.51
Z	Z_1	190.40	55.97
	Z_2	154.12	43.43
	Z_3	189.56	55.48
	Z_4	169.05	47.80
a	a_1	156.10	42.78
	a_2	217.96	57.89
b	b_1	202.07	53.19
	b_2	210.32	58.52
d	d_1	175.17	46.01
	d_2	154.98	43.98
e	e_1	199.50	53.72
	e_2	154.60	42.06
g	g_1	186.95	51.24
h	h_1	201.25	55.55

	h_2	167.22	45.96
j	j_1	179.67	49.17
	j_2	174.52	48.61
n	n_1	162.20	44.22
	n_2	151.53	41.97
q	q_1	121.43	32.80
	q_2	141.92	39.10
r	r_1	156.60	43.23
	r_2	149.24	41.07
t	t_1	111.81	32.55
	t_2	174.52	48.61

Appendix XX: Average Calculated Annual Gonadal Equivalent Dose (AGED) and Radium Equivalent Activity, (Ra_{eq}) in $Bqkg^{-1}$ for Soil Samples

BLOCK	Annual Gonadal Equivalent Dose (AGED)		Radium equivalent activity (Ra_{eq})	
	Range	Average	Range	Average
A	111.03 – 136.86	122.70±13.39	29.60 – 36.39	33.24±3.40
B	152.50 – 202.03	171.76±21.89	39.85 – 53.17	46.04±5.52
C	126.05 – 173.09	150.02±19.38	35.96 – 47.08	41.11±4.75
D	106.33 – 170.49	146.71±29.43	30.60 – 47.41	41.04±8.04
E	100.95 – 206.92	151.40±53.02	29.97 – 58.97	42.84±14.55
F	131.39 – 274.40	180.02±64.35	35.89 – 76.98	50.08±18.37
G	169.05 – 231.14	204.42±29.93	47.80 – 63.29	55.64±7.39
H	109.58 – 158.00	135.11±22.23	29.59 – 43.37	37.86±6.61
J	91.87 – 155.52	130.86±30.13	27.35 – 43.22	37.03±7.61
K	104.36 – 205.14	148.85±48.37	29.25 – 57.83	41.63±13.41
L	154.14 – 205.27	182.89±21.25	40.69 – 55.34	48.96±6.08
M	142.59 – 153.62	147.99±6.13	38.82 – 42.31	40.25±1.65
N	120.45 – 244.92	156.40±59.19	34.36 – 68.88	43.76±16.76
P	131.80 – 153.80	139.97±10.12	33.71 – 40.35	36.91±2.73
Q	105.70 – 250.21	194.17±64.19	29.57 – 69.55	53.60±17.31
R	167.22 – 211.48	183.43±21.01	45.03 – 59.11	50.13±6.43
S	136.36 – 172.10	156.20±15.13	37.48 – 46.63	42.94±3.89
T	120.96 – 267.65	210.84±62.88	32.83 – 74.72	58.57±18.03
U	99.27 – 256.89	178.32±64.35	28.61 – 70.16	48.97±16.99
V	128.51 – 360.48	195.54±110.31	32.49 – 102.34	53.12±32.96
W	158.33 – 220.34	189.85±31.53	40.45 – 59.25	50.86±9.57
X	57.36 – 275.38	186.35±106.41	18.09 – 77.57	51.67±29.07
Y	95.08 – 182.45	148.45±39.66	28.01 – 53.13	43.07±11.16
Z	154.12 – 190.40	175.79±17.49	43.43 – 55.97	50.17±5.64
a	156.10 – 217.96	187.03±43.74	42.78 – 57.89	50.34±10.68
b	202.07 – 210.32	206.20±5.84	53.19 – 58.52	55.85±3.77
d	154.98 – 175.17	165.08±14.28	43.98 – 46.01	45.00±1.44
e	154.60 – 199.50	177.05±31.75	42.06 – 53.72	47.89±8.24
g	186.95	186.95±0.00	51.24	51.24±0.00
h	167.22 – 201.25	184.24±24.06	45.96 – 55.55	50.76±6.78
j	174.52 – 179.67	177.10±3.64	48.61 – 49.17	48.89±0.40
n	151.53 – 162.20	156.86±7.55	41.97 – 44.22	43.09±1.59
q	121.43 – 141.92	131.67±14.49	32.80 – 39.10	35.95±4.46
r	149.24 – 156.60	152.92±5.20	41.07 – 43.23	42.15±1.53
t	111.81 – 174.52	143.17±44.34	32.55 – 48.61	40.58±11.35

Appendix XXI: Annual Effective Dose Rate, AEDE ($mSvy^{-1}$) and Excess Lifetime Cancer Risk (ELCR) as Calculated from Computed Soil Radio Activities for Soil Samples

BLOCK	Sample no.	Annual effective dose rate, AEDE			Excess Lifetime Cancer Risk (ELCR)
		Outdoor	Indoor	Total	
A	A_1	0.05	0.07	0.12	0.41
	A_2	0.05	0.07	0.12	0.40
	A_3	0.04	0.06	0.10	0.34
	A_4	0.04	0.06	0.10	0.34
B	B_1	0.07	0.10	0.17	0.61
	B_2	0.06	0.08	0.14	0.49
	B_3	0.05	0.08	0.13	0.46
	B_4	0.06	0.09	0.15	0.53
C	C_1	0.05	0.08	0.13	0.45
	C_2	0.05	0.08	0.13	0.47
	C_3	0.04	0.07	0.11	0.39
	C_4	0.06	0.09	0.15	0.53
D	D_1	0.04	0.06	0.10	0.33
	D_2	0.06	0.09	0.15	0.52
	D_3	0.06	0.09	0.15	0.53
	D_4	0.05	0.07	0.12	0.44
E	E_1	0.07	0.10	0.17	0.57
	E_2	0.04	0.05	0.09	0.32
	E_3	0.07	0.11	0.18	0.65
	E_4	0.04	0.06	0.10	0.34
F	F_1	0.05	0.07	0.12	0.40
	F_2	0.10	0.15	0.25	0.85
	F_3	0.05	0.08	0.13	0.46
	F_4	0.06	0.09	0.15	0.51
G	G_1	0.06	0.09	0.15	0.53
	G_2	0.07	0.10	0.17	0.58
	G_3	0.08	0.12	0.20	0.69
	G_4	0.08	0.12	0.20	0.71
H	H_1	0.05	0.08	0.13	0.47
	H_2	0.06	0.08	0.14	0.48
	H_3	0.04	0.06	0.10	0.33

	H_4	0.04	0.07	0.11	0.39
J	J_1	0.05	0.08	0.13	0.48
	J_2	0.05	0.08	0.13	0.48
	J_3	0.04	0.07	0.11	0.38
	J_4	0.03	0.05	0.08	0.29
K	K_1	0.06	0.09	0.15	0.53
	K_2	0.04	0.06	0.10	0.35
	K_3	0.04	0.06	0.10	0.32
	K_4	0.07	0.11	0.18	0.63
L	L_1	0.06	0.10	0.16	0.56
	L_2	0.05	0.08	0.13	0.47
	L_3	0.07	0.11	0.18	0.63
	L_4	0.07	0.10	0.17	0.57
M	M_1	0.05	0.08	0.13	0.46
	M_2	0.05	0.08	0.13	0.47
	M_3	0.05	0.07	0.12	0.44
	M_4	0.05	0.07	0.12	0.44
N	N_1	0.05	0.07	0.12	0.40
	N_2	0.05	0.07	0.12	0.40
	N_3	0.04	0.06	0.10	0.38
	N_4	0.09	0.13	0.22	0.76
P	P_1	0.05	0.07	0.12	0.42
	P_2	0.05	0.07	0.12	0.41
	P_3	0.05	0.07	0.12	0.40
	P_4	0.05	0.08	0.13	0.46
Q	Q_1	0.07	0.10	0.17	0.59
	Q_2	0.04	0.06	0.10	0.33
	Q_3	0.09	0.13	0.22	0.77
	Q_4	0.08	0.12	0.20	0.70
R	R_1	0.06	0.09	0.15	0.51
	R_2	0.07	0.11	0.18	0.65
	R_3	0.07	0.10	0.17	0.57
	R_4	0.06	0.09	0.15	0.51
S	S_1	0.05	0.07	0.12	0.42
	S_2	0.06	0.09	0.15	0.50
	S_3	0.05	0.08	0.13	0.48
	S_4	0.06	0.09	0.15	0.53

T	T_1	0.08	0.12	0.20	0.71
	T_2	0.09	0.14	0.23	0.83
	T_3	0.08	0.12	0.20	0.70
	T_4	0.04	0.06	0.10	0.37
U	U_1	0.06	0.09	0.15	0.54
	U_2	0.04	0.05	0.09	0.31
	U_3	0.06	0.09	0.15	0.55
	U_4	0.09	0.13	0.22	0.79
V	V_1	0.05	0.08	0.13	0.45
	V_2	0.13	0.19	0.32	1.12
	V_3	0.04	0.07	0.11	0.38
	V_4	0.05	0.07	0.12	0.43
W	W_1	0.06	0.09	0.15	0.51
	W_2	0.08	0.11	0.19	0.67
	W_3	0.05	0.08	0.13	0.47
	W_4	0.07	0.11	0.18	0.66
X	X_1	0.10	0.14	0.24	0.83
	X_2	0.05	0.07	0.12	0.42
	X_3	0.10	0.15	0.25	0.85
	X_4	0.02	0.03	0.05	0.19
Y	Y_1	0.06	0.09	0.15	0.54
	Y_2	0.03	0.05	0.08	0.30
	Y_3	0.07	0.10	0.17	0.57
	Y_4	0.05	0.08	0.13	0.45
Z	Z_1	0.07	0.10	0.17	0.60
	Z_2	0.05	0.08	0.13	0.48
	Z_3	0.07	0.10	0.17	0.59
	Z_4	0.06	0.09	0.15	0.53
a	a_1	0.05	0.08	0.13	0.48
	a_2	0.08	0.11	0.19	0.66
b	b_1	0.07	0.10	0.17	0.61
	b_2	0.07	0.11	0.18	0.65
d	d_1	0.06	0.09	0.15	0.53
	d_2	0.06	0.08	0.14	0.48
e	e_1	0.07	0.10	0.17	0.61
	e_2	0.05	0.08	0.13	0.47
g	g_1	0.07	0.10	0.17	0.57

h	h_1	0.07	0.11	0.18	0.62
	h_2	0.06	0.09	0.15	0.51
j	j_1	0.01	0.01	0.02	0.05
	j_2	0.01	0.01	0.02	0.08
n	n_1	0.06	0.09	0.15	0.50
	n_2	0.05	0.08	0.13	0.47
q	q_1	0.04	0.06	0.10	0.33
	q_2	0.04	0.06	0.10	0.36
r	r_1	0.06	0.08	0.14	0.48
	r_2	0.06	0.08	0.14	0.46
t	t_1	0.04	0.06	0.10	0.35
	t_2	0.06	0.09	0.15	0.54

Appendix XXII: Annual Effective Dose Rate, AEDE ($mSvy^{-1}$) and Excess Lifetime Cancer Risk (ELCR) as Calculated from Computed Soil Radio-Activities

BLOCK	Annual effective dose rate, AEDE ($mSvy^{-1}$)						Excess Lifetime Cancer Risk (ELCR)	
	Outdoor		Indoor		Total			
	Range	Average	Range	Average	Range	Average	Range	Average
A	0.04 – 0.05	0.04±0.01	0.06 – 0.07	0.06±0.01	0.10 – 0.12	0.11±0.01	0.34 – 0.41	0.37±0.04
B	0.05 – 0.07	0.06±0.01	0.08 – 0.10	0.09±0.01	0.13 – 0.17	0.15±0.02	0.46 – 0.61	0.52±0.06
C	0.04 – 0.06	0.05±0.01	0.07 – 0.09	0.08±0.01	0.11 – 0.15	0.13±0.02	0.39 – 0.53	0.46±0.06
D	0.04 – 0.06	0.05±0.01	0.06 – 0.09	0.08±0.02	0.10 – 0.15	0.13±0.03	0.33 – 0.53	0.45±0.09
E	0.04 – 0.07	0.05±0.02	0.05 – 0.11	0.08±0.03	0.09 – 0.18	0.13±0.05	0.32 – 0.65	0.47±0.16
F	0.05 – 0.10	0.06±0.02	0.07 – 0.15	0.10±0.03	0.12 – 0.24	0.16±0.06	0.40 – 0.85	0.56±0.20
G	0.06 – 0.08	0.07±0.01	0.09 – 0.12	0.11±0.02	0.15 – 0.20	0.18±0.03	0.53 – 0.71	0.63±0.09
H	0.04 – 0.06	0.05±0.01	0.06 – 0.08	0.07±0.01	0.10 – 0.14	0.12±0.02	0.33 – 0.48	0.42±0.07
J	0.03 – 0.05	0.05±0.01	0.05 – 0.08	0.07±0.02	0.08 – 0.13	0.11±0.03	0.29 – 0.48	0.41±0.09
K	0.04 – 0.07	0.05±0.02	006 – 0.11	0.08±0.03	0.09 – 0.18	0.13±0.04	0.32 – 0.63	0.46±0.15
L	0.05 – 0.07	0.06±0.01	0.08 – 0.11	0.10±0.01	0.13 – 0.18	0.16±0.02	0.47 – 0.63	0.56±0.07
M	0.05 – 0.05	0.05±0.00	0.07 – 0.08	0.08±0.00	0.12 – 0.13	0.13±0.01	0.44 – 0.47	0.45±0.02
N	0.04 – 0.09	0.06±0.02	0.06 – 0.13	0.08±0.03	0.10 – 0.22	0.14±0.05	0.38 – 0.76	0.48±0.18
P	0.05 – 0.05	0.05±0.00	0.07 – 0.08	0.07±0.01	0.12 – 0.13	0.12±0.01	0.40 – 0.46	0.42±0.03
Q	0.04 – 0.09	0.07±0.02	0.06 – 0.13	0.10±0.03	0.10 – 0.22	0.17±0.06	0.33 – 0.77	0.60±0.20
R	0.06 – 0.07	0.06±0.01	0.09 – 0.11	0.10±0.01	0.15 – 0.18	0.16±0.02	0.51 – 0.65	0.56±0.07
S	0.05 – 0.06	0.05±0.01	0.07 – 0.09	0.08±0.01	0.13 – 0.15	0.14±0.01	0.42 – 0.53	0.48±0.05
T	0.04 – 0.09	0.07±0.02	0.06 – 0.14	0.11±0.03	0.10 – 0.23	0.19±0.06	0.37 – 0.83	0.65±0.20
U	0.04 – 0.09	0.06±0.02	0.05 – 0.13	0.09±0.03	0.09 – 0.22	0.16±0.06	0.31 – 0.79	0.55±0.19
V	0.04 – 0.13	0.07±0.04	0.07 – 0.19	0.10±0.06	0.11 – 0.32	0.17±0.10	0.38 – 1.12	0.60±0.35

W	0.05 – 0.08	0.07±0.01	0.08 – 0.11	0.10±0.02	0.13 – 0.19	0.16±0.03	0.47 – 0.67	0.58±0.10
X	0.02 – 0.10	0.07±0.04	0.03 – 0.15	0.10±0.06	0.05 – 0.25	0.16±0.09	0.19 – 0.85	0.57±0.33
Y	0.03 – 0.07	0.05±0.01	0.05 – 0.10	0.08±0.02	0.08 – 0.17	0.13±0.04	0.30 – 0.57	0.47±0.12
Z	0.05 – 0.07	0.06±0.01	0.08 – 0.10	0.09±0.01	0.14 – 0.17	0.16±0.02	0.48 – 0.60	0.55±0.06
a	0.05 – 0.08	0.07±0.01	0.08 – 0.11	0.10±0.02	0.13 – 0.19	0.16±0.04	0.48 – 0.66	0.57±0.13
b	0.07 – 0.07	0.07±0.00	0.10 – 0.11	0.11±0.00	0.17 – 0.18	0.18±0.01	0.61 – 0.65	0.63±0.03
d	0.06 – 0.06	0.06±0.00	0.08 – 0.09	0.09±0.01	0.14 – 0.15	0.14±0.01	0.48 – 0.53	0.51±0.03
e	0.05 – 0.07	0.06±0.01	0.08 – 0.10	0.09±0.02	0.13 – 0.17	0.15±0.03	0.47 – 0.61	0.54±0.10
g	0.07	0.07±0.00	0.10	0.10±0.00	0.16	0.16±0.00	0.57	0.57±0.00
h	0.06 – 0.07	0.06±0.01	0.09 – 0.11	0.10±0.01	0.15 – 0.18	0.16±0.02	0.51 – 0.62	0.57±0.07
j	0.01 – 0.01	0.01±0.00	0.01 – 0.01	0.01±0.00	0.02 – 0.02	0.02±0.00	0.05 – 0.08	0.06±0.02
n	0.05 – 0.06	0.06±0.00	0.08 – 0.09	0.08±0.00	0.13 – 0.15	0.14±0.01	0.47 – 0.50	0.48±0.02
q	0.04 – 0.04	0.04±0.00	0.06 – 0.06	0.06±0.00	0.10 – 0.10	0.10±0.00	0.33 – 0.36	0.34±0.02
r	0.05 – 0.06	0.05±0.00	0.08 – 0.08	0.08±0.00	0.14 – 0.14	0.14±0.00	0.46 – 0.48	0.47±0.02
t	0.04 – 0.06	0.05±0.02	0.06 – 0.09	0.08±0.02	0.10 – 0.15	0.13±0.04	0.35 – 0.54	0.44±0.13

Appendix XXIII: Thorium Decay Series

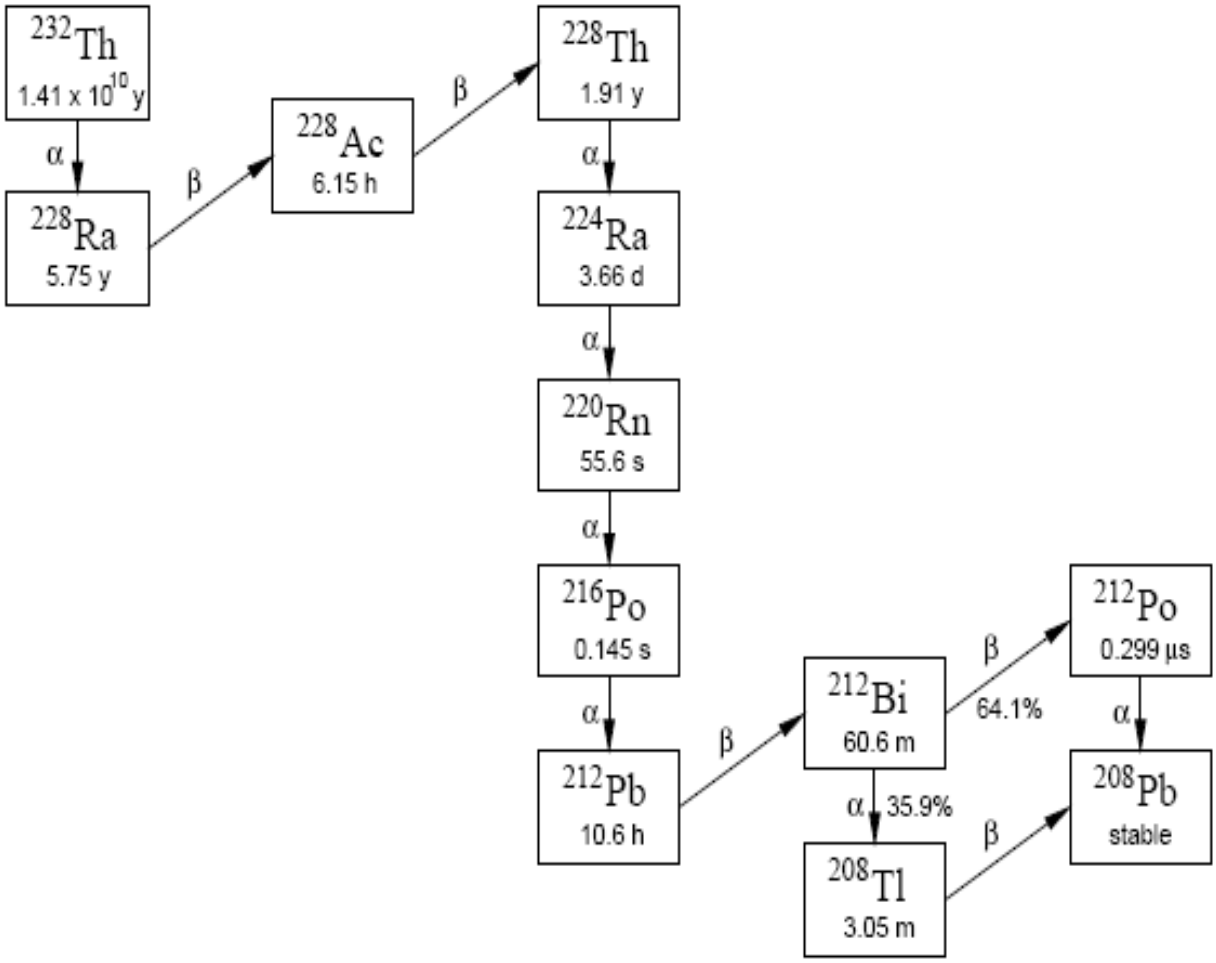

Appendix XXIV: Uranium Decay Series

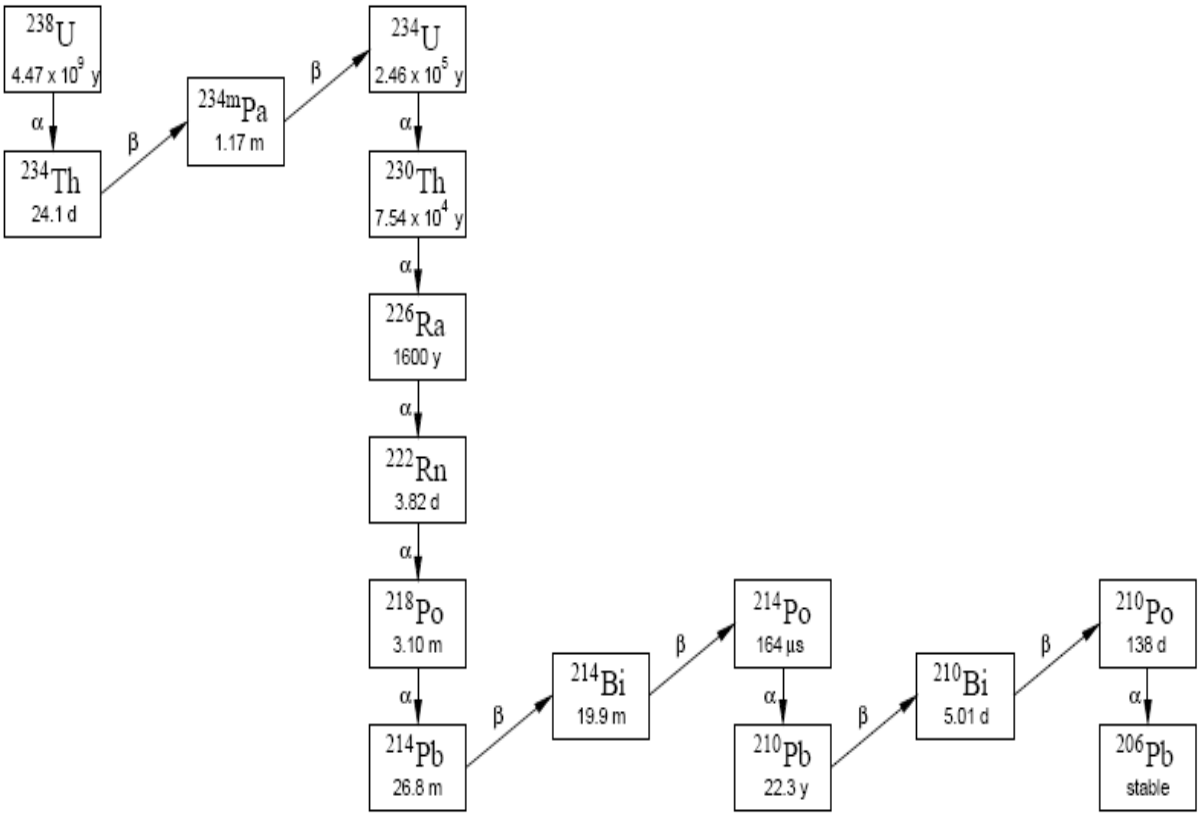

Appendix XXV: Table for Magnetic Anomaly Map

Magnetometer readings, nT					
Block	Easting, X - axis	Northing, Y - axis	Corrected magnetic reading, nT	IGRF reading, nT	Magnetic anomaly difference, nT (From IGRF calculator – corrected magnetic reading) Z - axis
D_1	341250	278250	33515.0	34080.9	-565.9
D_2	341250	277750	33766.0	34082.0	-316.0
D_3	340750	278250	33934.0	34082.6	-148.6
D_4	340750	277750	33860.0	34081.7	-221.7
E_1	340250	278250	34119.0	34082.2	36.8
E_2	340350	277750	33747.5	34081.4	-333.9
E_3	339750	278250	33827.5	34081.8	-254.3
E_4	339750	277750	34225.0	34081.0	144.0
F_1	339250	278250	33290.0	34081.4	-791.4
F_2	339250	277750	33791.0	34080.6	289.6
F_3	338750	278250	34108.0	34081.1	26.9
F_4	338750	277750	33929.5	34080.3	-150.8
G_1	339250	277250	33765.0	34079.9	-314.9
G_2	339250	276750	33872.0	34079.1	-207.1
G_3	338750	277250	33899.0	34079.6	-180.6
G_4	338750	276750	33933.0	34078.7	-145.7
H_1	340250	277250	34500.5	34080.6	419.9
H_2	340250	276750	34302.0	34079.8	222.2
H_3	339750	277250	33825.0	34080.3	-255.3
H_4	339750	276750	33353.0	34079.5	-726.5

J_1	341250	277250	34170.0	34081.4	88.6
J_2	341250	276750	-	34080.5	-
J_3	340750	277250	34232.0	34081.0	151.0
J_4	340750	276750	34106.0	34080.2	25.8
P_3	342750	276250	33958.5	34081.0	-122.5
P_4	342700	275750	33924.0	34080.0	-156.0
Q_1	342250	276250	34056.5	34086.6	-30.1
Q_2	342250	275750	33775.5	34079.7	-304.2
Q_3	341750	276250	34049.0	34080.2	-31.2
Q_4	341750	275750	33948.0	34079.4	-131.4
R_1	341250	276250	33994.5	34079.8	-85.3
R_2	341250	275750	33767.0	34079.0	-312.0
R_3	340750	276250	33875.0	34079.5	-204.5
R_4	340750	275750	33944.5	34078.7	-134.2
S_1	340250	276250	34468.0	34079.1	388.9
S_2	340250	275750	33959.0	34078.2	-119.2
S_3	339750	276250	34391.5	34078.8	312.7
S_4	339750	275750	34236.0	34077.9	158.1
T_1	339250	276250	34220.5	34078.4	142.1
T_2	339250	275750	33914.8	34083.5	-168.7
T_3	338750	276250	34321.0	34077.2	243.1
T_4	338750	275750	33965.0	34077.9	-112.2
U_1	339250	275250	33978.0	34076.7	-98.7
U_2	339250	274750	34137.0	34076.0	61.0

U_3	338750	275250	33844.0	34076.3	-232.3
U_4	338750	274750	33966.0	34075.7	-109.7
a_1	338250	278250	33909.5	34080.7	-171.2
a_2	338250	277750	34086.0	34079.9	6.1
b_1	338250	277250	33949.0	34079.2	-130.2
b_2	338250	276750	34103.5	34078.3	25.2
d_2	338250	275750	34112.5	34076.8	35.7
d_1	338250	276250	33943.5	34077.5	-134.0

Appendix XXVI: Magnetic Data Correction

Base station: Day 1. Date: 15/06/2018						
Time	Easting	Northing	Magnetic reading, nT			
07:00	340900	277008	33997			
11:05			34210			
14:25			34176			
Magnetometer readings, nT						
Block	Time	Easting	Northing	Magnetic reading, nT	Correction	New Magnetic reading, nT
J_1	08:30	341250	277250	34244	-74.0	34170.0
J_2	Houses	341250	276750	-	-	-
J_3	10:22	340750	277250	34402	-17.0	34232.0
J_4	10:50	340750	276750	34304	-198.0	34106.0
D_1	15:40	341250	278250	33671	-156.0	33515.0
D_2	16:00	341250	277750	33916	-150.0	33766.0
D_3	15:18	340750	278250	34095	-161.0	33934.0
D_4	14:25	340750	277750	34027	-167.0	33860.0
Base station: Day 2. Date: 16/06/2018						
Time	Easting	Northing	Magnetic reading, nT			
14:35	340900	277008	34152			
16:20			34132			
18:55			34096			
Magnetometer readings, nT						
Block	Time	Easting	Northing	Magnetic reading, nT	Correction	New Magnetic reading, nT
R_1	15:05	341250	276250	33987	7.5	33994.5
R_2	16:05	341250	275750	33752	15.0	33767.0
R_3	15:20	340750	276250	33865	10.0	33875.0
R_4	15:40	340750	275750	33932	12.5	33944.5
P_3	18:25	342750	276250	33911	47.5	33958.5
P_4	18:10	342700	275750	33879	45.0	33924.0
Q_1	17:30	342250	276250	34019	37.5	34056.5
Q_2	17:55	342250	275750	33733	42.5	33775.5
Q_3	17:06	341750	276250	34020	29.0	34049.0
Q_4	16:45	341750	275750	33923	25.0	33948.0
Base station: Day 3. Date: 07/09/2018						
Time	Easting	Northing	Magnetic reading, nT			
06:40	340900	277008	34096			
09:54			34073			

13:04			34069			
15:30			34051			
Block	Time	Easting	Northing	Magnetic reading, nT	Correction	New Magnetic reading, nT
E_1	16:57	340250	278250	34069	50.0	34119.0
E_3	17:07	339750	278250	33775	52.5	33827.5
F_1	17:21	339250	278250	33237	53.0	33290.0
F_3	17:48	338750	278250	34053	55.0	34108.0
G_1	08:05	339250	277250	33750	15.0	33765.0
G_2	11:00	339250	276750	33847	25.0	33872.0
G_3	08:20	338750	277250	33883	16.0	33899.0
G_4	10:44	338750	276750	33907	26.0	33933.0
H_1	07:10	340250	277250	34493	7.5	34500.5
H_2	11:46	340250	276750	34276	26.0	34302.0
H_3	07:25	339750	277250	33816	9.0	33825.0
H_4	11:22	339750	276750	33327	26.0	33353.0
S_1	12:20	340250	276250	34442	26.0	34468.0
S_2	12:46	340250	275750	33931	28.0	33959.0
a_1	18:10	338250	278250	33851	58.5	33909.5
a_2	18:27	338250	277750	34025	61.0	34086.0
b_1	08:50	338250	277250	33931	18.0	33949.0
b_2	09:28	338250	276750	34080	23.5	34103.5
Base station: Day 4. Date: 08/09/2018						
Time	Easting	Northing	Magnetic reading, nT			
06:30	340900	277008	34037			
08:50			33973			
13:20			33958			
15:25			33936			
18:30			33895			
Block	Time	Easting	Northing	Magnetic reading, nT	Correction	New Magnetic reading, nT
E_2	08:15	340350	277750	33715	32.5	33747.5
E_4	07:40	339750	277750	34200	25.0	34225.0
F_2	07:22	339250	277750	33776	15.0	33791.0
F_4	07:00	338750	277750	33917	12.5	33929.5
T_1	12:30	339250	276250	34148	72.5	34220.5
T_2	10:24	339250	275750	33846	68.8	33914.8
T_3	12:00	338750	276250	34251	70.0	34321.0
T_4	10:46	338750	275750	33905	60.0	33965.0

S_3	13:05	339750	276250	34314	77.5	34391.5
S_4	10:00	339750	275750	34181	55.0	34236.0
U_1	16:50	339250	275250	33858	120.0	33978.0
U_2	17:28	339250	274750	34009	127.0	34137.0
U_3	16:02	338750	275250	33734	110.0	33844.0
U_4	17:43	338750	274750	33836	130.0	33966.0
d_2	11:15	338250	275750	34050	62.5	34112.5
d_1	11:40	338250	276250	33876	67.5	33943.5

Appendix XXVII: Diurnal Correction as Done on Day 1 Magnetic Measurement

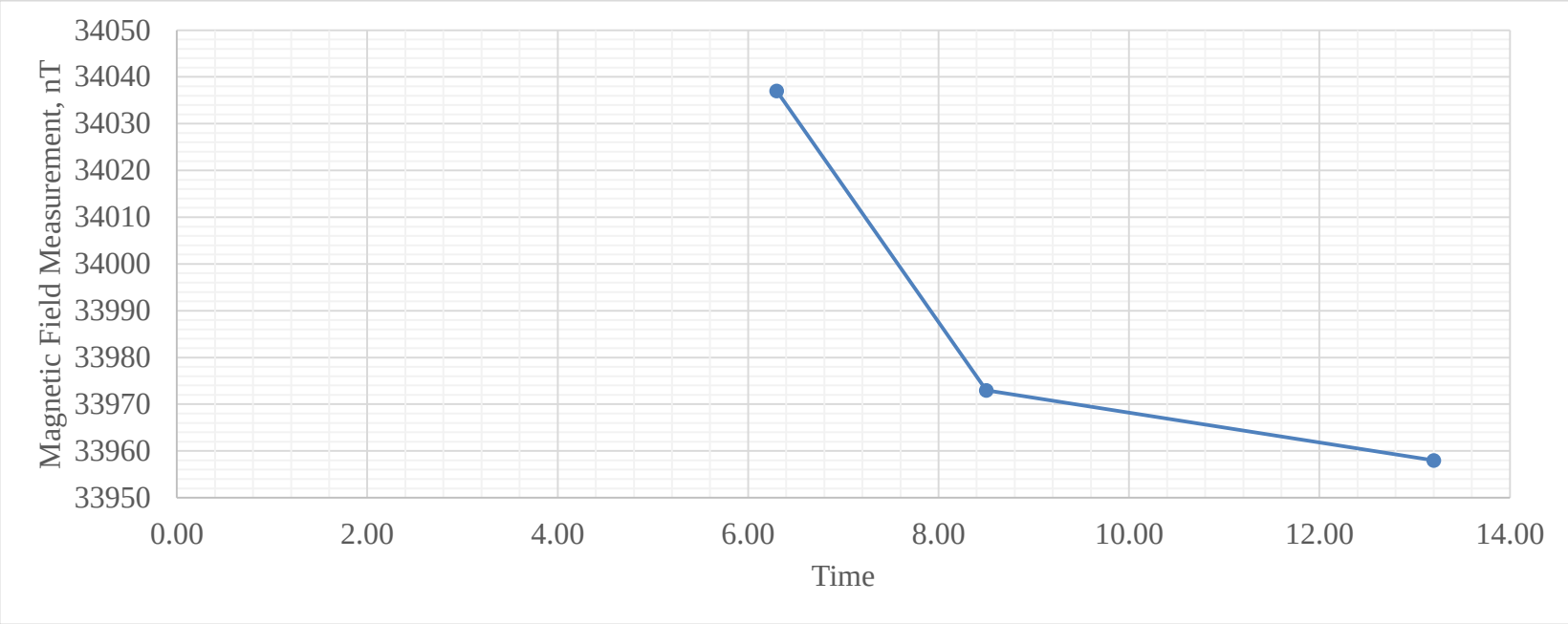

Appendix XXVIII: Diurnal Correction as Done on Day 2 Magnetic Measurement

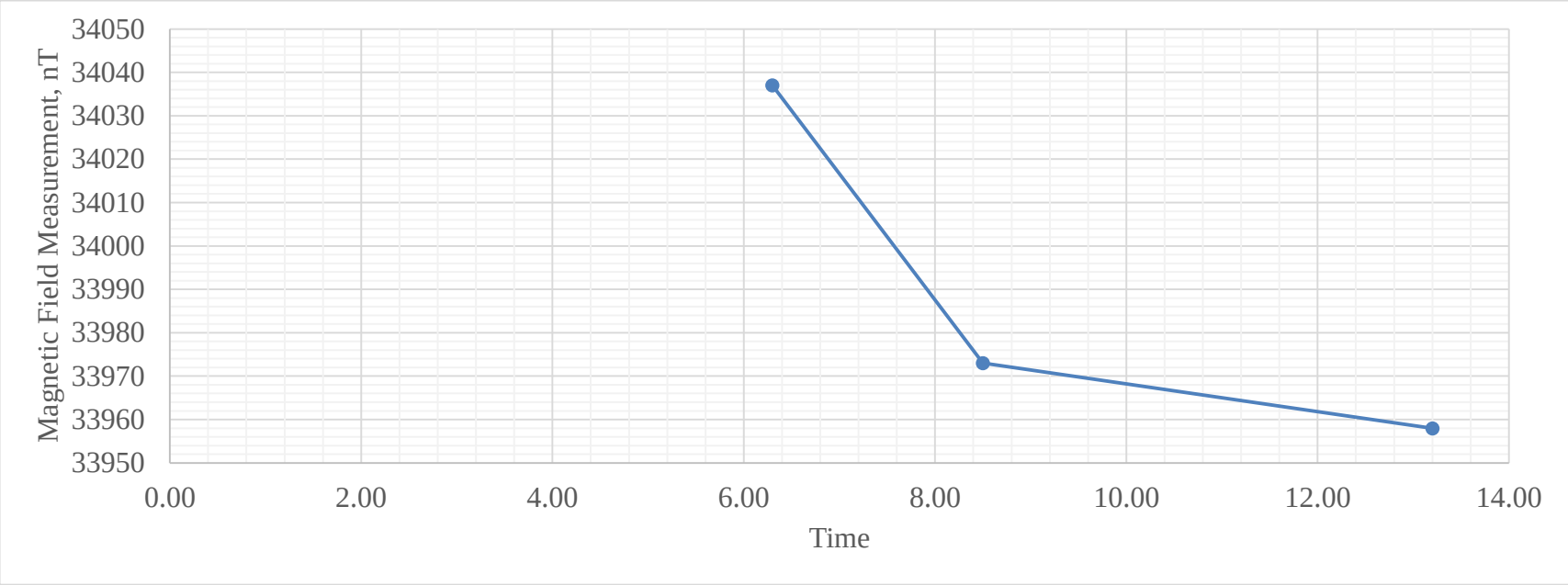

Appendix XXIX: Diurnal Correction as Done on Day 3 Magnetic Measurements

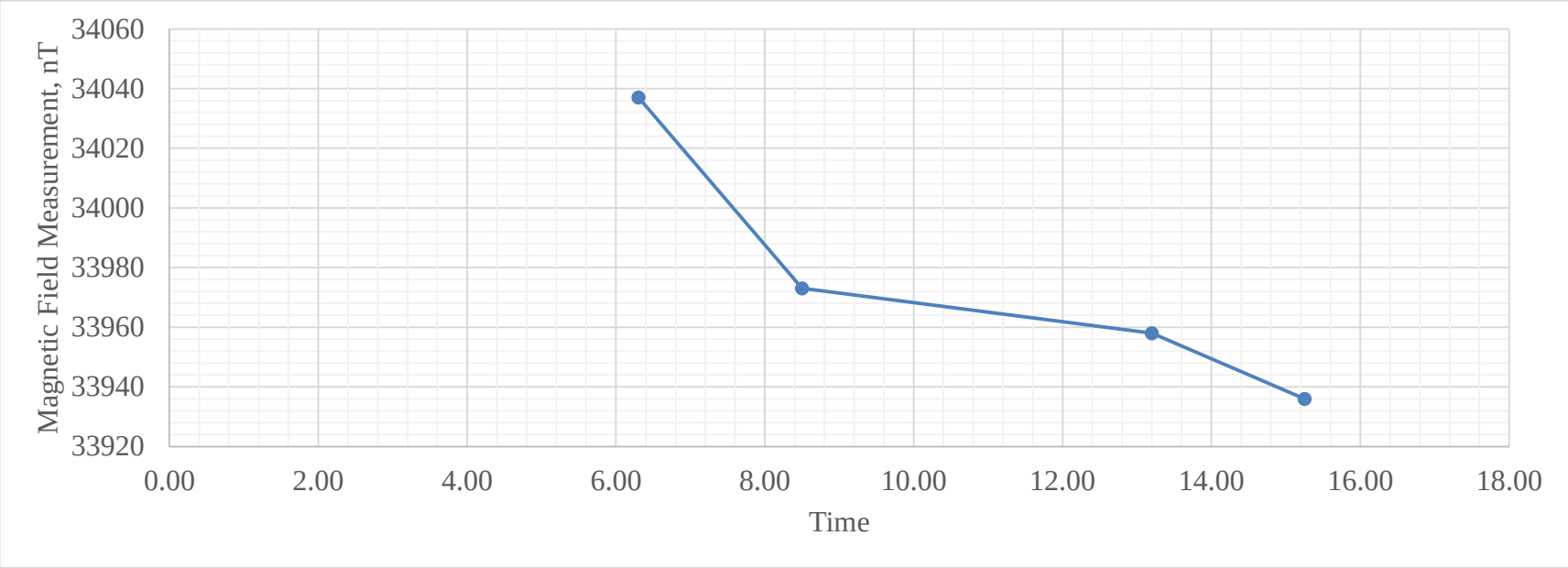

Appendix XXX: Diurnal Correction as Done on Day 4 Magnetic Measurements

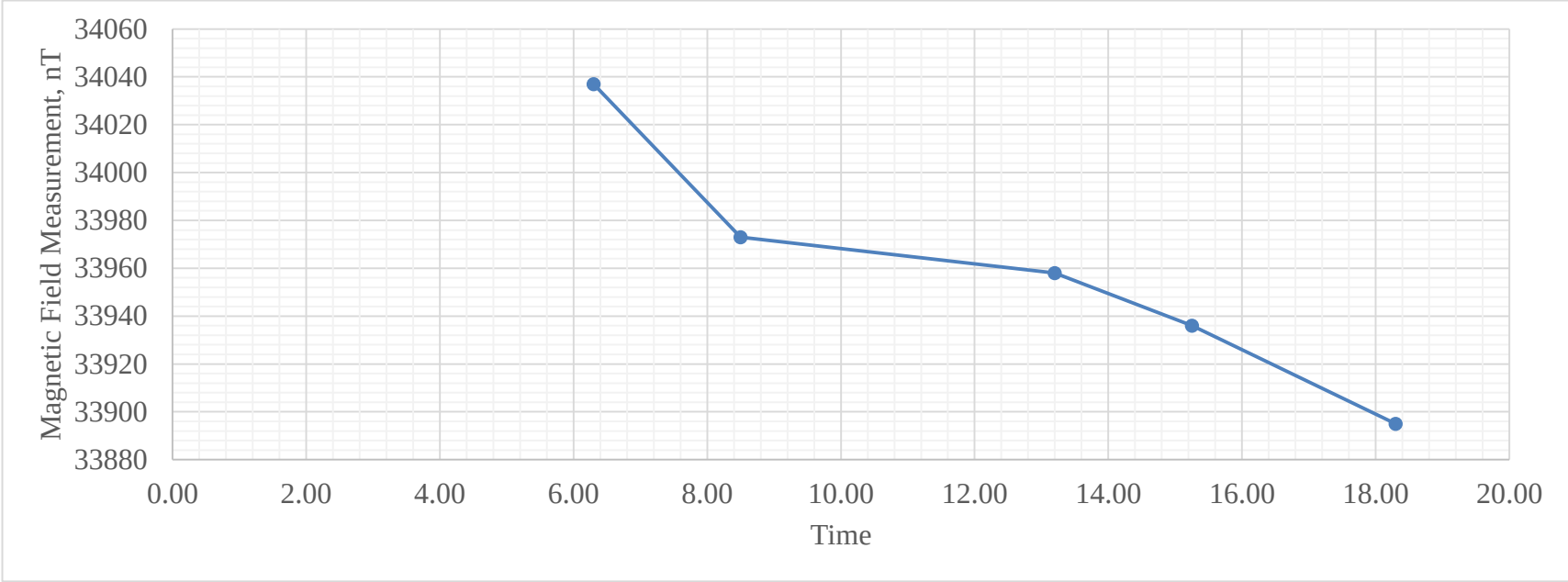

Appendix XXXI: Magnetic Data from IGRF Calculator

Base station: Day 1. Date: 15/06/2018					
Magnetometer readings, nT					
Block	Easting	Northing	Latitude	Longitude	Magnetic anomaly, nT (From IGRF calculator)
J_1	341250	277250	2.507569°	37.572144°	34081.4
J_2	341250	276750	2.503046°	37.572149°	34080.5
J_3	340750	277250	2.507564°	37.567648°	34081.0
J_4	340750	276750	2.503041°	37.567653°	34080.2
D_1	341250	278250	2.516613°	37.572134°	34080.9
D_2	341250	277750	2.512091°	37.572139°	34082.0
D_3	340750	278250	2.516608°	37.567638°	34082.6
D_4	340750	277750	2.512086°	37.567643°	34081.7
Base station: Day 2. Date: 16/06/2018					
Magnetometer readings, nT					
Block	Easting	Northing	Latitude	Longitude	Magnetic anomaly, nT (From IGRF calculator)
R_1	341250	276250	2.498524°	37.572154°	34079.8
R_2	341250	275750	2.494002°	37.572158°	34079.0
R_3	340750	276250	2.498519°	37.567657°	34079.5
R_4	340750	275750	2.493997°	37.567662°	34078.7
P_3	342750	276250	2.498539°	37.585642°	34081.0
P_4	342700	275750	2.494016°	37.585198°	34080.0
Q_1	342250	276250	2.498534°	37.581146°	34086.6
Q_2	342250	275750	2.494012°	37.581151°	34079.7
Q_3	341750	276250	2.498529°	37.57665°	34080.2
Q_4	341750	275750	2.494007°	37.576655°	34079.4
Base station: Day 3. Date: 07/09/2018					
Block	Easting	Northing	Latitude	Longitude	Magnetic anomaly, nT (From IGRF calculator)
E_1	340250	278250	2.516603°	37.563141°	34082.2
E_3	339750	278250	2.516598°	37.558645°	34081.8
F_1	339250	278250	2.516593°	37.554149°	34081.4
F_3	338750	278250	2.516588°	37.549653°	34081.1
G_1	339250	277250	2.507549°	37.554159°	34079.9
G_2	339250	276750	2.503027°	37.554164°	34079.1
G_3	338750	277250	2.507544°	37.549663°	34079.6
G_4	338750	276750	2.503022°	37.549668°	34078.7

H_1	340250	277250	2.507556°	37.563151°	34080.6
H_2	340250	276750	2.503037°	37.563656°	34079.8
H_3	339750	277250	2.507554°	37.558655°	34080.3
H_4	339750	276750	2.503032°	37.55866°	34079.5
S_1	340250	276250	2.498514°	37.563161°	34079.1
S_2	340250	275750	2.493992°	37.563166°	34078.2
a_1	338250	278250	2.516583°	37.545157°	34080.7
a_2	338250	277750	2.512061°	37.545162°	34079.9
a_3	338250	277250	2.507539°	37.545167°	34079.2
a_4	338250	276750	2.503017°	37.545172°	34078.3
Base station: Day 4. Date: 08/09/2018					
Block	Easting	Northing	Latitude	Longitude	Magnetic anomaly, nT (From IGRF calculator)
E_2	340350	277750	2.512082°	37.564046°	34081.4
E_4	339750	277750	2.12076°	37.55865°	34081.0
F_2	339250	277750	2.512071°	37.554154°	34080.6
F_4	338750	277750	2.512066°	37.549658°	34080.3
T_1	339250	276250	2.498504°	37.554169°	34078.4
T_2	339250	275750	2.493982°	37.554174°	34083.5
T_3	338750	276250	2.493977°	37.549678°	34077.2
T_4	338750	275750	2.498499°	37.549673°	34077.9
S_3	339750	276250	2.498509°	37.558665°	34078.8
S_4	339750	275750	2.493987°	37.55867°	34077.9
U_1	339250	275250	2.48946°	37.554179°	34076.7
U_2	339250	274750	2.484938°	37.554184°	34076.0
U_3	338750	275250	2.489455°	37.549683°	34076.3
U_4	338750	274750	2.484933°	37.549688°	34075.7
d_2	338250	275750	2.493972°	37.545181°	34076.8
d_1	338250	276250	2.498494°	37.545176°	34077.5

Appendix XXXII: Background Radiation Measuring Instrument

Appendix XXXIII: GPS Instruments

Appendix XXXIV: Magnetometer